Vol. 285, No. 3, January 28, 1994
Completing Volume 285
ISSN 0003-2670

ANALYTICA CHIMICA ACTA

An international journal devoted to all branches of analytical chemistry

ELSEVIER

ANALYTICA CHIMICA ACTA

Scope. *Analytica Chimica Acta* publishes original papers, rapid publication letters and reviews dealing with every aspect of modern analytical chemistry. Reviews are normally written by invitation of the editors, who welcome suggestions for subjects. Letters can be published within **four months** of submission. For information on the Letters section, see inside back cover.

Submission of Papers

Americas

Prof. Harry L. Pardue
Department of Chemistry
1393 BRWN Bldg, Purdue University
West Lafayette, IN 47907–1393
USA

Tel:(+1-317) 494 5320
Fax:(+1-317) 496 1200

Computer Techniques

Prof. J.T. Clerc
Universität Bern
Pharmazeutisches Institut
Baltzerstrasse 5, CH-3012 Bern
Switzerland

Tel:(+41-31) 6314191
Fax:(+41-31) 6314198

Prof. Sarah C. Rutan
Department of Chemistry
Virginia Commonwealth University
P.O. Box 2006
Richmond, VA 23284-2006
USA
Tel:(+1-804) 367 1298
Fax:(+1-804) 367 7517

Other Papers

Prof. Alan Townshend
Department of Chemistry
The University
Hull HU6 7RX
Great Britain

Tel:(+44-482) 465027
Fax:(+44-482) 466410

Prof. Willem E. van der Linden
Laboratory for Chemical Analysis
Department of Chemical Technology
Twente University of Technology
P.O. Box 217, 7500 AE Enschede
The Netherlands
Tel:(+31-53) 892629
Fax:(+31-53) 356024

Prof. Paul Worsfold
Dept. of Environmental Sciences
University of Plymouth
Plymouth PL4 8AA
Great Britain

Tel:(+44-752) 233006
Fax:(+44-752) 233009

Submission of an article is understood to imply that the article is original and unpublished and is not being considered for publication elsewhere. *Anal. Chim. Acta* accepts papers in English only. There are no page charges. Manuscripts should conform in layout and style to the papers published in this issue. See inside back cover for "Information for Authors".

Publication. *Analytica Chimica Acta* appears in 16 volumes in 1994 (Vols. 281–296). *Vibrational Spectroscopy* appears in 2 volumes in 1994 (Vols. 6 and 7). Subscriptions are accepted on a prepaid basis only, unless different terms have been previously agreed upon. It is possible to order a combined subscription (*Anal. Chim. Acta* **and** *Vib. Spectrosc.*).
Our p.p.h. (postage, packing and handling) charge includes surface delivery of all issues, except to subscribers in the U.S.A., Canada, Australia, New Zealand, China, India, Israel, South Africa, Malaysia, Thailand, Singapore, South Korea, Taiwan, Pakistan, Hong Kong, Brazil, Argentina and Mexico, who receive all issues by air delivery (S.A.L.–Surface Air Lifted) at no extra cost. For Japan, air delivery requires 25% additional charge of the normal postage and handling charge; for all other countries airmail and S.A.L. charges are available upon request.

Subscription orders. Subscription prices are available upon request from the publisher. Subscription orders can be entered only by calendar year and should be sent to: Elsevier Science B.V., Journals Department, P.O. Box 211, 1000 AE Amsterdam, The Netherlands. Tel: (+31-20) 5803 642, Telex: 18582, Telefax: (+31-20) 5803598, to which requests for sample copies can also be sent. Claims for issues not received should be made within six months of publication of the issues. If not they cannot be honoured free of charge. Readers in the U.S.A. and Canada can contact the following address: Elsevier Science Inc., Journal Information Center, 655 Avenue of the Americas, New York, NY 10010, U.S.A. Tel: (+1-212) 6333750, Telefax: (+1-212) 6333990, for further information, or a free sample copy of this or any other Elsevier Science journal.
Advertisements. Advertisement rates are available from the publisher on request.

US mailing notice – Analytica Chimica Acta (ISSN 0003-2670) is published 3 times a month (total 42 issues) by Elsevier Science B.V. (Molenwerf 1, Postbus 211, 1000 AE Amsterdam). Annual subscription price in the USA US$ 3035.75 (valid in North, Central and South America), including air speed delivery. Second class postage paid at Jamaica, NY 11431. *USA Postmasters*: Send address changes to Anal. Chim. Acta, Publications Expediting, Inc., 200 Meacham Av., Elmont, NY 11003. Airfreight and mailing in the USA by Publications Expediting.

ANALYTICA CHIMICA ACTA

An international journal devoted to all branches of analytical chemistry

(Full texts are incorporated in CJELSEVIER, a file in the Chemical Journals Online database available on STN International; Abstracted, indexed in: Aluminum Abstracts; Anal. Abstr.; Biol. Abstr.; BIOSIS; Chem. Abstr.; Curr. Contents Phys. Chem. Earth Sci.; Engineered Materials Abstracts; Excerpta Medica; Index Med.; Life Sci.; Mass Spectrom. Bull.; Material Business Alerts; Metals Abstracts; Sci. Citation Index)

VOL. 285 NO. 3 JANUARY 28, 1994

CONTENTS

(Continued overleaf)

Analytica Chimica Acta, 285 (1994) 247–263
Elsevier Science B.V., Amsterdam

Mathematical modelling and optimisation of a coulometric sensor–actuator system based on three-dimensional diffusion

Spas D. Kolev [1] and Willem E. van der Linden

MESA Research Institute, Department of Chemical Technology, University of Twente, P.O. Box 217, 7500 AE Enschede (Netherlands)

Wouter Olthuis and Piet Bergveld

MESA Research Institute, Department of Electrical Engineering, University of Twente, P.O. Box 217, 7500 AE Enschede, (Netherlands)

(Received 16th September 1993)

Abstract

A mathematical model describing the processes taking place in a measuring cell with a coulometric sensor–actuator system was developed both for the cases of titration of strong and weak protolytes. It takes into consideration the three dimensional diffusion which ocurrs in the volume of the measuring cell. The boundary conditions express the fact that the walls of the measuring cell are impermeable to the chemical species participating in the protolytic interactions and that a constant current is applied at the actuator electrode. The model was numerically solved by the implicit alternating-direction finite-difference method. Experimental titrations of diluted solutions of nitric, acetic and butyric acid and potassium hydroxide with various concentrations were performed. The good agreement between the experimental results and the predictions of the model confirmed its validity and showed that the model can be used successfully for the quantitative description of real sensor–actuator systems. On the basis of model simulations, some important guidelines for manufacturing sensor–actuator systems with optimal design with respect to their performance (e.g., high sampling rates) were formulated. The conditions under which the general three-dimensional model can be reduced to a two dimensional one for speeding up the computations were determined. They cover most of the sensor–actuator systems currently used in practice. It was shown that the one-dimensional model, used until now, failed to describe quantitatively real sensor–actuator systems and can be applied only for deriving qualitative trends.

Keywords: Coulometry; Sensors; Diffusion equation; Mathematical modelling; Sensor–actuator system; Titration

Acid or base concentrations can be determined by performing an acid–base titration with coulometrically generated hydronium (H_3O^+) or hydroxyl (OH^-) ions at an actuator electrode in close proximity to a pH sensor. A schematic representation of the sensor–actuator device is given in Fig. 1. The titrant can be generated by the electrolysis of water at the actuator which usually is a noble metal electrode [1,2]:

$$6H_2O \Rightarrow 4H_3O^+ + 4e^- + O_2$$

at the anode

$$2H_2O + 2e^- \Rightarrow 2OH^- + H_2$$

at the cathode

Correspondence to: W.E. van der Linden, MESA Research Institute, Department of Chemical Technology, University of Twente, P.O. Box 217, 7500 AE Enschede (Netherlands).

[1] Permanent address: Faculty of Chemistry, University of Sofia, 1 James Bourchier Ave., BG-1126 Sofia (Bulgaria).

SSDI 0003-2670(93)E0572-O

The pH sensor which is used as an indicator electrode monitors the changes in pH at its surface in time. A pH-sensitive ISFET can be successfully utilized [1–3]. The time dependence of the pH is similar to the dependence of the pH on the volume of the titrant added in classical titrations and for this reason is also referred to as titration curve.

The equivalence time, t_{eq}, which is determined as the inflection point of the titration curve, depends on the acid or base concentration of the sample solution.

Apart from the determination of acid or base concentrations, the coulometric sensor–actuator device has been used as the basic element of a carbon dioxide sensor [4] and has also been successfully applied as a pH-static enzyme sensor [5]. Recently, a modified version of this system has been shown to be able to determine the buffer capacity of a solution [6].

An early attempt to find an analytical expression between t_{eq} and the acid or base concentration was based on the statistics of the mean square distance that an ion travels in a given time interval and on the amount of generated titrant in that time interval [1]. A more sophisticated approach to describe the coulometric sensor–actuator system took the non-zero distance between the sensor and actuator into account [7]. The model was based on one-dimensional semi-infinite diffusive mass transport and was solved analytically giving an explicit relationship for calculating the equivalence time [7]. In addition to diffusive mass transfer, the effect of migration has been included and a one-dimensional diffusion–migration model has been developed, based on the solution of the Nernst-Planck equations [8].

The main advantage of the one-dimensional model is the relatively simple and little time-consuming numerical solution, and the possibility to derive some analytical expressions which can be used for a better understanding of the influence of some of the parameters on the behaviour of the system.

Their main drawbacks stem from the fact that in one dimension it is not possible to describe: (i) the complexity of the diffusion transport of all species participating in the chemical interactions; (ii) the influence of the geometrical dimensions of the actuator electrode and the sensor as well as the measuring cell. For these reasons the results obtained from these models had only a limited validity and required an extra fitting parameter in order to describe the multi-dimensional reality. For the adequate description and effective optimisation of sensor–actuator systems used in practice a general mathematical model overcoming these drawbacks is necessary. In the present paper the development of such a model and its experimental verification is reported. Some guidelines for optimising the design of sensor–actuator systems based on model simulation are also formulated.

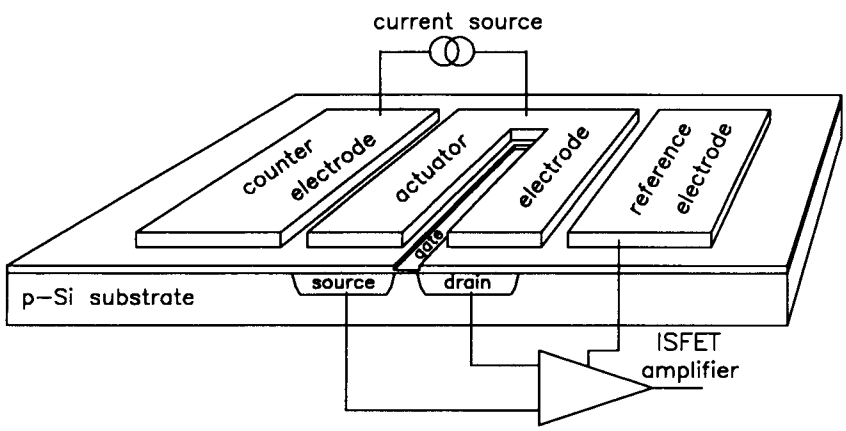

Fig. 1. The basic elements of an ISFET based sensor–actuator system.

DEVELOPMENT OF THE MATHEMATICAL MODEL

The mathematical model proposed in the present study describes the sensor–actuator system schematically presented in Fig. 2 and is based on the following assumptions: (i) the mass transfer is the result only of Fickian diffusion, i.e., no migration or convective transport (resulting from either stirring or buoyancy) is taken into account; (ii) the walls of the vessel where the measurements are performed, i.e., the measuring cell, which are assumed to be rectangular, are impermeable to the interacting chemical species; (iii) the current at the actuator electrode is kept constant during measurements and no side reactions either at the actuator electrode or in the bulk of the solution take place; (iv) the protolytic interactions are assumed to be very fast so equilibrium is instantaneously established; (v) in the case of strong protolytes which are fully dissociated only the diffusion of the hydronium and the hydroxyl ions is taken into account while for weak protolytes the diffusion of all chemical species participating in the protolytic interaction is considered; (vi) the counter electrode is assumed to be far from the actuator electrode so that the chemical species generated there cannot influence the processes taking place at the sensor in the time interval during which measurements are performed; (vii) both the sensor and the actuator are assumed to lie at the same level as the bottom of the measuring cell; (viii) the signal measured is proportional

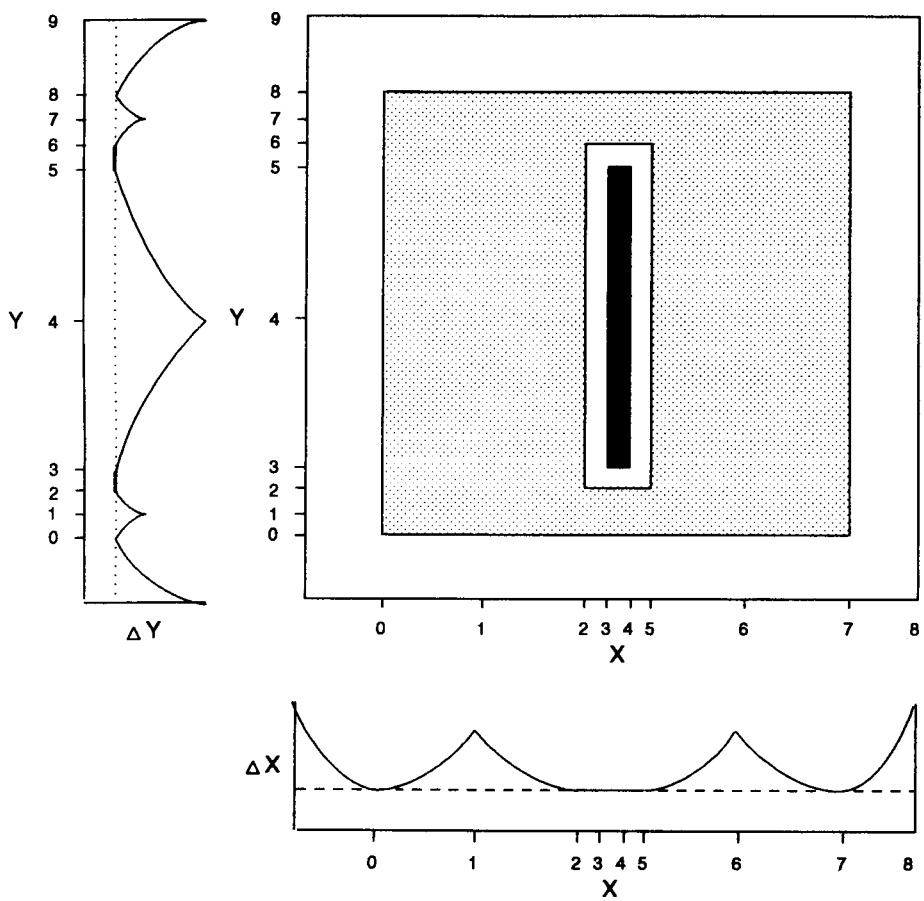

Fig. 2. Scheme of the bottom of the measuring cell and illustration of the way how the increments in X and Y direction vary. The dotted area refers to the actuator while the filled area refers to the sensor (ΔX and ΔY represent steps in the spatial grid).

to the averaged pH over the sensor surface. Assumption (i) will hold in the presence of a sufficiently high concentration of supporting electrolyte [8]. Otherwise migration and probably buoyancy effects should be considered. With regard to assumption (ii), it can be said that in the case the walls of the measuring cell are situated far from the sensor–actuator ensemble, infinite diffusive mass transfer in x and y directions and semi-infinite diffusive mass transfer in z direction will be encountered.

The chemical equilibrium which must be considered in the case of a strong protolyte is the dissociation of water. The symbols and their definitions are given in Table 1.

$$H_2O + H_2O \rightleftharpoons H_3O^+ + OH^- \quad (1)$$

with

$$K_W = c_{OH^-} c_{H_3O^+} \quad (2a)$$

The position of many solution equilibria depends on the electrolyte concentration of the medium. For this reason the concentration equilibrium constants (e.g., ion product of water, K_W, and the dissociation constants of acids and bases) must be corrected for the ionic strength, μ, of the solutions.

$$K_W = K_W^t f_{H_3O^+}^{-1} f_{OH^-}^{-1} \quad (2b)$$

where K_W is the concentration ion product of water, K_W^t is the thermodynamic ion product of water and f are the activity coefficients of the H_3O^+ and OH^- ions. They can be calculated according to the Debye-Hückel equation [9] (Appendix A).

In the case of a weak acid or a weak base besides Equilibrium 1 the corresponding dissociation process should be taken into account:

$$H_2O + HA \rightleftharpoons H_3O^+ + A^- \quad (3)$$

with dissociation constant

$$K_a = c_{A^-} c_{HA} / c_{HA} \quad (4)$$

$$H_2O + B \rightleftharpoons OH^- + HB^+ \quad (5)$$

with dissociation constant

$$K_b = c_{HB^+} c_{OH^-} / c_B \quad (6)$$

where $K_a = K_a^t f_{H_3O^+}^{-1} f_{A^-}^{-1}$ and $K_b = K_b^t f_{OH^-}^{-1} f_{HB^+}^{-1}$ (Appendix A).

TABLE 1

Symbols and definitions [a]

a	Coefficient defined in Eqns. 10e and 11e
b	Coefficient defined in Eqns. 10f, 11f and 12e
c	Concentration (mol m^{-3})
c_0	Initial concentration (mol m^{-3})
C	$= c/c_0$. Dimensionless concentration
D_m	Diffusion coefficient (m^2 s^{-1})
D	$= D_m/D_{mG}$. Dimensionless diffusion coefficient
f	Activity coefficient
F	= 96486.332. Faraday constant (C mol^{-1})
h	Exact value of the exponential coefficient
H	Approximate value of the exponential coefficient
j	Current density (A m^{-2})
J	$= -jL/\eta F D_{mG} c_0$. Dimensionless current density
K_w^t	Thermodynamic ion-product of water (mol^2 m^{-6})
K_w	Concentration ion-product of water (mol^2 m^{-6})
K_w'	$= K_w/(c_0)^2$. Dimensionless ion-product of water
K^t	Thermodynamic dissociation constant (mol m^{-3})
K	Concentration dissociation constant (mol m^{-3})
K'	$= K/c_0$. Dimensionless dissociation constant
L	$= \max\{X^8, Y^9\}$. Characteristic length (m)
M	Degree of miniaturisation
n	Number of increments in a given direction
N	Total number of increments in a given direction
Q	Approximate value of the spatial increment in a given direction (m)
S	$= Q/L$. Approximate dimensionless value of the spatial increment in a given direction
s	Exact dimensionless value of the spatial increment in a given direction
t	Time (s)
x, y, z	Directed distances in a Cartesian coordinate system (m)
X, Y, Z	$= x/L,\ y/L,\ z/L$. Dimensionless directed distances in a Cartesian coordinate system
α, β	Coefficients defined in Table 2
$\Delta\Psi$	$= \Delta X, \Delta Y, \Delta Z$. Dimensionless spatial increments
$\Delta\Psi^*$	Coefficient defined in Table 2
η	Charge of a given ion
λ	Ratio between the square root of the equivalence times calculated by the three and the two dimensional model
μ	Ionic strength
θ	$= D_{mG} t/L^2$. Dimensionless time
ρ	Effective diameter of a hydrated ion (m)
Ψ	$= X, Y, Z$. Dimensionless directed distances in a Cartesian coordinate system

[a] Subscripts: G refers to generated species; T refers to titrated species, Ψ refers to X, Y, or Z, eq refers to equivalence time, exp refers to experimental set-up, sim refers to data used in the simulations, subscripts H_3O^+, OH^-, HA, A^-, B, and HB^+ refer to H_3O^+, OH^-, HA, A^-, B, and HB^+. Superscripts: t refers to thermodynamic, j refers to regions of the sensor–actuator system, and * refers to concentrations established after the chemical reaction step.

The diffusion of the chemical species of interest (H_3O^+ and OH^- in the case of a strong protolyte and H_3O^+, OH^-, HA, A^-, B, and HB^+ in the case of a weak one) is described by Fick's second law in dimensionless quantities and variables.

$$\frac{\partial C_G}{\partial \theta} = \frac{\partial^2 C_G}{\partial X^2} + \frac{\partial^2 C_G}{\partial Y_2} + \frac{\partial^2 C_G}{\partial Z^2} \quad (7)$$

$$\frac{1}{D_i}\frac{\partial C_i}{\partial \theta} = \frac{\partial^2 C_i}{\partial X^2} + \frac{\partial^2 C_i}{\partial Y^2} + \frac{\partial^2 C_i}{\partial Z^2} \quad (8)$$

where subscript G refers to the generated species (i.e., H_3O^+ or OH^-) while subscript i refers to: H_3O^+ in the case of a strong acid; OH^- in the case of a strong base; H_3O^+, HA, and A^- in the case of a weak acid; and OH^-, B, and HB^+ in the case of a weak base.

In the case of a strong protolyte the diffusion of only two chemical species (the generated and the titrated species) should be considered, i.e., H_3O^+ or OH^-. Equations 7 and 8 allow to calculate their concentrations for a given time moment, i.e., C_G and C_T. As a result of their chemical interactions their concentrations will be modified to C_G^* and C_T^*. The resultant concentrations can be calculated by relationships derived on the basis of Eqn. 2.

$$\begin{aligned} C_G^* &= C_G - G_T && \text{if} \quad C_G > C_T \\ C_G^* &= K'_W/(C_T - C_G) && \text{if} \quad C_G < C_T \\ C_G^* &= \sqrt{K'_W} && \text{if} \quad C_G = C_T \end{aligned} \quad (9a)$$

$$\begin{aligned} C_T^* &= C_T - G_G && \text{if} \quad C_T > C_G \\ C_T^* &= K'_W/(C_G - C_T) && \text{if} \quad C_T < C_G \\ C_T^* &= \sqrt{K'_W} && \text{if} \quad C_T = C_G \end{aligned} \quad (9b)$$

As an example of the titration of a weak protolyte the titration of a weak acid (HA) will be considered. Equations 7 and 8 allow to calculate for a given moment the following concentrations: $C_{H_3O^+}$, C_{OH^-}, C_{A^-} and C_{HA}. As a result of the interactions between the hydronium and hydroxyl ions their concentrations will change. At the same time hydronium ions can be generated as a result of the dissociation of the weak acid HA leading to an additional change of C_{OH^-} and $C_{H_3O^+}$. Obviously the concentrations of HA and A^- will also change. The magnitude of this change, i.e., b (Table 1), can be determined by substituting the concentrations after reaction ($C^*_{H_3O^+}$, $C^*_{A^-}$ and C^*_{HA}, respectively) in Eqn. 4 and subsequently solving the resultant equation. Taking into consideration the dissociation of water (Eqn. 1) and the value of a (Table 1), the actual values of the concentrations of H_3O^+, OH^-, HA and A^- in the time moment under consideration can be calculated. Depending on the concentrations of H_3O^+, OH^- and HA obtained by Eqns. 7 and 8 the following cases with the corresponding relationships for $C^*_{OH^-}$, $C^*_{H_3O^+}$, $C^*_{A^-}$, and C^*_{HA} can be distinguished:

if $C_{OH^-} \leq C_{H_3O^+}$:

$$C^*_{H_3O^+} = a + b \quad (10a)$$

$$C^*_{OH^-} = K'_W/(a + b) \quad (10b)$$

$$C^*_{A^-} = C_{A^-} + b \quad (10c)$$

$$C^*_{HA} = C_{HA} - b \quad (10d)$$

where

$$a = C_{H_3O^+} - C_{OH^-} \quad (10e)$$

$$b = \left[-(a + C_{A^-} + K'_a) + \sqrt{(a + C_{A^-} + K'_a)^2 - 4(aC_{A^-} - K'_a C_{HA})} \right]/2 \quad (10f)$$

if $C_{H_3O^+} < C_{OH^-} < (C_{H_3O^+} + C_{HA})$

$$C^*_{H_3O^+} = b \quad (11a)$$

$$C^*_{OH^-} = K'_W/b \quad (11b)$$

$$C^*_{A^-} = C_{A^-} + a + b \quad (11c)$$

$$C^*_{HA} = C_{HA} - a - b \quad (11d)$$

where

$$a = C_{OH^-} - C_{H_3O^+} \quad (11e)$$

$$b = \frac{-(a + C_{A^-} + K'_a) + \sqrt{(a + C_{A^-} + K'_a)^2 - 4K'_a(a - C_{HA})}}{2} \quad (11f)$$

if $C_{OH^-} = C_{H_3O^+} + C_{HA}$:

$$C^*_{H_3O^+} = b \quad (12a)$$

$$C^*_{OH^-} = K'_W/b \quad (12b)$$

$$C^*_{A^-} = C_{A^-} + C_{HA} \quad (12c)$$

$$C^*_{HA} = b(C_{A^-} + C_{HA})/K'_a \quad (12d)$$

$$b = \sqrt{\frac{K'_a K'_W}{C_{A^-} + C_{HA} + K'_a}} \quad (12e)$$

if $C_{OH^-} > C_{H_3O^+} + C_{HA}$:

$$C^*_{H_3O^+} = K'_W/(C_{OH^-} - C_{HA} - C_{H_3O^+}) \quad (13a)$$

$$C^*_{OH^-} = C_{OH^-} - C_{HA} - C_{H_3O^+} \quad (13b)$$

$$C^*_{A^-} = C_{A^-} + C_{HA} \quad (13c)$$

$$C^*_{HA} = C_{H_3O^+}(C_{A^-} + C_{HA})/K'_a \quad (13d)$$

The initial conditions of Eqns. 7 and 8 are:
for $\theta = 0$:

$$C_G(X, Y, Z, 0) = 0.0$$

and

$$C_T(X, Y, Z, 0) = 1.0 \quad (14)$$

For strong protolytes the titrated species are either H_3O^+ or OH^- with initial concentration equal to that of the corresponding fully dissociated acid or base (C_T). In the case of a weak acid the relationships for calculating the initial concentrations of chemical species of interest are the following [9]:

$$C^*_{H_3O^+} = \frac{-K'_a + \sqrt{K'^2_a + 4K'_a C_{HA}}}{2} \quad (15a)$$

if $C_{HA} \gg K'_a$, $C^*_{H_3O^+} = \sqrt{K'_a C_{HA}}$

$$C^*_{OH^-} = K'_W/C^*_{H_3O^+} \quad (15b)$$

$$C^*_{A^-} = C^*_{H_3O^+} - C^*_{OH^-} \quad (15c)$$

$$C^*_{HA} = C_{HA} + C^*_{A^-} \quad (15d)$$

Similarly the relationships for calculating the initial concentrations of H_3O^+, OH^-, B and HB^+ for weak bases can be derived.

The boundary conditions of Eqns. 7 and 8 are the following:

$$\left(\frac{\partial C(X, Y, Z, \theta)}{\partial \Psi}\right)_{\Psi = 0, \Psi^j} = 0 \quad (16a)$$

$$\left(\frac{\partial C(X, Y, Z, \theta)}{\partial Z}\right)_{Z = Z^0} = 0 \quad (16b)$$

where Ψ and j are X and 8, and Y and 9, respectively (Fig. 2).
At the bottom of the measuring cell, i.e., $Z = 0$, the boundary condions are:
for the generated species (Eqn. 7):

$$\left(\frac{\partial C_G(X, Y, Z, \theta)}{\partial Z}\right)_{Z=0} = \begin{cases} 0 & \text{for } X^0 > X > X^7 \text{ or } Y^0 > Y > Y^8 \\ & \text{or } X^5 > X > X^2 \\ & \text{and } Y^6 > Y > Y^2 \\ J & \text{for } X^7 > X > X^0 \text{ and } Y^2 > Y > Y^0 \\ & \text{or } Y^8 > Y > Y^6 \end{cases} \quad (16c)$$

for the chemical species whose diffusion is described by Eqn. 8:

$$\left(\frac{\partial C(X, Y, Z, \theta)}{\partial Z}\right)_{Z=0} = 0 \quad (16d)$$

The signal monitored during the measurements, according to the assumptions on which the model is built, is proportional to the averaged pH over the area of the sensor.

$$\mathrm{pH}(\theta) = -\int_{Y^3}^{Y^5}\int_{X^3}^{X^4} \log C_{H_3O^+}(X, Y, 0, \theta)\,\mathrm{d}X\,\mathrm{d}Y \quad (17a)$$

For comparison the logarithm of the average concentration of the H_3O^+ ions was also calculated.

$$\log \overline{C_{H_3O^+}}(\theta) = \log \int_{Y^3}^{Y^5}\int_{X^3}^{X^4} C_{H_3O^+}(X, Y, 0, \theta)\,\mathrm{d}X\,\mathrm{d}Y \quad (17b)$$

The time needed for reaching the equivalence point of the titration curve [$\mathrm{pH}(\theta)$] was determined as the maximum of $\partial \mathrm{pH}(\theta)/\partial\theta$ which is actually its inflection point.

Though in the general case the model considers a three dimensional space it is possible to reduce the corresponding equations to two (X, Z) and even to one (X) dimensions. In the two-dimensional case all the partial derivatives with respect to Y in the equations comprising the model are set to zero and $Y^j = 0$ for $j = 0$–9. In

the one dimensional case besides setting the derivatives with respect to Y and Z to zero and $Y^j = 0$ for $j = 0$–9 and $Z^0 = 0$ and assuming that $X^0 = X^1 = X^2 = 0$ and $X^5 = X^6 = X^7 = X^8 = 1$ (Fig. 2), some additional changes in the boundary conditions of Eqn. 7 should be made, i.e.,:

$$\left(\frac{\partial C_G(X, \theta)}{\partial X}\right)_{X=0} = J$$

and

$$\left(\frac{\partial C_G(X, \theta)}{\partial X}\right)_{X=1} = -J \qquad (18)$$

NUMERICAL SOLUTION OF THE MODEL

The modification of Brian [10] of the implicit alternating-direction finite difference method (IADFDM) for two spatial variables [11] was selected for the numerical solution of Eqns. 7 and 8. The main advantages offered by this method are its unconditional stability and the possibility to apply the Gaussian elimination method for the solution of the sets of implicit equations in X, Y and Z directions because of their tridiagonal matrices. The IADFDM has been successfully applied to problems involving multidimensional diffusive and convective mass transport [12–14].

A mixed uniform/non-uniform space grid was used for reducing the computation time. The construction of this grid was oriented to the sensor–actuator geometry presented in Fig. 2. The highest density of nodes was located at the boundaries of the actuator and in its slit where the sensor (ISFET gate) was situated. In the areas far from these boundaries both within or outside the actuator surface the spatial increments ($\Delta\Psi$) increased exponentially because there the variations in the concentration gradients are smaller and less grid points are necessary for an accurate representation.

$$\Delta\Psi_i = s_\Psi^j \exp\left[h_\Psi^j i\right] \qquad (19)$$

where s_Ψ^j is the basic increment and h_Ψ^j is the exponential coefficient in the jth region in direction Ψ where $\Psi = X, Y, Z$. The regions with uniform and non-uniform exponentially increasing or decreasing spatial increments in X and Y directions are schematically presented in Fig. 2. In Z direction the increments are monotonously increasing in an exponential way.

The algorithm for constructing the three dimensional space grid can be summarised in the following steps:

(1) Selection of the approximate values of the basic increments S_Ψ (Eqn. 19) in all regions of a given direction ($\Psi = X, Y, Z$) and the approximate values of the corresponding exponential coefficients H_Ψ.

(2) Calculation of the exact values of the basic increments and the exponential coefficients so that the boundaries of the walls of the measuring cell, the actuator and the sensor are coinciding with grid lines in the corresponding X, Y or Z direction. If this condition does not hold, the initial dimensions of the sensor actuator system will change when partial differential Eqns. 7 and 8 are decomposed into implicit finite-difference equations. In the regions with uniform space grid (Fig. 2) the exact values of the increments (s_Ψ^j) and their number ($n_{\Psi_i}^j$) can be determined by the following equations:

$$n_\Psi^j = (\Psi^j - \Psi^{j-1})/S_\Psi \qquad (20)$$

$$s_\Psi^j = (\Psi^j - \Psi^{j-1})/n_\Psi^j \qquad (21)$$

where for $\Psi = X$, $j = 3$, 4, 5, and for $\Psi = Y$, $j = 3$, 6 (Fig. 2); $n_{\Psi_i}^j$ is the closest integer to the expression on the right hand-side of Eqn. 20;

In the regions with non-uniform space grid (for $\Psi = X$, $j = 0$, 1, 2, 6, 7, 8; for $\Psi = Y$, $j = 0$, 1, 2, 4, 5, 7, 8, 9; and for $\Psi = Z$, $j = 0$ (Fig. 2)) it can be written:

$$s_\Psi^j = S_\Psi \qquad (22)$$

$$n_\Psi^j = \frac{1}{H_\Psi} \ln\left(1 + H_\Psi \frac{\Psi^j - \Psi^{j-1}}{s_\Psi^j}\right) \qquad (23)$$

The derivation of Eqn. 23 is given in Appendix B. The exact value of the exponential coefficient (h_Ψ^j) was determined as the root of the following equation:

$$\frac{\Psi^j - \Psi^{j-1}}{s_\Psi^j} - \sum_{i=0}^{i=n_\Psi^j - 1} \exp\left[h_\Psi^j I\right] = 0 \qquad (24)$$

where $I = i$ for exponentially increasing increments and $I = n_\Psi^j - i - 1$ for exponentially de-

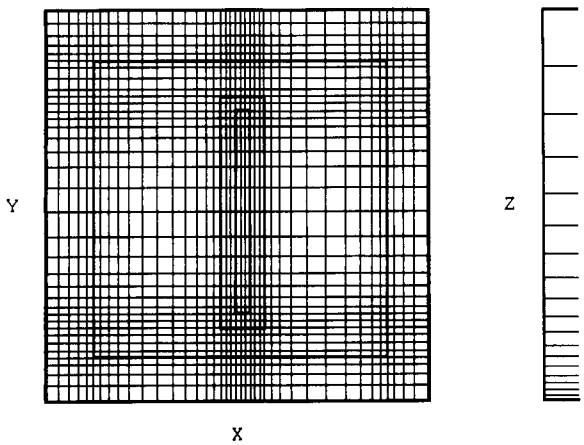

Fig. 3. Spatial grid in the measuring cell. Left, XY plane at $Z = 0$; right, XZ or YZ plane at arbitrary Y or X, respectively.

creasing increments. Equation 24 was numerically solved by the regula falsi method.

(3) Calculation of the coordinates of the nodes of the space grid:
for exponentially increasing increments,

$$\Psi_{i+1} = \Psi^{j-1} + \sum_{I=0}^{I=i} s_{\Psi}^{j} \exp\left[h_{\Psi}^{j} I\right] \qquad (25a)$$

for exponentially decreasing increments,

$$\Psi_{i+1} = \Psi^{j-1} + \sum_{I=0}^{I=i} s_{\Psi}^{j} \exp\left[h_{\Psi}^{j}\left(n_{\Psi}^{j} - I - 1\right)\right] \qquad (25b)$$

where $i = I + \sum_{k=0}^{k=j-1} n_{\Psi}^{j}$ and I varies from 0 to $n_{\Psi}^{j} - 1$. The space grid constructed according to the algorithm outlined above and used in the model simulations is illustrated in Fig. 3.

The formulas for finite-difference representation of the first and second derivatives necessary for decomposing the partial differential Eqns. 7 and 8 into the corresponding implicit finite-difference equations are given in Table 2 [14]. They were derived on the basis of Taylor's expansion [11].

An important step in developing the numerical procedure for the solution of the model is the integration of the pH and $C_{H_3O^+}$ over the whole surface of the sensor. The main difficulty arises from the fact that during the period when the equivalence part of the titration curve is formed very large differences in the concentration of H_3O^+ ions and the corresponding pH values evolve at the sensor surface which may lead to significant errors in the numerical integration. This effect is most profound in the direction of X while it is not significant in the direction of Y. The magnitude of these errors can be reduced either by increasing the number of grid nodes in the direction of X within the area of the sensor or by using formulas for numerical integration based on interpolating polynomials of higher degree (up to the 6th degree). The latter option seems to be more attractive because it does not lead to longer computation times. As far as the grid nodes in the direction of X within the sensor area are equally spaced the Newton-Cotes formulas [11] are appropriate. The numerical integration in the direction of Y was performed using the simple Trapezoidal rule.

The equivalence point of the titration curve was determined by its numerical differentiation. For improving the precision, the titration curve was approximated by an interpolating polynomial

TABLE 2

Finite-difference formulas for the partial derivatives in X, Y and Z in Eqns. 7 and 8 and their boundary conditions 16a–16e [a]

Ψ	X, Y	Z
0	$\partial C/\partial\Psi = 0$	$\partial C/\partial\Psi = J$
	$\partial^2 C/\partial\Psi^2 = 2(C_1 - C_0)/(\Delta\Psi_1)^2$	$\partial^2 C/\partial\Psi^2 = 2(C_1 - C_0)/(\Delta\Psi_1)^2 - 2J/\Delta\Psi_1$
$0 < \Psi < \Psi^j$	$\partial C/\partial\Psi = (C_i - C_{i-1})/\Delta\Psi_i$	$\partial C/\partial\Psi = (C_i - C_{i-1})/\Delta\Psi_i$
	$\partial^2 C/\partial\Psi^2 = (\alpha_i C_{i-1} - 2C_i + \beta_i C_{i+1})/\Delta\Psi_i^*$	$\partial^2 C/\partial\Psi^2 = (\alpha_i C_{i-1} - 2C_i + \beta_i C_{i+1})/\Delta\Psi_i^*$
Ψ^j	$\partial C/\partial\Psi = 0$	$\partial C/\partial\Psi = 0$
	$\partial^2 C/\partial\Psi^2 = 2(C_{N-1} - C_N)/(\Delta\Psi_N)^2$	$\partial^2 C/\partial\Psi^2 = 2(C_{N-1} - C_N)/(\Delta\Psi_N)^2$

[a] $N = \sum_{k=0}^{k=j} n_{\Psi}^{k}$; $\alpha = 2\Delta\Psi_{i+1}/(\Delta\Psi_i + \Delta\Psi_{i+1})$; $\beta = 2\Delta\Psi_i/(\Delta\Psi_i + \Delta\Psi_{i+1})$; $\Delta\Psi_i^* = \Delta\Psi_i\Delta\Psi_{i+1}$; and $j = 8$ for $\Psi = X$, $j = 0$ for $\Psi = Y$, $j = 0$ for $\Psi = Z$.

of nth degree ($n = 1$–4) [11]. When the time increment was not small enough for reasons of speeding up the computations, slight fluctuations in the equivalence part of the titration curve were generated. In such cases the first derivative of the titration curve in its equivalence part appeared to be noisy and caused difficulties in determining the exact position of the inflection point. For eliminating this undesirable effect a smoothing procedure based on the Savitzky-Golay algorithm [15] prior to the numerical differentiation of the titration curve was applied.

In the case of a two dimensional space the implicit alternating-direction finite-difference method [11] was used while in the one dimensional case the classical implicit finite-difference method [11] was applied.

For speeding up the computations the sensor–actuator geometry was examined for the existence of symmetry in both X and Y directions. In the case of symmetry in one direction only half of the system was considered thus reducing the computation time by one half. In the case of symmetry in both X and Y directions only one fourth of the grid nodes were necessary for the calculations thus speeding up the computations by four times in comparison with the standard case of asymmetry in both X and Y directions.

The computer program calculating the titration curve, i.e., pH(θ), and log $C_{H_3O^+}$ (Eqn. 17) was written in ANSIC and GNUCC and run on VAX/VMS or PC, respectively. The graphical representation of curves: pH(θ), $\overline{C_{H_3O^+}}(\theta)$, and $\partial pH(\theta)/\partial\theta$ and of the concentration distribution of the titrant and the titrated species as contour or three-dimensional plots was performed by another program written in Microsoft® Quick C® Version 2.5 and run on a PC.

EXPERIMENTAL

Preparation of the gold actuator–ISFET sensor device

For the experiments described in this paper, a pH-sensitive ISFET was used as the sensing device. The ISFET was fabricated following the standard NMOS processing steps, with an added tantalum oxide gate dielectric on top of the silicon oxide [3]. The generation of ions was performed at a gold actuator electrode, deposited around the gate. This thin gold film (0.6 μm) was evaporated on a Ti/Ag adhesion promoting layer. The actuator electrode was patterned using standard photolithographic techniques. A layer of polyimide was spun on the wafer in which holes were etched both to contact the ISFET and the actuator electrode, and to free the area of the actuator electrode to be exposed to the solution. A cross-section of the device is shown in Fig. 4. After dicing the wafer, the chips were glued on a piece of printed circuit board of 1×5 cm and connected to the available copper strips with bonding wires. The copper strips, the bonding wires and the edges of the chip were covered with epoxy for insulation and protection.

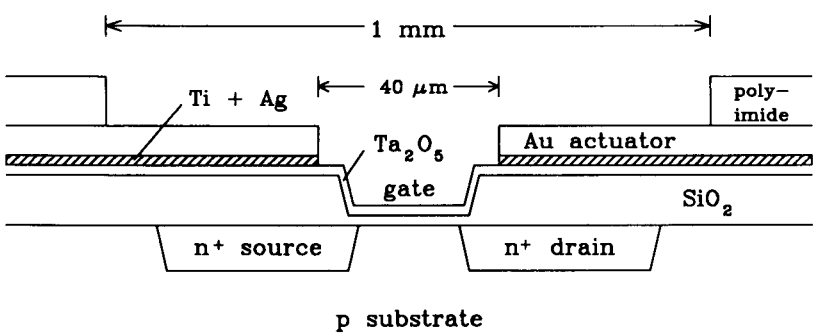

Fig. 4. Cross-section of the Ta_2O_5–ISFET sensor with the gold actuator electrode.

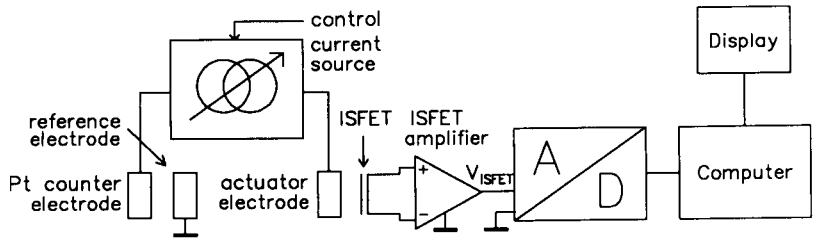

Fig. 5. Schematic representation of the measuring set-up.

Measurement set-up

All measurements have been carried out with the set-up as shown in Fig. 5. The ISFET amplifier keeps both the drain current and the drain-source voltage constant at 100 μA and 0.5 V, respectively. All coulometric titrations were carried out in a 0.1 M KNO_3 supporting electrolyte at room temperature. The constant actuator electrode current was generated by a computer controlled current source. The time t_{eq} was determined by the position of the extreme of the first derivative of the resulting titration curve.

VERIFICATION OF THE MODEL

The validity of the model was checked by experimental results for the titration of strong (nitric acid and potassium hydroxide) and weak (acetic acid and *n*-butyric acid) protolytes outlined earlier in the paper. The diffusion coefficients of the chemical species participating in the protolytic interactions and the corresponding dissociation constants are presented in Table 3. The dimensions of the experimental sensor–actuator system used in the calculations are given in Table 4. The current density in all experiments was 20 A m^{-2}. During the experiments the sensor–actuator system operated in a measuring cell considerably exceeding the dimensions of the actuator electrode. To reduce the computation time the dimensions of the measuring cell were scaled down assuming that the sensor–actuator ensemble was x^0 μm and y^0 μm from the side walls and the solution layer above it was z^0 μm thick (Figs. 2 and 3). In all the simulations it was assumed for simplicity that $x^0 = y^0 = z^0$ ranging from 300 to 2000 μm. For such dimensions of the measuring cell the processes taking place in the surrounding of the actuator did not affect the concentration of the titrated species at the boundaries of the measuring cell (Figs. 2 and 3), i.e., it was constant thus corresponding to the real situation during the experiments. The agreement between the experimental and the theoretically calculated values of the square root of the equivalence time is illustrated in Fig. 6. Real time (t) is used instead of the dimensionless time (θ) in Fig. 6 and subsequent figures to improve clarity of

TABLE 3

Diffusion coefficients, ion radii and dissociation constants [9,16]

Ions and molecules	$10^9 D_m$ (m^2 s^{-1})	ρ (Å)	$10^2 K_a^t$ (mol m^{-3})
H_3O^+	9.33	9	
OH^-	5.27	3.5	
CH_3COO^-	1.09	4	
$C_3H_7COO^-$	0.868	4	
CH_3COOH	1.21		1.75
C_3H_7COOH	0.93		1.54

TABLE 4

Dimensions of the sensor–actuator system in μm (Fig. 1) (exp refers to the experimental set-up and sim refers to data used in the simulations)

j	$X^j_{exp} - X^{j-1}_{exp}$	$Y^j_{exp} - Y^{j-1}_{exp}$	$X^j_{sim} - X^{j-1}_{sim}$	$Y^j_{sim} - Y^{j-1}_{sim}$
1	240	112.5	200	200
2	240	112.5	200	200
3	12.5	25	10	10
4	15	250	10	210
5	12.5	250	10	210
6	240	25	200	10
7	240	112.5	200	200
8		112.5		200

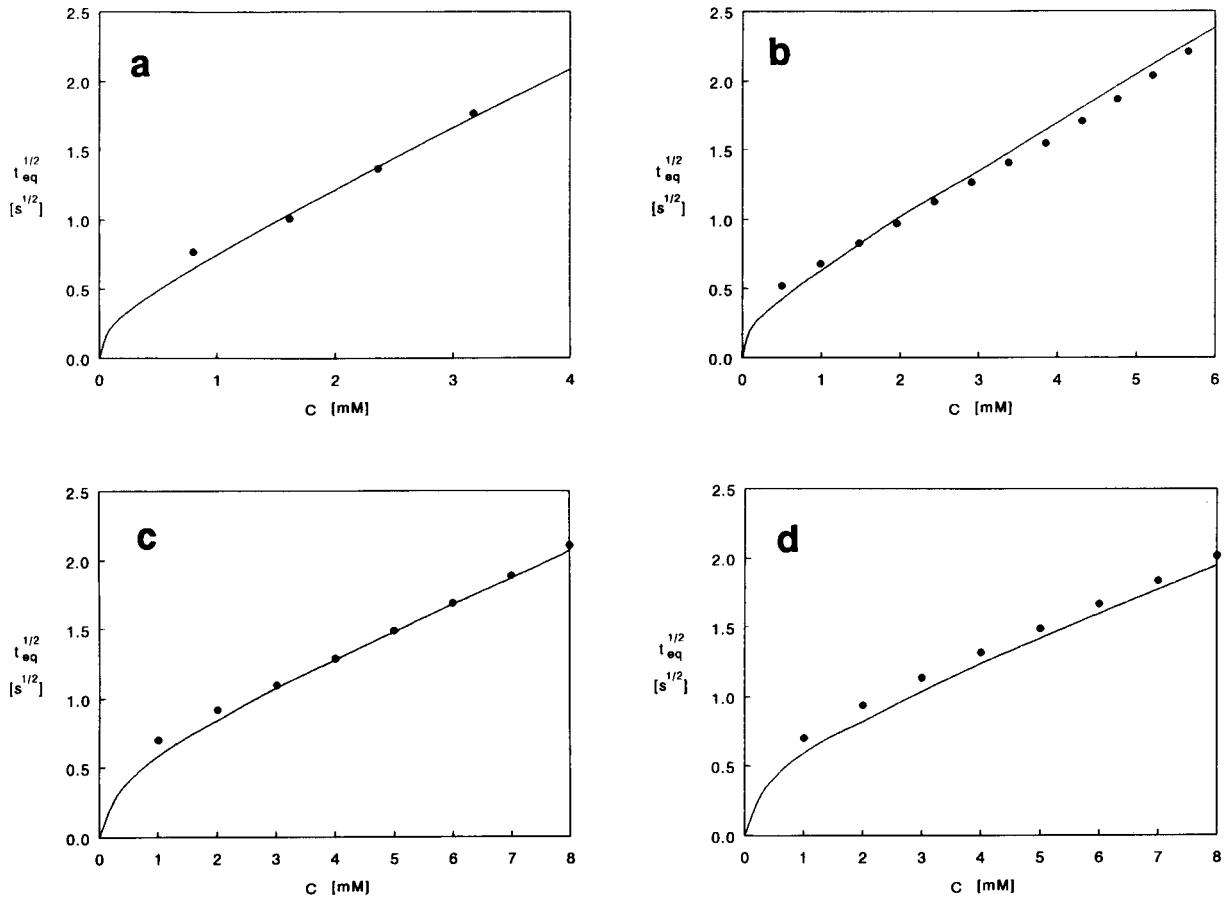

Fig. 6. Experimental (•) and theoretically calculated (bold line) values for the square root of the equivalence time versus concentration for: (a) nitric acid; (b) potassium hydroxide; (c) acetic acid; (d) *n*-butyric acid.

presentation. It should be emphasised that in the model simulations only fundamental physical constants with values taken from the literature and the real geometrical dimensions of the experimental sensor–actuator system were used. For this reason the good agreement between theory and experiments proved cogently the validity of the model.

MODEL SIMULATIONS

The mathematical model outlined above can be used not only for describing or predicting the titration curves monitored at a given coulometric sensor–actuator system but also for a better understanding of the behaviour of the system. The latter can be achieved by elucidating the influence of the main parameters of the system under investigation on the titration curve and in particular on the equivalence time. The most important geometrical dimensions of the sensor–actuator system are the width of the actuator, the distance of the sensor from the actuator and the ratio between the length and the width of the sensor. Another important question concerning the manufacturing of sensor–actuator systems is how miniaturisation affects their behaviour and to what extent the symmetry of the sensor with respect to the slit influences the titration curve and the equivalence time. In the subsequent paragraphs these questions will be discussed on

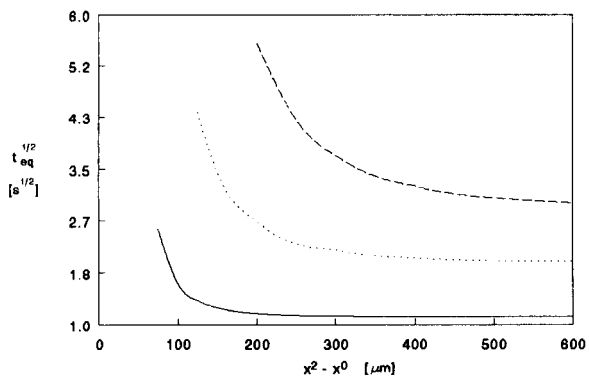

Fig. 7. Influence of the actuator width on the square root of the equivalence time in the case of titration of (———) 0.002 M, (· · ·) 0.004 M, and (— — —) 0.006 M strong acid.

the basis of results from model simulations. The dimensions of the sensor–actuator system, if not stated otherwise, were those presented in Table 4. The titration of a strong acid with values of the diffusion coefficients of the OH^- and H_3O^+ ions given in Table 3 and a concentration equal to 0.002 mol l^{-1} was considered. The current density at the actuator was assumed to be 20 A m^{-2} throughout the simulations.

Width of the actuator

The width of the actuator is one of the main parameters of the system determining the equivalence time. During the simulations the width (x^2–$x^0 = x^7$–$x^5 = y^2$–$y^0 = y^8$–y^6, Fig. 2) was varied from 75 to 600 μm. As can be expected the wider the actuator is the shorter the equivalence time becomes reaching an asymptotic value (Fig. 7) which corresponds to infinite width. For small widths the equivalence time dramatically increases. This effect can be explained by the fact that for such sizes of the actuator conditions of spherical diffusion prevail before the equivalence time is reached. This phenomenon is illustrated in Fig. 8a by the spatial distribution of the titrant at the bottom of the measuring cell after the equivalence time has been reached. Only one fourth of the measuring cell is considered because of the symmetry in x and y directions. Under the conditions of spherical diffusion the expansion of the region around the actuator where the titrated species are practically depleted is much slower than before the establishment of the spherical diffusion regime. For wider actuator electrodes the equivalence time is much shorter because it is reached before the spherical diffu-

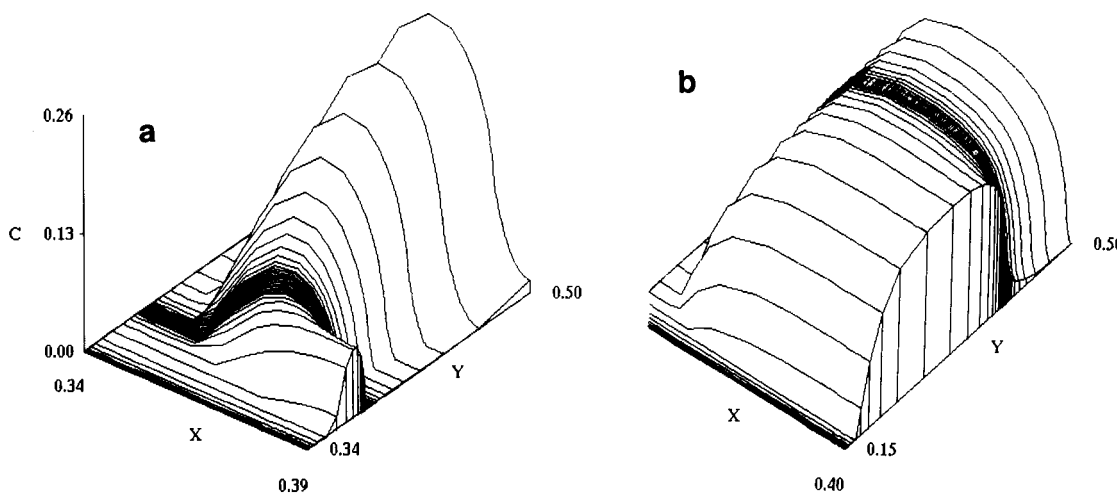

Fig. 8. Spatial distribution of the hydroxyl ions, right after the equivalence time for width of the actuator, (a) 75 μm and (b) 500 μm (titration of 0.002 M strong acid).

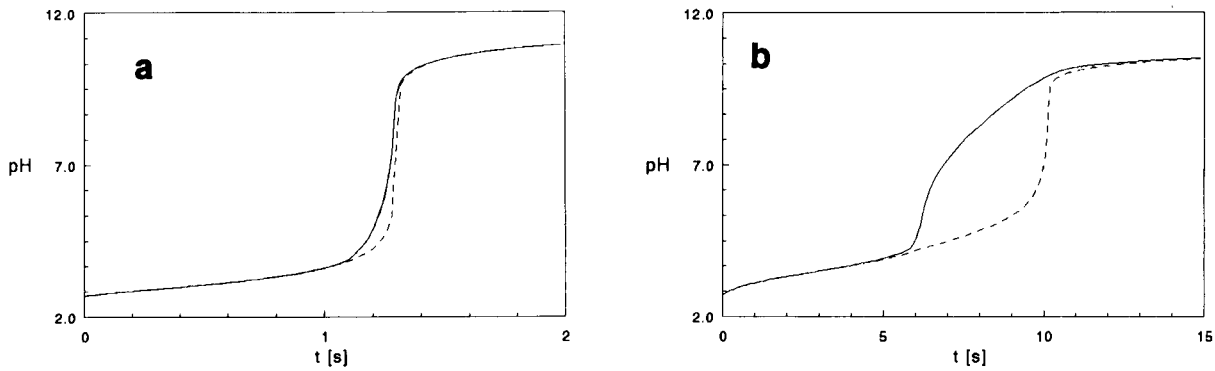

Fig. 9. Titration (———) and log $\overline{C_{H_3O^+}}(t)$ (· · ·) curves for width of the actuator, (a) 500 μm and (b) 75 μm (titration of 0.002 M strong acid).

sion has been fully developed. In Fig. 8b it can be seen that there are still traces of linear diffusion in the central part of the actuator after the equivalence time has been reached. The shapes of the titration curves obtained before and after the spherical diffusion has been established differ considerably. In the former case they are fairly symmetrical with respect to the inflection point and slightly differ from the negative logarithm of the averaged over the sensor surface concentration of the H_3O^+ ions, i.e., log $\overline{C_{H_3O^+}}(t)$ (Fig. 9a). In the case of spherical diffusion, i.e., narrow actuator, the titration curves are not symmetrical and the difference between pH(t) and log $\overline{C_{H_3O^+}}(t)$ is considerable (Fig. 9b). The equivalence part of pH(t) extends over a long period of time which may cause significant difficulties in the precise determination of the equivalence time. For higher concentrations of the titrated acid the critical width of the actuator below which the equivalence time grows very fast increases (Fig. 7). On the basis of the considerations made above it can be concluded that in constructing sensor–actuator devices the actuator width should be selected in the asymptotic part of the dependence of the equivalence time on the actuator width (Fig. 7). Attention should be paid to the concentration range within which the measurements will be performed.

Distance between the actuator and the sensor

The distance between the sensor and the actuator (x^3–$x^2 = x^5$–$x^4 = y^3$–$y^2 = y^6$–y^5, Fig. 2) was varied from 0 to 20 μm. Within this range the equivalence time was reached before the establishment of spherical diffusion. An almost linear relationship between the equivalence time (t_{eq}) and the sensor–actuator distance (x^3–x^2) was observed (Fig. 10).

Symmetry of the sensor with respect to the actuator slit

The positioning of the sensor in the centre of the actuator slit could pose some difficulties during the manufacturing of these devices. For this reason it is important to know what will be the impact of asymmetry on the equivalence time and the shape of the titration curves. Simulations

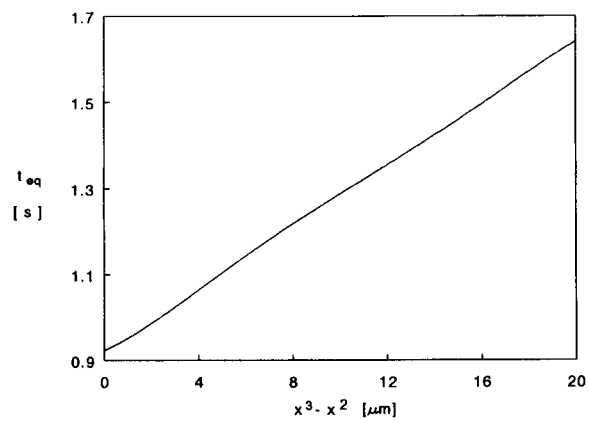

Fig. 10. Influence of the distance between the sensor and the actuator, i.e., x^3–$x^2 = x^5$–$x^4 = y^3$–$y^2 = y^6$–y^5, on the equivalence time (titration of 0.002 M strong acid).

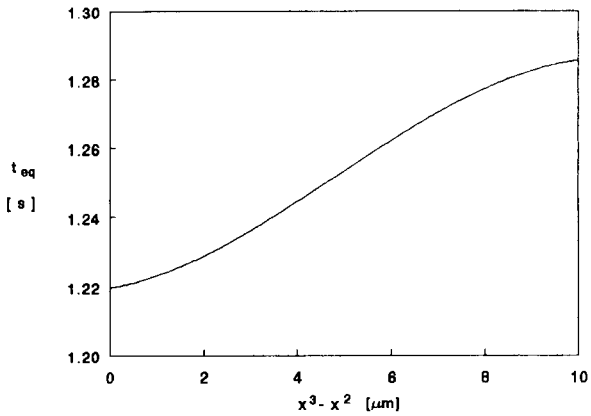

Fig. 11. Effect of asymmetry of the sensor with respect to the actuator (x^3-x^2 is varied while x^5-x^2 is fixed at 30 μm and y^3-y^2 and y^6-y^5 are kept equal to 10 μm) on the equivalence time (titration of 0.002 M strong acid).

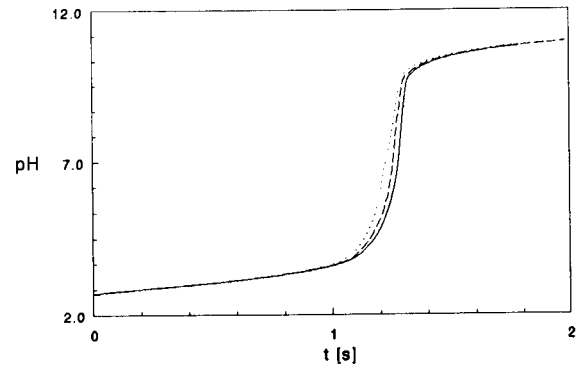

Fig. 12. Titration curves in the case of (···) $x^3-x^2=0$ μm and $x^5-x^4=20$ μm; (— — —) $x^3-x^2=4$ μm and $x^5-x^4=16$ μm; and (———) $x^3-x^2=10$ μm and $x^5-x^4=10$ μm (titration of 0.002 M strong acid).

were performed assuming symmetry in the direction of y ($y^3-y^2=y^6-y^5$, Fig. 2) and asymmetry in the direction of x. The distance x^3-x^2 was varied from 0 to 10 μm keeping the slit length constant, i.e., $x^5-x^2=30$ μm (Fig. 2, Table 4). The dependence of the equivalence time on the distance x^3-x^2 is illustrated in Fig. 11. As can be seen the asymmetry slightly affects the equivalence time and in the extreme case when $x^3-x^2=0$ μm and $x^5-x^4=20$ μm the equivalence time is decreased only by 5.4% with respect to the symmetrical case. In Fig. 12 titration curves calculated for different extent of asymmetry are presented. It can be seen that the greater the asymmetry is the lower the slope of the equivalence part the titration curve is (Fig. 12).

On the basis of the simulation results it can be concluded that if during manufacturing the sensor is placed slightly asymmetrically with respect to the actuator slit there will be no significant consequences on the behaviour of the system.

Miniaturisation

Miniaturisation of detectors is of vital importance for various fields of chemical analysis (e.g., chromatography, FIA, in vivo measurements, etc.). In this connection it is interesting to elucidate how miniaturisation of the sensor–actuator system considered in this study will affect its behaviour. In the subsequent considerations miniaturisation will be considered relative to the standard set of parameter values given in Table 4. The degree of miniaturisation, M, is the linear scaling-up or -down factor. For the standard set it is equal to 1.0. During the simulations M was varied from 0 to 2. Values of M greater than 1 (i.e., scaling-up) were taken for comparison. Its influence on the equivalence time is presented in Fig. 13. The relationship between M and t_{eq} is linear for values of M greater than 0.2 while for smaller values t_{eq} rapidly decreases to 0. In this region maximal gain in sampling frequency can be achieved. It should be taken into considera-

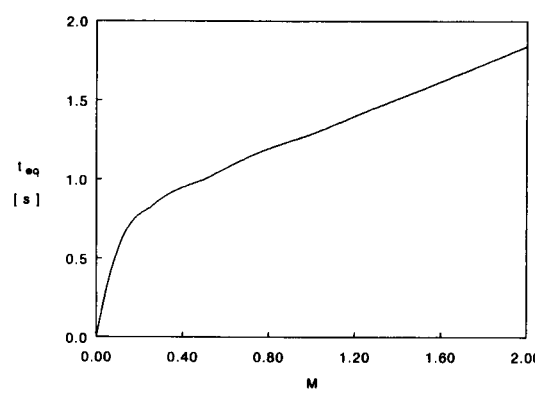

Fig. 13. Influence of miniaturisation on the equivalence time. (titration of 0.002 M strong acid; M is the degree of miniaturisation; $M=1$ is taken for standard set).

tion that the influence of M on t_{eq} is also concentration dependent.

Possibilities for reducing the number of spatial coordinates

The substantial disadvantage of using three-dimensional models is the considerable consumption of computation time. The reduction of only one spatial variable in the model decreases dramatically the computation time from several hours to several minutes. In the one-dimensional case the computation time is in the order of seconds. Knowing under which conditions one can simplify the model without loosing precision, can speed up the computations by several orders of magnitude. Obviously, the most important parameter determining the possibility to neglect the diffusion in the direction of y (Fig. 2) without creating substantial errors in the predictions is the width-to-length ratio of the slit of the actuator, $(y^6-y^2)/(x^5-x^2)$ (Fig. 2). For very large ratios the slit can be considered as infinitely long and diffusion in the direction of y practically will not affect the processes taking place. Under such conditions the two dimensional model should describe adequately the titration curve, i.e., there should be no difference between the results obtained by the two- and three-dimensional models. When the width to length ratio is decreased diffusion in the direction of y will start to affect the overall diffusion process thus decreasing the equivalence time in comparison with the infinite case. The discrepancy between the two- and three-dimensional models that will be observed can be represented as the ratio between the square root of the equivalence times calculated by the three and the two-dimensional models, λ. As could be expected, the simulations showed that λ was equal to 1 for high width to length ratios and decreased when the ratio was reduced (Fig. 14a and b). Varying the sensor area, the strength and the concentration of the titrated protolyte showed that the width to length ratio of the slit almost solely determines the applicability of the two dimensional model. For values of this ratio greater than 10 the error in calculating the square root of the equivalence time is less than 1.5%. By comparing the shape of the titration curves it can be

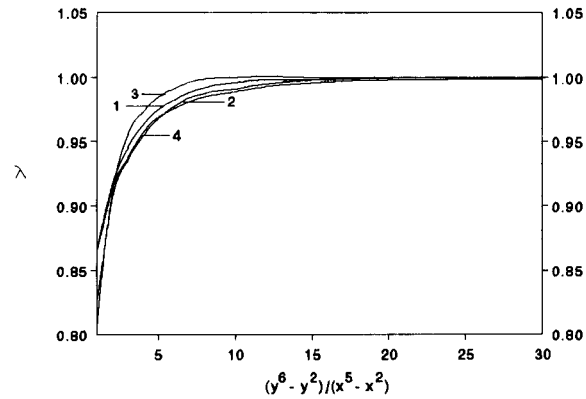

Fig. 14. Effect of the ratio between the width and length of the slit of the actuator on λ in the case of: (1) 0.002 M acetic acid, (2) 0.001 M nitric acid, (3) 0.002 M nitric acid, (4) 0.002 M nitric acid when the area of the set of the slit.

said that for ratios not much greater than 10 the equivalence part of the titration curves calculated by the three-dimensional model is not so steep as in the case of the two dimensional model and the inflection point is slightly shifted to the upper region of the equivalence part of the titration curve (Fig. 15). By increasing λ this difference decreases and the pH(t) and log $\overline{C_{H_3O^+}}(t)$ curves (Eqn. 17) almost totally overlap. Concerning the one dimensional case, it can be said that under no circumstances it can describe a real sensor–actuator system. It cannot take into account the dimensions of the actuator and the diffusion and reaction above the bottom of the measuring cell.

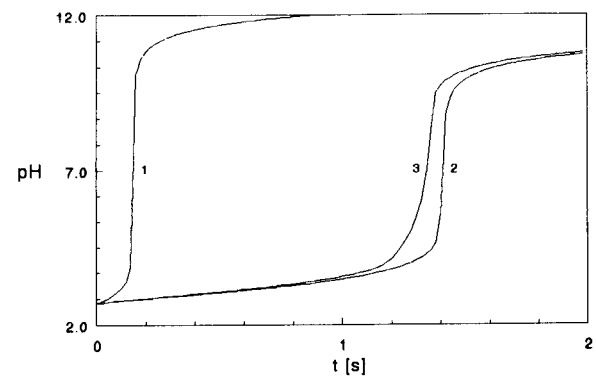

Fig. 15. Titration curves calculated by the (1) one; (2) two- and (3) three-dimensional model for $\lambda = 10$. (titration of 0.002 M strong acid).

For this reason the time interval necessary for the total depletion of the titrated protolyte in the slit was calculated to be much shorter than in reality. The equivalence time predicted by this model was by more than one order of magnitude lower than the one predicted by the three-dimensional model. For this reason it can be concluded that the one-dimensional model can be used only for drawing qualitative conclusions concerning the parameters of the sensor–actuator system it takes into account, e.g., diffusion coefficients of the protolytes, current density, length of the slit and the sensor. When reliability is important or quantitative results are aimed at, the two or the three dimensional models should be preferred.

Conclusions

A general mathematical model describing the behaviour of a coulometric sensor–actuator system was developed. It takes into account the three-dimensional diffusion which takes place in real systems. The boundary conditions depict the impermeability of the walls of the measuring cell at the bottom of which the detector is placed and the constant current applied at the actuator electrode. These boundary conditions allow to take into consideration the influence of the depletion of the titrated species in the finite volume of the measuring cell on the titration curve monitored by the sensor. The very good agreement of the predictions of the model, when only basic physical constants are used, with experimental results is a convincing proof of its validity. It shows that the model can be used successfully for the quantitative description of the behaviour of real sensor–actuator systems. On the basis of model simulations, some important conclusions concerning the geometrical dimensions of sensor–actuator systems with optimal design can be drawn. In order to achieve small equivalence times, i.e., high sampling rates, the actuator should be wide enough to assure that the equivalence time is reached before spherical diffusion regime has been established. Another option for increasing the sampling throughput is the miniaturisation of the system. The simulations showed that not too much efforts should be put in placing the sensor absolutely symmetrically in the slit of the actuator because slight displacements from the symmetrical position will hardly affect the behaviour.

The conditions under which the two-dimensional model can be used for speeding up the computations were determined. They cover most the sensor–actuator systems used currently in practice.

This study has been carried out as part of an European Economic Community action for cooperation in science and technology with Central and Eastern European countries for 1993 and financed by the Commission of the European Communities. The authors are grateful to Mr. E.H.J. Satink for carrying out most of the measurements.

APPENDIX A

For ionic strength of the solution not greater than 0.1 the activity coefficients of the various ions can be evaluated using the Debye-Hückel expression [9]:

$$-\log f_i = \frac{0.509\eta_i^2\sqrt{\mu}}{1 + 0.33\rho\sqrt{\mu}} \qquad \text{(A1)}$$

where $\mu = \frac{1}{2}\Sigma_i c_i \eta_i^2$ is the ionic strength of the solution and ρ is the so-called ionic radius in Å [9] (Table 3).

APPENDIX B

Derivation of Eqn. 23

Let us consider the region stretching from Ψ_{j-1} to Ψ_j and assume that it is divided into n_Ψ^j increments. Taking into consideration Eqn. 24 it can be written that:

$$\Psi^j - \Psi^{j-1} = \int_0^{n_\Psi^j} s_\Psi^j \exp[H_\Psi i]\, \mathrm{d}i \qquad \text{(B1)}$$

The integral on the right hand-side of Eqn. B1 can easily be solved analytically (Eqn. B2).

$$\Psi^j - \Psi^{j-1} = \frac{s_\Psi^j}{H_\Psi}\left(\exp\left[H_\Psi n_\Psi^j\right] - 1\right) \qquad \text{(B2)}$$

Equation B2 can be rearranged with respect to n_{Ψ}^{j} giving Eqn. 23.

REFERENCES

1 W. Olthuis, B.H. van der Schoot, F. Chavez and P. Bergveld, Sensors Actuators, 17 (1989) 279.
2 W. Olthuis, J. Luo, B.H. van der Schoot, J.G. Bomer and P. Bergveld, Sensors Actuators, B1 (1990) 416.
3 P. Bergveld and A. Sibbald, Analytical and Biomedical Applications of Ion-selective Field-effect Transistors, (Comprehensive Analytical Chemistry, Vol. XXIII), Elsevier, Amsterdam, 1988.
4 B.H. van der Schoot and P. Bergveld, Sensors Actuators, 13 (1988) 251.
5 B.H. van der Schoot and P. Bergveld, Anal. Chim. Acta, 233 (1990) 49.
6 J. Luo, W. Olthuis, P. Bergveld, M. Bos and W.E. van der Linden, Sensors Actuators, in press.
7 W. Olthuis, J. Luo, B.H. van der Schoot, P. Bergveld, M. Bos and W.E. van der Linden, Anal. Chim. Acta, 229 (1990) 71.
8 J. Luo, W. Olthuis, B.H. van der Schoot, P. Bergveld, M. Bos and W.E. van der Linden, Anal. Chim. Acta, 237 (1990) 71.
9 D.A. Skoog, D.M. West and F.J. Holler, Fundamentals of Analytical Chemistry, Saunders College Publishing, New York, 1988.
10 P.L.T. Brian, AIChE J., 7 (1961) 367.
11 B. Carnahan, H.A. Luther and J.O. Wilkes, Applied Numerical Methods, Wiley, New York, 1969.
12 S.D. Kolev and W.E. van der Linden, Anal. Chim. Acta, 257 (1992) 51.
13 S.D. Kolev and W.E. van der Linden, Anal. Chim. Acta, 257 (1992) 331.
14 S.D. Kolev, J.H.M. Simons and W.E. van der Linden, Anal. Chim. Acta, 273 (1993) 71.
15 A. Savitzky and M.J.E. Golay, Anal. Chem., 36 (1964) 1627.
16 D.R. Lide (Ed.), CRC Handbook of Chemistry and Physics, CRC Press, Boca Raton, FL, 1992.

Analytica Chimica Acta, 285 (1994) 265–269
Elsevier Science B.V., Amsterdam

Evanescent sensing in doped sol-gel glass films

John E. Lee and S. Scott Saavedra [a]

Department of Chemistry, 227 Old Chemistry, University of Arizona, Tucson, AZ 85721 (USA)

(Received 11th June 1993; revised manuscript received 14th September 1993)

Abstract

Bromophenol blue, a pH indicator, was entrapped in porous glass films prepared by the sol-gel method. The colorimetric response of the films to pH was assessed visibly and by attenuated total reflectance spectrometry. The entrapped indicator was nonleachable and responded to solution pH changes in a reversible manner. The immobilization of indicator molecules in porous sol-gel films appears to be a particularly promising approach to optical waveguide sensor development.

Keywords: Attenuated total reflectance; Colorimetry; Bromophenol blue; Indicators; Porous glass films; Sol-gel method

Optical sensing using immobilized indicators is a rapidly developing area in chemical and biochemical analysis [1,2]. Although the properties desired of an immobilized indicator phase will vary depending on the intended application, in general the ideal immobilization technique should produce a highly stable assembly of molecules that remain sterically accessible to dissolved ligands. Covalent attachment to a functionalized support [3] and physical entrapment, either in a porous polymer matrix [4] or behind a selectively porous membrane [5], are two commonly employed approaches. Entrapment is the technically simpler technique, but the response time of an entrapped indicator to a dissolved analyte is often relatively slow. Furthermore, the organic polymers typically used as entrapment matrices are labile and optically inferior compared to inorganic materials.

Recently, the entrapment of optical indicators in porous, optically clear glasses prepared by sol-gel techniques has been reported. Avnir and coworkers [6–10] have entrapped low molecular weight indicators and enzymes in sol-gel glass monoliths. Soluble analytes diffused into the gels and reacted with immobilized indicators. Colorimetric detection of pH, metal ions, inorganic anions, and glucose was demonstrated. Ellerbee et al. [11] entrapped metalloproteins in sol-gel glass monoliths. Visible absorbance spectrophotometry was used to show that in both wet and dried gels, entrapped proteins could reversibly bind soluble ligands.

Thin, transparent films can also be produced via sol-gel technology [12]. Here, a pH indicator was entrapped in a sol-gel film coated on the surface of a glass slide. The slide was utilized as an attenuated total reflection (ATR) element while the sol-gel film functioned as a pH-sensitive cladding. A fast and reversible response to solution pH was observed.

Correspondence to: S.S. Saavedra, Department of Chemistry, 227 Old Chemistry, University of Arizona, Tucson, AZ 85721 (USA).

EXPERIMENTAL

Sol-gel film preparation

All chemicals were used as received. Tetraethylorthosilicate (TEOS, 99 + %) and bromophenol

SSDI 0003-2670(93)E0539-J

blue were obtained from Aldrich. HCl and buffer components were obtained from Aldrich and Baker. Sols were prepared from a starting mixture of 1 ml of TEOS, 164 μl of deionized water, 112 μl of 0.04 M HCl, and 50 μl of 69 mg/ml bromophenol blue in water. The mixture was sonicated at room temperature for 2 h in a vented container, capped, and incubated at room temperature. After the sol formed a single phase (in about 3 h), it was stored overnight at 4°C in a sealed container. The coating solution was prepared by diluting the sol with 1.75 ml of 10 mM pH 6 phosphate buffer. Sol-gel films were formed on glass microscope slides (Clay Adams) by spin coating [13]. Prior to coating, the slides were precleaned by sonication for 30 min in a 2% (v/v) aqueous solution of PCC-54 surfactant (Pierce), rinsed in deionized water, and dried overnight at 150°C. About 2 ml of coating solution was applied to each slide through a 0.45 μm syringe filter, followed by spinning at 1500 rpm for 2 min. After coating, films were stored in contact with air in a covered dish at room temperature in the dark.

A Gaertner Scientific Model L116C ellipsometer was used to measure the amplitude ratio (Ψ) and phase difference (Δ) of 633 nm light reflected from a sol-gel film coated on a glass slide. The incidence angle was 70°. Film thickness and refractive index were determined through iterative computation [14] by constraining the film thickness to be $\leqslant 2000$ Å. This assumption is reasonable based on the spinning rate and water-like viscosity of the coating solution. Bromophenol concentrations were determined by absorbance spectrometry using an $\epsilon_{592\ nm}$ of 70 300 $M^{-1}\ cm^{-1}$ (our measurement).

ATR spectrophotometry.

In Fig. 1 is shown the instrumental arrangement used to record the pH response of sol-gel films. The slide was mounted in a flow cell constructed from a Lucite housing and a silicone gasket. The liquid in the flow cell volume contacted only the coated side of the slide. The polarized 457.9 nm line of an air-cooled argon laser (Ion Laser Technology, Model 5500A) was launched into the slide using a fused silica prism that was coupled to the uncoated side of the slide with an index matching fluid. Light propagated in the slide by total internal reflection at an angle of approximately 64°. A silicon photodiode (Metrologic Instruments, Model 45–540) was used to measure the light intensity after the beam was coupled out of the slide by a second prism. The beam underwent about 26 reflections over the 4.8 cm distance between the prisms.

Buffers were introduced into the flow cell from a syringe through an inlet port and exited through an outlet port. A mixed buffer consisting of 0.05 M phosphate, citrate, and formate provided buffer capacity over the range of pH 2.0 to pH 8.0. Spectrophotometric response curves were acquired by injecting buffers in order of increasing

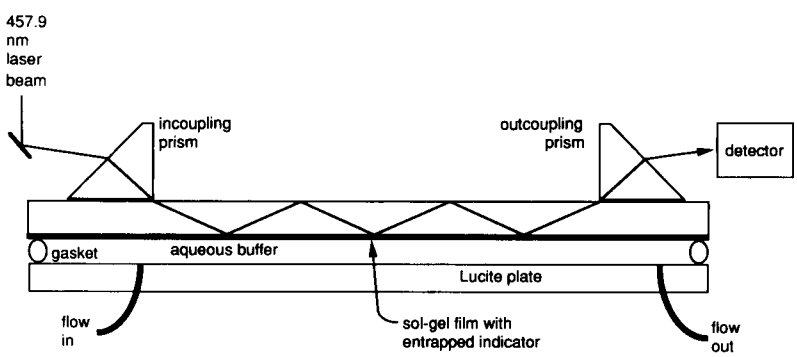

Fig. 1. Instrumental arrangement for ATR spectrometry of a sol-gel film coated on a glass slide. The 457.9 nm line of an argon ion laser was coupled into and out of the coated slide with a pair of fused silica prisms. The slide was mounted in a flow cell that allowed solutions to be introduced to and flushed from the coated side of the slide. Outcoupled light was detected with a silicon photodiode.

pH. When measurements were repeated, the pH was first returned to 2.0, then increased to the pH of interest.

RESULTS AND DISCUSSION

Coating solutions were prepared with a high indicator concentration, 1.62 mM, to enable color changes to be detected by eye. After drying for one day at room temperature, films were a slight yellow color characteristic of the protonated form of bromophenol blue. The film surfaces appeared smooth and no cracks could be detected by phase-contrast microscopy. Upon immersion in pH 8 phosphate buffer, films turned visibly blue within 2 s. Upon addition of an excess of acid, the films reverted to their initial yellow color within 2 s. Films were soaked in pH 8 phosphate buffer for eight days to remove any free indicator. Some fraction of the indicator was leached out during soaking, but this amount was not quantified. After soaking, the visibly detected response of the films to pH was intact. Thereafter, films were stored in ambient air in a covered dish in the dark, and were hydrated only when pH response was assessed visibly or measured spectrometrically. The visible pH response was maintained for a period of at least 12 months. Although numerous films were prepared and tested for visible response, further characterization was performed on only two films (denoted A and B) from the same batch prepared under identical conditions.

The pH response of film A was assessed spectrometrically by measuring the attenuated total reflectance of 457.9 nm light. The relative outcoupled intensity of waveguided light is plotted as a function of pH in Fig. 2A. This curve was recorded after drying the film for three months as described above. The film responded to pH changes over the range of pH 3–6 with a midpoint at about pH 4.5, which is greater than the published pK_a of 4.1 for bromophenol blue [15]. The difference in pK and the shape of the curve show that the chemical environment of the dye was altered by entrapment in the sol-gel. The negative surface charge of the glass probably affected the response of the indicator. More importantly, the broad shape of the curve clearly indicates that entrapment produced a distribution of chemically inequivalent microenvironments that differ in response to solution pH.

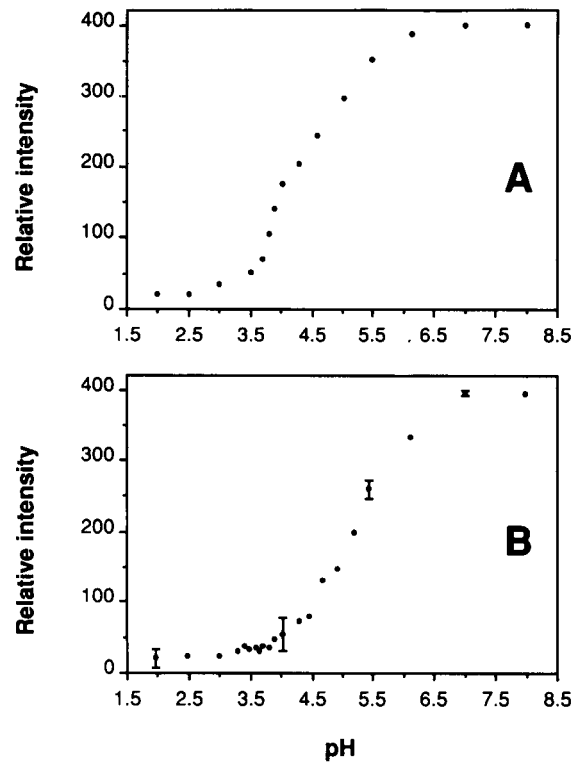

Fig. 2. (A) pH response curve of sol-gel film A measured three months after the film was fabricated. A mixed buffer consisting of phosphate, citrate, and formate (50 mM each) was used to span the pH range of 2–8. The flow cell was flushed with several volumes of buffer at each pH, 5 min were allowed to elapse, and the outcoupled 457.9 nm light intensity was measured. Measurements were made sequentially from lowest to highest pH. (B) pH response curve of sol-gel film A measured 12 months after the film was fabricated (9 months after curve A was recorded). The curve was recorded as described for A except that 10 min was allowed to elapse between flushing and intensity measurements. Error bars representing standard deviations are plotted for measurements that were repeated ($n = 3$) in sequence after stepping the pH back to the starting value of 2.0.

Nine months later (one year after fabrication), the pH response of film A was assessed again both visibly and using ATR spectrometry. The spectrometric response curve is shown in Fig. 2B

and demonstrates that the film remained sensitive to pH after prolonged storage. However, two differences from previous experiments were apparent. One, although the response of the film to pH changes could still be detected visibly, the response time was several minutes, much slower than earlier measurements. Second, the midpoint of the titration curve shifted to approximately pH 5.2, or about half a pH unit higher than the curve in Fig. 2A. The origin of these changes is unknown but is probably related to structural evolution of the film during storage. It is well known that sol-gel based materials that have not been thermally densified continue to undergo slow polymerization and shrinkage long after gelation has occurred [16]. The difference in film response with storage time indicates that these processes were incomplete even after drying for three months at room temperature.

After the titration curve in Fig. 2B was recorded, additional measurements at four pH values were made by lowering the pH to 2.0 followed by sequential increases to pH 4.0, 5.4, and 7.0. Error bars representing the standard deviations ($n = 3$) of these measurements are plotted in Fig. 2B. It is evident that the dependence of outcoupled light intensity on pH is quite reproducible. The average standard deviation of the four points that were repeated, expressed as a percentage of the total intensity change between pH 3.5 and 7.0, was 3.6%.

After storage for 12 months, ellipsometry was used to measure the thickness and refractive index of film B. Measurements were made at 10 different spots on the film surface. The mean thickness and refractive index were 85 ± 15 nm and 1.43 ± 0.016, respectively. The absorbance of film A measured in the transmission mode was 0.0087 a.u. Assuming that the molar absorptivity of dissolved bromophenol blue is unaffected by sol-gel entrapment, for an 85-nm pathlength 0.0087 a.u. corresponds to a bromophenol blue concentration of 15 μmol/cm^3. This concentration is 9-fold higher than the indicator concentration in the coating solution. The increase was likely due to shrinkage of the film during drying, which was not measured here but is a well studied aspect of sol-gel processing [16].

Bulk, monolithic TEOS gels prepared with entrapped bromophenol blue also responded reversibly to solution pH. However, response times for bulk gels were on the order of hours, much longer than those of the films. A thin film therefore has the advantage of fast response but at the expense of diminished pathlength and hence low sensitivity. The optical pathlength in the sol-gel films employed here can be estimated using a ray optics approximation [17,18]. Based on the propagation angle in the glass slide (64°) and the refractive indices of the film ($n = 1.43$) and the slide ($n = 1.51$), the light in the film is predicted to be propagating rather than evanescent. Using a reflection density of 5 reflections/cm of beam propagation in the slide, the optical pathlength in the film is calculated to be 2.7 μm/cm. This relatively insensitive experimental arrangement was overcome by using a high concentration of entrapped bromophenol blue. However, since the optical pathlength is inversely proportional to waveguide thickness, substantially enhanced sensitivity should be achievable by using a waveguide much thinner than 1 mm. In the integrated optical regime, where the waveguide thickness is on the order of 1 μm, reflection densities of up to several thousand/cm of beam propagation (based on a ray optics approximation of thin film waveguiding behavior) are realized, which produces a corresponding increase in pathlength [18,19]. For example, a 0.5 μm thick planar waveguide ($n = 1.6$) supported on a glass substrate and coated with a 85 nm thick sol-gel film will support 1900 reflections/cm. The light in the film will be evanescent with a 90 nm pathlength (effective thickness) per reflection [17,18], from which an optical pathlength of 170 μm/cm is calculated. This represents a 63-fold increase over the glass slide geometry. The sensitivity of ATR sensing using sol-gel derived thin films should therefore be greatly enhanced by coating the film on a planar integrated optical waveguide. Such enhanced sensitivity may be useful, for example, in trace metal ion sensing using an entrapped chelating agent.

This work was partially supported by the Materials Characterization Program at the Univer-

sity of Arizona. We thank Lin Yang of the University of Arizona for assisting with the ellipsometer.

REFERENCES

1 M.A. Arnold, Anal. Chem., 64 (1992) 1015A.
2 R.E. Dessey, Anal. Chem., 61 (1989) 1079A.
3 M.J. Goldfinch and C.R. Lowe, Anal. Biochem., 138 (1984) 430.
4 O.S. Wolfbeis and H.E. Posch, Anal. Chim. Acta, 185 (1986) 321.
5 M.A. Arnold and T.J. Ostler, Anal. Chem., 58 (1986) 1137.
6 S. Braun, S. Shtelzer, S. Rappoport and D. Avnir, J. Non-Cryst. Solids, 147 and 148 (1992) 739.
7 S. Shtelzer, S. Rappoport, D. Avnir, M. Ottolenghi and S. Braun, Biotechnol. Appl. Biochem., 15 (1992) 227.
8 S. Braun, S. Shtelzer, R. Zusman, D. Avnir and M. Ottolenghi, Materials Lett., 10 (1990) 1.
9 R. Zusman, C. Rottman, M. Ottolenghi and D. Avnir, J. Non-Cryst. Solids, 122 (1990) 107.
10 B. Iosefzon-Kuyavskaya, I. Gigozin, M. Ottolenghi, D. Avnir and O. Lev, J. Non-Cryst. Solids, 147 and 148 (1992) 808.
11 L.M. Ellerby, C.R. Nishida, F. Nishida, S.A. Yamanaka, B. Dunn, J.S. Valentine and J.I. Zink, Science, 255 (1992) 1113.
12 C.J. Brinker, A.J. Hurd, P.R. Schunk, G.C. Frye and C.S. Ashley, J. Non-Cryst. Solids, 147 and 148 (1992) 424.
13 S.S. Saavedra and W.M. Reichert, Appl. Spectrosc., 44 (1990) 1210.
14 R.M.A. Azzam and N.M. Bashara, Ellipsometry and Polarized Light, North-Holland, Amsterdam, 1987, pp. 315–320.
15 E. Bishop, Indicators, Pergamon, Oxford, 1972. p. 67.
16 C.J. Brinker and G.W. Scherer, Sol-Gel Science, Academic Press, San Diego, CA, 1990.
17 N.J. Harrick, Internal Reflection Spectroscopy, Harrick Scientific, Ossining, NY, 2nd edn., 1979, pp. 41–50.
18 S.S. Saavedra and W.M. Reichert, Anal. Chem., 62 (1990) 2251.
19 S.S. Saavedra and W.M. Reichert, Langmuir, 7 (1991) 995.

Analytica Chimica Acta, 285 (1994) 271–276
Elsevier Science B.V., Amsterdam

Paraquat sensors based on cyclotetrasiloxanes

Bahruddin Saad, Mazlina Tahir, Mohd. N. Ahmad, Muhammad I. Saleh and Md. S. Jab

School of Chemical Sciences, Universiti Sains Malaysia, 11800 Penang (Malaysia)

Abas Hj Hussin

School of Pharmaceutical Sciences, Universiti Sains Malaysia, 11800 Penang (Malaysia)

(Received 13th April 1993; revised manuscript received 14th September 1993)

Abstract

A solvent polymeric membrane electrode that exhibits a significant potentiometric response toward paraquat ion is described. The membrane is prepared by incorporation of neutral octamethylcyclotetrasiloxane (**I**) or its phenyl derivative (**II**) and potassium tetrakis(4-chlorophenyl)borate as membrane additive in a thin film of poly(vinyl chloride) plasticized with *o*-nitrophenyl octyl ether. The electrodes exhibit near-Nernstian slopes, fast dynamic response times of about 20 s and a useful pH range of 4–11 and display an insignificant or low response towards common inorganic cations, copper(II), glucose, urea and diquat ions. Determinations of 12.9 and 25.7 mg l^{-1} of paraquat dichloride in each of water, electrolyte solution (consisting of 0.14 M sodium chloride, 1 mM calcium chloride, 1 mM magnesium chloride and 5 mM potassium chloride in Tris buffer, pH 7.0) and normal artificial serum, using an electrode based on **I** were satisfactory. Electrochemical features of these electrodes versus those based on the dibenzo-30-crown-10 system reported earlier are compared.

Keywords: Ion selective electrodes; Potentiometry; Sensors; Cyclotetrasiloxanes; Herbicides; Membrane electrodes; Paraquat

Paraquat, the common name for 1,1′-dimethyl-4,4′-bipyridinium cations, was first introduced as a broad-spectrum contact herbicide in 1962 [1]. Since then it has been used extensively in more than 130 countries [2]. This herbicide is extremely toxic and is often encountered in cases of accidental and suicidal poisonings [1,3]. In fact, it has been banned in countries such as Germany, Sweden and Norway, although not necessarily for toxicological reasons [2]. Despite these shortcomings, paraquat has many advantageous agrochemical properties unrivalled by any other herbicides: it is a relatively non-selective, contact herbicide that is rapidly inactivated on contact with most types of soil [1,2]. Hence no biologically active residues remain in the soil and planting and sowing can be carried out almost immediately after spraying [1,2].

Various techniques have been described for the determination of paraquat. A common method involves spectrophotometry where the absorbance of the paraquat radical after being reduced by reagents such as sodium dithionite [4,5], ascorbic acid [6] and potassium tetraiodomercurate [7] was measured. Generally, the radical formed is not very stable [7,8] owing to its rapid oxidation by atmospheric oxygen, requiring immediate determination of the absorbance, although a flow-injection approach overcame this stability problem [8]. Other methods include thin-layer chromatography [9,10], gas chromatography [11], liquid chromatography [3,12,13], po-

Correspondence to: B. Saad, School of Chemical Sciences, Universiti Sains Malaysia, 11800 Penang (Malaysia).

SSDI 0003-2670(93)E0522-9

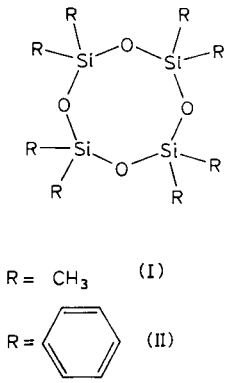

Fig. 1. Structures of octamethylcyclotetrasiloxane (I) and octaphenylcyclotetrasiloxane (II).

larography [14] and radioimmunoassay [15]. Generally, these techniques are slow because of the need for extensive sample pretreatment. A more rapid and simplified approach is offered by potentiometric sensors.

Earlier studies with neutral carrier potentiometric sensors have dealt essentially with metal cation sensing. The selection of suitable neutral carriers aided by structural studies on interactions between the carriers and ions have resulted in the development of diquat and paraquat ion sensors [16,17]. Other organic ion sensors responsive towards guanidinium [18,19], amphetaminium [20], primaquinium [21], adenosinium [22], etc., have also been reported. These studies suggest that the sensing of organic ions using macrocyclic polyethers and their derivatives is viable.

Moody et al. have described several interesting paraquat sensors based on crown ethers [16,17] and ion exchangers [16,23]. Although they exhibit good response features, the performance of these electrodes with real samples has yet to be demonstrated. Strong interference from potassium ions with the dibenzo-30-crown-10 (DB30C10) system, the most promising neutral carrier-type sensor investigated [16], is evident. In contrast, the paraquat sensors described here suffer negligible interference from potassium ions.

The evaluation of octamethylcyclotetrasiloxane (**I**) and its phenyl derivative (**II**) (Figure 1) as electroactive components for potentiometric paraquat sensing and its application to the determination of paraquat background solutions are described in this paper.

EXPERIMENTAL

Reagents

Reagents and materials used were obtained from the following sources: *o*-nitrophenyl octyl ether (NPOE), high-molecular-mass poly(vinyl chloride) (PVC) and potassium tetrakis(4-chlorophenyl)borate (KTPB) from Aldrich (Milwaukee, WI), paraquat dichloride, Sigma artificial serum, tris(2-ethylhexyl) phosphate, dioctylphenyl phosphonate, urea, glucose and Trizma base buffer from Sigma (St. Louis, MO) and octamethylcyclotetrasiloxane (**I**) and octaphenylcyclotetrasiloxane (**II**) from Fluka (Buchs, Switzerland). Chlorides of metal ions were all of analytical-reagent grade and distilled, doubly deionized water was used throughout.

Electrode preparation and measurement

The PVC-immobilized sensors were prepared as membranes and assembled into conventional ion-selective electrodes using established procedures [24]. The master membrane composition is given in Table 1. For membranes 2 and 4, a 50% mole ratio of KTPB as membrane additive, relative to sensors **I** and **II**, respectively, was added to the membrane.

TABLE 1

Membrane compositions used

Membrane No.	Composition (% mass ratio)			
	Sensor	NPOE [a]	PVC	KTPB [b]
1	3.7 (**I**) [c]	65.4	30.9	
2	3.6 (**I**) [c]	63.5	30.0	3.0
3	3.7 (**II**) [d]	65.4	30.9	
4	3.6 (**II**) [d]	64.7	30.5	1.1

[a] *o*-Nitrophenyl octyl ether. [b] Potassium tetrakis(4-chlorophenyl)borate. [c] Octamethylcyclotetrasiloxane. [d] Octaphenylcyclotetrasiloxane.

TABLE 2

Electrochemical characteristics of paraquat electrodes [a] using cyclotetrasiloxanes compared with those reported based on dibenzo-30-crown-10 [16]

Electrode No.	Slope (mV per decade)	Detection limit (M)	Useful pH range	log $k^{pot}_{PQT.B}$ (separate solution method, except values in parentheses)								
				B = Li	B = Na	B = K	B = Ca	B = Mg	B = Cu	B = diquat	B = glucose	B = urea
1	13.3	6.0×10^{-5}	–	Not determined owing to poor slope								
2	31.2	6.3×10^{-6}	3.5–12.5	−2.84	−3.78	−2.42	−4.12	−4.47	−4.42	−0.51	−4.75	−4.11
					(−3.10) [b]	(−2.31) [b]						
3	12.8	1.0×10^{-4}		Not determined owing to poor slope								
4	26.8	7.3×10^{-6}	4.0–11.0	−4.44	−4.19	−3.75	−4.37	−4.42	−4.22	−0.44	−4.51	−4.66
					(−3.42) [b]	(−2.06) [b]						
5 (DB30C10) [c]	19.0	–	–	+0.5	+2.8	+10	−0.5	−2.0	–	+4.0		
6 (DB30C10 [c] + additive)	30.1	–	–	−2.0	−2.0	−0.5	−4.0	−4.0	–	−0.5		

[a] All membranes plasticized with NPOE. [b] Mixed solution method. [c] Dibenzo-30-crown-10.

Electrochemical measurements were made with a Orion digital ionanalyzer (Model 701A) versus an Orion 90-02 Ag/AgCl double-junction reference electrode (Orion, Cambridge, MA). Electrode calibrations were effected by adding successive aliquots of a known concentration of sample to water (20 cm^3). Owing to scarcity of the paraquat dichloride, the selectivity coefficients were mainly determined using the separate solution method containing a 0.01 M paraquat dichloride concentration as described previously [21,25]. The mixed solution method at a fixed concentration of interferent ion (1 mM) was also used to measure a few ions using the standard IUPAC recommendations [26]. The electrodes were conditioned before use by immersion for 24 h in 0.1 M paraquat salt solution. A similar solution was used as the internal filling solution. The electrodes were stored in this solution between measurements.

Determination of paraquat

Solutions containing 12.9 and 25.7 mg l^{-1} of paraquat salt, were prepared in each of the following media: (i) water, (ii) electrolyte solution consisting of 0.14 M sodium chloride, 5.0 mM potassium chloride, 1 mM calcium chloride and 1 mM magnesium chloride in Tris buffer (pH 7.0) and (iii) artificial serum prepared by dissolving 1.3713 g of Sigma normal control serum in 50 cm^3 of water. The standard addition procedure as described previously [21] was used for the determination of paraquat.

RESULTS AND DISCUSSION

Response characteristics of the electrodes

The key electrochemical characteristics of the paraquat electrode are summarized in Table 2. Membranes containing no additive yield paraquat electrodes that not only give poor slopes and high detection limits but also are noisy (electrodes 1 and 3). However, a marked increase in electrode quality with respect to slope, e.m.f. stability and detection limit was achieved with membranes that were incorporated with a 50% mole ratio of KTPB relative to sensors with both **I** and **II** (electrodes 2 and 4, Table 2). The need for incorporation of a membrane additive to promote the electrode response is also observed for paraquat electrodes based on DB30C10 [16] and other potentiometric sensing systems [21,27]. Dynamic response times of 20 s are typical of these electrodes. The effect of common plasticizers such as dioctyl phenyl phosphonate, NPOE and tris(2-ethylhexyl) phosphate on the electrode response was also investigated. It was found that, with the exception of NPOE, the other plasticizers result in electrodes with erratic responses and with poor slopes.

The response of the electrodes in the presence of a few common inorganic ions, copper(II), glucose, urea and diquat ions was evaluated mainly using the separate solution method. Copper(II) sulphate was evaluated as it is an emetic ingredient that is added to paraquat formulations in order to minimize injury due to accidental consumption of the herbicide [28], and diquat is added in certain formulations to increase the herbicidal effectiveness against a wider range of weeds [3,4]. The selectivity characteristics of this electrode, with the exception of potassium ions, are at least comparable to those reported earlier [16] based on DB30C10 (Table 2). A marked improvement in the selectivity over potassium ions with the proposed electrode compared with those reported earlier is evident. A strong response of the reported electrode towards potassium is not surprising in view of the fact that DB30C10 has been used for constructing potassium-selective electrodes [29].

Determination of paraquat in different background solutions

Table 3 summarizes the results obtained using electrode 2 for the determination of different

TABLE 3

Determination of paraquat dichloride in different background solutions using known addition method with electrode 2

Background solution	Paraquat concentration (mg l^{-1})			
	Present	Found [a]	Present	Found [a]
Water	25.7	24.1 ± 1.2	12.9	9.8 ± 0.8
Electrolyte	25.7	23.5 ± 1.6	12.9	9.2 ± 0.8
Artificial Serum	25.7	22.8 ± 0.8	12.9	9.5 ± 0.6

[a] Mean ± standard deviation ($n = 4$).

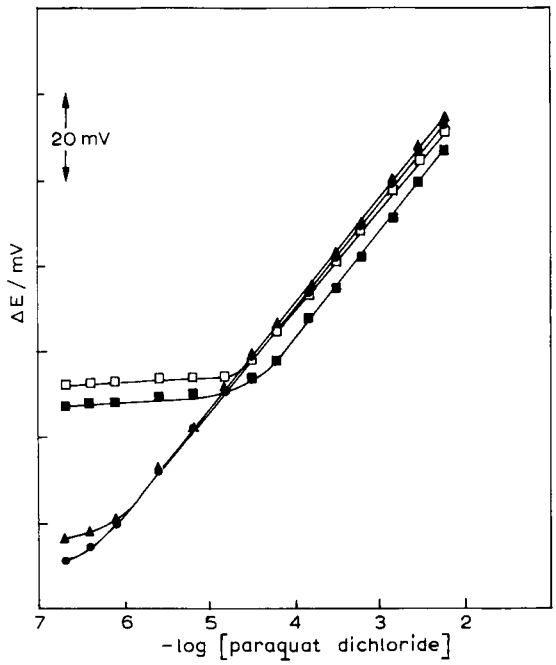

Fig. 2. Typical calibrations of electrode 2 in (●) water, (▲) Tris buffer, (□) electrolyte and (■) artificial serum solutions. See text for compositions.

paraquat ion levels in various background solutions. The results for the determination of 25.7 mg l^{-1} of paraquat salt are especially satisfactory in view of the fact that for potentiometric measurements errors of 5–20% are common [21,25, 30]. Adsorbtion of the herbicide on glass surfaces of vessels has also been reported [11]. Typical calibrations of the electrode in the different background solutions studies are shown in Fig. 2. The electrolyte solution was prepared to mimic the major electrolytes present in normal blood serum. Even in protein-containing solution, a linear dynamic range of 10^{-4}–10^{-2} M is obtained. The detection limits as determined according to IUPAC recommendations [26] in electrolyte and artificial serum solution are 2.5×10^{-5} and 2.0×10^{-5} M, respectively.

Conclusion

For viable paraquat sensors to be realised using **I** and **II**, it is essential to add the membrane additive KTPB. NPOE was found to be the most suitable plasticizer. The fact that this electrode is subject to negligible interferences from both inorganic cations and also protein-containing solutions lends makes it promising for paraquat sensors for the analysis of body fluids. For the proposed electrode to be used in the analysis of herbicide formulations, more studies need to be done, especially with respect to the response in the presence of various other formulation ingredients such as anti-foaming agents, anti-corrosion inhibitors and surfactants. The problematic nature of the latter with regard to ion-selective electrode responses has already been documented [31,32].

The authors acknowledge the support of the Ministry of Science, Technology and Environment of Malaysia through its Intensification of Research in Priority Areas via grant 123/2304/2504.

REFERENCES

1 G.R. Sagar, Hum. Toxicol., 6 (1987) 7.
2 J.A. Vale and G.N. Volans, Hum. Toxicol., 6 (1987) 3.
3 R. Gill, S.C. Qua and A.C. Moffat, J. Chromatogr., 255 (1983) 483.
4 S.H. Yuen, J.E. Bagness and D. Myles, Analyst, 92 (1967) 375.
5 A. Calderbank and S.H. Yuen, Analyst, 90 (1965) 99.
6 P. Shivhare and V.K. Gupta, Analyst, 116 (1991) 391.
7 M. Ganesan, S. Natesan and V. Ranganathan, Analyst, 104 (1979) 258.
8 E.H. Guijarro, P.Y. Sedeno and L.M.P. Diez, Anal. Chim. Acta, 199 (1987) 203.
9 G.S. Tadjer, J. Forensic Sci., 12 (1967) 549.
10 H.D. Crone and E.M. Smith, J. Chromatogr., 77 (1973) 234.
11 A.J. Cannard and W.J. Criddle, Analyst, 100 (1975) 848.
12 Y. Kawano, J. Audino and M. Edlund, J. Chromatogr., 115 (1975) 289.
13 D.C. Paschal, L.H. Needham, Z.J. Rollen and J.A. Liddle, J. Chromatogr., 177 (1979) 85.
14 P.Y. Sedeno, J.M.P. Carrazon and L.M.P. Diez, Mikrochim. Acta, III (1985) 279.
15 R.A. Braithwaite, Hum. Toxicol., 6 (1987) 83.
16 G.J. Moody, R.K. Owusu and J.D.R. Thomas, Analyst, 112 (1987) 121.
17 G.J. Moody, R.K. Owusu and J.D.R. Thomas, Analyst, 113 (1988) 65.

18 M. Bochenska and J. Biernat, Anal. Chim. Acta, 162 (1984) 369.
19 F.N. Assubaie, G.J. Moody and J.D.R. Thomas, Analyst, 114 (1989) 1545.
20 S.S.M. Hassan and E.M. Elnemma, Anal. Chem., 61 (1989) 2189.
21 B. Saad, Z.A. Zahid, S.A. Rahman, M.N. Ahmad and A.H. Hussin, Analyst, 117 (1992) 1319.
22 Y. Umezawa, M. Kataoka, W. Takami, E. Kimura, T. Koide and H. Nada, Anal. Chem., 60 (1988) 2392.
23 G.J. Moody, R.K. Owusu and J.D.R. Thomas, Analyst, 112 (1987) 1347.
24 A. Craggs, G.J. Moody and J.D.R. Thomas, J. Chem. Educ., 51 (1974) 541.
25 B. Saad, K. Kanapathy, M.N. Ahmad, A.H. Hussin and Z. Ismail, Talanta, 38 (1991) 1399.
26 G.G. Guilbault, Ion-Sel. Electrode Rev., 1 (1979) 139.
27 D. Ammann, Ion-Selective Microelectrodes, Springer, Berlin, 1986, p. 53.
28 L.J. Onyon and G.N. Nolans, Hum. Toxicol., 6 (1987) 19.
29 O. Ryba and J. Petranek, J. Electroanal. Chem., 44 (1973) 425
30 G.J. Moody, R.K. Owusu and J.D.R. Thomas, Anal. Lett., 21 (1988) 1653.
31 A. Craggs, G.J. Moody, J.D.R. Thomas and B.J. Birch, Analyst, 105 (1980) 426.
32 A.J. Frend, G.J. Moody, J.D.R. Thomas and B.J. Birch, Analyst, 108 (1983) 1072.

Analytica Chimica Acta, 285 (1994) 277–285
Elsevier Science B.V., Amsterdam

Effect of cysteine on the speciation of arsenic by using hydride generation atomic absorption spectrometry

Xiao-Chun Le, William R. Cullen and Kenneth J. Reimer

Department of Chemistry, University of British Columbia, Vancouver, B.C. V6T 1Z1 (Canada)

(Received 15th June 1993; revised manuscript received 8th September 1993)

Abstract

The use of hydride generation techniques for arsenic species is pH dependent. Identical responses can not be obtained from arsenite, arsenate, monomethylarsonic acid (MMAA) and dimethylarsinic acid (DMAA) when the same acid concentration is used. Thus some methods commonly used for the direct determination of total arsenic under compromised conditions are subject to error. This error is eliminated by the addition of 2% cysteine to samples prior to hydride generation. In the presence of cysteine the optimum condition for the determination of these arsenic species is in the same range, and a single arsenic species can be used for calibration. This finding is applied to the determination of arsenic in human urine by using flow injection, hydride generation, and atomic absorption spectrometry methodology. The effect of cysteine and thioglycerol is reported in detail, and it is proposed that arsenate, MMAA and DMAA all in the As(V) state, are reduced to the As(III) state as organo-sulfur-arsenic(III) compounds through the reaction between the arsenic species and the thiol. These products, organosulfur derivatives of arsenic(III), easily react with tetrahydroborate(III) under similar conditions to afford the arsines without interference from cysteine. Non-thiol-containing amino acids such as methionine, glycine and histidine do not react with arsenic species in this way, and therefore they do not affect the pH dependence of the generation of arsenic hydride species.

Keywords: Atomic absorption spectrometry; Flow injection; Hydride generation; Arsenic speciation; Human urine; Cysteine; Environment

The determination of arsenic in environmental and biological systems is gaining increasing importance, mainly because of the ubiquitous nature of this element and the toxic characteristics of some arsenic species. Natural waters have been reported [1–5] to contain arsenite, arsenate, monomethylarsonic acid (MMAA) and dimethylarsinic acid (DMAA), which are all toxic and the relative toxicity decreases in the above order [6]. In addition to these toxic arsenic species, approximately 20% of arsenic present in a river water reference material was reported as unidentified species [7]. Although not identified in natural waters, an essentially non-toxic compound [8–10], arsenobetaine, has been found in biological tissues [5,11,12] and in human urine samples [13–17]. The presence of elevated levels of arsenobetaine in human urine has been ascribed to the ingestion of seafood, particularly crustaceans, which often contain this compound as the major arsenic species [5,11,12].

The hydride generation technique with its major advantages of high sensitivity and relative simplicity has been widely used for arsenic determination at trace levels. Various arsines can

Correspondence to: W.R. Cullen, Department of Chemistry, University of British Columbia, Vancouver, B.C. V6T 1Z1 (Canada).

SSDI 0003-2670(93)E0541-E

be formed. Arsenite and arsenate give AsH_3, MMAA gives CH_3AsH_2, and DMAA gives $(CH_3)_2AsH$, upon reaction with sodium tetrahydroborate(III). The gaseous arsines can be introduced to a variety of spectrometric detectors for measurement. Braman and Foreback [1] pointed out that the formation of the arsines was pH dependent and was related to the pK_a values of the individual arsenic acids. This pH dependency was further demonstrated by Anderson et al. [18]. Hinners [19] also emphasized the critical effect of acid concentration on the hydride generation responses from arsenite, arsenate, MMAA and DMAA, and was unable to find a compromised acid concentration under which the same response could be obtained from the four arsenic species. Thus, when 4–10 M hydrochloric acid was used, DMAA gave only 15% (or less) of the signal that was obtained from the same amount of arsenite, whereas at a lower acidity (pH 4.8), arsenate and MMAA were severely underestimated. Similar observations were also reported by Arbab-Zavar and Howard [20]. In a method reported by Aggett and Aspell [21], however, total arsenic in environmental water samples was evaluated by using 5 M hydrochloric acid as the hydride generation reaction medium and inorganic arsenite as the standard. As clearly indicated by the work of others [19,20] this method underestimates DMAA, which is often present in natural waters. Similar errors exist in other reports [22,23] and the problem has not been solved.

We have previously reported [24–27] that cysteine successfully reduces matrix interferences in the determination of arsenic, antimony, germanium, and tin when hydride generation techniques are used. We have recently found that when cysteine is added to samples, arsenite, arsenate, MMAA and DMAA give the same response under the same optimum acid concentration when quantitated by using hydride generation. Thus the determination error described above can be eliminated. We now wish to report some detailed studies on the effect of cysteine and related compounds on the speciation of arsenic by using hydride generation, and the development of a simple method for the determination of arsenic in human urine.

EXPERIMENTAL

Instrumentation

A system coupling flow-injection analysis with hydride generation atomic absorption spectrometry (FIA–HGAAS) was used as described previously [28,29]. It consists of a peristaltic pump (Gilson Minipuls 2), a Rheodyne six-port sample injection valve, a lab-made continuous hydride generator, an atomic absorption spectrometer equipped with an air–acetylene flame atomizer (Varian Model AA-1275), and an open-ended T-shaped quartz absorption tube (11.5 cm × 0.8 cm i.d.) mounted in the AA flame. Atomic absorption signals of arsenic were measured at 193.7 nm wavelength and were recorded on a Hewlett Packard 3390A integrator. A 500-W domestic microwave oven (Toshiba, Japan) was used for the digestion of urine samples.

A system that employed hydride generation followed by cryogenic trapping, gas chromatographic separation and atomic absorption detection was also used for arsenic speciation. The basic operations used for hydride generation and cryogenic trapping are similar to those reported [2,3,30]. Some modifications [31,32] have been made for GC separation and sample introduction. A Jarrell-Ash 810 atomic absorption spectrophotometer and a Hewlett Packard 5830A gas chromatograph were used.

Reagents

Standard solutions of arsenite, arsenate, MMAA, DMAA, arsenobetaine, arsenocholine, and tetramethylarsonium were prepared as described previously [24,28]. Sodium tetrahydroborate(III), L-cysteine (BDH), methionine, glycine, histidine and thioglycerol (Sigma) and other reagents used were all of analytical reagent grade or better.

Samples

Urine samples were collected from a 30-year old, healthy male before and after the ingestion of crab meat. The subject refrained from eating seafood for at least 3 days immediately before this experiment was conducted. Live crabs were purchased from a local seafood market in Van-

couver (Canada) and were steam cooked. Following the ingestion of crab meat, urine samples were collected for three consecutive days. A sample was also collected prior to the ingestion of crab. The urine samples were stored at 4°C and were analyzed within 3 days of collection.

Procedures

FIA–HGAAS. Method one: Urine samples were directly analyzed for arsenic by using FIA–HGAAS. A 100-μl sample was injected into a deionized water carrier stream by using a sample injection valve. The injected sample met with a continuously introduced hydrochloric acid stream and a sodium tetrahydroborate(III) stream at two T-joints. Arsines were generated and separated from liquid waste in a lab-made gas–liquid separator apparatus as discussed previously [28]. The gaseous arsines were then swept by a continuous flow of nitrogen carrier gas into a quartz absorption tube mounted in the air–acetylene flame for AA measurement. Initially both peak height and peak area of signals were measured. It was found that the peak height measurements gave a lower standard deviation and this was therefore used for quantitation. Standard arsenite solutions were used for calibration.

Method two: Cysteine, 0.2 g, was dissolved in each 10 ml urine sample. The solution was left for 10–20 min at room temperature, and the samples were analyzed for arsenic in the same way as described in method one, except that a lower acid concentration was used (see Table 1). Standard arsenite solutions and a blank, treated in the same way, were used for calibration.

Method three: Urine samples were first subjected to batch type microwave digestion [29] as follows. The urine sample or standard (40 ml), potassium persulfate (4.5 g), and sodium hydroxide (2.7 g) were combined in a 125–ml Erlenmeyer flask. Six of such sample-containing flasks were placed in a microwave oven at one time. The microwave oven was then operated at full power for 3 min followed by a 3 min cooling period, and this heating and cooling cycle was repeated for another four times. After being cooled to room temperature, the samples were each diluted to 50 ml with deionized water. Determination of arsenic in the digested samples was also carried out by using FIA–HGAAS as described above in method one, except that arsenate was employed as standard for calibration.

Hydride generation gas chromatography atomic absorption spectrometry (HG–GCAAS). The sample, hydrochloric acid, and sodium tetrahydroborate(III), each 3 ml, were pumped, at a flow-rate of 3 ml min^{-1}, into the gas–liquid separator apparatus [28] via a 2-m reaction coil. Arsines generated from the reaction were separated from waste, passed through an acetone–dry ice bath to remove moisture, and trapped in a Teflon U-tube (30 cm × 0.3 cm i.d.) cooled in liquid nitrogen. After 6 min of trapping, the liquid nitrogen was removed and the U-tube was warmed up by using a hot water bath (70°C). The trapped arsines were released and swept with the aid of the helium carrier gas into a PTFE GC column (50 cm × 0.3 cm i.d.) packed with Porapak-PS (80–100 mesh). The GC oven temperature was kept at 50°C for the initial 0.5 min and then linearly increased to 150°C at a rate of 30°C min^{-1}. Individual arsine species were separated on the GC column and were subsequently introduced into a quartz absorption tube heated internally with a hydrogen–air flame for AA measurement [20]. Chromatograms were recorded on a Hewlett Packard 3390A integrator capable of both peak height and peak area measurements.

TABLE 1

Experimental conditions for hydride generation

	Method One	Method Two	Method Three
Microwave digestion	NO	NO	YES
Cysteine	NO	2%	NO
HCl Conc.	3 M	0.5 M	3 M
HCl flow rate	3.4 ml min^{-1}	3.4 ml min^{-1}	3.4 ml min^{-1}
$NaBH_4$ Conc.	0.65 M	0.65 M	0.65 M
$NaBH_4$ flow rate	3.4 ml min^{-1}	3.4 ml min^{-1}	3.4 ml min^{-1}

RESULTS AND DISCUSSION

Effect of acid concentration on arsine generation in the absence of cysteine

Figure 1 shows the atomic absorption responses of arsenic derived from arsenite, arsenate, MMAA and DMAA in aqueous solution as a function of concentration of hydrochloric acid. It is clear that responses from each arsenic species depend differently on acid concentration and that there is no acid concentration at which an equal response from the four arsenic species can be obtained. Similar effects were observed when nitric acid was used instead of hydrochloric acid. Also, peak area measurement showed the same effect of acid concentration on the responses from these arsenic species. These results along with those reported [18,20,33], demonstrate that each arsenic species has its own requirement on acid concentration to achieve optimum response by hydride generation. This is why errors can easily arise in the direct determination of total arsenic from the use of a compromised acid concentration and a calibration based on a single arsenic species [21–23].

Effect of cysteine

When 2% cysteine is present in the aqueous arsenic solution, the pH dependence of hydride generation of the same four arsenic compounds is shown in Fig. 2. As compared to Fig. 1, the optimum acid concentration for maximum sensitivity is shifted to a much lower level in the presence of cysteine. Also, in the acid concentration range of 0.3–0.7 M, maximum and identical responses are obtained from all the four arsenic species. Furthermore, since all four arsenic species give the same response, a single arsenic species can be used for calibration. When thioglycerol, another thiol-containing (–SH) compound was used instead of cysteine, similar effects to those shown in Fig. 2 were noted.

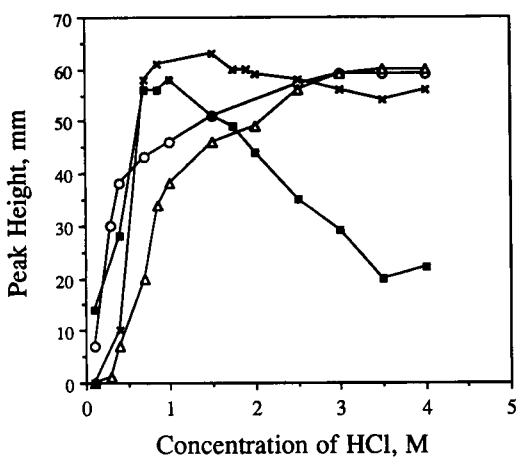

Fig. 1. Effect of hydrochloric acid concentration on hydride generation responses from 20 ng ml^{-1} of (○) arsenite, (△) arsenate, (×) MMAA and (■) DMAA in H_2O.

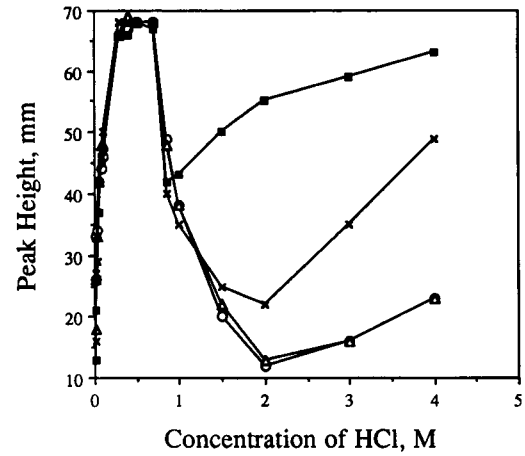

Fig. 2. Effect of hydrochloric acid concentration on hydride generation responses from 20 ng ml^{-1} of (○) arsenite, (△) arsenate, (×) MMAA and (■) DMAA in 2% cysteine aqueous solution.

Anderson et al. [18] have obtained similar results when using mercaptoacetic acid. Thus in the absence of any other acid, the optimum concentration of mercaptoacetic acid was found to be 0.1 M for the determination of arsenite, arsenate, MMAA and DMAA; but unfortunately, severe interferences from a number of transition metal ions were encountered [18]. These interferences can be reduced efficiently [24,34] by using cysteine. Furthermore, a relatively wider optimum acid concentration range (0.3–0.7 M) is available when cysteine is used compared with mercaptoacetic acid (0.1 M). An obvious advantage of having a wider optimum concentration range is that it is easier to keep experimental conditions

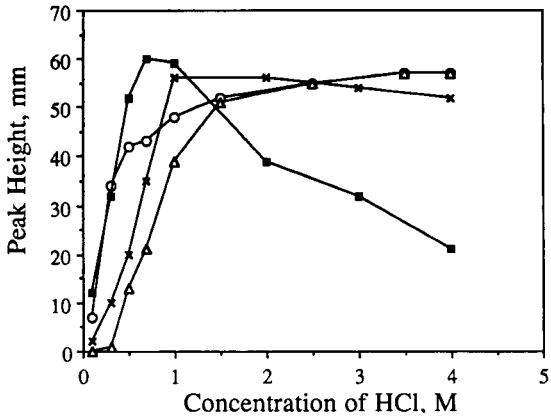

Fig. 3. Effect of hydrochloric acid concentration on hydride generation responses from 20 ng ml^{-1} of (○) arsenite, (△) arsenate, (×) MMAA and (■) DMAA in 2% methionine aqueous solution.

within this range in order to maintain the maximum sensitivity and the minimum deviation.

Other amino acids such as methionine, glycine and histidine were also studied in the same manner to evaluate how they might affect the optimum acid concentration for arsenic determination. The effect of hydrochloric acid concentration on the responses from arsenic species with 2% methionine present in each arsenic standard solution is shown in Fig. 3. Very little difference is seen compared with Fig. 1, indicating that methionine has little effect. The presence of added glycine or histidine has likewise little effect.

The significant effect by cysteine and thioglycerol and the lack of effect by methionine, glycine and histidine is probably due to the presence of the thiol group (–SH) in cysteine and thioglycerol. Cullen et al. [35,36] have shown that methylarsenicals can be easily reduced by a variety of thiols and dithiols including cysteine, glutathione, dithiothreitol, 2,3-dimercaptopropanol, and lipoic acid. The reactions were found to be quantitative and stoichiometric [35]. Chen et al. [34] have shown that arsenate is readily reduced to arsenite by cysteine. Therefore, it is reasonable to propose that the following reactions take place in the presence of thiol compounds, such as cysteine:

$$\begin{array}{ccccc} As(OH)_3 & & As(SR)_3 & & AsH_3 \\ AsO(OH)_3 & & As(SR)_3 & & AsH_3 \\ & \xrightarrow{RSH} & & \xrightarrow{NaBH_4} & \\ CH_3AsO(OH)_2 & & CH_3As(SR)_2 & & CH_3AsH_2 \\ (CH_3)_2AsO(OH) & & (CH_3)_2As(SR) & & (CH_3)_2AsH \end{array}$$

where $R = -CH_2CH(NH_2)COOH$ for cysteine and $-CH_2CH(OH)CH_2OH$ for thioglycerol. Initially the arsenic species react with the thiols to form $As(SR)_3$, $CH_3As(SR)_2$, and $(CH_3)_2As(SR)$ which are all in the As(III) state. These organo sulfur derivatives of arsenic(III) probably require similar condition to react with tetrahydroborate(III) to produce arsines, accounting for the observation that the optimum acid concentration for reduction of the four arsenic species lies in the same range.

The proposed mechanism indicates that although intermediate arsenic sulfur compounds are formed, the final product arsines do not incorporate cysteine. This is experimentally proven by using a modified [31,32] hydride generation – cold trap – gas chromatography with atomic absorption detection, a similar technique to that employed by Braman et al. [2], Andreae [3], and Vien and Fry [30]. Figure 4 shows signals from arsenite, arsenate, MMAA and DMAA in the absence (a) and presence (b) of cysteine. In both

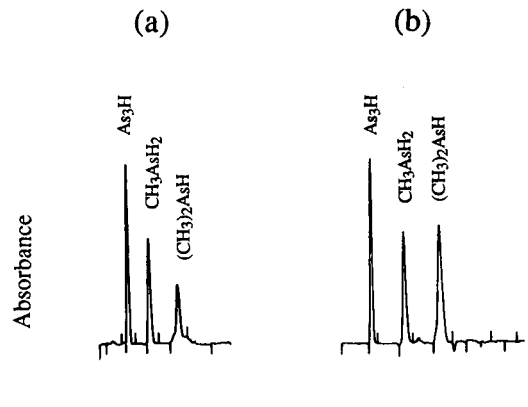

Fig. 4. Chromatograms obtained by using hydride generation/cold trapping/GC-AAS. (a) without cysteine, and (b) with cysteine.

cases, AsH_3, CH_3AsH_2, and $(CH_3)_2AsH$ are produced from the hydride generation reaction. The fact that the presence of cysteine has no effect on the arsines produced from individual arsenic species makes it applicable not only for total arsenic determination but also for arsenic speciation studies. In the latter case it may be used to reduce interferences in speciation of arsenic by using hydride generation.

Effect of varying the reaction coil length

The reaction time was studied by changing the length of the reaction coil between the gas–liquid separator and the point of mixing of the sample and reagents. Figure 5 shows the responses from the four arsenic species when either no reaction coil or a 2-m reaction coil is used. Fig. 5a and b were obtained from arsenic compounds in the presence of cysteine and they show that the responses from the arsenicals are approximately the same with or without the reaction coil. This indicates a fast reduction in the presence of cysteine and consequently no reaction coil is required. However, when cysteine is absent from the arsenic solutions, as shown in Fig. 5c and d, the responses are not maximized in the absence of the reaction coil, indicating incomplete reaction. When a 2-m reaction coil is added, the reaction is

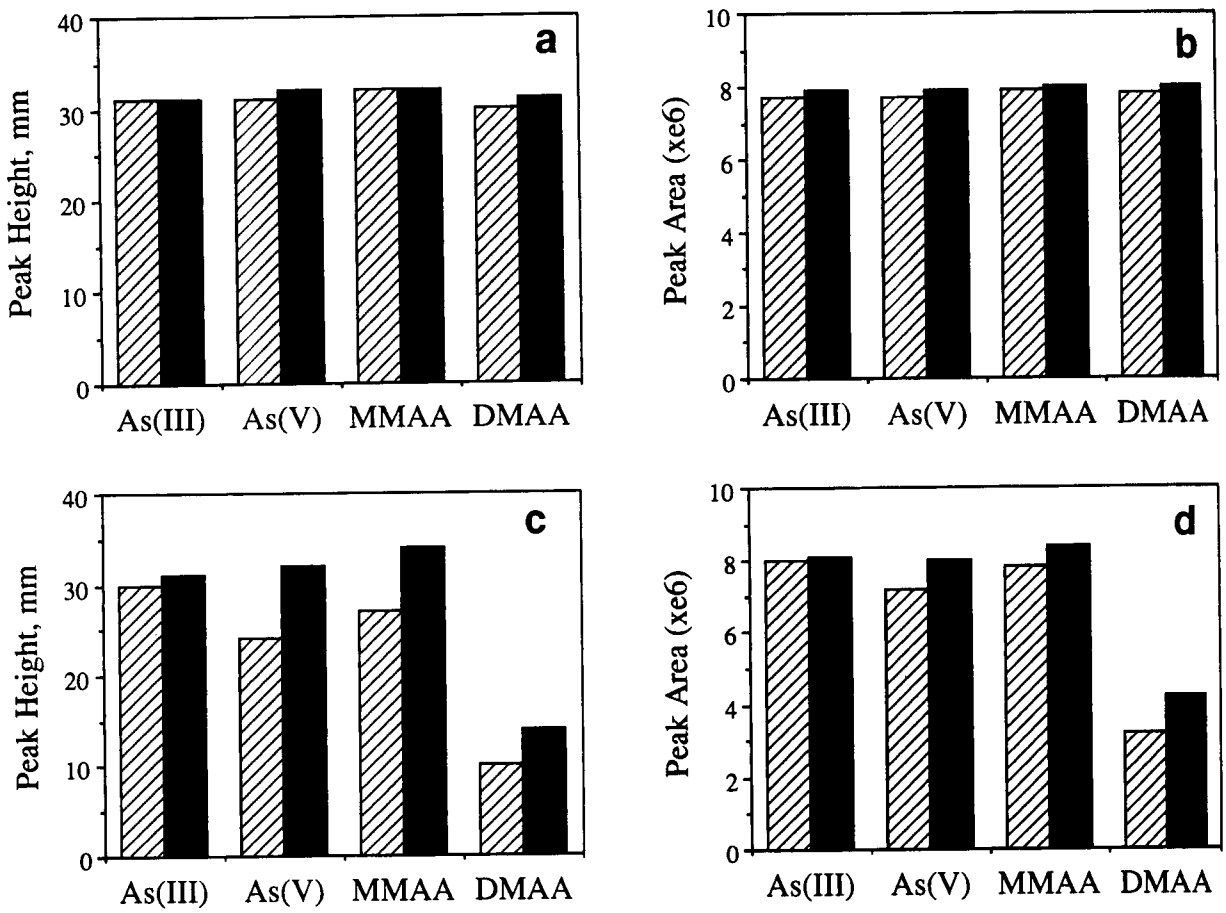

Fig. 5. (a) Comparison of peak height of hydride generation signals from arsenic species in 2% cysteine obtained with (black columns) and without (hatched columns) a 2-m reation coil. (b) Same as (a) but peak area. (c) Comparison of peak height of hydride generation signals from arsenic species in H_2O obtained with and without a 2-m reation coil. Key as in (a). (d) Same as (c) but peak area.

complete and full responses are obtained. Further lengthening the reaction coil up to 5 m did not produce any further increase of the arsenic signals.

It seems that cysteine enhances the rate of arsine generation. The mechanism proposed above suggests that the pentavalent arsenic species, arsenate, MMAA, and DMAA are all reduced to their trivalent oxidation state by cysteine prior to the reaction with tetrahydroborate(III). Consequently, faster reactions with tetrahydroborate(III) are possible from these pre-reduced arsenic species. It is well established [1–3,18–21,37–40] that the production of an arsine from arsenite is substantially faster than from the pentavalent arsenicals. In the absence of cysteine or other common reducing agents such as potassium iodide, both the pre-reduction and hydride formation would be carried out by reacting with tetrahydroborate(III).

Application–determination of arsenic in human urine

Organoarsenic compounds such as arsenobetaine have been found to be present in urine samples following the ingestion of seafood. Arsenobetaine does not form a hydride on treatment with tetrahydroborate(III) and therefore needs to be decomposed prior to its quantitation by hydride generation technique. Our previous work [28,29] showed that arsenobetaine was completely decomposed to arsenate by using potassium persulfate and sodium hydroxide with the aid of microwave heating. This approach is adapted here to measure total arsenic in urine samples.

To take the matrix effect into consideration, optimization was carried out by maximizing responses from both arsenic in standard aqueous solutions and arsenic in a typical urine sample. Acid concentration, sodium tetrahydroborate(III) concentration, amount of cysteine, sample and reagent flow rate, and carrier gas flow rate, were optimized to reach maximum sensitivity and signal reproducibility. It was found that the effects of these parameters are similar for arsenic in urine samples and in standard solution, and the optimum conditions are summarized in Table 1.

TABLE 2

Recovery of arsenic species spiked into urine sample

Urine sample spiked with arsenicals	Recovery, %		
	Method one	Method two	Method three
20 ppb As(III)	98±2	96±6	97±2
20 ppb As(V)	90±2	[b]	98±3
20 ppb DMAA	57±3	98±3	92±2
10 ppb 4As mixture [a]	78±6	97±2	91±2
20 ppb 4As mixture [a]	88±5	99±3	[b]
50 ppb AB	0	0	98±6
50 ppb AC	0	0	97±3
50 ppb Me_4As^+	0	0	96±6

[a] 4As mixture contains equal amount of arsenite, arsenate, MMAA and DMAA. [b] not evaluated.

Recovery of arsenic species spiked into a urine sample was studied and compared by using three procedures: (i) direct analysis without addition of cysteine, (ii) direct analysis in the presence of cysteine, giving total hydride-forming arsenic concentration, and (iii) determination of total arsenic after microwave oven decomposition. Recovery results are summarized in Table 2. It is clearly seen that in the absence of cysteine, when 3 M HCl is used as reaction medium for all arsenic species, DMAA gives only 57% of the signal as calibrated against arsenite. Consequently when arsenic mixtures containing equal amount of arsenite, arsenate, MMAA and DMAA are spiked into the urine sample, the recovery is also incomplete as calibrated against arsenite. These results support the conclusion of Hinners [19] and Arbab-Zavar and Howard [20] who state that when total arsenic was measured against arsenite calibration, DMAA would be underestimated. However, when cysteine is added to the urine sample, complete recovery from all the arsenicals studied is achieved as shown in Table 2. Arsenobetaine (AB), arsenocholine (AC) and the tetramethylarsonium ion (Me_4As^+) do not form a hydride, with or without cysteine; however, after microwave oven decomposition, quantitative recoveries from these organoarsenicals, which have been converted to arsenate, are also obtained (Table 2).

Determination of arsenic in urine samples collected from an individual who had ingested some

TABLE 3

Concentration of arsenic in urine samples measured by using three methods

Urine sample No.	Collection time [b] (h)	Concentration of arsenic (ng ml^{-1}) (mean ± S.D.) [a]		
		Method one	Method two	Method three
1	−1	12.8±0.4	14.7±0.4	17.0±0.5
2	1	13.2±0.4	16.7±0.4	28.2±0.8
3	4	12.0±0.4	13.0±0.4	64.0±2.0
4	6	11.0±0.4	12.4±0.3	91.3±2.8
5	9	10.0±0.4	11.3±0.3	98.5±3.0
6	11	10.0±0.3	11.0±0.3	95.6±2.9
7	16	6.8±0.3	7.3±0.3	78.3±2.5
8	20	14.0±0.4	17.3±0.4	39.0±1.1
9	29	6.0±0.3	7.0±0.3	31.5±1.0
10	32	6.0±0.3	7.0±0.3	29.5±1.0
11	36	7.0±0.3	8.7±0.3	32.0±1.1
12	39	5.5±0.3	6.4±0.3	25.5±0.8
13	41	11.0±0.4	11.3±0.3	21.8±0.6
14	50	12.5±0.4	14.7±0.4	17.9±0.8
15	62	12.8±0.4	15.3±0.4	18.0±0.5

[a] From three or four replicate measurements. [b] Time zero is the time of ingestion of the crab meat.

crab meat was carried out and compared by using the three methods described in the procedure section. Table 3 lists the results of the time course study. In the presence of added cysteine, the mean value of the concentration of total hydride-forming arsenic for the 15 samples analyzed is 11.6 ng ml^{-1}. This represents the sum of arsenite, arsenate, MMAA and DMAA. In the absence of cysteine, however, the arsenic concentration is consistently underestimated in each sample, and the mean value from the 15 samples analyzed is 10.0 ng ml^{-1}. Thus on average a 13.8% error is present. In samples 2 and 8 in particular, the error is as high as 20%. This is not surprising since urine samples often contain DMAA [13–17] and DMAA concentration is underestimated in the absence of cysteine.

After microwave digestion, all arsenic compounds are converted to arsenate, and determination by hydride generation against arsenate calibration gives the total arsenic concentration. The difference in arsenic concentration measured between method 3 and method 2 is due to the hidden organoarsenic compounds which do not form a hydride. We have recently identified the major hidden organoarsenic compound in the crab and in the urine samples after ingestion of crab meat to be arsenobetaine, by using liquid chromatography (LC) with inductively coupled plasma mass spectrometry (ICPMS) detection [41]. Determination of arsenic in the microwave digested urine samples reveals that the highest concentration of arsenobetaine is excreted between 4 and 20 h after the ingestion of crab (Table 3). These results are in good agreement with other reports [13–17] and further demonstrate the fast excretion of arsenobetaine from the human body in an unchanged form. The methods 2 and 3 reported here are easy to use for the determination of trace amounts of arsenic and provide a convenient means to differentiate between the more toxic hydride-forming arsenicals which might be present in environmental/biological samples and other essentially non-toxic organoarsenic compounds.

This work is partly supported by the Natural Sciences and Engineering Research Council of Canada and the Canadian Department of Fisheries and Oceans. The authors thank the Canada's Killam Trust and its Scholarship Committee for awarding a Killam Predoctoral Fellowship to X.C.L.

REFERENCES

1 R.S. Braman and C.C. Foreback, Science, 182 (1973) 1247.
2 R.S. Braman, D.L. Johnson, C.C. Foreback, J.M. Ammons and J.L. Bricker, Anal. Chem., 49 (1977) 621.
3 M.O. Andreae, Anal. Chem., 49 (1977) 820.
4 M.O. Andreae, Deep Sea Res., 25 (1978) 391.
5 W.R. Cullen and K.J. Reimer, Chem. Rev., 89 (1989) 713.
6 W.R. Penrose, CRC Crit. Rev. Environ. Control, 4 (1974) 465.
7 R.E. Sturgeon, K.W.M. Siu, S.N. Willie and S.S. Berman, Analyst, 114 (1989) 1393.
8 M. Vahter, E. Marafante and L. Dencker, Sci. Total Environ., 30 (1983) 197.
9 T.R. Irvin and K.J. Irgolic, Appl. Organomet. Chem., 2 (1988) 509.
10 T. Kaise, S. Watanabe and K. Itoh, Chemosphere, 14 (1985) 1327.
11 J.S. Edmonds, K.A. Francesconi, J.R. Cannon, C.L. Raston, B.W. Skelton and A.H. White, Tetrahedron Lett., 18 (1977) 1543.

12 M. Burow and M. Stoeppler, in P. Bratter and P. Schramel (Eds.), Trace Element and Analytical Chemistry in Medicine and Biology, Vol. 4, De Gruyter, Berlin, 1987, p. 145.
13 V. Foa, A. Colombi and M. Maroni, Sci. Total Environ., 34 (1984) 241.
14 E.A. Crecelius, Environ. Health Perspect., 19 (1977) 147.
15 J.P. Buchet, R. Lauwerys and H. Roels, Int. Arch. Occup. Environ. Health, 48 (1981) 71.
16 B.S. Chana and N.J. Smith, Anal. Chim. Acta, 197 (1987) 177.
17 H. Yamauchi, K. Takahashi, M. Mashiko, J. Saitoh and Y. Yamamura, Appl. Organomet. Chem., 6 (1992) 383.
18 R.K. Anderson, M. Thompson and E. Culbard, Analyst, 111 (1986) 1143.
19 T.A. Hinners, Analyst, 105 (1980) 751.
20 M.H. Arbab-Zavar and A.G. Howard, Analyst, 105 (1980) 744.
21 J. Aggett and A.C. Aspell, Analyst, 101 (1976) 341.
22 F.D. Pierce, T.C. Lamoreaux, H.R. Brown and R.S. Fraser, Appl. Spectrosc., 30 (1976) 38.
23 P. Seyler and J.M. Martin, Marine Chem., 29 (1990) 277 and 34 (1991) 137.
24 X.-C. Le, W.R. Cullen, K.J. Reimer and I.D. Brindle, Anal. Chim. Acta, 258 (1992) 307.
25 I.D. Brindle and X.-C. Le, Analyst, 113 (1988) 1377.
26 I.D. Brindle, X.-C. Le and X.-F. Li, J. Anal. At. Spectrom., 4 (1989) 227.
27 I.D. Brindle and X.-C. Le, Anal. Chim. Acta, 229 (1990) 239.
28 X.-C. Le, W.R. Cullen and K.J. Reimer, Appl. Organomet. Chem., 6 (1992) 161.
29 X.-C. Le, W.R. Cullen and K.J. Reimer, Talanta, 40 (1993) 185.
30 S.H. Vien and R.C. Fry, Anal. Chem., 60 (1988) 465.
31 K.J. Reimer, Appl. Organomet. Chem., 3 (1989) 474.
32 W.R. Cullen and H. Li, unpublished results.
33 H. Narasaki and M. Ikeda, Anal. Chem., 56 (1984) 2059.
34 H. Chen, I.D. Brindle and X.-C. Le, Anal. Chem., 64 (1992) 667.
35 W.R. Cullen, B.C. McBride and J. Reglinski, J. Inorg. Biochem., 21 (1984) 179.
36 W.R. Cullen, B.C. McBride and J. Reglinski, J. Inorg. Biochem., 21 (1984) 45.
37 B. Welz and M. Melcher, Analyst, 109 (1984) 573.
38 D.D. Siemer, P. Koteel and V. Jariwala, Anal. Chem., 48 (1976) 836.
39 P.D. Goulden and P. Brooksbank, Anal. Chem., 46 (1974) 1431.
40 T. Nakahara, Prog. Anal. At. Spectrosc., 6 (1983) 163.
41 X.-C. Le, W.R. Cullen and K.J. Reimer, unpublished results.

Analytica Chimica Acta, 285 (1994) 287–292
Elsevier Science B.V., Amsterdam

Single-phase liquid–liquid extraction in monosegmented continuous-flow systems

Ileana Facchin, José W. Martins, Patrício G.P. Zamora and Celio Pasquini

Instituto de Química, Universidade Estadual de Campinas, C.P. 6154, CEP 13081-970 Campinas, São Paulo (Brazil)

(Received 4th June 1993; revised manuscript received 31st August 1993)

Abstract

Monosegmented continuous-flow analysis (MCFA) was evaluated for the realization of automatic single-phase liquid–liquid extraction. The single-phase mixture is generated by confluence of three solutions (isobutyl methyl ketone–thenoyltrifluoroacetone (IBMK-TTA), aqueous sample solution and ethanol). The resulting homogeneous solution is passed through a sample loop of an MCFA manifold and introduced into a reaction coil. Rapid and almost complete reaction between the analyte and complexing agent is obtained in the single phase. Subsequently, the single-phase monosegment containing the analyte complexed by TTA is broken into two phases (organic and aqueous) by adding saturated $NaNO_3$ solution. The organic portion containing the extracted analyte finally occupies the superior part of the monosegment and is passed through an on-line spectrophotometric detector. The system does not make use of a segmenter or separation device such as is usually employed in continuous-flow extraction methods. The sensitivity of the MCFA single-phase approach is closer to that of the conventional manual extraction method while samples can be processed at 60–80 h^{-1}.

Keywords: Flow system; Sample preparation; UV–Visible spectrophotometry; Extraction; Monosegmented continuous-flow analysis; Single-phase liquid–liquid extraction

The classical two phase liquid–liquid extraction methodology is usually employed for analytical purposes to achieve one or more of the following objectives: to allow the use of water-insoluble reagents; to improve the selectivity of the detection technique, removing the analyte from its matrix; and to improve the sensitivity by increasing the enrichment factor and/or by isolating the analyte in a medium (one of the phases) where enhanced analytical signals are observed.

Early in the development of flow-injection analysis (FIA), it was adapted to perform liquid–liquid extractions automatically [1,2]. Although two-phase flow extraction methodology has been proved to be very efficient in meeting the above objectives, two of the necessary stages, segmentation and separation of the immiscible phases, are frequently reported as being restrictive [3]. The segmentation must be uniform with very reproducible flow-rates and specially designed devices are necessary. High flow-rates can disrupt the uniformity. The extraction step is performed in a coil where the aqueous and organic segments travel side-by-side. The transfer of the analyte from one phase to the other is governed by the film of one of the phases produced on the wall of the extraction tube and by the interfacial area between two neighbouring segments of distinct phases [3–5]. The overall process is influenced by several equilibrium constants and by the viscosity

Correspondence to: C. Pasquini, Instituto de Quimica, Universidade Estadual de Campinas, C.P. 6154, CEP 13081-970 Campinas, São Paulo (Brazil).

SSDI 0003-2670(93)E0538-I

and surface tension of the liquids and is frequently kinetically unfavourable owing the short residence time of the segments in the extraction coil possible in FIA systems.

Recently, a batch procedure for single-phase liquid–liquid extraction has been described [6]. In this procedure the analyte and the reagent are both initially present in a single phase composed of three components. One is an organic solvent as isobutyl methyl ketone (IBMK), containing any suitable extracting reagent, the second is an aqueous phase containing the analyte and the last is a common solvent (e.g., ethanol) for water and for the organic solvent, capable of, in a suitable proportion, maintaining the mixture as a single phase. The resulting three-component, single-phase mixture retains some of the useful characteristics of the organic phase employed in conventional batch or flow liquid–liquid two-phase extraction such as a high solubility of organic reagents and non-polar compounds. Other combinations of solvents such as water–ethanol–cyclohexane [7], water–ethanol–isoamyl alcohol [8], water–ethanol–chloroform [9] and water–acetone–benzene [10] have also been employed to achieve single-phase extraction in batch procedures.

The single-phase method also presents the possibility of a reaction between an extracting and a chromogenic reagent to occur in a homogeneous medium. After the reaction, the addition of an excess of a polar solvent (e.g., water) will break down the system into two phases. The organic, now immiscible, phase almost instantaneously extracts the product of the reaction between the reagent and the analyte formed in the single phase.

It can be clearly seen that the single-phase approach shows some potential advantages that suggest its investigation as an alternative procedure for automating liquid–liquid extraction in continuous-flow systems. These advantages come mainly from the fact that a liquid–liquid flow extraction system based on single-phase principles would not require a segmentation stage because a reaction, if necessary, will be processed in a homogeneous medium. In consequence, simpler continuous-flow systems with less restrictive requirements could be employed. Also, the direct contact between reagent and the sample certainly could improve the reaction velocity, an important factor in continuous-flow analysis where the sample residence time is usually short. Further, the organic phase could, after in-line addition of excess water, be isolated in order to carry the analyte to a suitable detector.

This paper reports on the use of the single-phase liquid–liquid extraction approach in continuous-flow systems. Although, in principle, an FIA system could be used to confirm the potential of single-phase extraction, monosegmented continuous-flow analysis [11,12] (MCFA) was first evaluated because this technique allows the construction of a simple flow manifold that does not require either a segmenter or a separation device.

MCFA was introduced in 1985 by Pasquini and de Oliveira [11]. The main characteristic of this flow analysis principle is the introduction of the sample between two air bubbles, defining a monosegment. Dispersion is restricted and the two bubbles mark the regions of the flow which contain the sample. Therefore, samples can be easily identified and re-sampled [12] if necessary. Subsequently, other names as segmental flow-injection analysis have been proposed for the same principle as MCFA [13,14].

The MCFA single-phase liquid–liquid system was applied to the spectrophotometric determination of Fe(III) performed by the use of the ternary single-phase water–ethanol–IBMK + thenoyltrifluoroacetone (TTA) as extracting–chromogenic reagent.

EXPERIMENTAL

Phase diagram

A phase diagram for the water–ethanol–IBMK system is shown in Fig. 1. This diagram is employed to establish the composition (in mass %) of the ternary mixtures which will originate single-phase systems. The mixtures whose composition lies above the limit line will exist as a homogeneous solution. It should be noted that the addition of excess water to any stable single-phase mixture will bring the new composition below the

limit line and a two-phase system will be formed. The compositions of these two phases are dictated by the initial single-phase composition and by the amount of water added to it. The point marked above the limit line represents the ternary composition employed in this work. This composition has volumetric fractions in the ratio 0.62 : 0.45 : 0.50 of ethanol, aqueous sample and IBMK–TTA, respectively.

Monosegmented flow system and sample processing

Figure 2 depicts the MCFA manifold employed to evaluate the single-phase liquid–liquid extraction of Fe(III). Absolute ethanol was pumped through Viton pumping tube. The IBMK–TTA solution was pumped by displacement with water. Sample was aspirated and mixed with ethanol and IBMK–TTA solution in a 270-μl magnetically stirred glass chamber. From the chamber the mixture passes through a bubble-removal device similar to that described previously [15]. The homogeneous single phase is then pumped through a 300-μl loop and this volume is introduced into the reaction coil as a monosegment, between two air bubbles. The coil is made of 20 cm × 2 mm i.d. polyethylene tubing. A

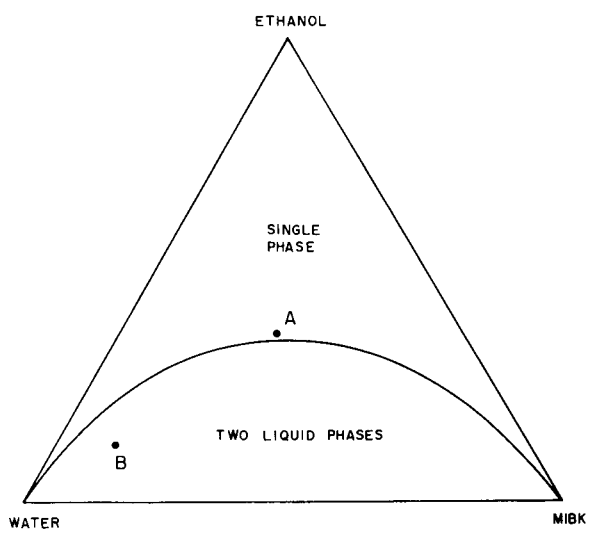

Fig. 1. Phase diagram for the ternary mixture of water, ethanol and IBMK. (A) Single-phase composition employed in this work; (B) final composition after single-phase breaking.

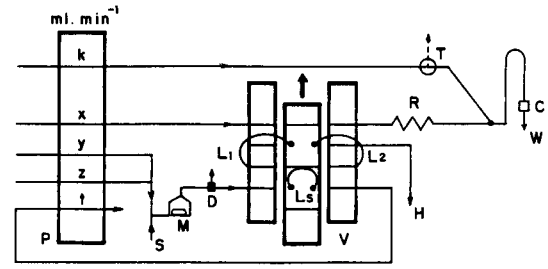

Fig. 2. Monosegmented continuous-flow manifold for single-phase liquid–liquid extraction. P = peristaltic pump; S = sample inlet; M = mixing chamber; D = bubble-removal device; V = sampler valve; Ls = 300-μl sample loop; L_1 and L_2 = 30-μl air loops; H = to water aspirator; R = reaction coil; T = three-way solenoid micro-valve; C = detector/flow cell; C = waste line; k, x, y, z and t are flow-rates equal to 2.40, 1.20 0.62 (ethanol), 0.50 (IBMK) and 1.57 ml min^{-1}, respectively.

water stream, pumped through a Tygon tube, carries the monosegment to another confluence point where an appropriate volume of saturated $NaNO_3$ aqueous solution is added.

The addition of the saturated solution is controlled by a three-way solenoid micro-valve. The valve timing is controlled automatically by a circuit that detects the passage of bubbles using optical switches in a similar manner to that described elsewhere [16]. When the first bubble passes the confluence point the valve is turned on and the saturated solution is added to the single-phase monosegment. When the second bubble has almost reached the confluence point the valve is turned off. After this operation, the monosegment has more than twice its initial volume and is carried towards the detector by the water flow.

From the confluence point, the monosegment passes through a tube in the form of an inverted U acting as a separator as shown in Fig. 3(I). The U form was made from an initial segment of 35 cm × 2 mm i.d. and a final segment of 25 cm × 3 mm i.d., both of polyethylene tubing. The end of the inverted U was connected directly to the detector glass tube.

The two phases (organic and aqueous) start to form in the ascending portion of the separator but the organic phase is dispersed in the aqueous phase. When the second bubble turns through the U section and descends in direction of the

detector, the organic phase starts to accumulate (owing to its lower density in relation to the aqueous phase) at the end of the monosegment just before the second air bubble. This bubble forms a barrier that prevents the organic phase from passing behind to the carrier water flow.

Spectrophotometric detector

A simple spectrophotometric detector [17], based on a light-emitting diode (LED) and a light-dependent resistor (LDR), was employed for on-line detection of the analytical signal. The LED has a maximum emission intensity at 560 nm. The light emitted passes perpendicularly through a 2 mm i.d. glass tube and reached the LDR, which is connected to one of the arms of a Wheatstone bridge. Changes in the light intensity reaching the LDR cause bridge imbalance and the imbalance potential is sent to a potentiometric recorder.

Analytical signal

Figure 3(II) shows a typical signal obtained on the chart recorder. The signals obtained are identified as (1) the passage of the first air bubble of the monosegment, (2) the aqueous phase originating from the broken single-phase, (3) the analytical signal which corresponds to the absorbance of the organic phase containing the extracted analyte and (4) the second bubble of the monosegment. Double peaks are observed for signals 1 and 4 owing to the refractive index change at the two liquid/gas interfaces that exist in each bubble.

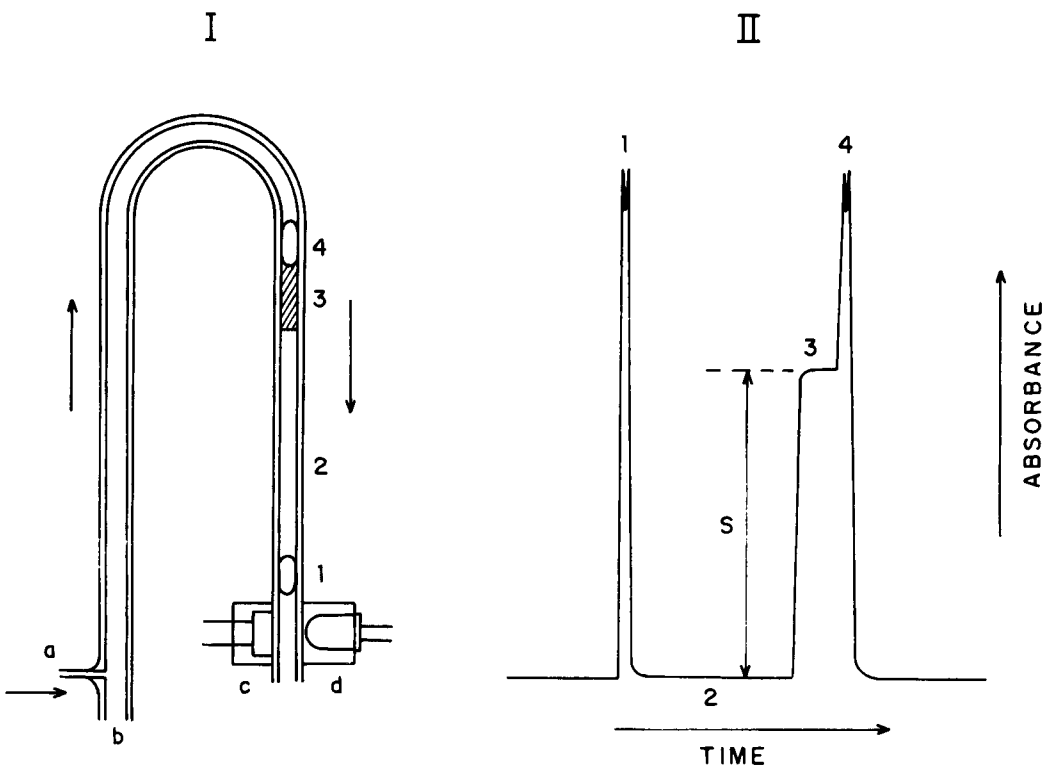

Fig. 3. (I) Schematic diagram of the final step of the single-phase liquid–liquid extraction in MCFA. a = Saturated $NaNO_3$ solution inlet; b = polyethylene tube; c = LDR sensor; d = LED source. (II) Typical analytical signal. 1 = First monosegment air bubble; 2 = aqueous phase; 3 = organic phase; 4 = second air bubble; S = analytical signal obtained during passage of the organic phase through the detector.

Reagents and solutions

The IBMK–TTA solution was prepared by dissolving the appropriate amount of analytical-reagent grade TTA in IBMK (Carlo Erba) to obtain a 0.05 M solution.

Fe(III) working standard solutions in the range 1–30 mg l^{-1} were prepared by suitable dilution of a 1000 mg l^{-1} stock standard solution. All standard solutions were in 1×10^{-3} M HNO_3 medium. The pH of the standard solutions was about 2.6.

Saturated $NaNO_3$ solution was prepared by stirring an excess of the salt in water for 1 h and filtering off the remaining insoluble salt.

RESULTS AND DISCUSSION

Calibration graphs for the Fe(III)–TTA complex present in the unbroken single-phase monosegment and for the broken (two-phase) monosegment were obtained with the MCFA system. The linear regression equations of the calibration signals for Fe(III) concentrations in the range 2–30 mg l^{-1} were $A = 0.179\ (\pm 8.8 \times 10^{-3}) C_{Fe(III)} - 0.47\ (\pm 0.98)$ with a correlation coefficient (r) of 0.997 in the single-phase monosegment and $A = 0.597\ (\pm 1.5 \times 10^{-2}) C_{Fe(III)} - 2.65 \times 10^{-2}\ (\pm 0.58)$, $r = 0.998$, after phase separation, where A is the absorbance expressed in arbitrary units (signal height in cm) and $C_{Fe(III)}$ denotes the iron(III) concentration in the sample expressed in mg l^{-1}.

A factor of 3.34 was found between the slopes of the broken (extracted) and unbroken (single-phase) calibration graphs. A ratio equal of 2.83 was expected based on the dilution of the aqueous sample in the monosegment and total transfer of the iron complex to the original IBMK volume present in the single-phase monosegment after the two phases have been formed. The increase in the absorbance could be attributed to the smaller IBMK volume obtained after the phases have been separated. However, the increase should be greater (4.5 instead of 3.3). The formation of the iron complex in the single phase, at the composition employed in this work, was verified to be close to 100%. As observed previously [6], the extraction of Fe(III) under these conditions is also nearly 100%. Therefore, the molar absorptivity of the complex or the formation of new specimens in the organic phase should be investigated in the future. Also, as the automatic procedure is different to the manual procedure [6] with regard to phase separation (stirring is found in the automatic procedure whereas in the manual procedure all efforts are made to avoid it), the real extraction efficiency of the MCFA system needs to be further evaluated.

The precision of the method was evaluated by measuring ten times a 10 mg l^{-1} solution of Fe(III). After extraction, the relative standard deviation of the ten signals was 1.5%. The broken monosegment [Fig. 3(II)] takes 45 s to pass through the detector, allowing up to 80 samples to be processed per hour.

The use of the single-phase approach to liquid–liquid extraction within an MCFA system results in a simple manifold offering high performance in terms of sample throughput and sensitivity. No segmenter is needed. Therefore, no attention needs to be paid to uniformity and stability, which is necessary when the two-phase approach is employed in continuous-flow systems.

In the single-phase approach the contact between the analyte and the extracting–chromogenic reagent is complete. The kinetics of the reaction are favourable although the monosegmented system could, if necessary, couple with long residence times [11]. In the present case, the Fe(III)–TTA reaction occurs almost instantaneously in the single phase. A short reaction coil was necessary only to transport the single phase to the break point.

Flow-injection systems could also make use of the single-phase approach. The absence of a segmenter and the favourable kinetics represent advantages over the two-phase approach. However, there will certainly be some disadvantages. Owing to the mixture of ethanol with the aqueous sample, air bubbles are formed together with the single phase in the mixing chamber. The removal of the gas bubbles is easily achieved in MCFA. Slow aspiration (slightly greater than the volume of the gas bubbles formed) also removes a small portion of a homogeneous single phase. There-

fore, this operation does not have an adverse effect on the precision. On the other hand, this process can cause serious problems if applied to an FIA system because the aspiration is not uniform and distinct portions of the sample zone can be removed from injection to injection.

Another advantage of the MCFA approach resides in the recovery of the organic phase without the use of a separation device. This feature is only possible owing to the presence of air bubbles in the system. In fact, the bubbles are important in two respects, first in relation to the identification of the portion of the flow that contains the sample. This allows, for example, the addition of the saturated $NaNO_3$ solution only in the necessary volume. In consequence, excessive consumption of the solution is avoided and detection can be effected at a slower flow-rate. The second bubble is important to keep the organic phase over the aqueous phase similarly as in a conventional batch liquid–liquid extraction procedure.

Although, in this initial work, only an organic phase (IBMK) with a lower density than water was employed, preliminary evaluation of a single phase containing water–ethanol–chloroform [9] has demonstrated that phase separation is also obtained, in almost the same way, when an organic solvent (chloroform) with a higher density than water is employed. The difference is that the phase separation occurs in the ascending portion of the inverted U. Also, a non-inverted U separator could be used if some degree of mixing between phases is to be obtained, before final separation, in order to improve the extraction ratio. Therefore, a general statement can be made regarding the separation process: phase separation will occur when the carrier flow direction is opposite to the natural tendency of the organic solvent to move up or down in the monosegment, as predicted by the density difference between the solvent and the aqueous phase. For example, if (as with chloroform) the density of the solvent is higher than that of the aqueous phase, after phase breaking, it will try to descend, to the bottom of the segment. The flow should then carry the segment upwards. The detector should be placed in the first leg of the inverted U or in the second leg of a normal U separator. Analytical signals will show the same profile as that in Fig. 3(II).

The restriction of the organic phase in a well defined zone of the monosegment allow the development of simple procedures for signal acquisition, without the requirement for phase isolation. Automatic, computer-controlled data acquisition is being developed in which the sampled points immediately before the second bubble detection are identified with the analytical signal. Also, under computer control, the organic or the aqueous phase could be re-sampled to another parallel continuous-flow manifold.

In this work, the possibility of using different ratios between the aqueous sample and IBMK was not investigated. However, the potential exists for that ratio to lead to higher enrichment factors by, for example, creating a single phase with an IBMK–sample composition of 1 + 4.

REFERENCES

1 B. Karlberg and S. Thelander, Anal. Chim. Acta, 98 (1978) 1.
2 H. Bergamin F°., J.X. Medeiros, B.F. Reis and E.A.G. Zagatto, Anal. Chim. Acta, 101 (1978) 9.
3 V. Kuban, CRC Crit. Rev. Anal. Chem., 22 (1991) 477.
4 L. Nord, K. Backstrom, L.G. Danielsson, L.G., F. Ingman and B. Karlberg, Anal. Chim. Acta, 194 (1987) 221.
5 C.A. Lucy and F.F. Cantwell, Anal. Chem., 61 (1989) 107.
6 J.F. Silva and W. Martins, Talanta, 39 (1992) 1307.
7 A. Capri Neto, MSc Thesis, UNICAMP, Campinas, 1987.
8 N.M.R.L. Alba, MSc Thesis, UNICAMP, Campinas, 1978.
9 L.H. Seron, MSc Thesis, UNICAMP, Campinas, 1981.
10 J. Silva, MSc Thesis, UNICAMP, Campinas, 1978.
11 C. Pasquini and W.A. de Oliveira, Anal. Chem., 57 (1985) 2575.
12 C. Pasquini, Anal. Chem., 58 (1986) 2346.
13 L.C. Tian, X.P. Xu and Z.L. Zhi, Anal. Chim. Acta, 238 (1990) 183.
14 J.A. Borzitsky, A.V. Dvinin, O.M. Petrukin and Yu. Urusoz, Anal. Chim. Acta, 274 (1993) 125.
15 I.L. Mattos, E.A.G. Zagatto and, A.O. Jacintho, Anal. Chim. Acta, 214 (1988) 247.
16 I.B.S. Cunha and C. Pasquini, Analyst, 117 (1992) 905.
17 C. Pasquini and I.M. Raimundo, Jr., Quim. Nova, 7 (1984) 24.

Analytica Chimica Acta, 285 (1994) 293–299
Elsevier Science B.V., Amsterdam

Multi-site detection in flow analysis

Part 3. Periodate tubular electrode with low inner volume as a relocatable detector

José A. Gomes Neto, Ana Rita A. Nogueira [1], H. Bergamin Filho and Elias A.G. Zagatto
Centro de Energia Nuclear na Agricultura, Universidade de São Paulo, Caixa Postal 96, 13400-970 Piracicaba SP (Brazil)

José L.F. Costa Lima and M. Conceição B.S.M. Montenegro
Faculdade de Farmácia, Universidade do Porto, Porto (Portugal)

(Received 17th August 1993)

Abstract

Periodate oxidation was exploited for the determination of sucrose and glycerol with potentiometric monitoring of the remaining periodate. For this task, a tubular electrode with a small inner volume and a fast response time was used in a flow-injection procedure with multi-site detection. With parallel monitoring, two almost identical systems shared the same detection unit. After peak maximum measurement, the detector was displaced to the other analytical channel, and then washing time was no longer a limiting factor with respect to sampling rate. The approach was applied to the determination of glycerol in soaps, detergents and lixivia samples. The sampling rate was improved by 85% relative to a comparable conventional flow-injection system without impairing other favourable analytical characteristics. The reagent consumption was only 190 μg of $NaIO_4$ per determination. With serial monitoring, measurements were made at two manifold sites under different sample processing conditions. In this way, sucrose was determined in sugar-cane juice and syrups by monitoring the sample zone prior to and after in-line acidic hydrolysis. The proposed system is very stable, no baseline drift being observed during 4-h operation periods. It provides 50 measurements per hour and yields precise results (R.S.D. usually $< 2\%$) in agreement with liquid chromatography. Clarification of the sample is not required.

Keywords: Flow injection; Potentiometry; Glycerol; Multi-site detection; Periodate tubular electrode; Sucrose; Waters

In flow-based methodologies with multi-site detection [1], after the measurement the detector is moved from its original site to another position. Although potentially beneficial, the approach may be limited by the inner volume of the detector, as was stressed in previous papers [1,2], where expected improvements in sampling rates were not so pronounced owing to the large inner volume of the spectrophotometric flow cell plus accessories. As tubular potentiometric detectors without an inner reference solution [3] can be constructed with very small inner volumes, they become attractive as relocatable detectors.

Oxidation by periodate is a widely used reaction in carbohydrate chemistry, and proceeds at room temperature under mild conditions [4]. It has often been used for the determination of reducing sugars and glycerol [5–7], but in flow

Correspondence to: E.A.G. Zagatto, Centro de Energia Nuclear na Agricultura, Universidade de São Paulo, Caixa Postal 96, 13400-970 Piracicaba SP (Brazil).
[1] Present address: Empresa Brasileira de Pesquisa Agropecuária, P.O. Box 339, S. Carlos 13560 SP, Brazil.

SSDI 0003-2670(93)E0518-C

analysis the relatively slow oxidation has often been the limiting factor with respect to sampling rate. This drawback is minimized by taking advantage of multi-site detection [1], especially when a flow-through detector with a small inner volume and fast response time is available.

The aim of this work was to investigate the use of a small inner-volume periodate-selective electrode [8] as a movable detector in flow systems. Two situations were considered, namely those involving parallel and those involving serial periodate monitoring.

In the former approach, two almost identical systems sharing the detector are proposed for the analysis of lixivia and waste waters with high glycerol contents in the soap industry. With serial monitoring, a flow system was developed for sucrose determination in sugar-cane juice and syrups. The sample zone was monitored at two manifold sites prior to and after partial and reproducible in-line sucrose hydrolysis.

EXPERIMENTAL

Apparatus

The system consisted of an MLW DP 2-2 peristaltic pump (Veb Labortechnik, Ilmenau, Germany), a B352 electronically operated commutator (Micronal, São Paulo, Brazil), a B375 digital potentiometer (Micronal), an REC61 strip-chart recorder (Radiometer, Copenhagen, Denmark), polyethylene tubing (0.7 mm i.d.) and accessories. The Reactor B_2 (see Fig. 2) was built up by coiling thin polyethylene tubing (6 m × 0.3 mm i.d., wall thickness 0.2 mm) around a glass cylinder (0.5 cm o.d.) which was immersed in a model 102/1 thermostated water-bath (Fanem, São Paulo, Brazil). With this long and thin B_2 coil, the temperature of the water-bath could be raised to about 60°C without the formation of air bubbles.

Working and reference (Ag/AgCl) electrodes were assembled in a Perspex device [3] which was connected to the sliding bar of the commutator. The inner volume of the potentiometric cell plus accessories was determined as 45 μl according to a procedure used previously [1].

The periodate-selective electrode was prepared as described [8]. The sensor system consisted of ca. 10% tetraoctylammonium periodate in *o*-nitrophenyl octyl ether solution which was further immobilized in PVC. The final membrane composition was ca. 30% (w/w) PVC and 70% (w/w) of the sensor solution. It should be stressed that use of *o*-nitrophenyl octyl ether as the mediator solvent resulted in improved selectivity and fast response times relative to the previously used dibutyl phthalate [8].

Solutions

All solutions were prepared with distilled, deionized water and analytical-reagent grade chemicals.

A 0.1 M $NaIO_4$ stock solution was prepared by dissolving 10.69 g of $NaIO_4$ in 500 ml of water and was kept in an amber-coloured bottle.

For the determination of glycerol, a stock standard solution [10.00% (w/v) glycerol] was standardized iodimetrically [9]. Working standard solutions containing 0.05–0.20% (w/v) glycerol were freshly prepared by dilution of the stock standard solution with water. The combined reagent for the determination of glycerol (C′ and C″, see Fig. 1) was 0.003 M $NaIO_4$–0.5 M Na_2SO_4–0.1 M acetic acid–0.1 M sodium acetate.

Bottom lixivia, industrial brine, washing solutions and waters from evaporators and condensers were collected at a soap production plant. The samples were heated (50–60°C for about 10 min) and the resulting clear solutions were manually diluted (100 g of sample plus 500 g of water). Immediately before injection into the flow system, the samples were further diluted with water.

For sucrose determination, working standard solutions [0.10–0.50% (w/v)] were prepared daily in water. A 0.50% (w/v) invert sucrose standard prepared as in previous work [6] was used to check hydrolysis. The combined reagent (R_1 in Fig. 2) was 0.002 M $NaIO_4$–0.5 M Na_2SO_4–0.01 M Na_2HPO_4–0.01 M NaH_2PO_4. C, R_2 and R_3 were water, 2.0 M H_2SO_4 and 1.9 M NaOH–0.1 M Na_3PO_4, respectively. The NaOH concentration should be accurately adjusted if the pH of the discarded stream (W, Fig. 2) lies outside the range 6.5–7.2.

Procedure

The system for the determination of glycerol (Fig. 1) consisted of two almost independent channels sharing the detection unit. It was designed according to the single-line system proposed for the analysis of residues relevant to soap production [8]. A small sample plug was intercalated into the carrier stream C′ flowing through reactor B′ towards detection site a. During sample transportation, glycerol was oxidized by periodate at pH ≈ 4.7. The baseline potential was related to the periodate concentration, and sample passage through the detector resulted in a transient signal proportional to the periodate consumed, reflecting the glycerol content in the sample. The commutator was switched a few seconds after the peak maximum was reached, intercalating the next sample into the stream C″ and displacing the movable detector to monitor at site b. During sample processing inside B″, the trailing edge of the previous sample still flowing inside B′ was discarded without flowing through

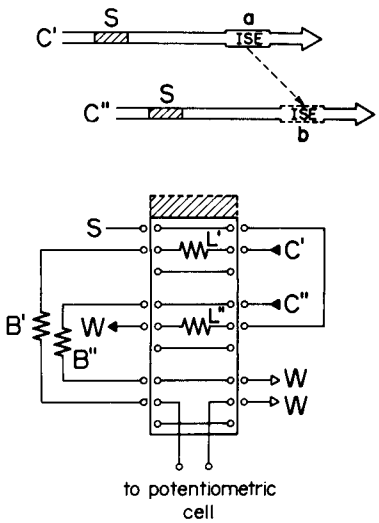

Fig. 1. Schematic representation and flow diagram of the system with parallel monitoring proposed for glycerol determination. S, sample (2.0 ml min^{-1}); L′ and L″, 6-cm (30-μl) sampling loops; C′ and C″, combined reagent (0.5 ml min^{-1}); B′ and B″, coiled reactors (100 cm); ISE, relocatable ion-selective electrode; a and b, monitoring sites; W, waste; black arrows, sites where pumping is applied; hatched area, movement of the commutator; interrupted lines, detector displacement.

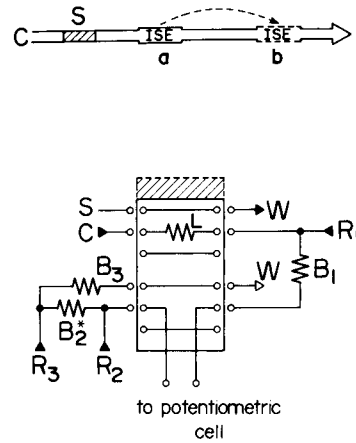

Fig. 2. Schematic representation and flow diagram of the system with serial monitoring proposed for sucrose determination. S, sample (1.0 ml min^{-1}); L, 50-cm (250-μl) sampling loop; C, water (0.4 ml min^{-1}); R_1, R_2 and R_3, reagents (0.4, 0.4 and 0.8 ml min^{-1}); B_1 and B_3, reactors (100 and 300 cm); B_2^*, heated coil (600 cm); temperature of the water-bath in which this coil and transmission line (200 cm) for R_2 addition are immersed, 60°C; other symbols as in Fig. 1.

the detector. In this way, the washing time was not a limiting factor with respect to the sampling rate. With the system in Fig. 1, effects of flow rate and commutation timing were studied.

The system for the determination of sucrose (Fig. 2) exploited serial monitoring to permit sample quantification prior to and after acidic hydrolysis. The sample was introduced into carrier stream C, reagent R_1 was added and periodate oxidation was initiated inside reactor B_1 under neutral conditions. The peak related to site a reflected mainly the concentrations of chemical species readily oxidized by periodate and reducing sugars occurring at higher concentrations such as fructose and glucose [4]. Thereafter, warm sulphuric acid solution (R_2) was added, promoting partial and reproducible sucrose hydrolysis inside the heated coil B_2. When most of the sample was flowing inside B_2, the commutator was switched to the loading position and the detector displaced downstream (site b). After neutralization of the sample zone by reagent R_3, further periodate oxidation proceeded inside coil B_3. Then, the recorded peak height related to site b referred also to the periodate consumed by the

hydrolysis products. The sucrose concentration in the sample was then evaluated after subtraction of signals related to both monitoring sites. After measurement of the peak maximum, the commutator was switched back to the position specified in Fig. 2 and the trailing edge of the dispersed zone was directly discarded. With this system, the effects of periodate concentration, flow-rates, temperature, acidity for hydrolysis and timing were studied.

RESULTS AND DISCUSSION

Determination of glycerol with parallel monitoring

The speed of the peristaltic pump is an important parameter to be considered in system design [8] as it is proportional to the washing time and to the mean available time for glycerol oxidation.

With the flow system outlined in Fig. 1, the peak heights observed for 0.20% (w/v) glycerol were 48.1, 75.0 and 119.5 mV when the flow-rate of C′ (or C″) was 1.0, 0.5 and 0.2 ml/min, respectively, which corresponded to about 30, 60 and 180 s for glycerol oxidation. Higher glycerol concentrations reaching the electrode should be avoided to prevent membrane deterioration, which was probably due to reduction of periodate ions in the membrane [8]. Therefore, the flow-rates of the sample carrier streams were set at 0.5 ml/min and the system was designed to allow a large dispersion (dispersion coefficient ca. 0.07). As a consequence, no pronounced modifications of slope, baseline stability or electrode response time were observed during extended working periods (4 h) and the electrode performance remained unchanged after at least 5 weeks. In addition, undesirable effects due to the establishment of concentration gradients along the sample zone, inherent to the single-line configuration, were not pronounced. The signal corresponding to 0.00% (w/v) glycerol was only 4.6 mV (Fig. 3). It should be stressed that the difference in peak heights for the same glycerol concentration (Fig. 3) which are not relevant in terms of the final results are due to the practical impossibility of designing identical sub-systems.

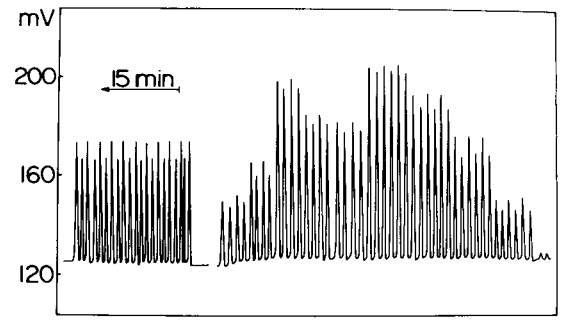

Fig. 3. Recorder tracing related to glycerol determination. The results relate to the system in Fig. 1 operated manually. From the left, recorded peaks refer to a lixivia sample processed ten times, five samples in duplicate, four standard solutions [0.20, 0.15, 0.10 and 0.05% (w/v) glycerol] in triplicate, and a blank (water) processed once. Higher signals correspond to site b.

Without detector relocation, the washing time was 55 s for a 1% carryover level (Fig. 4). This means a sampling rate of about 65 h^{-1} and a periodate consumption of 280 μg of $NaIO_4$ per determination. A remarkable improvement in sampling rate (85%) was achieved by relocating the detector immediately after measurement of the peak maximum, which reduced washing time to about 36 s. In this situation, 100 samples could be analysed per hour with a periodate consumption of 190 μg of $NaIO_4$ per determination, provided that the detector was able to monitor at the

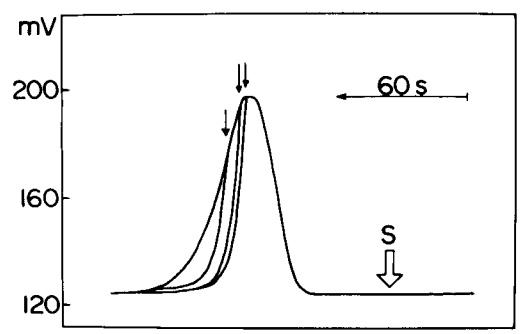

Fig. 4. Effect of detector relocation. Record tracings refer to a 0.20% (w/v) glycerol solution injected into the system in Fig. 1. All signals refer to site a. S, instant of sample injection. The broader peak corresponds to the situation without detector relocation. Instants of detector relocation/sample injection are specified by black arrows.

other channel. Studies on multi-site detection in n-channel systems with parallel monitoring are in progress.

The time for restoration of the baseline was almost independent of the instant of moving the detector (Fig. 4) and much shorter than those reported for spectrophotometric systems with multi-site detection [1,2]. This emphasizes the beneficial effect of the small inner volume of the potentiometric cell with accessories.

The proposed system does not require rigid temperature control; negligible variations in peak heights (< 2 mV) were noted after raising the ambient temperature from 25 to 30°C. It is suitable for on-line analysis related to industrial processes. A noteworthy feature of the proposed procedure is the linearity of the calibration equation ($r = 0.9982$, $n = 6$), which is a consequence of the combination of the Nerstian response of the detector and oxidation kinetics [4,6]. Reproducible results (S.D. < 0.5 mV) and a stable baseline were always observed and slope was > 58 mV per concentration decade. The accuracy can be assessed from Table 1.

Determination of sucrose with serial monitoring

The system for the determination of sucrose (Fig. 2) was based on that proposed previously for the spectrophotometric analysis of sugar-cane juice and molasses [6], but the coil volumes and flow-rates were lower in view of the small inner volume of the relocatable detector.

The flow-rate for R_3 was selected as relatively high. In this way, the need for a too concentrated R_3 solution was diminished, dilution at the last confluence became more pronounced and the ionic strength inside coil B_3 and the detector was decreased. The lengths of coils B_1 and B_3 were selected to permit similar available times for periodate reduction. Better heating conditions were attained by using a heated stream R_2 and a coil B_2 built up with thin-walled and small inner diameter tubing. The temperature of the water-bath was fixed at 60°C; increasing this temperature increased the possibility of the formation of air bubbles which impaired detection. The length of B_2 was a compromise between the available time for hydrolysis and hydrodynamic pressure. With $B_2 = 600$ cm, the mean sample residence time inside the tube was about 20 s and 32% hydrolysis was attained for sodium periodate and sulphuric acid concentrations of 0.002 and 2.0 M, respectively.

Hydrochloric acid has been widely used for sucrose hydrolysis and was also used when sucrose inversion was incorporated in flow-injection analysis [6]. However, this acid was not used here considering the need for high concentrations and the potentiometric selectivity towards chloride ($\log K^{pot} \approx -3.5$ [8]). For higher sucrose concentrations, lower periodate contents should be monitored, and the electrode response was more susceptible to the high chloride level. As a consequence, bending of the calibration graph became more pronounced, and injected solutions with sucrose concentrations $> 0.2\%$ (w/v) could not be analysed. As the potentiometric selectivity coefficient towards sulphate was more favourable ($\log K^{pot} < -5$), this drawback was circumvented by using sulphuric acid in R_2 and increasing the periodate concentration in reagent R_1.

The effects of acid concentration and temperature for hydrolysis were analogous to those already reported [6]. Lower sulphuric acid concentrations were not used; when it was < 1.0 M, the extent of hydrolysis was always $< 5\%$ On the other hand, the acid concentration could not be increased at will to avoid the need for special pumping tubes, bending of the calibration graph, high ionic strength and difficulties of pH adjustment inside coil B_3. R_2 was then chosen as 2.0 M H_2SO_4.

TABLE 1

Glycerol contents [% (w/w)] in lixivia and waters from a condenser as determined by the proposed procedure and by iodimetric titration [9].

Sample	Proposed procedure [a]	Titration [b]
Lixivia 1	32.5 (0.010)	30.0
Lixivia 2	32.7 (0.013)	32.5
Lixivia 3	35.6 (< 0.005)	35.4
Wash liquor 1	0.86 (0.007)	0.81
Wash liquor 2	0.54 (0.021)	0.59

[a] Numbers in parentheses are estimates of relative standard deviations (%), based on triplicate measurements. [b] Relative standard deviation of results $< 0.01\%$.

The periodate concentration also could not be modified at will. Preliminary tests confirmed the pronounced decrease in sensitivity [8] for concentrations > 0.01 M. A noisy baseline, slow response time and unacceptable calibration characteristics were observed for concentrations < 0.001 M. The periodate concentration in R_1 reagent was consequently selected as 0.002 M.

The HPO_4^{2-}–$H_2PO_4^-$ buffer system was chosen mainly because under neutral conditions the oxidation of fructose was faster than for other reducing agents present in the samples at significant concentrations [6,10]. Thus, the measurement reflected efficiently the amount of inverted sucrose. An increase in sensitivity could be achieved by selecting a more alkaline medium, as the oxidation of fructose would be accelerated and glucose would become relevant. At pH ≈ 10 (ammonium–ammonia buffer), the signal almost doubled but the procedure became more susceptible to the presence of other sugars. Moreover, an increase in the signal related to site a impaired the precision of the results owing to error propagation effects. The concentration of buffer components in reagent R_1 was kept low to minimize the consumption of sulphuric acid prior to hydrolysis. The phosphate concentration in R_3 was selected as a compromise between easy adjustment of pH inside coil B_3, ionic strength and solubility.

The proposed system (Fig. 2) is remarkably stable and no baseline drift is observed during extended working periods, which in turn confirms the stability of the periodate reagent. The recording tracings show two baselines (Fig. 5) corresponding to measuring sites a and b which are related to different periodate concentrations and temperatures. The difference in baseline could be minimized by adding a suitable amount of sodium periodate to R_3 and minimizing the differences in temperature between sites a and b. Experiments involving periodate addition to R_3 reagent and immersion of coil B_3 in cold water were carried out, but no pronounced improvement in results or electrode lifetime were noted. When R_3 was immersed in an ice-bath, tubing clogging due to precipitation effects was observed. Therefore, and in order to retain simplicity, the set-up outlined in Fig. 2 was maintained.

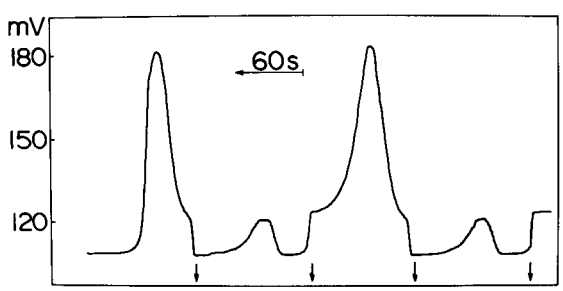

Fig. 5. Recorder tracing related to serial monitoring. The results relate to a diluted syrup sample (420 mg l^{-1} sucrose in the injected solution) processed with the system in Fig. 2. Lower and higher peaks correspond to monitoring sites a and b, reflecting situations prior to and after hydrolysis. Arrows indicate instants of detector relocation/sample injection.

The commutator can be operated any time after the peak reaches a maximum at site a provided that the baseline is restored before the sample arrives at site b. Next, commutation should be done immediately after reaching the peak maximum at site b so that most of the trailing portion of the sample zone is directly discarded. In this way, about 50 measurements can be performed per hour (Fig. 5).

The sensitivity could be improved by decreasing the flow-rates. This aspect was not exploited here in view of the high sucrose contents in the samples. As the system was designed with large dispersion, caramelization was not observed and the samples could be run without prior clarification.

The proposed procedure is potentially applicable to industrial process monitoring associated with sugar and ethanol production, as it is not susceptible to interferences by ethanol at concentrations up to 10% (v/v). As partial sucrose hydrolysis is involved, a precisely controlled water-bath should be available. Here, a 10% increase in the slope of the calibration equation was observed after a 1°C temperature increase. Analogously to the system of Fig. 1, good linearity of the calibration graph was attained.

Metal interferences are also negligible. For 10 mg l^{-1} of Mn(II), Mn(VI), Cu(II) and Cr(VI) in the injected solution, no measurable influence was observed on either the blank or the analytical

signals. Fe(III) concentrations higher than 5 mg l^{-1} cannot be tolerated. However, such levels are unlikely to be found in the assayed samples.

Results are obtained by expressing peak heights related to sites a and b as "apparent sucrose concentrations" and subtracting them. For this, both sucrose and inverted sucrose standards are needed. For most of the assayed samples, the signal related to site a was < 10% relative to that recorded at site b (see also Fig. 5). Therefore, a decrease in accuracy due to the presence of other species reacting with periodate and to error propagation effects is usually not relevant.

For a typical sugar-cane juice, the relative standard deviation (R.S.D.) of the results was < 2% for seven replicate determinations. A better precision (R.S.D. < 0.01%) was found for syrup analysis. After running ten juice samples already analysed by LC [11], no statistical differences between the two methods at the 95% confidence level were found.

Conclusions

Small inner volume detectors with fast response times are excellent as relocatable detectors, especially for parallel monitoring. With regard to this point, the system shown in Fig. 1 has been used in large-scale analyses without any major problems. The detector can be moved any instant after the peak maximum has been reached. Manual operation of the system is preferred.

Regarding serial monitoring, the beneficial effects of detector relocation are more worthwhile at site b (Fig. 2). As the trailing edge of the sample zone is not directly discarded after measurement at site a, the washing time of the first peak is not so relevant (see also Fig. 5). The system requires strict timing control, and in this case manual operation is not feasible.

Both systems can also be designed with computer-controlled three-way valves in order to improve versatility. Studies on this aspect are in progress.

This work was supported by the EC (Project CI1* CT92-0052), CNPq and JNICT. I.L. Mattos and S.M.B. Brienza are thanked for their participation in the earlier stages of the work. Funds from STRDA/P/CEN/554/92 Project are greatly appreciated.

REFERENCES

1 E.A.G. Zagatto, H. Bergamin F°., S.M.B. Brienza, M.A.Z. Arruda, A.R.A. Nogueira and J.L.F.C. Lima, Anal. Chim. Acta, 261 (1992) 59.
2 A.R.A. Nogueira, S.M.B. Brienza, E.A.G. Zagatto, J.L.F.C. Lima and A.N. Araújo, Anal. Chim. Acta, 276 (1993) 121.
3 J.L.F.C. Lima, M.C.B.M. Montenegro and A.M.R. Silva, J. Flow Injection Anal., 7 (1990) 19.
4 E.L. Jackson, in R. Adams, W.E. Bachmann, L.F. Fieser, J.R. Johnson and H.R. Snyder (Eds.), Organic Reactions, 4th edn., Vol. 2, Wiley, New York, 1947, pp. 341–364.
5 E.P. Diamandis and T.P. Hadjiioannou, Analyst, 107 (1982) 1471.
6 E.A.G. Zagatto, I.L. Mattos and A.O. Jacintho, Anal. Chim. Acta, 204 (1988) 259.
7 E.V. Willeman, Lever Brothers, UK, personal communication, 1983.
8 M.C.B.S.M. Montenegro, J.L.F. Costa Lima, I.L. Mattos, G. Oliveira Neto, J.A. Gomes Neto and E.A.G. Zagatto, Talanta, 40 (1993) 1563.
9 American Oil Chemists Society, Official Methods and Recommended Practices of the AOCS, 4th edn., Section D, Sampling and Analysis of Soap and Soap Products, AOCS Tentative Method Da 23-56, AOCS, Champaign, IL, 1991.
10 C.E. Efstathiou and T.P. Hadjiioannou, Anal. Chim. Acta, 89 (1977) 55.
11 C.O. Mariano and J.F. Silva, Jr., Sugar Azucar, 80 (1985) 31.

Analytica Chimica Acta, 285 (1994) 301–308
Elsevier Science B.V., Amsterdam

Potential of the continuous addition of reagent technique for chemiluminescent reaction-rate determinations

Juana Cepas, Manuel Silva and Dolores Pérez-Bendito

Department of Analytical Chemistry, Faculty of Sciences, University of Córdoba, E-14004 Córdoba (Spain)

(Received 16th June 1993; revised manuscript received 16th September 1993)

Abstract

The chemiluminescent (CL) reaction between luminol and hydrogen peroxide in the presence of copper(II) was used to assess the potential of the continuous addition of reagent (CAR) technique for CL determinations. This approach allows this type of reaction to be studied in terms of reaction rate, so maximum reaction-rate measurements can be compared with classical peak height measurements. The reaction-rate method provided better analytical features in the CL determination of copper(II): dynamic range, 1–700 ng ml^{-1}; precision (R.S.D.), ca. 3%; sample throughput, 48 samples h^{-1}. In addition, the CAR technique facilitates thorough, reproducible mixing of sample and reagents, in addition to recording the whole CL response curve and altering the rate of the CL process, which can be monitored with a straightforward data acquisition system.

Keywords: Chemiluminescence; Continuous addition; Copper; Reaction-rate determinations

Chemiluminescence (CL) reactions have proved to be powerful means for detecting various substances at very low concentrations [1–3]. Many CL reactions are very fast, so they give rise to imprecise measurements owing to irreproducible mixing of sample and reagents; consequently, systems for monitoring CL reactions should be designed primarily according to how sample and reagents are to be mixed. Several approaches have been developed to overcome the problems posed by discrete sampling devices [4–7], the flow-injection technique [8–14] being the most currently alternative. In our laboratory, the stopped-flow technique has been used to ensure reproducible mixing of sample and reagents in CL reactions, with the additional advantage that the whole CL intensity vs. time profile can thus be recorded [15–17]. The wealth of information provided by the whole transient signal allows CL to be monitored through reaction-rate measurements; in this way, the CL formation and decay rates can be related to the analyte concentration, thereby improving on the precision and selectivity of classical measurement parameters (e.g., peak hight intensity and area under the CL emission–time curve) [15].

In this work we studied the potential of the continous addition of reagent (CAR) technique for CL determinations. The theoretical foundation of the CAR technique was described elsewhere [18], and its applicability has been shown in a number of individual analyses and multideterminations on clinical, pharmaceutical, and agricultural samples based on various reactions [19–21]. The features of this approach rely on the following facts: (a) it provides thorough repro-

Correspondence to: D. Pérez-Bendito, Department of Analytical Chemistry, Faculty of Sciences, University of Córdoba, E-14004 Córdoba (Spain).

SSDI 0003-2670(93)E0524-B

ducible mixing of sample and reagents as a result of the special manner in which this operation is performed; (b) it enables recording of the whole CL response curve, which includes a wide linear portion on which CL determinations can be performed by reaction-rate measurements; and (c) it allows the rate of a given reaction to be altered (decreased, on account of its second-order nature), so the CL reaction can be monitored with a straightforward data acquisition system or even a simple recorder to obtain the whole CL response curve and subject it to appropriate measurements with a high accuracy. In this work, the CAR approach was tested on the determination of copper(II) by its enhancing effect on the classical reaction between luminol and hydrogen peroxide.

EXPERIMENTAL

Reagents

All chemicals used were of analytical-reagent grade and solutions were prepared in distilled water. A standard copper(II) solution was made by dissolving 1.000 g of pure copper metal in the minimum volume of (1 + 1) nitric acid and diluting to exactly 1 l with 1% (v/v) nitric acid. More dilute solutions were prepared by appropriate dilution with purified distilled water. Luminol was used as supplied to prepare a 1.75×10^{-3} M stock solution by dissolving 0.309 g of the compound in 0.1 M sodium carbonate (final pH 12.3, adjusted with sodium hydroxide) in a 1-l volumetric flask. Dilute solutions were prepared as needed. A stock solution (1.5 M) of hydrogen peroxide was made daily by dilution of concentrated (30%) hydrogen peroxide.

Apparatus

The instrumental set-up used to implement the CAR technique in CL determinations consisted of an addition unit composed of an autoburette (Metrohm Dosimat 665) and a stirrer which was fitted to a spectrofluorimeter (Perkin-Elmer 650-10S) operated in its energy mode (the band width of the emission monochromator was set at 20 nm) and furnished with a reaction vessel and a data acquisition and processing unit consisting of a PC compatible computer (Mitac PC-AT 12 MHz) equipped with a PC-Multilab PCL-711 ADC running a program developed by the authors for application of reaction-rate methods to CL determinations. This program performs the calculation of the maximum reaction rate and the maximum CL intensity as well as the calibration plots using both measured parameters.

Procedure

The reaction vessel of the CAR system was filled with a volume of the standard copper(II) solution containing between 100 ng and 7 μg, 2.0 ml of 1.75×10^{-4} M luminol at pH 12.3, 5.0 ml of 4.0 M sodium chloride and distilled water up to a final volume of 10 ml. Under these conditions, the final pH in the reaction vessel was 11.8. The reaction was started by adding 1.5 M hydrogen peroxide solution from the autoburette at a rate of 1 ml min^{-1}, with stirring. The light output of the reaction taking place in the reaction vessel was sensed by the spectrofluorimeter an at emission wavelength of 425 nm. The computer system recorded the full CL signal vs. time profile and calculated the two measured parameters (maximum reaction rate, determined within the first 5 s of reaction development, and peak-height), which were related to the copper(II) concentration by means of linear calibration plots.

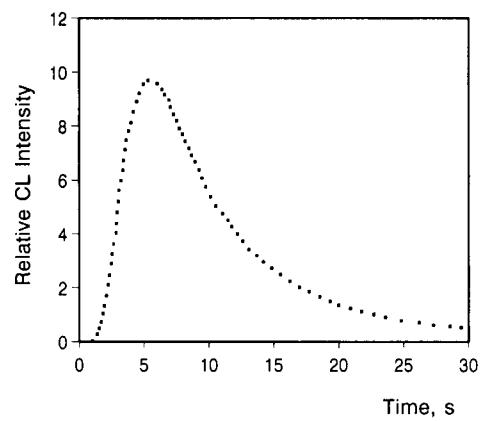

Fig. 1. CL intensity vs. time profile obtained in the CL-CAR determination of 30 ng ml^{-1} copper(II). Conditions: 1.5 M hydrogen peroxide, 1.0 ml min^{-1} addition rate, 3.5×10^{-5} M luminol, 2.0 M sodium chloride, pH 11.8.

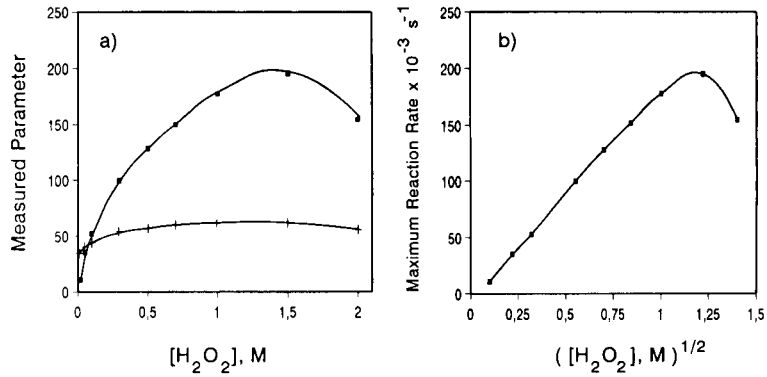

Fig. 2. (a) Dependence of the measured parameters on the hydrogen peroxide concentration; and (b) effect of the square root of oxidant concentration on the maximum reaction rate. (■) Maximum reaction rate ($\times 10^{-3}$ s^{-1}) and (+) peak height ($\times 10^{-2}$ V). Conditions: 100 ng ml^{-1} copper(II), 3.3×10^{-4} M luminol, 5.0 ml min^{-1} addition rate.

RESULTS AND DISCUSSION

The aim of this work was to assess the performance of the CAR technique in CL determinations. For this purpose, in a first stage, the quantitative aspects of the copper(II)/luminol/hydrogen peroxide system were studied by evaluating the influence of chemical and instrumental variables on the system. In a second step, the analytical features of the CL determination of copper(II) were determined and compared with those achieved by using other instrumental approaches.

Placement of luminol and hydrogen peroxide, the reagents for the application of the CAR technique to the copper(II)/luminol/hydrogen peroxide system was studied first. Preliminary experiments showed the sensitivity to copper(II) to be higher when hydrogen peroxide was placed in the addition unit. This also allowed the concentration of hydrogen peroxide in the autoburette to be varied over a wide range (high luminol concentrations in the autoburette gave rise to solubility problems). Figure 1 shows typical CL response curve provided by this approach using the spectrofluorimeter at 425 nm, after processing by the data acquisition system. As can be seen, the CL reaction was developed in a measurable time (ca. 30 s) in contrast to faster development in other mixing systems (ca. 5 s with the stopped-flow technique). This is of great interest for monitoring CL reactions since the CAR technique slows them down. In addition, the CL response–time

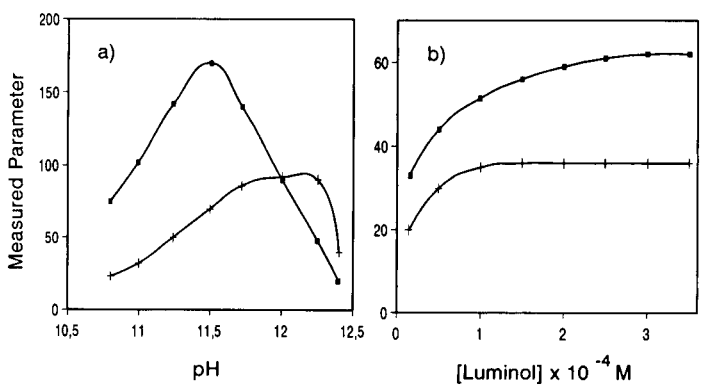

Fig. 3. Dependence of the measured parameters on (a) pH and (b) the luminol concentration. (■) Maximum reaction rate ($\times 10^{-3}$ s^{-1}) and (+) peak height ($\times 10^{-2}$ V). Conditions: (a) 75 ng ml^{-1} copper(II), 3.3×10^{-4} M luminol, 1.5 M hydrogen peroxide and 5.0 ml min^{-1} addition rate; (b) 50 ng ml^{-1} copper(II), 1.5 M hydrogen peroxide, 5.0 ml min^{-1} addition rate, pH 11.8.

curve includes a wide linear portion in its rise zone, arising from very nature of the CAR technique, which can readily be used to calculate the formation or maximum reaction rate by simple linear regression. This reaction-rate method and that based on measurement of the maximum CL intensity or peak height were selected methods for evaluating data in order to investigate the effect of variables and optimize them for the CL determination of copper.

Effect of variables

The effect of the hydrogen peroxide concentration added from the autoburette was studied over a broad range, viz. between 10^{-2} and 2.0 M. The results obtained by using maximum reaction rates and peak heights are shown in Fig. 2a. As can be seen, the maximum reaction rate increased with increasing hydrogen peroxide concentration up to 1.5 M, above which a quenching effect was observed; on the other hand, peak height measurements were less markedly variable. Figure 2b shows the variation of the maximum reaction rate with the square root of the oxidant concentration. Consistent with the theoretical foundation of the CAR technique [18], the two parameters were found to be linearly related. A hydrogen peroxide concentration of 1.5 M was chosen for further experiments based on the observed dependence of both measured parameters.

The effect of the pH on the CL reaction is shown in Fig. 3a; as can be seen, a strongly basic solution was required for the maximum development of the CL reaction. However, the maximum values obtained for each measured parameter were slightly different: the maximum reaction rate peaked at pH 11.5, whereas the peak height was maximal at pH ≈ 12. The difference between both can be ascribed to the different relative contributions of the formation (maximum reaction) and decay rate to the peak height of the CL signal. In fact, eventhough the maximum reaction rate started to decreased above pH 11.5, if the decay rate was affected to a similar extent, then the maximum signal achieved in the CL reaction would be virtually constant (pH between 11.7 and 12.2). pH 11.8, adjusted with 10.0 ml of 1.0 M sodium carbonate (pH 12.3), was chosen for further experiments, as a compromise. The same carbonate solution was also used to prepare that of luminol, which was thus at an appropriate pH for development of the CL reaction.

The influence of the luminol concentration on the CL reaction is illustrated in Fig. 3b. The measured parameters increased steadily with increasing luminol concentration. Virtually stable responses were obtained at concentrations above 2.0×10^{-4} M; a 3.3×10^{-4} M luminol concentration (10 ml of 2.0×10^{-3} M in 60 ml of the above-mentioned basic solution) was eventually chosen for subsequent work. This solution provided the maximum response after 24 h at room temperature [15], after which it remained stable for at least 4 weeks.

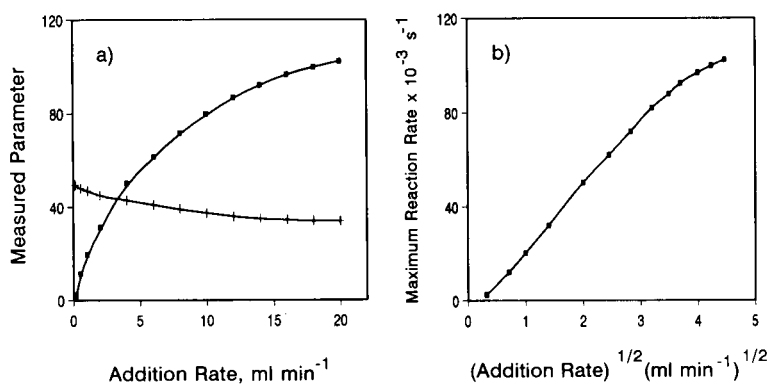

Fig. 4. Effect of the addition rate on the CL reaction. (a) Influence on (■) the maximum reaction rate ($\times 10^{-3}$ s^{-1}) and (+) peak height ($\times 10^{-2}$ V); (b) classical plot of maximum reaction rate versus square root of addition rate. Conditions: 50 ng ml^{-1} copper(II), 3.3×10^{-4} M luminol, 1.5 M hydrogen peroxide, 6.0 ml min^{-1} addition rate, pH 11.8.

The effect of the rate of addition of hydrogen peroxide (1.5 M) was assessed over a wide range (between 0.1 and 20 ml min^{-1}). The CL intensity vs. time curves obtained behaved disparately towards maximum reaction rate and peak height measurements, as shown in Fig. 4a. Figure 4b shows a typical linear plot of maximum reaction rate vs. square root of addition rate, consistent with theoretical postulates of the CAR technique [18]; the linear dependence was observed up to an addition rate of ca. 16 ml min^{-1}. A rate of 6.0 ml min^{-1}, which lay within the straight portion of the plot, was selected for further experiments. While higher addition rates resulted in shorter reaction times, they also decreased maximum CL intensities.

The initial sample volume, V_0, is a central instrumental variable in the CAR technique. Thus, V_0 normally ranges between 60 and 80 ml, which results in a high reagents consumption and it is accasionally inappropriate for the determination of species in minute amounts of samples (e.g., biological, forensic and same geological materials). The above described experiments were performed using a special rectangular reaction vessel ($100 \times 40 \times 40$ mm, $v \approx 100$ ml) made of Herasil quartz whose sides were optically polished (V_0 was 60 ml), furnished to the spectrofluorimeter. A minireaction vessel was used in this work to reduce the initial sample volume. So, the spectrofluorimeter sample compartment was replaced with small, commercially available magnetic stirrer which can support a 25-ml beaker placed in front of the photomultiplier. With this device, V_0 can be decreased down to ca. 10 ml. Using this instrumental set-up required changing the above-selected values of the variables. Thus, the new optimal concentration of luminol was obtained by adding 2.0 ml of 1.75×10^{-4} M solution in 0.1 M sodium carbonate (pH 12.3); also, the addition rate was decreased by a factor of 6 (V_0 was reduced from 60 to 10 ml), so the 1.5 M hydrogen peroxide solution was added from the autoburette at 1.0 ml min^{-1}.

The influence of species with potential matrix effects on the CL determination of copper(II), viz. the presence of electrolytes and solvents modifying the ionic strength and dielectric constant, respectively, of the reaction medium, was also tested. In both cases, the values obtained were referred to the increment in these parameters from the above-selected conditions. Ionic strengths (adjusted with sodium chloride) up to 2.5 M behaved similarly towards both measured parameters, as shown in Table 1. These results are significant to the application of the proposed method to the determination of copper in real samples; however, if a high ionic strengths were used, the contribution of this parameter from the real sample would be virtually negligible. A 2.0 M concentration was chosen which also increased the sensitivity of the CL determination, especially when reaction-rate measurements were performed. Variations in the dielectric constant (adjusted with methanol and ethanol) had virtually

TABLE 1

Influence of the matrix composition on the CL determination of copper(II)

Variable	Maximum reaction rate (10^{-2} s^{-1})	Peak height (10^{-1} V)
Sodium chloride (M)		
0	6.4	4.5
0.05	7.0	4.6
0.10	7.4	4.8
0.25	8.4	4.8
0.50	10.0	5.1
1.0	12.4	5.4
1.5	13.8	5.7
2.0	14.2	6.2
2.5	14.3	6.3
Ethanol content (%)		
0	14.1	6.3
3.3	10.0	4.8
6.6	8.0	4.5
10	7.0	4.5
13.3	6.5	5.0
16.6	6.7	5.5
33.3	6.0	6.5
Methanol content (%)		
0	13.1	5.8
3.3	9.4	5.2
6.6	8.3	5.1
10	7.3	5.1
13.3	6.5	5.2
16.6	6.0	5.3
25	5.2	5.6
33.3	4.8	5.8

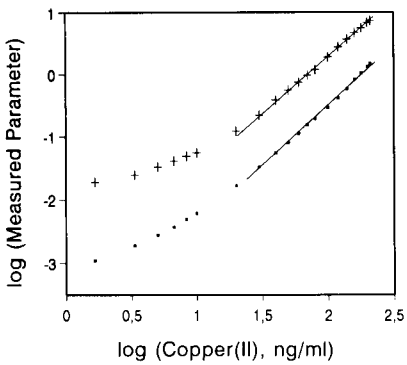

Fig. 5. Log–log calibration curves for the determination of copper(II) by the luminol/hydrogen peroxide reaction as implemented by the CAR technique at 3.5×10^{-4} M luminol concentrations. (■) maximum reaction rate and (+) peak height measurements. Other experimental conditions as described in Procedure.

no effect on the peak height of the CL signal, but decreased the maximum reaction rate (see Table 1). Therefore, these solvents should not be used in the CL determination of copper, which poses no special problems since the treatment to which real samples must be subjected for determining this metal ion usually involves no organic solvents.

Analytical results

Solutions containing different amounts of copper(II) were analysed under the selected conditions by the maximum reaction rate and peak height methods; the log–log working curves obtained are shown in Fig. 5. As can be seen, there was no linear relationship between measurements and the concentration of copper(II); however, these plots can be fitted to the equation $y = a + bx^2$, where y is the measured parameter, x the copper(II) concentration and a and b two constants. Thus, the following equations were obtained in the CL determination of copper:

maximum reaction rate

$$= -9.5\times10^{-4} + 3.3\times10^{-5}[\text{copper(II)}]^2 \quad (n = 20,\ r = 0.998) \qquad (1)$$

peak height

$$= 7.1\times10^{-3} + 1.7\times10^{-4}[\text{copper(II)}]^2 \quad (n = 20,\ r = 0.997) \qquad (2)$$

where the copper(II) concentration is expressed in ng ml^{-1}. By using these plots, the determination of copper(II) was feasible over a wide range (1–210 ng ml^{-1}).

Although this option allows the mathematical linearization of the working curves, it is also interesting to explain their shapes chemically (in other words, to implement chemical linearization). As shown in Fig. 5, there is a virtually linear dependence of the measured parameters on the copper(II) concentration at high concentrations of this metal ion (above ca. 50 ng ml^{-1}). Deviations at lower concentrations can be attributed to a decrease in the actual concentration of copper(II) in the reaction vessel due to the potential formation of the luminol–copper(II) complex, which was previously reported in the literature [22]. Thus, if the working curves are obtained in the presence of lower luminol concentrations, a linear dependence should be found at lower copper(II) concentrations. This is confirmed by Fig. 6, where straight lines were obtained at the maximum reaction rate [between 10 and 700 ng ml^{-1} copper(II)] and peak height [between 10 and 250 ng ml^{-1} copper(II)], in the corresponding log–log working curves. The luminol concentration used in these experiencies was 3.5×10^{-5} M, i.e., ten times lower than that used in Fig. 5.

It is interesting to note the behaviour observed when the CL reaction was developed at high

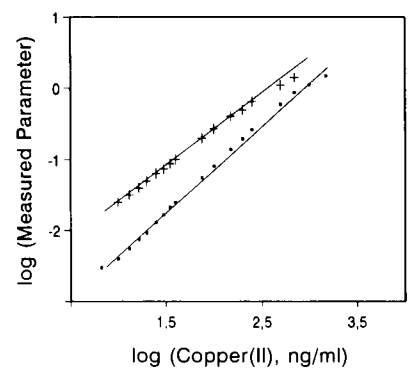

Fig. 6. Log–log calibration curves for the determination of copper(II) by the luminol/hydrogen peroxide reaction at 3.5×10^{-5} M luminol concentration. (■) maximum reaction rate and (+) peak height measurements. Other experimental conditions as described in *Procedure*.

TABLE 2

Comparison of the performance of the reaction-rate and peak height methods in the CL determination of copper(II) using 3.5×10^{-5} M luminol by the CAR technique

Figure of merit	Maximum reaction-rate method	Peak height method
Dynamic linear range (ng ml^{-1})	10–700	10–250
Detection limit (ng ml^{-1}) [a]	0.30	0.25
Precision (R.S.D.) (%)	2.48 [b]	3.66 [b]
	5.05 [c]	7.12 [c]
Sample frequency (h^{-1})	48	30

[a] [Luminol] = 3.5×10^{-4} M. [b] [Cu(II)] = 5 ng ml^{-1}. [c] [Cu(II)] = 40 ng ml^{-1}.

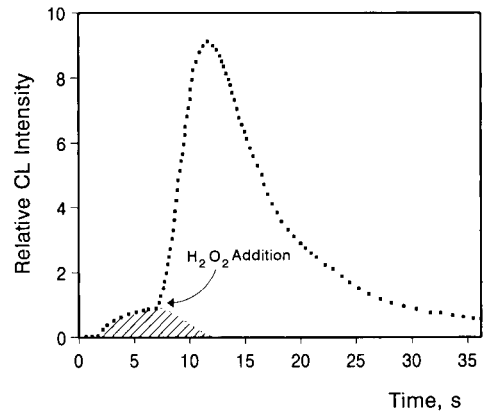

Fig. 7. Effect of dissolved oxygen on the CL determination of copper(II). The shaded portion denotes reaction development with no addition of hydrogen peroxide from the autoburette. The other portion corresponds to the normal CAR procedure (oxidant addition). [Copper(II)] = 300 ng ml^{-1} and the other experimental conditions as described in *Procedure*.

copper(II) concentrations (above 250 ng ml^{-1}). The CL started before any H_2O_2 was added owing to the presence of dissolved oxygen, which acted as an oxidant (shaded portion in Fig. 7); when H_2O_2 was added, the typical CL-CAR curve was recorded. This phenomenon had a slight effect on maximum reaction-rate measurements, which decreased somewhat at as a result, and a more marked effect on peak height measurements if data acquisition was started simultaneously with H_2O_2 addition. The decrease in the maximum reaction rate confirms the known fact that the metal does not have a purely catalytic effect on this CL reaction. While the reaction is due to the atmospheric oxygen, part of the copper becomes inactive and hence unrecyclable.

Based on these experiments, two different procedures can be used for the CL determination of copper(II): for concentrations between 10 and 700 ng ml^{-1}, the best luminol concentration is 3.5×10^{-5}, whereas for lower concentrations (between 1 and 10 ng ml^{-1}) 3.5×10^{-4} M luminol can be used in conjunction with Eqns. 1 and 2 to run calibration graphs.

Other analytical features were determined by using the maximum reaction rate and peak height methods (Table 2). The detection limits given were calculated according to IUPAC [23] by using Eqns. 1 and 2 for the calibration graphs; the precision of the proposed methods was checked on 11 samples containing copper(II) concentrations within both calibration curves: 5.0 and 40 ng ml^{-1} copper(II); the sample throughput was calculated from the time taken to perform three replicate analyses including sample changeover in the CAR system (ca. 20 s). As can be seen, both measured parameters can be used for the CL determination of copper(II); however, reaction-

TABLE 3

Comparison of the copper(II) dynamic ranges/detection limits afforded by the proposed CAR method and other recent CL procedures

System	Dynamic range or detection limit (ng ml^{-1})	Observations	Ref.
Luminol/H_2O_2	1–20	Use of a copolymer as enhancer	24
Luminol/H_2O_2	5	FIA system coupled to ion chromatography	25
Luminol/MnO_4^-	10–2000	Inhibitory effect of copper(II)	26
Luminol/H_2O_2	1–700	Reaction-rate measurements by the CAR technique	This paper
	0.3		

TABLE 4

Selectivity provided by the different measurement methods used for the CL determination of 50 ng copper(II) ml^{-1}

Metal ion	Tolerated concentration ($ng\ ml^{-1}$)		Selectivity factor [a]
	Maximum reaction rate	Peak height	
Co(II)	100	50	2.0
Fe(III)	100	100	1.0
Mn(II)	100	50	2.0
Cr(III)	< 50	< 50	–
Ni(II)	50	50	1.0
Hg(II)	5000	5000	1.0
Ag(I)	5000	5000	1.0

[a] Ratio between the tolerated concentrations by the reaction-rate and peak height method.

rate measurements provide quite good values of all the parameters assayed.

We believed it was of interest to compare the proposed method (reaction-rate measurements) with other recently reported methods based on similar chemical systems. The results in Table 3 show that the CAR method is a useful alternative for the CL determination of copper(II), as it provides a lower detection limit and wider dynamic range than the other methods, and requires very simple intrumentation.

The species tested in the selectivity study were those metal ions that show an enhancing effect on the reaction of luminol with hydrogen peroxide. The maximum tolerated limit of each foreign species assayed was taken to be 100 for a copper(II) concentration of 50 ng ml^{-1}. As can be seen from Table 4, the selectivity was better for the reaction-rate measurement method because of its kinetic nature. A selectivity factor (reaction-rate versus peak height measurements) of 2.0 was found for cobalt(II) and manganese(II), two metal ions that are usually determined by these CL reactions. A similar behaviour was found when decay rate measurements were used in stopped-flow CL spectrometry [15].

These analytical features testify to the reliability of reaction-rate measurements for the CL determination of copper(II) and the usefulness of the CAR technique for monitoring CL reactions.

The authors gratefully acknowledge financial support from the Dirección General Interministerial de Ciencia y Tecnología (DIGICyT) for the realization of this work as part of Project PB91-0840.

REFERENCES

1 M.L Grayeski, Anal. Chem., 59 (1987) 1243A.
2 J.S. Lancaster and P.J. Worsfold, Anal. Proc. (London), 26 (1989) 362.
3 S.W. Lewis and P.J. Worsfold, Anal. Proc. (London), 29 (1992) 10.
4 U. Isacsson and G. Wettermark, Anal. Chim. Acta, 83 (1976) 227.
5 D.F. Marino and J.D. Ingle, Jr., Anal. Chem., 51 (1979) 2051.
6 L.J. Kricka and G.H.G. Thorpe, Analyst, 108 (1983) 1274.
7 N. Dan, M.L. Lau and M.L. Grayeski, Anal. Chem., 63 (1991) 1766.
8 A.A. Alwarthan and A. Townshend, Anal. Chim. Acta, 196 (1987) 135.
9 S.A. Al-Tamrah and A. Townshend, Anal. Chim. Acta, 202 (1987) 247.
10 K. Hool and T.A. Nieman, Anal. Chem., 60 (1988) 834.
11 B. Yan and P.J. Worsfold, Anal. Chim. Acta, 236 (1990) 287.
12 R.E. Milofsky and J.W. Birks, Anal. Chem., 62 (1990) 1050.
13 N. Hanakoa, H. Tanaka, A. Nakamoto and M. Takada, Anal. Chem., 63 (1991) 2680.
14 K. Robards and P.J. Worsfold, Anal. Chim. Acta, 266 (1992) 147.
15 D. González-Robledo, M. Silva and D. Pérez-Bendito, Anal. Chim. Acta, 217 (1989) 239.
16 D. González-Robledo, M. Silva and D. Pérez-Bendito, Anal. Chim. Acta, 228 (1990) 123.
17 S. Ventura, M. Silva and D. Pérez-Bendito, Anal. Chim. Acta, 266 (1992) 301.
18 A. Velasco, M. Silva and D. Pérez-Bendito, Anal. Chem., 64 (1992) 2359.
19 D. Pérez-Bendito, M. Silva and A. Gómez-Hens, Trends Anal. Chem., 8 (1989) 302.
20 M. Silva, Analyst, 118 (1993) 681.
21 J. Cepas, M. Silva and D. Pérez-Bendito, Analyst, 118 (1993) 923.
22 R. Delumyea, Ph.D Thesis, Wayne State University, Detroit, MI, 1974.
23 G.L. Long and J.D. Winefordner, Anal. Chem., 55 (1983) 712A.
24 H. Karatani, Anal. Sci., 4 (1988) 393.
25 B. Yan and P.J. Worsfold, Anal. Chim. Acta, 236 (1990) 287.
26 X. Lu, M. Lu, W. Shi and F. Yin, Huanjing Huaxue, 9 (1990) 69.

Analytica Chimica Acta, 285 (1994) 309–320
Elsevier Science B.V., Amsterdam

Chemiluminescent detection of amino acids using in situ generated $Ru(bpy)_3^{3+}$

Warren A. Jackson and Donald R. Bobbitt

Department of Chemistry and Biochemistry, University of Arkansas, Fayetteville, AR 72701 (USA)

(Received 8th June 1993; revised manuscript received 8th September 1993)

Abstract

A technique for the detection of underivatized amino acids based on the chemiluminescent (CL) reaction between in situ generated $Ru(bpy)_3^{3+}$ and the amino acid is described. Glassy carbon was found to be an ideal material for the in situ generation of $Ru(bpy)_3^{3+}$ from $Ru(bpy)_3^{2+}$ in alkaline pH in the presence or absence of an organic modifier such as acetonitrile. The CL emission from the glassy carbon thin-layer flow cell used for the in situ studies was found to be dependent upon the concentration of $Ru(bpy)_3^{2+}$ in the carrier buffer, the buffer flow-rate through the cell, and the applied potential at the working electrode. The detection scheme was applied to high performance ion-exchange chromatography (HPIEC) by utilizing a column packed with a polystyrene–divinylbenzene anion-exchange resin. The technique was found to provide a linear response over 3 orders of magnitude for leucine, a representative amino acid. Limits of detection (LOD) ranged from 100 fmol for proline to 22 pmol for serine at a S/N of 6. The CL–flow-injection analysis response of injected leucine was found to decay less than 8% over the course of 40 h of continuous electrolysis of $Ru(bpy)_3^{2+}$ in the detection cell. The method is also shown to be applicable to the sensitive detection of PTH–glycine. Arguments toward the future miniaturization of the detection scheme in order to facilitate application to capillary electrophoresis and subsequent development of new protein sequencing methodologies will be presented.

Keywords: Chemiluminescence; Amino acids; $Ru(bpy)_3^{3+}$

Amino acid analysis continues to be an important area of investigation in the fields of chemical and biochemical analysis. Improvements in amino acid analysis and protein sequencing methodology are essential for the continued advancement of many areas of biotechnology and genetic engineering, including those involving recombinant DNA procedures and gene cloning [1]. Currently available techniques for amino acid analysis usually involve pre- or post-column derivatization to enhance detection, since most amino acids have no inherent fluorophore or chromophore. These derivatization methods may involve reaction of the amino acid with either ninhydrin [2], phenylisothiocyanate [3], dansyl chloride [4], *o*-phthalaldehyde [5], 9-fluorenylmethyl chloroformate or other derivatizing agents [6] in order to facilitate detection using conventional UV–visible or fluorescence spectroscopy. Other methods involve attachment of a chemiluminescent (CL) probe to the amino acid [7,8]. In general, preparation of amino acid derivatives can be problematic as the procedures are often labor intensive, some derivatives may not be stable, and the moiety added to enhance detection may dominate the physio-chemical properties of the complex. This can complicate the separation of the various amino acid derivatives.

Correspondence to: D.R. Bobbitt, Department of Chemistry and Biochemistry, University of Arkansas, Fayetteville, AR 72701 (USA).

SSDI 0003-2670(93)E0540-N

Under many circumstances one would like to be able to detect the amino acid of interest without the need for derivatization. Several methods are currently available for the direct detection of the amino acids. Welch et al. [9] have applied potential sweep-pulsed coulometric detection (PS-PCD) at a gold electrode following liquid chromatography (LC) for the determination of free amino acids. Luo et al. [10] have used constant-potential detection at a Cu wire electrode for the detection of underivatized amino acids following LC and flow-injection analysis (FIA). Detection limits for both methods are in the 1–100 pmol range which is not adequate in order to address a number of significant problems of current interest. For example, the study of proteins involved in intracellular communication and growth regulation will require amino acid analysis at levels substantially below the capability of the presently available techniques.

Interest in amino acid analysis is not limited to methods which can only determine the gross amino acid composition of proteins and peptides. One important goal in the area of biological analysis involves the need to develop detection methodology based upon new technologies which can be applied to the sequence analysis of proteins. Sequence analysis underlies the basic understanding of the relationship between structure and function in proteins. Currently, sequencing technology is based upon the Edman degradation [11], which involves reaction of a protein at the N-terminus with an isothiocyanate and yields a thiohydantoin (TH) derivative of the N-terminal amino acid, and a peptide, one amino acid shorter in length. The phenyl group of the phenyl-TH derivative provides a means for detection using absorption spectroscopy following the chromatographic separation of the derivative. Derivatives are identified by their characteristic retention times. Currently, limits of detection are in the 5 pmole range for the phenyl thiohydantoin (PTH) derivatives [1] which is limited by the molar absorptivity of the phenyl moiety. As discussed earlier, improvements in detection technology which will allow sequencing of proteins at levels 1–2 orders-of magnitude below that which is presently available are needed [1].

Toward this end, other isothiocyanates have been prepared and used to derivatize amino acids. Fluorescein isothiocyanate (FITC) derivatives of amino acids have been prepared and detected at sub-attomolar levels [12], but the reaction between FITC and the amine terminus of a protein or peptide is inefficient which creates error in the sequence analysis of proteins limiting the analysis to 25 residues, or less [13]. Azo-derivatives have been proposed as a means to enhance detection through a larger extinction coefficient. However, steric constraints make the chemistry unreliable. Methyl isothiocyanate (MITC) has also been used to sequence peptides [14]; detection of these derivatives was accomplished by mass spectrometry. Other isothiocyanate derivatives are also reactive toward amino acids and could feasibly be used in a protein sequencing scheme. Thus in improving the detection aspects of the Edman procedure by eliminating the need for the phenyl-TH derivative, the reaction chemistry may also be improved leading to higher reaction efficiencies and more reliable sequencing information over larger residue ranges.

Recently, a new technique for the detection of underivatized amino acids has been described by Brune and Bobbitt [15]. In this technique, $Ru(bpy)_3^{3+}$ was shown to undergo a chemiluminescent reaction with free amino acids and the chemiluminescence was maximized at pH values near the pK_a of the N-terminal amine site. The overall reaction sequence is shown below [15].

$$^{+}H_3NCRHCO_2^- + OH^- \rightleftharpoons H_2NCRHCO_2^- + H_2O$$

$$H_2NCRHCO_2^- + Ru(bpy)_3^{3+} \longrightarrow H_2\dot{N}^{+}RHCO_2^- + Ru(bpy)_3^{2+}$$

$$H_2\dot{N}^{+}CRHCO_2^- \longrightarrow H_2N\dot{C}RCO_2^- + H^+$$

$$H_2N\dot{C}RCO_2^- + Ru(bpy)_3^{3+} \longrightarrow HNCRCO_2^- + Ru(bpy)_3^{2+*} + H^+$$

$$HNCRCO_2^- + H_2O \longrightarrow RCOCO_2^- + NH_3$$

$$Ru(bpy)_3^{2+*} \longrightarrow Ru(bpy)_3^{2+} + h\nu$$

Experimental evidence in support of this mecha-

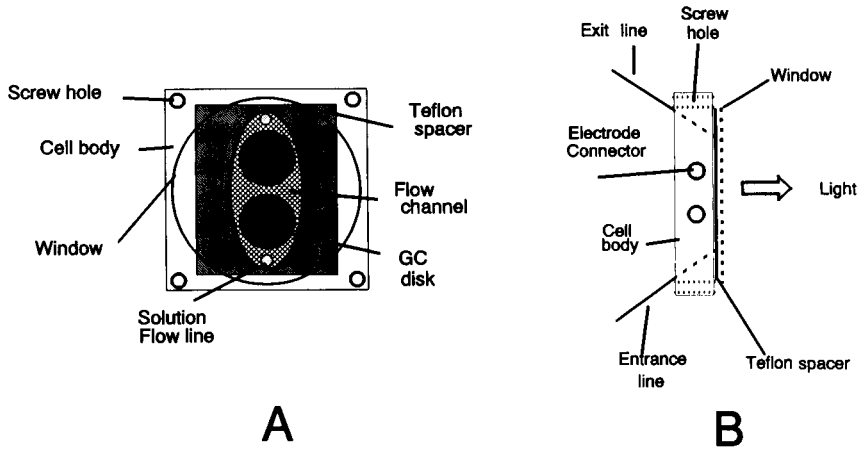

Fig. 1. Diagram of flow-cell used for the in situ studies: (A) front view, (B) side-view.

nism has shown that the overall reaction efficiency depends strongly on the pH at which the reaction occurs and on the electron donating/withdrawing characteristics of groups attached to the α-carbon of the amino acid [16]. Stoichiometric studies produced a ruthenium–amine mole ratio of 2:1. The chemiluminescence resulting from the reaction of an amino acid and $Ru(bpy)_3^{3+}$ was found to offer a sensitive method for the detection of underivatized amino acids. Further, it has also been shown that secondary amino acids luminescence more efficiently than primary acids with a concomitant reduction in the limit of detection [17]. This detection scheme can also be applied to the detection of other compounds which contain a primary, secondary or tertiary amine functionality [18,19], including conceivably, TH derivatives of amino acids. As described earlier, protein sequencing strategies are currently based on the Edman reaction which yields PTH derivatives that are detected by absorption spectroscopy. It is likely that the $Ru(bpy)_3^{3+}$-based CL technique can also be used to sensitively detect phenyl and other TH derivatives thus extending the versatility of current protein sequencing strategies.

Experimentally, the method involves electrochemically generating the $Ru(bpy)_3^{3+}$ from $Ru(bpy)_3^{2+}$ at a remote site followed by pumping of the active $Ru(bpy)_3^{3+}$ reagent to the site of detection where it is mixed with a stream containing the amino acid. Problems with this arrangement include degradation of the $Ru(bpy)_3^{3+}$ to $Ru(bpy)_3^{2+}$ before it reaches the detection cell and dilution of the amino acid stream, both of which reduce detectability. Also, the need to merge two streams prior to detection will make it difficult to miniaturize this configuration for application to modern microseparation techniques such as capillary electrophoresis (CE).

Downey and Nieman [20] have reported upon a promising technique where $Ru(bpy)_3^{2+}$ can be immobilized in Nafion which has been coated onto a glassy carbon disk. $Ru(bpy)_3^{3+}$ was electrochemically generated from the $Ru(bpy)_3^{2+}$ at the GC electrode following incorporation of $Ru(bpy)_3^{2+}$ into the Nafion. This approach was used in a flowing stream configuration, and the CL response was examined for several analytes. Oxalate, tripropylamine, and NADH were all found to provide a significant CL signal. Immobilization of the $Ru(bpy)_3^{2+}$ in this fashion provides a substantial improvement in terms of convenience of production of the active CL reagent, $Ru(bpy)_3^{3+}$. However, since the authors provided no LOD or response linearity data for the amino acids examined, the utility of this approach for the sensitive detection of amino acids remains unclear.

In situ electrochemical generation of $Ru(bpy)_3^{3+}$ at both glassy carbon and Pt [21] electrodes under hydrodynamic conditions has

been demonstrated, and has also been used to quantitate oxalate in synthetic urine samples [22]. Downey and Nieman [20] report both "solution" and "Nafion" data for a few studies in order to contrast the chemical behavior of immobilized and solution-phase $Ru(bpy)_3^{2+}$. However, very little experimental information was given for the "solution" studies, and amino acids were not reported to be detected by the "solution" method.

In this work, in situ generation of the active $Ru(bpy)_3^{3+}$ reagent from $Ru(bpy)_3^{2+}$, in solution, at the site of detection, is used to detect underivatized amino acids at the optimum pH of 10. $Ru(bpy)_3^{2+}$, present in the carrier buffer or mobile phase is electrochemically converted to $Ru(bpy)_3^{3+}$ within the detection cell at a glassy carbon electrode. Amino acids are detected by the light generated upon their reaction with the $Ru(bpy)_3^{3+}$ present in the detection cell. The method was found to be a more convenient approach for generating $Ru(bpy)_3^{3+}$ and provided better limits of detection than those reported earlier [15,16].

Application of this reaction sequence to the detection of underivatized amino acids following HPIEC separation will be presented, along with results describing the linearity, LOD, and stability of the method. Preliminary results will also be given for the detection of PTH–amino acids using this scheme. These results may have use in directing the development of new strategies for protein sequencing.

EXPERIMENTAL

Apparatus

Figure 1 schematically depicts the detection cell used for the in situ generated $Ru(bpy)_3^{3+}$ studies. The cell is similar, but more simple in design than the one reported by Downey and Nieman [20]. It consists of a modified thin-layer electrochemical cell obtained from Bioanalytical Systems (West Lafayette, IN) which has two 3 mm glassy carbon (GC) disks imbedded into the cell body. The body was modified by drilling two holes (0.055″ in diameter) through the cell body along the solution-flow axis (defined by the orientation of the two electrodes) which were used as solution inlet and exit ports. A length of 0.010″ or 0.007″ i.d. PTFE tubing was pulled through one of the drilled holes and trimmed flush with the face of the flow-cell. The seal formed between the tubing and the cell body was liquid-tight and this tube served as the solution inlet line for the cell. A second length of tubing, 0.035″ i.d., was pulled through the other hole in the cell body and this served as the solution exit. The GC disk nearest to the entrance line served as the working electrode, while the other GC disk served as the auxiliary electrode. The flow channel and internal volume (15 μl) of the thin-layer cell were defined by an oval opening cut into a PTFE gasket (0.030″ in thickness) which was attached to the cell body with silicon cement. A glass cover slide was affixed to the external face of the teflon gasket with the silicon cement thereby sealing the flow channel and allowing observation of chemiluminescence from within the cell flow channel.

The reference electrode port was a glass tube 1″ in diameter and 3″ in length. The tube was held vertically with the bottom opening sealed by a rubber septum. The exit line of the flow cell was inserted through the septum and this provided electrical connection between the reference electrode (saturated calomel electrode (SCE)) and the flow cell. Potential control was achieved with a PAR (Princeton, NJ) Model 363 potentiostat/galvanostat. A second glass tube was also inserted through the septum to a depth of 1″ and this served as a drain tube.

The flow cell was mounted onto an aluminum plate which was then directly fastened to the housing of a photomultiplier tube (PMT) (Hamamatsu, NJ, Model R928). The entire apparatus was covered with black cloth to minimize the collection of stray light at the PMT. PMT current was monitored with a Keithley (Cleveland, OH) model 485 picoammeter, the output of which was sent to a personal computer through a RS232 interface after being filtered with a 0.15 s time constant.

All FIA and chromatographic studies employed an ISCO (Lincoln, NE) Model LC5000 syringe pump which was coupled to either the detection cell (FIA studies) or the HPIEC col-

umn through a Rheodyne (Cotati, CA) Model 7125 syringe injector equipped with a 20-μl injection loop. Chromatographic studies employed an Alltech (Deerfield, IL) anion exchange column packed with a polymeric 10 μm Anion/R resin and involved addition of $Ru(bpy)_3^{2+}$ directly to the chromatographic mobile phase. The column effluent was taken directly to the detection cell.

Procedure

The procedure used for preparation of the GC electrodes prior to the experimental studies involved several steps which are outlined below. Initially, the cell body into which the electrodes were imbedded was subjected to a gross sanding using No. 600 grit SiC paper to remove any contaminates which may have penetrated the electrodes. The cell body and electrodes were then skid polished on felt or microcloth (Buehler, Lake Bluff, IL) to a mirror finish with a 5-μm alumina suspension, followed by a polishing with a 0.3-μm suspension (both from Buehler). The cell body was then washed by sonication for at least 2 min in three separate portions of deionized water to dislodge any imbedded alumina from the electrodes. Following surface preparation of the electrodes, the PTFE gasket and glass cover slide were attached with silicon cement, as described previously.

Reagents

All amino acid standards and PTH–glycine were purchased from Sigma (St. Louis, MO) and used without further purification. $Ru(bpy)_3^{3+}$ is known to oxidize Cl^- to Cl_2 under some conditions [23]. So, to prevent possible complications due to the formation of reactive Cl_2 at the glassy carbon electrode surface, $Ru(bpy)_3Cl_2$ which was purchased from Aldrich (Milwaukee, WI) was converted into the perchlorate salt prior to use. All other chemicals were reagent grade and used as received.

Chromatographic mobile phases were prepared from water which was deionized by a mixed-bed ion-exchange cartridge (Model No. 09-034-3, Fisher, Pittsburgh, PA).

RESULTS AND DISCUSSION

Signal stability

As outlined earlier, the $Ru(bpy)_3^{3+}$-based chemiluminescence reaction is well suited to the detection of amino acids. Demonstrated detection limits are at the level needed for recently identified applications requiring low level amino acid analysis, the system does not require chemical modification of the amino acid prior to detection to facilitate the analysis, and the reaction chemistry is relatively straightforward and well studied. Further, the fact that the active reagent, $Ru(bpy)_3^{3+}$, can be electrochemically prepared from a relatively inert form makes the experimental system very versatile. However, the need to prepare the reagent away from the site of utilization, and then pump it to the reaction zone does not make miniaturization of the system very practical. Therefore, studies were initiated to investigate the potential of preparing $Ru(bpy)_3^{3+}$ at the site of utilization. As mentioned previously, glassy carbon has been used to generate $Ru(bpy)_3^{3+}$ in situ [20,21]. GC was also found to be attractive for our application due to its available potential range, inertness of the surface to fouling under the experimental conditions utilized in these studies, and the ability of the surface to support chemiluminescent emission without quenching.

Glassy carbon is commonly used as an electrode material in thin-layer electrochemical detection cells and has been shown to provide for the sensitive detection of many important biological compounds either by direct electrochemical analysis, or the electrochemistry may be preceded by LC separation [24]. Due to the chemical nature of many of the compounds which are amenable to direct detection at GC surfaces, and the availability of high-efficiency silica-based chromatographic stationary phases, LC with electrochemical detection at a GC electrode is most often performed in acidic or neutral aqueous buffers. Also, many of the compounds of biological interest are easily oxidized on GC and thus the positive applied potential at the working electrode is not large. Previous studies employing in situ generated $Ru(bpy)_3^{3+}$ at GC have mostly been conducted at pH 5–7, where the optimum

CL intensity is observed for oxalate [20,21]. $Ru(bpy)_3^{3+}$ is known to be very stable in acidic solution, but is reduced in alkaline solution to $Ru(bpy)_3^{2+}$ through a reaction with hydroxide ion [25]. Because of this reaction, the lifetime of the active CL reagent, $Ru(bpy)_3^{3+}$, at pH 10 is greatly reduced in comparison to its lifetime at pH 5–7 [25]. Since studies cited earlier [15] have clearly demonstrated that the chemiluminescent reaction of amino acids and $Ru(bpy)_3^{3+}$ is optimum at pH 10, our study was initiated to assess the possibility of using GC in alkaline media at a relatively large positive operating potential for the in situ generation of the CL active reagent, $Ru(bpy)_3^{3+}$. The experimental conditions established through these studies should be applicable to postulated future applications which will require the use of GC fibers of micrometer dimensions for detection with high efficiency separation systems.

The CL signal produced upon FIA introduction of leucine into the detection cell was used to measure the stability of the in situ generation technique. For this evaluation, $Ru(bpy)_3^{2+}$ was added to the FIA carrier stream at various concentrations, and the CL peak height for a standard sample of leucine was used to monitor system response. During the initial utilization of a freshly polished electrode, the magnitude of the leucine signal decreased slowly over time and would reach a level of approximately 90% of initial activity after 6–10 h of continuous electrolysis of $Ru(bpy)_3^{2+}$. Following an overnight relaxation period in which the flow cell was stored in the operating buffer, the activity of the electrode would return to a response level representing 95–100% of the final activity achieved before the relaxation period. Upon continued use, the leucine response would then decay slowly, reaching a level of 95–98% of this activity after 8–12 h of use. Additionally, the leucine response was found to decay less than 8% over a 40-h period of constant electrolysis of $Ru(bpy)_3^{2+}$. In general, the signal became more stable as the electrode was used for the generation of $Ru(bpy)_3^{3+}$.

On rare occasions it was observed that the in situ generated CL signal would exhibit instability and degrade with time. Concomitant with the decrease in CL, the overall electrode current density was found to increase. Since the large positive potential needed to oxidize the $Ru(bpy)_3^{2+}$ to $Ru(bpy)_3^{3+}$ is also sufficiently positive to conceivably achieve solvent breakdown, the increased current density is believed to be from the electrochemical evolution of molecular oxygen. The oxygen produced by the electrode could be affecting the luminescence reaction since molecular oxygen is known to quench excited states of luminescent transition metal complexes [26].

Although the exact cause of the instability of the CL signal is not known, electrode preparation (polishing) is believed to be an important parameter in obtaining a stable CL signal from the GC electrode. The behavior of GC toward specific redox couples has already been shown to depend upon polishing procedures and materials [27]. It is conceivable that inconsistencies in the polishing procedures are responsible for the differences in electrode activities encountered during some of these experiments. In general, rigorous application of the surface preparation procedures outlined in the experimental section provided an active surface which was stable for at least 40 h of continuous use, as indicated previously.

Optimization of chemiluminescent response

The chemiluminescent reaction of $Ru(bpy)_3^{3+}$ with amino acids is dependent upon several experimental parameters. FIA was used as a means to introduce a precisely defined quantity of amino acid into the detection cell in order to optimize the CL response with respect to electrode potential, solution flow-rate through the cell, and the concentration of $Ru(bpy)_3^{2+}$ in the carrier stream. These studies were conducted by measuring the CL response as each parameter under consideration was varied. The effect of pH was not investigated because the pH dependence of this CL reaction has already been well established [15].

Figure 2 is a plot of the background CL signal obtained as a function of electrode potential in a pH 10 borate/acetate buffer. As expected, the data show that electrode potential is an important parameter to consider in optimizing the CL efficiency of the thin-layer cell. The small hysteresis which exists between forward and reverse

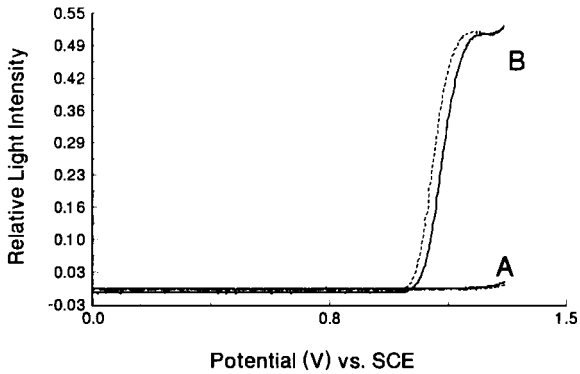

Fig. 2. Background chemiluminescence from the thin-layer cell as a function of applied potential. Buffer, 25 mM boric acid–75 mM sodium acetate adjusted to pH 10; flow-rate, 0.25 ml min^{-1}; potential sweep rate, 10 mV s^{-1}; PMT voltage, 700 V. CL signal filtered with a 5 ms time constant. Key: (A) 0.0 mM $Ru(bpy)_3^{2+}$ present in the buffer; (B) 1.0 mM $Ru(bpy)_3^{2+}$ present in buffer; (straight line), positive-going sweep; (dashed line), negative-going sweep.

CL intensities increases with increasing potential scan rate and is believed to be related to the lifetime of $Ru(bpy)_3^{3+}$. This effect can be understood by considering that if the rate of change of production of $Ru(bpy)_3^{3+}$ at the electrode surface is greater than the rate of consumption of $Ru(bpy)_3^{3+}$ by OH^- (to yield CL), then a hysteresis will develop in which the intensity of the CL for the reverse sweep will exceed that of the forward sweep since the concentration of $Ru(bpy)_3^{3+}$ at any given potential during the reverse sweep will be larger than that of the forward sweep.

The effect of electrode potential on the chemiluminescent response was evaluated using FIA to introduce 0.2 nmol samples of Asp into the detection system as the potential of the working electrode was varied from 1.05 to 1.50 V vs. the SCE. The maximum S/N was achieved at 1.20 to 1.30 V, which corresponds to the potential where the oxidation of $Ru(bpy)_3^{2+}$ proceeds at close to its diffusion limited rate. At potentials more positive than 1.50 V vs. SCE, it is possible that solvent degradation starts to occur and products from this reaction could interfere with the $Ru(bpy)_3^{3+}$ CL reaction with amino acids.

The chemical reaction sequence which is responsible for the CL requires that two molecules of $Ru(bpy)_3^{3+}$ be in proximity to the amino acid. This makes solution flow-rate a parameter which can influence the CL efficiency in the cell. Flow-rate was optimized by the FIA introduction of a standard sample of Asp while the carrier stream flow-rate was varied from 0.1 to 1.0 ml min^{-1}. These rates were chosen as being indicative of that which could be expected for the majority of LC applications using conventional diameter columns. Further, the linear flow-rate in the cell can be used to evaluate appropriate cell dimensions and flow-rates in order to apply this detection sequence to other, recently developed separation modes.

From these studies, it was determined that the S/N was maximized at the lowest flow-rates tested (0.1 ml min^{-1}), and it was minimum at the higher flow-rates of 0.5–1.0 ml min^{-1}. However, the variation in the response of the detection system is small and the S/N varied by only a factor of 2 over this flow-rate range. These results were expected after considering that at the lower flow-rates, the residence time of the amino acid sample in the cell is maximized. At a flow-rate of 250 μl min^{-1}, the residence time in the 15-μl detection cell is approximately 2 s. Given the stoichiometric relationship between the $Ru(bpy)_3^{3+}$ and amino acid, the short residence time suggests that the amino acid will have a smaller probability of interacting with a second $Ru(bpy)_3^{3+}$ molecule within the lifetime of the radical species formed in the first step as the flow-rate increases. Thus, the flow channel utilized for these studies may not be optimized for these volumetric flow-rates and a more convoluted design, exhibiting more opportunities for interaction between the reactants may provide improvement in the experimental S/N.

The concentration of $Ru(bpy)_3^{2+}$ in the carrier stream ultimately determines the concentration of $Ru(bpy)_3^{3+}$, the active CL reagent, at the electrode surface. This is a very important parameter in determining the magnitude of the CL signal obtained for a particular amino acid. Figure 3 shows the linear relationship between the signal obtained for a fixed amount of Asp and the concentration of $Ru(bpy)_3^{2+}$ in the mobile phase. The linearity of the plot strongly suggests that the

$Ru(bpy)_3^{3+}$ is the reagent limiting the CL reaction within the flow-cell. This is not unreasonable since only a small portion of the $Ru(bpy)_3^{2+}$ available contacts the working electrode and is converted to $Ru(bpy)_3^{3+}$. This makes the effective concentration of $Ru(bpy)_3^{3+}$, the active CL reagent, relatively small within the flow-cell channel even though the concentration of $Ru(bpy)_3^{2+}$ in the carrier stream might be relatively large compared to the concentration of amino acid under study. Concentrations of $Ru(bpy)_3^{2+}$ greater than 1 mM were not investigated since 1 mM is near the upper solubility limit of $Ru(bpy)_3^{2+}(ClO_4)_2$. Since 1 mM $Ru(bpy)_3^{2+}$ was found to provide the optimum S/N, studies which employed aqueous buffers without any organic solvent added as a modifier utilized 1 mM $Ru(bpy)_3^{2+}$ to maximize the CL S/N. A concentration of 0.25 mM $Ru(bpy)_3^{2+}$ was used in studies where the carrier stream was a buffer containing 5–10% ACN to avoid precipitation of $Ru(bpy)_3^{2+}$ within the flow cell channel.

Relative CL response

Brune and Bobbitt [16] have previously shown that the CL intensity of the reaction of primary amino acids with $Ru(bpy)_3^{3+}$ varies with the electron-withdrawing character of the R-group attached to the α-carbon of the amino acid. The CL intensity was found to be greatest for amino acids with an R-group which exhibited poor electron-withdrawing characteristics. The same trend of CL intensity was observed in the present study, with leucine having the highest and serine the lowest CL intensities of the amino acids examined. Proline is a secondary amino acid and shows a greater luminescent intensity than the primary amino acids. This same relative response has previously been reported for the reaction of primary and secondary amines with $Ru(bpy)_3^{3+}$ [18]. Table 1 lists the relative CL intensities of a select group of 5 amino acids evaluated using the in situ generated $Ru(bpy)_3^{3+}$ detection system. The group possesses side chain functionalities representing many of the types of functionalities exhibited by the 20 naturally occurring amino acids. The relative order of luminescent intensity observed for this group of 5 is the same as that reported earlier [15], but there is a larger difference in intensities between the most and least intensely luminescencing amino acid. The flow-cell used by Brune was a coiled glass reactor with an internal volume of 80 μl which allowed for more completeness of the CL reaction in the detection zone. As a consequence, this provided more efficient collection of the light generated in the detection region. The coiled nature of the cell design also provided some degree of mixing of the amino acid and $Ru(bpy)_3^{3+}$. In comparison, the cell used in the current study had a 15-μl internal volume and the solution flow channel did not allow for extensive mixing of the electrogenerated

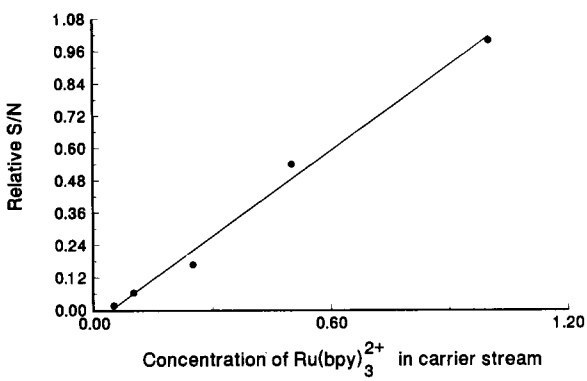

Fig. 3. Plot of S/N of flow-injection CL response of 10 μM Asp as a function of the concentration of $Ru(bpy)_3^{2+}$ in carrier stream. Buffer composition and flow-rate as in Fig. 2B; PMT voltage, 850 V; applied potential, 1.20 V vs. SCE.

TABLE 1

Relative CL intensities and limits of detection for several of the amino acids

Amino acid [a]	CL efficiency [b]	LOD [c]
Proline	1	5.0 nM (100 fmol)
Leucine	0.17	45 nM (1 pmol)
Aspartic acid	0.05	90 nM (2 pmol)
Phenylalanine	0.04	160 nM (3 pmol)
Serine	0.002	1.1 μM (22 pmol)

[a] All solutions buffered at pH 10 with 25 mM boric acid–75 mM sodium acetate buffer. [b] Intensities normalized to proline. Values represent comparison of FIA responses for 1.2 nmol of amino acid injected. [c] LODs estimated from the following injected concentrations in the FIA mode: proline, 30 nM; leucine, 0.3 μM; aspartic acid, 1.2 μM; phenylalanine, 2.4 μM; serine, 12 μM.

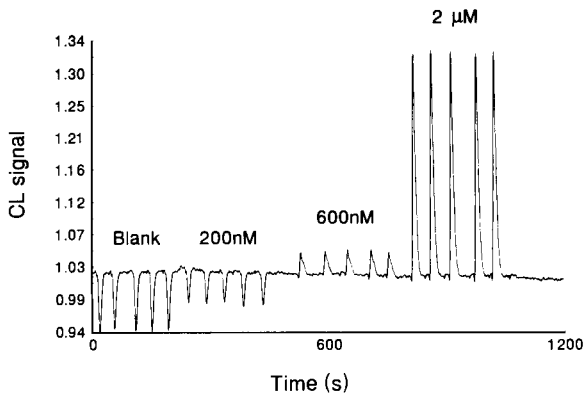

Fig. 4. Flow-injection CL response as a function of leucine concentration. Conditions as in Fig. 3.

$Ru(bpy)_3^{3+}$ and the amino acid in the detection zone.

The 5 amino acids tested show a concentration-dependent response which was linear over 2–3 orders of magnitude. Figure 4 shows the CL–FIA signal obtained for several concentrations of leucine. As mentioned previously, oxygen is known to quench excited states of luminescent transition metal complexes. Since the background CL response observed in this experiment is from an excited state of $Ru(bpy)_3^{2+}$, the negative blank response (relative to the analytical signal) is believed to be caused by differences in the concentration of dissolved oxygen in the carrier stream and the injected sample. Purging the sample with N_2 to remove dissolved oxygen prior to injection eliminated the negative response thus lending support to this postulate. The carrier buffer was shielded from atmospheric oxygen after being placed into the air-tight reservoir of the syringe pump used for the studies. The amino acid standard solutions and blank had the same oxygen concentration as the carrier buffer at the time of preparation, but continued to absorb atmospheric oxygen since they were not kept in an inert atmosphere. In support of this it was observed that the negative response of the blank increased slowly over time as it absorbed more oxygen. Therefore, sample and blank solutions were treated in an identical fashion to ensure identical oxygen concentrations. When the blank-corrected CL response for leucine was plotted as a function of leucine concentration, a linear relationship was established which exhibited a slope of 0.215 μA μM^{-1} (S.D. = 0.001 μA μM^{-1}), a y-intercept of -1×10^{-3} μA (S.D. = 0.08 μA) and an r^2 value of 0.9993 over 3 orders of magnitude thereby indicating very good linear correlation. Calibration plots of other amino acids show similar characteristics. The relative standard deviation (R.S.D.) of 27 injections of 0.1 mM leucine over a one hour period was found to be less than 5%, indicating excellent reproducibility. Table 1 lists the limit of detection for 5 amino acids. Due to uncertainty in both the blank and analyte signals caused by oxygen quenching of the background CL, the limit of detection was taken as the concentration of amino acid that would give a $S/N = 6$. These values were estimated from the lowest concentration of amino acid injected into the system (see footnote "c" on Table 1). These limits of detection represent an improvement of 3–10 times in the detectability of free amino acids by $Ru(bpy)_3^{3+}$-based CL [16]. These levels of detectability for underivatized amino acids are competitive with all currently available methods.

Chromatography

The in situ generation scheme can also be applied to the detection of amino acids following separation by HPIEC. A standard mixture of amino acids was separated and detected by the CL produced from the in situ generated $Ru(bpy)_3^{3+}$. The column used for the HPIEC separation of the various amino acids was packed with a polymeric anion-exchange resin. The separations were performed at pH 10 to ensure deprotonation of the amino group of the amino acid thereby facilitating reaction with the $Ru(bpy)_3^{3+}$. Since the separation and detection protocols both utilized a pH 10 buffer, it eliminated the need to introduce a post-column buffer as was required in earlier studies [16]. The separation mechanism under these conditions depended upon the carboxyl group of the amino acid to interact with the anionic exchange functionality of the stationary phase to effect separation.

CL detection of amino acids following chromatography was evaluated by using a chromatographic stationary phase which was resistant to

alkaline buffer conditions. $Ru(bpy)_3^{2+}$ was added directly to the pH 10 mobile phase. It was observed that $Ru(bpy)_3^{2+}$ has a strong affinity for the polystyrene–divinyl benzene (PS–DVB) backbone of the stationary phase and it adsorbed onto the packing material. The addition of 5% ACN to the mobile phase was found to significantly reduce the affinity of the $Ru(bpy)_3^{2+}$ for the packing material. By breakthrough analysis, it was determined that under conditions of 5% ACN, 0.8 μmol of $Ru(bpy)_3^{2+}$ was adsorbed onto the column which was used for the chromatographic studies. The adsorbed $Ru(bpy)_3^{2+}$ altered the interaction of the amino acids with the stationary phase and changes in the retention characteristics of the amino acids were observed. Apparently, the adsorbed $Ru(bpy)_3^{2+}$ reduced the number of anion-exchange sites which were available to eluting amino acids, since the k' values for all of the amino acids examined decreased after adsorption of $Ru(bpy)_3^{2+}$. Before adsorption of $Ru(bpy)_3^{2+}$, the k' values for Leu, Val, and Arg were 6.1, 1.9, and 0.2 respectively. After adsorption of $Ru(bpy)_3^{2+}$, the k' values for Leu, Val, and Arg changed to 2.9, 1.0, and 0.1, respectively. The packing material likely adsorbs no additional $Ru(bpy)_3^{2+}$ beyond that adsorbed during initial

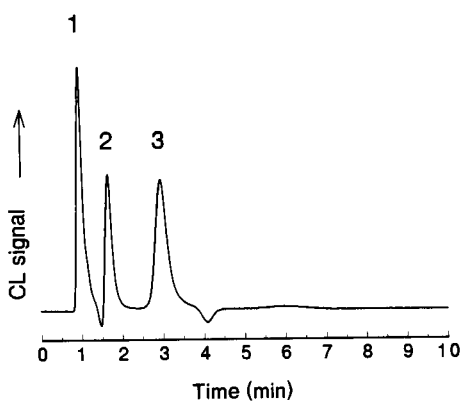

Fig. 5. HPIEC of amino acids using in situ chemiluminescence detection. Analytes: (1) 0.24 mM arginine, (2) 0.02 mM valine, (3) 0.02 mM leucine. Column dimensions, 150 mm×2.1 mm i.d.; stationary phase, Alltech Anion/R; mobile phase, 25 mM boric acid–75 mM sodium acetate adjusted to pH 10 with 5% ACN and 0.25 mM $Ru(bpy)_3^{2+}$ added; flow-rate, 0.33 ml min^{-1}; applied potential, 1.25 V vs. SCE; PMT voltage, 850 V.

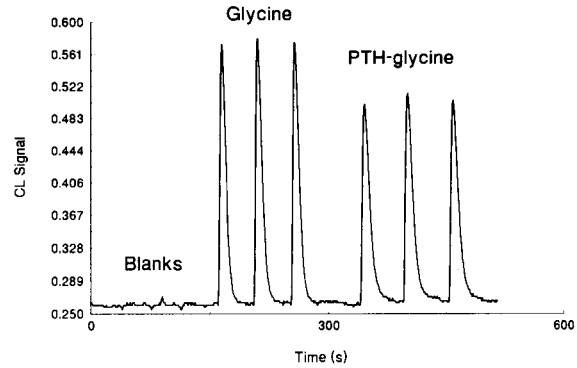

Fig. 6. Comparison of the FIA responses of 40 μM glycine and PTH–glycine with in situ chemiluminescence detection. Buffer, 25 mM boric acid–75 mM sodium acetate adjusted to pH 10 with 10% ACN and 0.25 mM $Ru(bpy)_3^{2+}$ added; applied potential, 1.2 V vs. SCE; PMT voltage, 900 V.

modification, since k' values for the amino acids changed less than 5% over the course of a 4-h period. Figure 5 shows a separation which employed a mobile phase containing 5% ACN. The small negative peaks observed at the beginning of the chromatogram were also present in the blank injection.

It is evident from Fig. 5 that the column used for the chromatographic separations shown in this study can not achieve high efficiency separation of amino acids. The results from these chromatographic studies do indicate though that the in situ generation detection scheme, when coupled to a high-efficiency analytical column will allow determination of free amino acids in various sample matrices under low level situations. Further, it is clear from these results that the in situ generation of $Ru(bpy)_3^{3+}$ at the site of utilization is feasible in a flowing stream.

Detection of PTH derivatized amino acids

PTH–amino acids possess a secondary amine functionality as a result of the formation of a phenyl thiohydantoin derivative from the originating amino acid. Based on previous studies of the relative luminescent intensities of primary versus secondary amines [18] and amino acids [15–17], the PTH derivatives should luminescence to a greater extent than the free, underivatized amino acids. Figure 6 shows the $Ru(bpy)_3^{3+}$ CL–FIA signal obtained for both glycine and

PTH–glycine in a pH 10 buffer containing 10% acetonitrile. It should be noted that the CL response of the electrode was not found to be stable over long periods of time in 10% ACN, but the organic solvent was needed to solubilize the hydrophobic PTH–glycine. This is the first report of the use of electrogenerated chemiluminescence to detect the PTH derivatives of amino acids. As is evident from the data, the PTH-derivative provided a signal which was of the same magnitude as the underivatized glycine. The reduction of the magnitude of the signal relative to what was expected may be due to the proximity of the aromatic ring in the PTH functionality to the N-terminal amine site in the PTH–amino acid. It has been previously shown using a series of aminobenzenes of the form $C_6H_5-(CH_2)_x-NH_2$, where x can vary from 0 to 3, that as the aromatic ring is moved away from the terminal amine site, the efficiency of the luminescent reaction increases. This same effect most likely governs the PTH-derivatives. However, even with the luminescence observed for the PTH–glycine, it is clear that the PTH-derivatives of the amino acids will provide, at a minimum, equivalent detection limits as the underivatized precursors. It is likely that this concentration detectability of the PTH amino acids by CL can be extrapolated to include detection at capillary dimensions since, unlike absorption measurements, there is no path-length dependence of the observed S/N measurement. This implies that the detectability exhibited by the CL method is already comparable to the results presented in a recent report of thermooptical detection of PTH amino acids following CE [28]. The quenching effect of the aromatic character of the phenyl-TH derivatives will not be a concern if other TH derivatives are utilized instead. Thus, the use of, for example, a methyl-TH derivative could allow more reliable reaction chemistry in the Edman sequence (i.e., minimize steric effects), and at the same time permit the limit of detection to possibly be reduced.

Conclusions

The chemiluminescent reaction of amino acids with in situ generated $Ru(bpy)_3^{3+}$ can provide for the sensitive and reproducible detection of underivatized and PTH derivatized amino acids following FIA introduction or HPIEC separation. Glassy carbon has been shown to be an ideal electrode material for the in situ generation of $Ru(bpy)_3^{3+}$, and, by proper surface preparation, a stable response can be achieved even under conditions of high pH and large positive potentials. Both the limit of detection and response linearity demonstrated in these studies are comparable to the best reported detection techniques for the underivatized amino acids.

These preliminary results suggest that the in situ approach for the generation of $Ru(bpy)_3^{3+}$ can also be applied to detection in CE. In this approach, $Ru(bpy)_3^{+2}$ would be present in the CE buffer and a GC fiber inserted into the end of the separation capillary could be used to prepare the active $Ru(bpy)_3^{3+}$ form. Electrochemical detection at a carbon fiber has already been applied to the monitoring of catechols and other easily oxidizable substances in CE by using a porous glass plug to electrically isolate the detection capillary from the separation capillary [29]. Modification of this configuration to facilitate light collection from the carbon fiber should make direct CL detection of amino acids possible. Work designed to evaluate the potential of coupling the in situ-generated $Ru(bpy)_3^{3+}$ detection protocol to capillary electrophoresis for the direct CL detection of amino acids is underway in our laboratory. In addition, studies are also underway to assess the feasibility of using methyl (or other) isothiocyanates in protein sequencing strategies which depend upon the CL reaction of the thiohydantoin derivatives with in situ generated $Ru(bpy)_3^{3+}$.

This work was supported, in part, by grant No. EHR-9108762 from the National Science Foundation. DRB also acknowledges the support of the Camille and Henry Dreyfus Foundation through a teacher-scholar fellowship. Many helpful discussions with Dr. Stephen Brune are gratefully acknowledged.

REFERENCES

1 L.M. Smith, Anal. Chem., 60 (1988) 381A.
2 K. Samejima, W. Dairman, J. Stone and S. Udenfriend, Anal. Biochem., 42 (1971) 237.

3 B.A. Bidlingmeyer, S.A. Cohen and T.L. Tarrin, J. Chromatogr., 336 (1984) 93.
4 C. De Jong, G.J. Hughes, E. Van Wieringen and K.J. Wilson, J. Chromatogr., 241 (1982) 345.
5 P. Lindroth and K. Mopper, Anal. Chem., 51 (1979) 1667.
6 M. Albin, R. Weinberger, E. Sapp and S. Moring, Anal. Chem., 63 (1991) 417.
7 S. Spurlin and M.M. Cooper, Anal. Lett., 19 (1986) 2277.
8 K. Miyaguchi, K. Honda and K. Imai, J. Chromatogr., 316 (1984) 501.
9 L.E. Welch, W.R. LaCourse, D.A. Mead, Jr., D.C. Johnson and Terry Hu, Anal. Chem., 61 (1989) 555.
10 P. Luo, F. Zhang and R.P. Baldwin, Anal. Chem., 63 (1991) 1702.
11 L. Drobnica, P. Kristian and J. Augustin, in S. Patai (Ed.), The Chemistry of the Cyanates and their Thio Derivatives, Wiley, New York, 1977, p. 1187.
12 Y.-F. Cheng and N.J. Dovichi, Science, 242 (1988) 562.
13 K. Muramoto, H. Kawauchi and K. Tuzimura, Agric. Biol. Chem., 42 (1978) 1559.
14 F.F. Richards and R.E. Lovis, Methods Enzymol., 25 (1972) 314.
15 S.N. Brune and D.R. Bobbitt, Talanta, 38 (1991) 419.
16 S.N. Brune and D.R. Bobbitt, Anal. Chem., 64 (1992) 166.
17 L. He, K.A. Cox and N.D. Danielson, Anal. Lett., 23 (1990) 195.
18 J.B. Noffsinger and N.D. Danielson, Anal. Chem., 59 (1987) 865.
19 J.A. Holeman and N.D. Danielson, Anal. Chim. Acta, 277 (1993) 55.
20 T.M. Downey and T.A. Nieman, Anal. Chem., 64 (1992) 261.
21 I. Rubinstein and A.J. Bard, J. Am. Chem. Soc., 103 (1981) 512.
22 I. Rubinstein, C.R. Martin and A.J. Bard, Anal. Chem., 55 (1983) 1580.
23 J. Rabin, K. Hashimoto, Z.F. Liu and A. Fujishima, Langmuir, 9 (1993) 818.
24 D.A. Roston, R.E. Shoup and P.T. Kissinger, Anal. Chem., 54 (1982) 1417A.
25 P.K. Ghosh, B.S. Brunschwig, M. Chou, Carol Creutz and N. Sutin, J. Am. Chem. Soc., 106 (1984) 4772.
26 E.R. Carraway, J.N. Demas, B.A. DeGraff and J.R. Bacon, Anal. Chem., 63 (1991) 337.
27 G.N. Kamau, W.S. Willis and J.F. Rusling, Anal. Chem., 57 (1985) 545.
28 K.C. Waldron and N.J. Dovichi, Anal. Chem., 64 (1992) 1396.
29 R.A. Wallingford and A.G. Ewing, Anal. Chem., 59 (1987) 1762.

Analytica Chimica Acta, 285 (1994) 321–328
Elsevier Science B.V., Amsterdam

Flow-injection bioluminescent determination of ATP based on the use of the luciferin–luciferase system

Grith Gamborg and Elo H. Hansen [a]

Chemistry Department A, The Technical University of Denmark, Building 207, DK-2800 Lyngby (Denmark)

(Received 24th June 1993; revised manuscript received 29th September 1993)

Abstract

A flow-injection system is described for assay of low levels of ATP as based on reaction with luciferase–luciferin with ensuing detection of the bioluminescence generated. The system employs a dual-injection valve which permits simultaneous injection of individually metered zones of the ATP-containing sample and enzyme solutions. By appropriate configuration of the injection valve, any unused enzyme solution is recycled thereby saving this costly reagent. At a consumption of 30–50 μl of enzyme and sample solutions, respectively, a detection limit of ca. 10^{-10} M ATP was achieved. Aqueous ATP standard solutions in the nM and pM range proved very unstable, and had to be stabilised with addition of EDTA in order to yield reproducible readouts. The performance of the system is discussed and compared with previously published systems for this kind of assay, and it is concluded that the limit of detection primarily is dictated by the ambient contaminatory level of ATP.

Keywords: Enzymatic methods; Flow injection; ATP; Bacterial ATP; Dual-injection; Recycling

The assay of low levels of ATP (adenosine-5′-triphosphate) is analytically interesting, because it is inherently an indicator for the population of somatic cells and bacteria, and therefore it is an intriguing parameter to evaluate not only in medicine, but also in the food industry. During the past years various flow-injection analysis (FIA) approaches for determination of ATP have been investigated at this laboratory. Thus recently, a FIA procedure based on an enzyme amplification scheme with ensuing fluorimetric detection was developed [1]. The system utilized a combination of three enzymes, that is, hexokinase, pyruvate kinase and glucose-6-phosphate dehydrogenase, coimmobilized on CPG glass beads and contained within a 100-μl tubular reactor placed into the FIA manifold. In the presence of appropriate cofactors, as added to the carrier stream, ATP was repeatedly recycled in the enzyme reactor with the ultimate formation of NADH which was detected, advantage additionally being taken of the fact that fluorimetry is a very sensitive detection procedure. As it was shown, amplification factors up to 1000 with this system were readily feasible, permitting to reach a lower limit of detection of the order of 6 nM [1].

For many applications in the food industry, particularly for assaying bacterial activity, it is, however, imperative with even lower limits of detection (preferably 10^{-12} 10^{-14} M ATP, corresponding to a population of 10^6 to 10^4 bacteria per litre [2]). Therefore, attention was focused on assaying ATP by means of bioluminescence utilizing the luciferin–luciferase system [3,4]. In this multistep reaction sequence, which overall can be described by the following scheme:

$$\text{ATP} + \text{D-Luciferin} + \text{O}_2 \xrightarrow{\text{Luciferase, Mg}^{2+}} \text{Oxyluciferin} + \text{PP}_\text{i} + \text{AMP} + \text{CO}_2 + \text{light}$$

ATP is converted to adenosine monophosphate

Correspondence to: E.H. Hansen, Chemistry Department A, The Technical University of Denmark, Building 207, DK-2800 Lyngby (Denmark).

SSDI 0003-2670(93)E0561-K

with concurrent generation of pyrophosphate (PP_i) and light which is emitted at ca. 560 nm. Previously, FIA has proven itself a particular attractive vehicle for chemi- and bioluminescent assays because of its inherent accurate and reproducible timing of all events [5–7], thereby permitting to relate the light emission, which, in fact, is a function of the reaction rate that these reactions actually exhibit, directly to real concentrations. Unfortunately, it is very difficult to immobilize luciferase as demonstrated by several authors [8–15], and furthermore when immobilized the enzyme exhibits very poor storage- and usage-stability, and temperatures above 25°C denaturises it completely [8]. The use of solubilized enzyme therefore appears, at least for the time being, to be the only practical avenue to pursue. But luciferase is a very expensive enzyme, and consequently a system with practical potentials should exhibit a high degree of economy in order to be of interest. The Danish company Foss-Electric has marketed an ATP-measuring instrument (BactoScan) which uses ca. 38 μl enzyme solution per assay, and this quantity was therefore used as a measuring stick for developing the FIA system described in this communication.

During the early stages of this work, a paper by Miller et al. [16] was published describing a reversed FIA system with which the authors claimed that they could measure down to 10^{-14} M ATP. Seen from a practical point of view, their system does, however, have some drawbacks. Firstly, because it is reversed FIA system, that is, the sample is pumped continuously while the enzyme solution is injected, it uses a substantial amount of sample material. Secondly, the sampling frequency is rather low because the system has to be thoroughly washed when switching from sample to sample. And thirdly, and very importantly, it requires the injection of 50–75 μl enzyme solution per assay, which means that in order to fill the injection loop very likely at least 100–150 μl of the precious enzyme solution is called for. However, spurned by its surprisingly outstanding performance, it was decided to test the approach suggested by Miller et al. [16], and compare its performance with the FIA system described herein.

This communication thus describes the development of a FIA system for the assay of ATP where both the sample solution and the luciferase enzyme solution initially are injected as discrete zones and subsequently merged by confluence, and where it by proper configuration of the injection valve is feasible to recycle any luciferase which is not actually injected. Thereby, the consumption of the enzyme is restricted to only 30–50 μl of luciferase solution per assay, which should make this approach attractive for practical applications. It is also reported that it was not feasible to reproduce the very low detection limits claimed by Miller et al. [16], neither with their reversed FIA system nor with the present system. Possible explanations for this discrepancy are forwarded and discussed.

EXPERIMENTAL

Apparatus

The FIA manifolds used are shown in Fig. 1, where (A) is the system used in the preliminary investigations (see below) comprising two individual 6-port rotary valves, (B) is the reversed FIA system constructed according to the design proposed by Miller et al. [16] and incorporating a 6-port rotary valve with external sample loop to facilitate injection of the enzyme solution and (C) is the ultimately designed FIA system comprising a 12-port rotary valve permitting simultaneous injection of sample solution and enzyme (for actual operation of the valve, see below). In all three systems the carrier streams were propagated by a peristaltic pump (Mini-S-840, Ismatec, Switzerland), which pump also served for delivery of enzyme–sample solutions to the valve(s). The detector was a specially constructed unit (Foss-Electric, Denmark, used in their commercial instrument BactoFoss), consisting of a photomultiplier (PM; Hamamatsu R2801-01) furnished with a small acrylic cell (mixing chamber) of a volume of 157 μl attached directly to the surface of the PM-tube by a tooled block. The readout from the PM was fed to a recorder (Radiometer REC 80, furnished with a REA 112 High Sensitivity Unit) and concurrently to a computer for on-line data

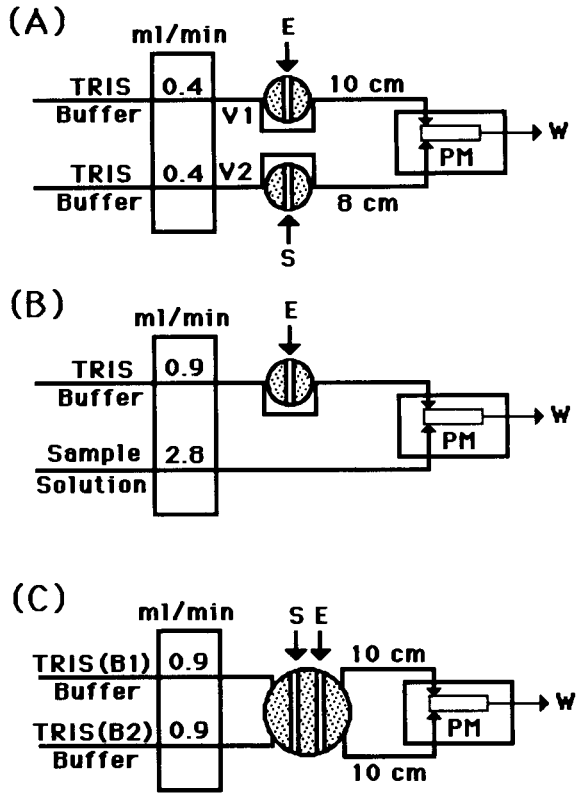

Fig. 1. FIA manifolds used in the present investigation, where (A), which comprizes two individually manually operated 6-port injection valves (V1 and V2) for introduction of ATP-sample (S) and enzyme (E) solutions, respectively, is the system used in the preliminary investigations; (B) is the reversed FIA system constructed according to the design proposed by Miller et al. [16]; and (C) is the system incorporating a dual injection valve whereby sample and enzyme solutions can be injected simultaneously. PM = photomultiplier; and W = waste.

acquisition. In all cases, peak heights were used for evaluation. All connecting lines in the FIA manifolds consisted of 0.5 mm i.d. Microline tubing. In order to prevent fibre optic effects of ambient light along the tubings all connecting lines in the FIA manifolds were shielded by black sleeving. All experiments were performed at room temperature, and no attempts were made in order to thermostate the FIA manifolds.

Reagents

HPLC-grade water was used throughout (except in the preliminary investigations, see below, where distilled water was used). In all three FIA systems the carrier solution (B1 and B2 in Fig. 1C) consisted of 0.10 M Tris buffer and 2.1 mM EDTA prepared by dissolving 12.14 g of Tris and 0.75 g of Na_2EDTA in a little less than 1 l of water. The pH was adjusted to 7.74 by addition of 2 M acetic acid and the solution was finally diluted to 1000 ml with water.

Standards of ATP were prepared from a 50 μM stock solution by appropriate dilution with the Tris–EDTA buffer of pH 7.74. The stock solution was made by weighing precisely 6.9 mg of ATP (Sigma) and diluting to 250 ml with the buffer. All substandards were made freshly prior to actual analysis.

The luciferin–luciferase mixture used in these investigations was donated by Foss-Electric. Each preparation came in a prepacked ampule which were to be dissolved in 1.5 ml of 0.1 M Tris buffer (pH 7.74). Unfortunately, it was not reported by the supplier how many units of enzymes each ampule contained so that the activity in the final solution is unknown to these authors. Yet, it is known that it in addition to the the enzyme (luciferase) it contains the appropriate levels of the necessary cofactors (luciferin and Mg^{2+}), plus preservating and stabilising agents. During experiments the enzyme-containing reservoir (ER, Fig. 2) was cooled by water (ca. 15°C) in order to prevent thermal degradation. (Foss-Electric reports that their dissolved enzyme mixture is stable for 8 h at 10°C. Generally, the individual experimental series based on the dissolution of a single ampule lasted typically 1–2 h, and during this period no degradation was observable).

Utmost care was taken in order to prevent contamination from ambient ATP during preparation of all solutions. Thus, all glassware was thorougly cleansed prior to use by soaking for 8 h in 0.1 M HCl, drying at 100°C and thorough rinsing in HPLC-grade water. Disposable pipettes were used throughout, the experimental area was regularly cleansed with alcohol, and the use of gloves was mandatory.

Operation of the dual-injection valve

The system requiring simultaneous injection of sample and enzyme solutions and recycling of any

unused enzyme solution requires that at least an 8-port rotary valve with individual access to each port is available. In the present case, a 12-port valve was at disposal, where 8 of the communicating ports were used (see Fig. 2, where ports 4–7/16–20 are unused and superfluous for the present purpose). It operates in the following way: In the LOAD position (left) enzyme solution is delivered from the enzyme reservoir (ER) via the pump to port 13 which by communication with ports 1 and 23 fills the enzyme loop (50 μl, bold line), surplus solution going to waste via port 11 and loop L, which has a volume identical to that of the enzyme loop (50 μl). At the same time, sample (ATP) is administered via ports 21/9 thereby filling the sample loop (50 μl, thin line) which communicates with ports 15/3. During this operation, buffer solutions B1 and B2 are via ports 14/2 and 22/10 directed to the detector (D). In the INJECT position (right), buffer solution B2 carries via ports 14/1 and 23/10 the enzyme solution towards the detector, and simultaneously the sample solution is propelled to the detector by buffer solution B1 via ports 22/9 and 15/2. During this position of the valve, the enzyme solution from reservoir ER is recycled through ports 13/12, and the solution in loop L is emptied by gravity because port 24 is open to the air. When the valve is switched to the LOAD position, it is meticulously observed exactly when loop L has been filled with solution, indicating that the carrier which previously was in the enzyme loop now has been replaced by fresh enzyme solution (and the sample loop simultaneously has been filled with new sample solution), whereupon the valve is turned for the next injection. Following this pattern, that is, only loading the valve immediately prior to an actual analysis, only the metered amount of enzyme solution will be required for each assay, the surplus being returned to the enzyme container.

RESULTS AND DISCUSSION

Preliminary investigations

Because the enzyme–reagent mixture is the dominating price-determining factor, it was initially decided to base the design of the flow-injection system on the multi-injection principle, that is, on separate introductions of both sample and reagent solutions, injected into separate carrier

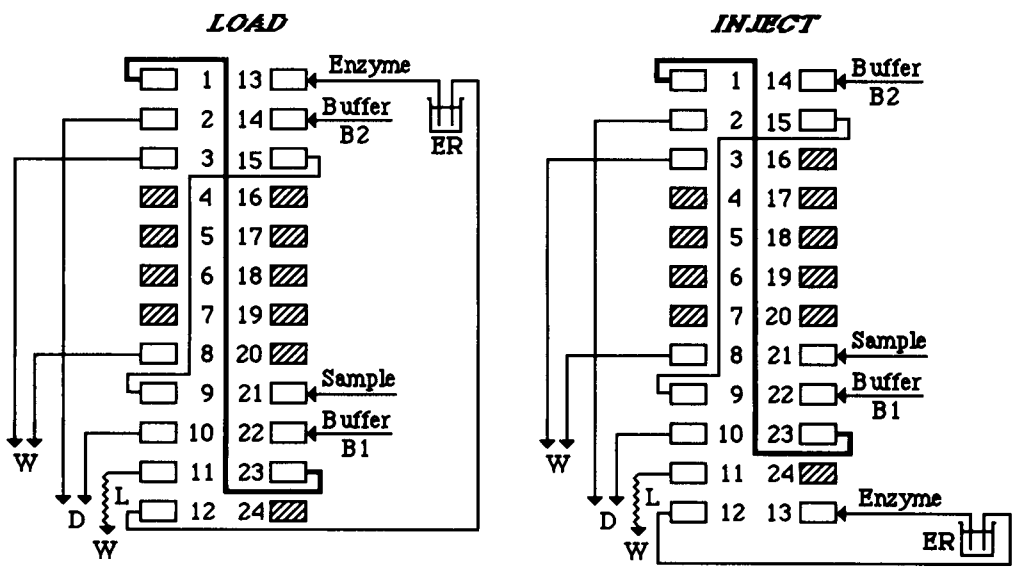

Fig. 2. Configuration of the dual injection valve, used in manifold (C) of Fig. 1, in the LOAD and INJECT positions. For operational details, see text (Experimental). The hatched ports denote the ones which are unused/permanently open.

streams which are merged either shortly before entering the flow cell in the detector or mixed directly inside the flow cell. The system used is depicted in Fig. 1A, which consists of two separate, manually operated 6-port roratory valves, where valve V1 is used for the enzyme solution and valve V2 for the sample solution (already in this system provisions were made to effect recirculation of any unused enzyme; cf. the description made in connection with the dual-injection valve). Using the specially constructed detector, where the flow cell had a volume of 157 μl, it was found that the best results were obtained by merging and mixing directly in the flow cell, which because of its rather large volume acts as small mixing chamber where the two streams meet head-on in one end and leaves at the other end (see Fig. 1). The volume of the enzyme zone was 20 μl and that of the sample zone was 40 μl, while the conduits from injection valve V1 and V2 to the flow cell were 10 and 8 cm, respectively. In this manner, it was ensured that the smaller enzyme zone upon introduction was enveloped within the larger sample zone.

The system was calibrated with ATP standards in the concentration range 10^{-6} to 10^{-14} M, all standards prepared as described in the Experimental part, except that doubly distilled water was used. However, it was observed that the standards below ca. 10^{-8} M were rather unstable, yielding with time progressively lower readouts so that it was difficult to reproduce the individual measurements. And the lower the concentration, the more unstable were the solutions. Since a possible reason for the decreased light emission might be ascribed to degradation of ATP in the standards, e.g., by hydrolysis, it was obviously necessary to stabilize them. According to Eriksen [4] addition of EDTA should be able to effect such stabilisation of ATP in aqueous solution. Considering that the enzyme mixture contains magnesium ions as a necessary cofactor for the light emitting reaction, it might not be thought advisable to employ EDTA as stabilising agent. However, it is known that the reaction between Mg and EDTA is a relatively slow process [17], and since the residence time in FIA is short and all events taking place are characterized by a high degree of accurate and reproducible timing, it was anticipated that the complexation reaction could be partly kinetically discriminated so that sufficient magnesium ions would be available for the light emitting sequence (besides, the level of magnesium ions in the enzyme solution is rather high, that is, of the order of 1 mM).

Therefore, a new series of standards were prepared where the 0.1 M Tris buffer used as diluent was spiked with 2.1 mM EDTA. This treatment had a remarkable effect on the standards, which as revealed by the reproducible readouts obtained repeatedly over several hours of operation indicated that the standards indeed had been stabilised. A perfectly linear relationship between the light emission and concentration was obtained in the calibration range 1.0×10^{-10} to 4.0×10^{-8} M ATP (totally 9 standards, each run in triplicate; regression coefficient 0.9973). Next, the carrier buffer streams were additionally spiked with EDTA at the same concentration level (in order to verify if the same buffer solution, for convenience, could be used both as carrier streams and as diluent for the standards), and readouts identical to those of before were obtained. The EDTA added therefore does not appear to pose any restrictions on the light emitting chemical reaction. In fact, ATP concentrations 10 times higher than the highest standard used for calibration could also be assayed without difficulty, so obviously sufficient magnesium ions are available. Yet, it cannot be ruled out that the presence of EDTA might indeed affect the measurement of lower ATP concentrations, but since it was found impossible to maintain the stability of the standards in these ultra-diluted solutions, there was no other choice than to add the stabilising agent. The addition of EDTA was therefore adopted in all ensuing experiments.

However, it was not possible to measure concentrations lower than 10^{-10} M ATP with the FIA system (i.e., similar readouts for the blank and the 1×10^{-10} M standard). In addition to the elaborate measures taken to maintain cleanliness to avoid ambient contamination (see Experimental), the water used for preparing all solutions was therefore replaced by HPLC-grade water which was certified to contain maximum 25

CFU/ml. Assuming that the average bacteria contains ca. 10^{-15} g ATP [2], this should correspond to a level of approximately 5×10^{-14} M ATP. Yet, even this precaution did not allow any further reduction of the dynamic measuring range.

One particular shortcoming of the hereto used system is that it requires the manual simultaneous operation of two individual valves, which might affect the reproducibility of measurement. In order to overcome this drawback, and considering the experience gained, it was decided to construct a second FIA dual-injection system, where the injections of the enzyme and sample zones could be completely synchronized, yet where emphasis still should be maintained with respect to consumption of enzyme solution per assay. This is possible by employing a rotary valve with minimum 8 individually accessible ports on both the rotor and stator. The finally designed system is depicted in Fig. 1C, and the operation of the dual-injection valve shown in Fig. 2 (for details, see below).

However, before embarking on experiments with this system, a reversed FIA system similar to the one proposed by Miller et al. [16] was constructed and thorougly tested in order to have a measure of comparison. As mentioned above, these authors have claimed to be able to measure down to 10^{-14} M ATP (which, in fact, is 5 times lower than the ATP level in the very pure HPLC-grade water used in this investigation), and they did not mention any difficulties in preparing these ultra diluted solution, neither did they appear to have any difficulties to maintain their stability (at least not referred to in their paper).

Experiments with the reversed flow-injection system

The reversed system is depicted in Fig. 1B and it is to the extent possible a complete replica of the manifold used by Miller et al. [16]. As to actual operation, the only difference is that the aqueous Tris solution used for the carrier stream and diluent of the standards contained EDTA (2.1 mM), and that the enzyme solution possibly is somewhat different in concentrations of the active ingredients (Miller et al. do neither offer

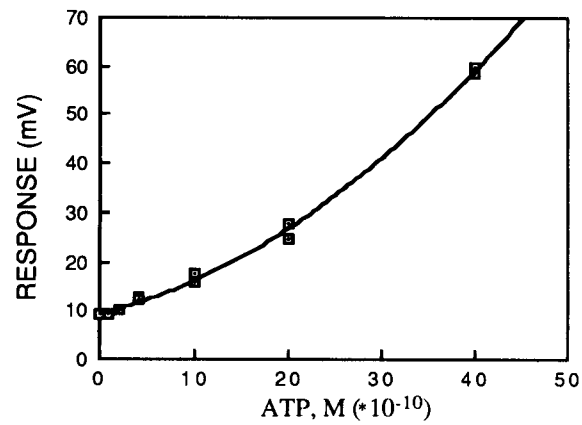

Fig. 3. Calibration curve for the reversed FIA system. The injected enzyme volume was 50 μl. Each standard was measured in dublicate.

any specific information as to the actual activity of the luciferase employed). Calibrated with a blank plus standards in the concentration range 8.0×10^{-11} to 4.0×10^{-9} M ATP (each standard measured in duplicate), the results obtained are depicted in Fig. 3. As it appears, the calibration curve is not a straight line, and the lowest concentration which it was possible to measure was 8×10^{-11} M ATP. This level, which interestingly is similar to the detection limit reported by Miller et al. for the assay of diluted cell suspensions, obviously corresponds to the level of contamination, despite the extreme precautions which were made. Yet, the level is still three to four decades poorer than that obtained by the same authors for pure aqueous standards analysed in an identical system. However, these results were taken as measuring stick for the performance of the system in Fig. 1C.

Experiments with the intergrated dual-injection system

The FIA manifold incorporating the double injection system is shown in Fig. 1C. Following the experience gained in the preliminary experiments, the injected sample and enzyme solutions volumes were each increased to 50 μl, which potentially should allow to reach a lower limit of detection [18] (provided ambient ATP contamination could be decreased or eliminated). Accord-

ingly, the conduits from the valve to the flow cell were also made identical, i.e., 10 cm each. In order to be as economical as possible in respect to enzyme solution, the system was designed so that any unused enzyme solution was recycled to the enzyme reservoir. The actual configuration of the valve in the LOAD and INJECT positions is depicted in Fig. 2 and the operation of it is explained in detail in the Experimental section.

In Fig. 4 is shown a calibration curve recorded for a blank plus ATP standards in the lowest concentration range, that is, $2–10 \times 10^{-10}$ M. Approximated to a linear relationship (although the points tend to reveal a slight curvature), the slope was 2.646 (10^{-10} M/mV) and the regression coefficient was 0.98. Compared to the calibration curve for the reversed FIA system, which in the same concentration range, and equally well approximated to a linear relationship, exhibited a slope of 0.798 (10^{-10} M/mV) and $r = 0.99$, the sensitivity and the absolute readouts for the dual-injection injection system in this concentration range were actually ca. twice that of the reversed FIA system. Yet, the limit of detection was more or less similar for the two systems, and also comparable to the one obtained with the system depicted in Fig. 1A, that is, the limit of detection did not become improved with the use of larger sample–enzyme volumes, but was obviously dictated by external factors, i.e., predominantly the ambient contaminatory level. Therefore, the injected enzyme and sample volumes could readily be reduced to, say, 30 μl each with the ensuing improved economy. With the set-up used, the residence time of the sample was ca. 25 s, which with the time of loading of the valve allowed a sampling frequency of the order of ca. 75 h^{-1}. The standard deviation for the individual standards in the lowest concentration range was slightly higher for the dual-injection system than for the reversed FIA system, but this is very likely due to the visually determined time of switching of the valve in the former one. No attempts were made to automate this switching process, but it should be readily automatable, for instance by incorporating a conductivity sensor in loop L which could ascertain when the enzyme loop precisely has been filled with fresh solution and hence is ready for injection.

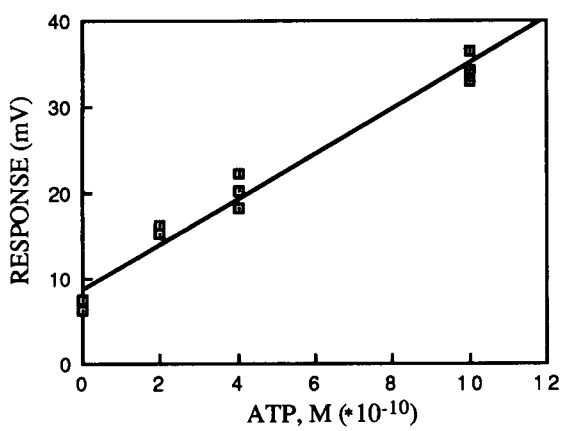

Fig. 4. Calibration curve for the dual injection system. The injected sample and enzyme volumes were each 50 μl. Each standard was measured in triplicate.

Conclusion

A dual-injection FIA system has been designed which at a consumption of 30–50 μl soluble enzyme solution per assay allows determination of low levels of ATP in aqueous samples and which via recycling of any unused amount of the precious enzyme solution permits a high degree of economy. The lowest level of ATP detectable is similar to that obtained with a reversed FIA system previously described by Miller et al. [16], but which consumes more enzyme per assay, requires much higher sample volumes, and which has a much lower sampling frequency. It has not been feasible to reproduce the very low limit of detection claimed by Miller et al. (10^{-14} M ATP) despite very elaborate procedures for cleanliness and pretreatment of vessels used. This might possibly be explained be the use of EDTA added as stabilising agent to the standards, but without this agent it was totally impossible to prepare stable and reliable standards in the lower ATP concentration range (i.e., lower than 10^{-8} M ATP). If the standards could be stabilized by any other means or prepared without addition of a stabiliser (interestingly and surprisingly, Miller et al. did not appear to run into these calibration difficulties, at least they do not make any mentioning of it in their publication), and/or if the

level of contamination from ambient ATP could be lowered, the dual-injection system, especially when fully operationally automated, promises to offer the economy, the capacity, the selectivity and the rapidity required for a practically applicable system. However, with the experience gained during this investigation, the present authors seriously doubt if it is indeed possible in practical work to reach much lower levels than 10^{-12} M ATP, which should also be of interest, because it would require so stern precautions that they would rarely be satisfied in practically operating laboratories.

No attempts were made in this investigation to ascertain ATP in practical samples. Firstly, because it was outside the scope of the present task, and secondly because a number of authors, including Miller et al. [16], already have demonstrated this feat with the luciferin–luciferase system.

The authors wish to express their appreciation to Foss-Electric (Drs. Martin Glensbjerg, Börkur Arnvidarsson and Helle Bækmark Andersen) for donation of the luciferase kits, loan of the detector device employed, and for constructive discussions. Thanks are also due to Julie Damms Foundation for partial financial support of the research activities described herein.

REFERENCES

1 E.H. Hansen, M. Gundstrup and H.S. Mikkelsen, J. Biotechnol., in press.
2 A. Decool, V. Goury, A. Tibi, S. Gibaud, F. Vincent and J.C. Darbord, Anal. Chim. Acta, 255 (1991) 423.
3 S. Brolin and G. Wettermark, Bioluminescence Analysis. VCH, Weinheim, 1992.
4 B.P. Eriksen, Ph.D. Thesis, Tech. Univ. Denmark, Lyngby, 1988.
5 B.A. Petersson, E.H. Hansen and J. Ruzicka, Anal. Lett., 19 (1986) 649.
6 E.H. Hansen, A. Arndal and L. Nørgaard, Anal. Lett., 23 (1990) 225.
7 E.H. Hansen, L. Nørgaard and M. Pedersen, Talanta, 38 (1991) 275.
8 K. Kurkijärvi, P. Turunen, T. Heinonen, O. Kolhinen, R. Raunio, A. Lundin and T. Lövgren, Methods Enzymol., 137 (1988) 171.
9 N.N. Ugarova, L.Y. Brovko and I. Berezin, Anal. Lett., 13 (1980) 881.
10 N.N. Ugarova, L.Y. Brovko and N.V. Kost, Enzyme Microbiol. Technol., 4 (1982) 224.
11 G.K. Wienhausen, L.K. Kricka, J.E. Hinkley and M. Deluca, Appl. Biochem. Biotechnol., 7 (1982) 463.
12 L.J. Blum, P.R. Coulet and D.C. Gautheron, Biotechnol. Bioeng., 27 (1985) 232.
13 J.J. Webster, B.G. Walker, S.R. Ford and F.R. Leach, J. Bioluminesc. Chemiluminesc., 2 (1998) 129.
14 N. Yu. Filippova, A.F. Duchovich and N.N. Ugarova, J. Bioluminesc. Chemiluminesc., 2 (1988) 419.
15 G. Gamborg, M.Sc. Thesis, Tech. Univ. Denmark, Lyngby, 1993.
16 J.N. Miller, M.B. Nawawi and C. Burgess, Anal. Chim. Acta, 266 (1992) 339.
17 E.H. Hansen and J. Ruzicka, Talanta, 20 (1973) 1105.
18 J. Ruzicka and E.H. Hansen, Flow Injection Analysis, Wiley, New York, 2nd edn., 1988.

Analytica Chimica Acta, 285 (1994) 329–333
Elsevier Science B.V., Amsterdam

UV–visible absorption and fluorescence characteristics of the luminescent label coumarin-6-sulphonyl chloride in homogeneous and micellar solutions

S.M.Z. Al-Kindy

Department of Chemistry, College of Science, Sultan Qaboos University, P.O. Box 36 Postal Code 123, Al-Khed, Muscat (Oman)

S.A. El-Sherbini

College of Applied Sciences, Arabian Gulf University (Bahrain)

M.H. Abdel-Kader

Department of Chemistry, Faculty of Science, United Arab Emirates University, P.O. Box 17551, Al-Ain (United Arab Emirates)

(Received 25th May 1993)

Abstract

This paper describes the study of the UV–visual absorption, fluorescence emission, and fluorescence excitation spectra of coumarin-6-sulphonyl chloride (C-6SCl) in various organic solvents and buffer solutions. In addition, the spectral behaviour in aqueous micellar systems of anionic and cationic surfactants was investigated. The spectral properties of the compound together with the determined pK values in the ground and excited state are discussed in relation to its electronic structure. The results reflect the importance of the medium effect on the analytical application of C-6SCl as a potential luminescent label for derivatization of amino and phenolic groups.

Keywords: UV–Visible spectrophotometry; Coumarin-6-sulphonyl chloride; Luminescence; Micellar solutions

Coumarin derivatives are of considerable photochemical, industrial, and analytical interest [1–6]. Photochemists have been intrigued by the selectivity of coumarins in forming photodimers of different conformation under controllable experimental conditions [7–9]. These compounds have been used as organic laser dyes and optical brightening agents [10,11]. From the analytical point of view, coumarin derivatives were the earliest fluorescent labels used in enzymatic assays [12,13]. In addition coumarin carboxylic acids have found applications as fluorescent probes for studying drug protein binding parameters [14].

Recently, a study has been made of a novel fluorescent and phosphorescent label coumarin-6-sulphonyl chloride (C-6SCl) which was obtained by straightforward sulphonation of the coumarin nucleus and was found to be highly stable [15,16]. This compound has found potential application in fluorimetric as well as phosphorimetric analysis of amino acids and phenols [16]. A quantitative derivatization reaction of C-6SCl with phenols and amino acids has been achieved giving stable derivatives which possess a reasonable molar ab-

Correspondence to: S.M.Z. Al-Kindy, Department of Chemistry, College of Science, Sultan Qaboos University, P.O. Box 36 Postal Code 123, Al-Khed, Muscat (Oman)

SSDI 0003-2670(93)E0537-H

sorptivity and a large Stokes shift. The luminescent properties of these derivatives met well with the requirements of an ideal label.

It is well documented, however, that the fluorescence properties of a molecule do not depend only on the structural characteristics of the molecule but are also a function of its environment. A knowledge of possible environmental effects on the spectral characteristics is therefore necessary for the utilization of such fluorescent labels to their maximum potential. Thus it was the aim of this work to investigate the effect of the medium on the spectral behaviour of C-6SCl in homogenous solutions of varying polarity and buffer solutions of different pH values. In addition, the spectral characteristics in aqueous micellar system of anionic and cationic surfactants were investigated. The results reflect the importance of the medium effect on the analytical application of C-6SCl as a potential luminescent label for derivatization of amino and phenolic groups.

EXPERIMENTAL

Materials

C-6SCl was synthesized and purified as described in the literature [17]. All the solvents used were spectroscopic grade and were used as received from Fluka. Aqueous buffer solutions were prepared as described by Bates and Bower [18]. The surfactants cetyltrimethylammonium bromide (CTABr, Fluka) and sodium dodecyl sulphate (SDS, Fluka) were purified by crystallization from methanol.

A stock solution (5×10^{-3} M) of C-6SCl was prepared in methanol and diluted with the appropriate solvent or buffer solution until the final solution contained not more than 1% methanol.

Instrumentation

UV–visible absorption spectra were recorded on a Beckman DU 8 spectrophotometer, using 1.0-cm matched quartz cells. The fluorescence measurements were made on a Perkin-Elmer LS-5B luminescence spectrometer. Fluorescence intensity was measured at right angles to the exciting light. The pH values of the buffer solutions were checked on an Orteck pH meter.

RESULTS AND DISCUSSION

Absorption spectra

The UV–visible absorption spectra of 5×10^{-5} M C-6SCl were measured in homogenous solutions of different polarity. As can be seen in Fig. 1, the absorption spectra exhibit more or less the same characteristics indicating that the electronic excitation processes are not sensitive to solvent polarity. The spectra display four overlapping peaks with maxima at about 310, 280, 270 and 240 nm.

The effect of the solvent is very slight. A small red shift of the first absorption band is observed in the case of highly polar solvents, e.g., water and dimethyl formamide (DMF). In addition, the first and second absorption bands in water and DMF exhibit relatively high absorbance values in comparison to the other solvents, in which there is a highly absorbing band at 240 nm. This behaviour can be ascribed to the difference in the

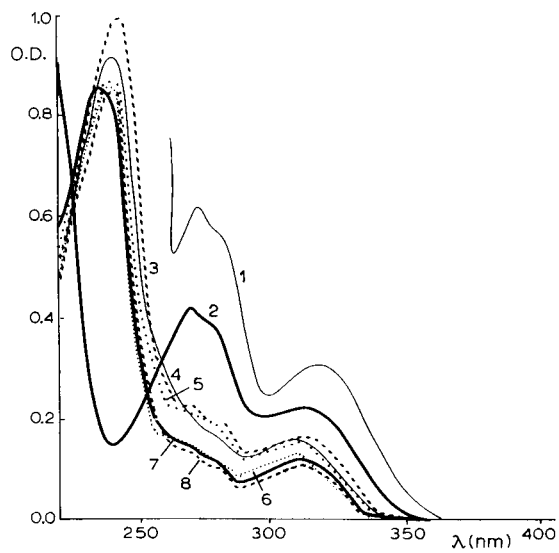

Fig. 1. Electronic absorption spectra of 5×10^{-5} M C-6SCl in various solvents: (1) DMF, (2) H_2O, (3) $CHCl_3$, (4) CH_3OH, (5) C_2H_5OH, (6) acetonitrile, (7) cyclohexane, (8) *n*-hexane.

transition probabilities in water and DMF compared to that in the other solvents.

The UV–visible absorption of 5×10^{-5} M C-6SCl in buffer solutions shows regular changes (Fig. 2). Within the pH range 1–7, the spectra display a single band with $\lambda_{max} = 305$ nm which does not show apparent variations with pH. This indicates that one form of the compound, most probably the neutral molecule, dominates under such conditions. With increasing pH, the absorbance of the band at 305 nm decreases, while a new band develops at longer wavelength ($\lambda_{max} = 328$ nm). The absorbance at the new band increases with increasing pH but tends to a limiting value at pH 10–11. A clear isosbestic point is observed at 316 nm indicating the existence of an equilibrium between the two species, most probably the normal lactone form of the coumarin nucleus and the ring opened form of the coumarin, which dominate at low and high pH, respectively. The pK value of this equilibrium can be determined from the following equation.

$$\mathrm{pH} = \mathrm{p}K_a + \log\frac{A - A_{min}}{A_{max} - A} + \log \gamma$$

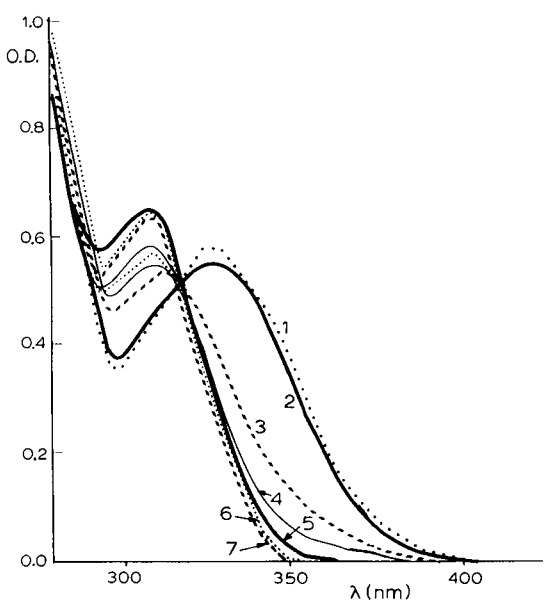

Fig. 2. Electronic absorption spectra of 5×10^{-5} M C-6SCl at different pH values: (1) 12, (2) 11, (3) 10, (4) 9, (5) 8, (6) 7, (7) 1.

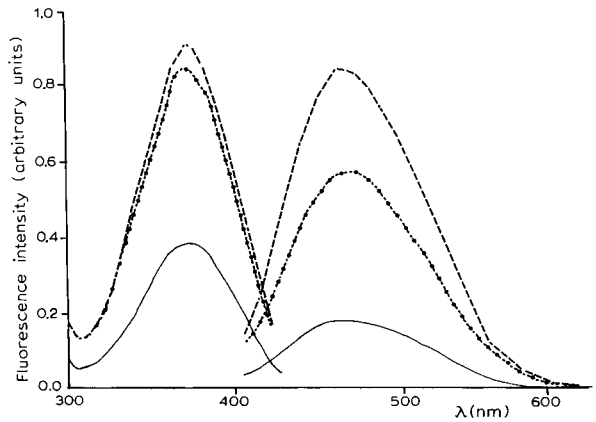

Fig. 3. Fluorescence emission ($\lambda_{ex} = 368$ nm) and excitation ($\lambda_{em} = 480$ nm) spectra of 5×10^{-6} M. C-6SCl at different pH values: ———, pH 9; •, pH 10; - - -, pH 11.

where A_{max} is the maximum absorbance for the acidic or basic form at a given wavelength, A_{min} is the minimum absorbance, and A is the measured absorbance at the same wavelength. The activity coefficient term (γ) may be approximated as unity, since a dilute solution of C-6SCl is used. The plot of $\log(A - A_{min}/A_{max} - A)$ vs. pH is linear, from which a value for pK_a of 10.9 is obtained. This value is in good agreement with the pK value of the coumarin nucleus reported by Carrety et al. (pKa = 9.95) [19] and Matto (pK_a = 10.7) [20]. This result indicates that there is no effect of the substituent on the reversible reaction of C-6SCl.

Fluorescence emission spectra

Investigation in buffer solutions. The fluorescence emission spectra of 5×10^{-6} M C-6SCl were measured in buffer solutions of varying pH values at $\lambda_{ex} = 368$ nm. As can be seen in Fig. 3, the spectra exhibit a very broad emission band with $\lambda_{max} = 480$ nm only at $\geqslant$ pH 9. The intensity of the band increases with increasing pH, but tends to a limiting value at pH 11. Within the pH range 1–8, C-6SCl does not fluoresce. This observation substantiates the findings of Gallivan [21] that coumarin and its derivatives are not fluorescent at room temperature in acidic or neutral medium. Under alkaline condition C-6SCl exhibits intense fluorescence. This has been ex-

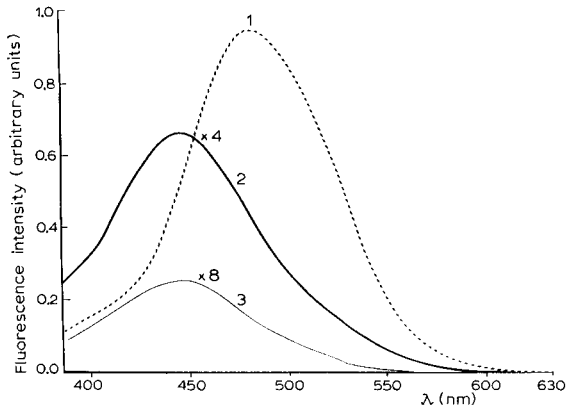

Fig. 4. Fluorescence emission spectra (λ_{ex} = 340 nm) of 5×10^{-6} M C-6SCl at different pH values, (1) pH 9, (2) pH 8, (3) pH 7.5.

plained as being a result of hydrolysis of the lactone ring by alkali to give yellow coumarinate ion [22,23].

The fluorescence emission of C-6SCl has also been studied in buffer solutions but excited at another wavelength (340 nm). It is of interest to observe that the fluorescence spectra exhibit a measurable broad emission band at pH 7.5 with λ_{max} = 440 nm. The fluorescence intensity is increased about tenfold at pH 8. This emission band is remarkably red shifted at pH 9 with λ_{max} = 480 nm (Fig. 4) and increases in intensity with increasing pH until a limiting value is obtained at pH 11. This indicates the presence of two different emitting species in the excited state. A plausible explanation of these two emitting species is that they may be the excited lactone form of the coumarin nucleus and the excited form of the ring opened product, which dominate at low and high pH, respectively.

The fluorescence spectra reveal that there is no measurable dissociation in the first excited state. Thus it was not possible to determine the equilibrium constant in the first excited state by fluorescence titration. Instead, the excited state equilibrium constant could be determined using a Förster cycle [24], in which the difference (ΔpK_a^*) between the pK_a of the ground state (pK_a) and of the excited states (pK_a^*), i.e., $\Delta pK_a^* = pK_a - pK_a^* = hC(\gamma_a - \gamma_b)/2.303KT$. $\Delta pK_a^* = 2.1 \times 10^{-3}\ \Delta\upsilon$ at 298K. υ is the frequency difference

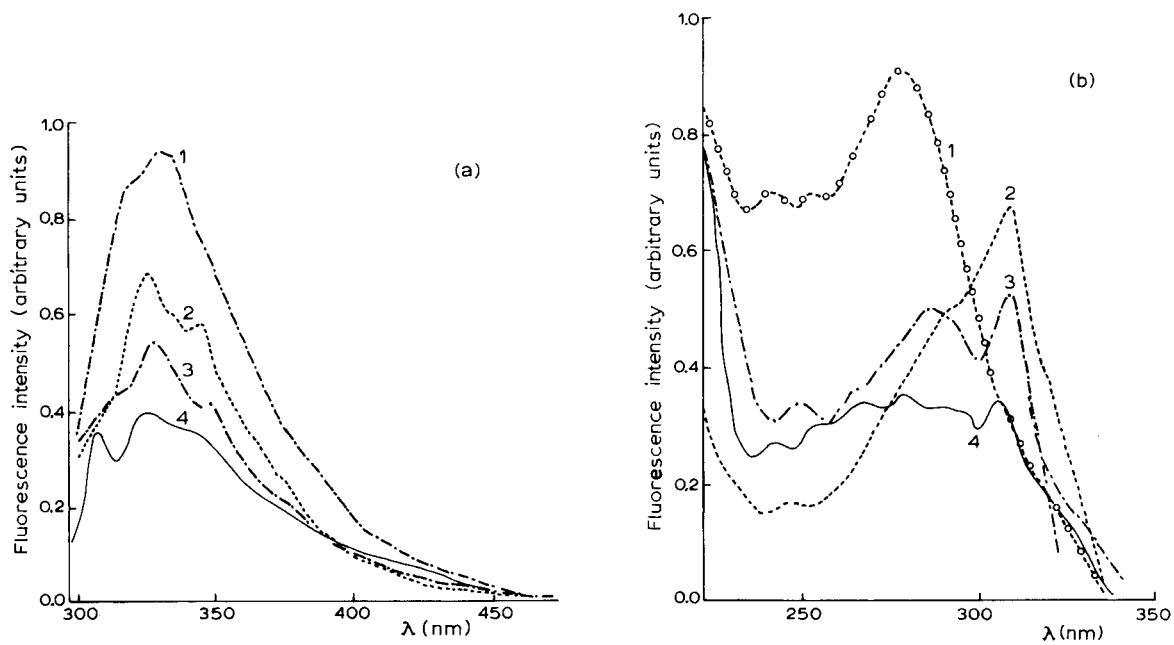

Fig. 5. (a) Fluorescence emission (λ_{ex} = 310 nm) and (b) fluorescence excitation spectra (λ_{em} = 355 nm) of 5×10^{-6} M in (1) CH_3CN, (2) 10^{-2} M SDS, (3) 5×10^{-3} M CTABr, (4) H_2O.

(in cm^{-1}) between the O–O bands of the electronic transition in the lactone form and ring opened product present at equilibrium. Taking an average value of $\Delta\upsilon = 2.0 \times 10^3$ cm^{-1} for the absorption and fluorescence transition, one can obtain $\Delta pK_a^* = 4.2$. Knowing that pK_a in the ground state is 10.9, thus pK_a^* in the first excited state is 6.7. As expected, the compound is considerably more acidic in the first excited state than in the ground state.

Investigations in micellar systems. The fluorescence emission and excitation spectra were measured in micellar systems of cationic (CTABr) and anionic (SDS) surfactants. Fig. 5a and b show the fluorescence emission of 5×10^{-6} M C-6SCl ($\lambda_{ex} = 310$ nm) and excitation spectra ($\lambda_{em} = 355$ nm) in aqueous solutions of 5×10^{-3} M CTABr, or 1×10^{-2} MSDS. The spectra of C-6SCl in water and acetonitrile are included for comparison. These spectra illustrate that the fluorescence and excitation spectra of C-6SCl are more or less the same in both band position and shape in anionic, or cationic surfactant micellar solutions and in water, indicating that C-6SCl is not incorporated into the micelle. The emission and excitation spectra in CTABr, SDS and water exhibit composite structural bands, which may be ascribed to the electrostatic interactions between C-6SCl and charged surfactants molecules as well as in aqueous solutions. The results show that C-6SCl fluorescence is only slightly affected by micellar media. This can be attributed to the fact that the difference in the solvation of the ground and excited state is too small to be measured. The fluorescence intensity is more sensitive to the effect of the medium than the spectral shift.

REFERENCES

1 L. Reio, J. Chromatogr., 1 (1958) 388.
2 J.B. Harbourne, Biochem. J., 74 (1960) 270.
3 R.A. Bernard, Nature, 182 (1958) 1171.
4 J.H. Copenhover and J.H. Carver, J. Chromatogr., 16 (1964) 229.
5 E. Sundt and A. Saccardi, Food Technol., 16 (1962) 89.
6 M. Trkovinik, M. Kules, I. Tabakovic and M. Zecevic, J. Chromatogr., 128 (1976) 227.
7 R. Anet, Can. J. Chem., 40 (1962) 1249.
8 G.S. Hammond, C.A. Stout and A.A. Lomola, J. Am. Chem. Soc., 86 (1964) 3103.
9 F.D. Lewis, D.K. Howard and J.D. Oxman, J. Am. Chem. Soc., 105 (1983) 3344.
10 S.A. Tuccio, K.H. Drexhage and G. Reynolds, Opt. Commun., 7 (1973) 248.
11 G.A. Reynolds and K.H. Drexhage, Opt. Commun., 13 (1975) 222.
12 R.H. Goodwin and F. Kavanagh, Arch. Biochem. Biophys., 36 (1952) 442.
13 S. Udenfriend, Fluorescence Assay in Biology and Medicines, Vol. 1, Academic Press, New York, 1962, p. 320.
14 S. Goya, A. Takadate, H. Fujino, M. Otagiri and K. Uekama, Chem. Pharm. Bull., 30 (1982) 1363.
15 S.M.Z. Al-Kindy, Ph.D. Thesis, Loughborough University of Technology, 1987.
16 S.M.Z. Al-Kindy and J.N. Miller, Anal. Chim. Acta 227 (1989) 145.
17 J.R. Merchant and R.C. Shah, J. Indian Chem. Soc., 34 (1957) 35.
18 R.G. Bates and V.E. Bower, Anal. Chem., 28 (1956) 1322.
19 E.R. Carrett, B.C. Lippold and J.B. Mielk, J. Pharm. Sci., 60 (1971) 396.
20 B.N. Matto, Trans. Faraday Soc., 53 (1957) 760.
21 J.R. Gallivan, Mol. Photochem., 2 (1970) 191.
22 M.H. Palmer, The Structure and Reactions of Heterocyclic Compounds, Arnold, London, 1967.
23 F.M. Dean, Naturally Occurring Oxygen Ring Compounds, Butterworth, London. 1963, p. 220.
24 T. Förster, Z. Elektrochem., 54 (1950) 42.

Analytica Chimica Acta, 285 (1994) 335–341
Elsevier Science B.V., Amsterdam

Simultaneous determination of organic and inorganic ultraviolet-absorbing compounds in human saliva by electrostatic ion chromatography

Wenzhi Hu and Hiroki Haraguchi

Department of Applied Chemistry, School of Engineering, Nagoya University, Furo-cho, Chikusa-ku, Nagoya 464-01 (Japan)

(Received 6th August 1993)

Abstract

Organic UV-absorbing compounds such as α-amylase and tryptophan and inorganic UV-absorbing compounds such as nitrite, nitrate, iodide and thiocyanate contained in human saliva were simultaneously determined by ion chromatography using a strong–strong positively–negatively charged zwitterionic stationary phase. When both positive and negative charges are close together in a single molecule of the stationary phase, the positively–negatively charged zwitterionic stationary phase provides a specific retention behaviour for the separation of inorganic anions and organic zwitterions. It was demonstrated in previous experiments that the separation of inorganic anions and organic zwitterions is caused by simultaneous electrostatic repulsive and attractive interactions between the same and opposite charges. Separation of inorganic anions and organic zwitterions using ion chromatography based on simultaneous electrostatic attraction–repulsion interactions between the same and opposite charges has been termed "electrostatic ion chromatography". This paper deals with a method for the improvement of the separation coefficient of electrostatic ion chromatography and a biological application.

Keywords: Ion chromatography; Saliva; UV-absorbing compounds

Many previous studies have demonstrated that the concentrations of inorganic and organic species in human saliva could be used as indicators for the diagnosis of the physiological and biological condition of an individual. The concentration of thiocyanates in saliva is a good indicator for the distinction between smokers and non-smokers [1]. The concentrations of other inorganic species are also considered to be good indicators for the diagnosis of the etiology of chronic respiratory diseases. Organic species such as α-amylase, which acts as a digestive enzyme, is also an important indicator.

Correspondence to: W. Hu, National Institute for Resources and Environment, 16-3 Onogawa, Tsukuba, Ibaraki 305 (Japan).

For the determination of thiocyanates in human saliva, numerous methods have been developed [2–6]. However, only a few papers have dealt with a method for the determination of other inorganic species such as nitrite [7] and nitrate [8], and organic species such as proteins [9] in human saliva. Most of the methods mentioned above, however, provide quantitative information about a single species, which is not satisfactory for a survey of complicate biological sources or for medical diagnosis.

To develop a method that is effective for the simultaneous determination of inorganic and organic species in human saliva, in this work we attempted to use electrostatic ion chromatography developed in a previous study [10]. Ion chromatography using a strong–strong positively–

0003-2670/94/$07.00
SSDI 0003-2670(93)E0517-B

negatively charged zwitterionic stationary phase for the separation of inorganic anions and organic zwitterions, based on simultaneous electrostatic attractive–repulsive interactions between the same and opposite charges has been termed "electrostatic ion chromatography" (EIC) [10].

Over a wide pH range, amino acids and proteins are also organic zwitterions, and therefore the simultaneous determination of amino acids and proteins and inorganic anions contained in human saliva should be successfully achievable using EIC.

EXPERIMENTAL

Apparatus

In this study, a microcolumn liquid chromatographic (LC) and a conventional LC system were employed. The microcolumn LC system used was the same as employed in previous work [10]. The conventional LC system was a Shimadzu (Kyoto) LC-6A system consisting of an LC-6A pump, a sample injector with an injection volume of 20 μl, an SPD-6A UV absorption detector and an EC-6A conductivity detector. The separation column used was ODS (L-Column, 250 × 4.6 mm i.d.) (Chemical Inspection and Testing Institute, Tokyo) coated with strong–strong positively–negatively charged zwitterionic bile micelles. The flow-rate of the mobile phase was 0.7 ml min^{-1}. All separations were carried out at room temperature.

Reagents

All reagents were of analytical-reagent grade and were used as received. Purified water was prepared using a Milli-Q system (Nihon Millipore Kogyo, Tokyo). The zwitterionic surfactants

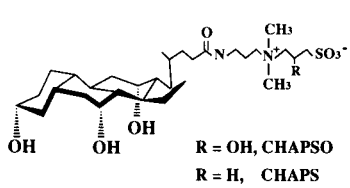

Fig. 1. Structures of CHAPS and CHAPSO.

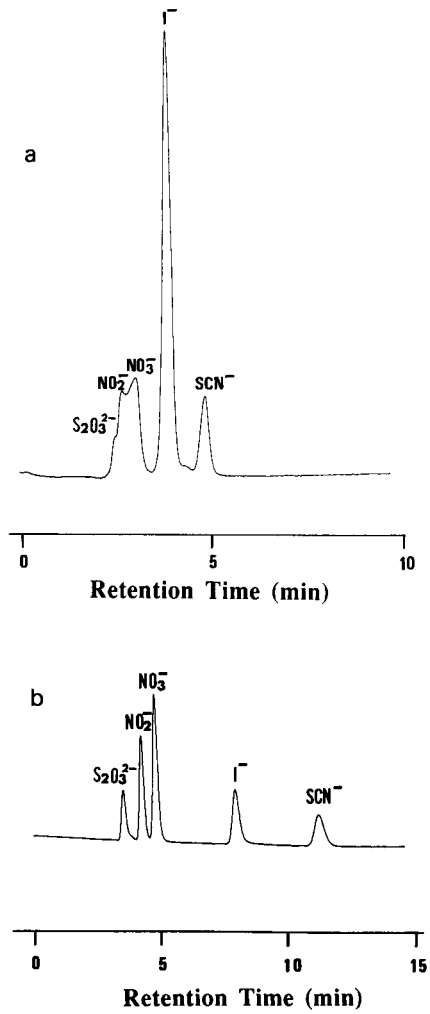

Fig. 2. Chromatograms of a mixture of inorganic solutes. Separation conditions: column, 150 × 0.35 mm i.d. packed with ODS and coated with CHAPS micelles; mobile phase, (a) pure water and (b) phosphate buffer; flow-rate, 2.8 μl min^{-1}; detection at 230 nm. Analyte: aqueous solution of 1 mM each of thiosulphate, nitrite, nitrate, iodide and thiocyanate.

3-[(3-cholamidopropyl)dimethylammonio]-1-propanesulphonate (CHAPS) and 3-[(3-cholamidopropyl)dimethylammonio]-2-hydroxy-1-propanesulphonate (CHAPSO) (Fig. 1) were obtained from Dojin (Kumamoto) and were used to form the strong–strong positively–negatively charged zwitterionic stationary phase. Inorganic anions used as the analytes were obtained as sodium salts from Wako (Osaka, Japan). Amino acids

were obtained from Sigma (St. Louis, MO). α-Amylase was obtained from *Bacillus subtilis* (activity about 20 units mg^{-1}).

Preparation of strong–strong positively–negatively charged zwitterionic stationary phase

An aqueous solution of 30 mM CHAPS or CHAPSO was passed through the ODS column for 80 min at a flow-rate of 0.7 ml min^{-1}. The column was then washed with pure water for at least 40 min at the same flow-rate.

RESULTS AND DISCUSSION

Effect of ion concentrations in the mobile phase

It was demonstrated previously [10] that the separation of inorganic anions and organic zwitterions could be simultaneously achieved by using EIC with pure water as the mobile phase. When an inorganic solute (cation and its counter anion) is passing through a strong–strong positively–negatively charged zwitterionic stationary phase, the analyte cation is attracted by the negative charge present in the zwitterionic stationary phase. However, the positive charge present in the same molecule of the stationary phase simultaneously repels the analyte cation. The counter anion of the analyte will have a similar electrostatic behaviour. Therefore, both the analyte cation and its counter anion cannot approach close to the zwitterionic stationary phase. The analyte cations and their counter anions are forced into a state of simultaneous electrostatic attraction–repulsion in the positively–negatively charged zwitterionic stationary phase, which has been termed an "ion-pairing-like" form [10].

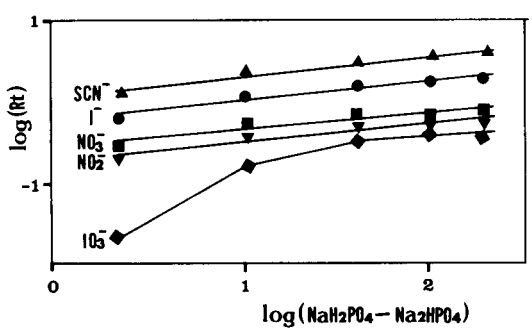

Fig. 3. Relationships between the logarithm of retention times of analytes and the logarithm of total ion concentrations in the mobile phase. Experimental conditions as in Fig. 2B.

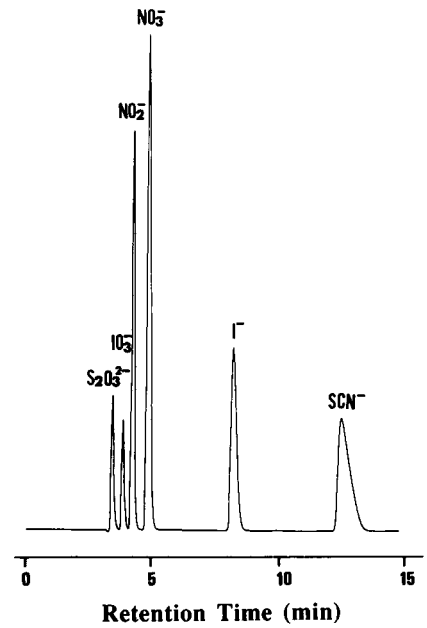

Fig. 4. Chromatogram of a mixture of inorganic solutes. Separation conditions: column, 250×4.6 mm i.d. packed with ODS and coated with CHAPS micelles; mobile phase, phosphate buffer; flow-rate, 0.7 ml min^{-1}; detection at 230 nm. Analyte: aqueous solution of 1 mM each of thiosulphate, iodate, nitrite, nitrate, iodide and thiocyanate.

Microcolumn LC system. Figure 2A shows a chromatogram of a mixture of inorganic solutes containing thiosulphate, nitrite, nitrate, iodide and thiocyanate obtained using a CHAPS micelle-coated stationary phase with water as the mobile phase. As can be seen, iodide and thiocyanate were baseline separated, but thiosulphate, nitrite and nitrate ions were not. Figure 2B shows a chromatogram of the same analytes as in Fig. 2A, obtained using 10 mM sodium phosphate–sodium dihydrogenphosphate (pH 6.8) instead of water as the mobile phase. As can be seen, the separation coefficient was improved by using the phosphate buffer as the mobile phase. The retention times of the analyte anions were also increased.

TABLE 1
Effect of mobile phase pH on retention time

pH [a]	Retention time (min)				
	IO_3^-	NO_2^-	NO_3^-	I^-	SCN^-
5.30	3.53	4.01	4.52	7.32	11.83
6.40	3.42	3.91	4.29	6.99	11.08
6.90	3.40	3.93	4.40	6.98	11.05
7.33	3.36	3.85	4.29	6.60	10.90

[a] The pH was adjusted with phosphate buffer [$NaH_2PO_4 + Na_2HPO_4$ (20 mM)].

Figure 3 shows the logarithm of the adjusted retention times of the analytes as a function of the logarithm of the total concentration of $NaH_2PO_4 + Na_2HPO_4$ in the mobile phase, where the whole mobile phase was fixed at pH 6.8. In conventional ion-exchange chromatography, the retention time decreases with increasing mobile phase ion concentration [11], in contrast to the present experiments, where the retention time increased. The separation achieved using EIC is due to the simultaneous electrostatic attractive–repulsive interactions between the same and opposite charges [10]. The results shown in Fig. 3 indicate that simultaneous electrostatic attractive–repulsive interactions between charges occur more easily in an ionic environment than in pure water.

The effect of the pH of the mobile phase was also examined by using the microcolumn system. The total concentration of phosphate buffer was fixed at 20 mM. The retention times of the inorganic anions were almost constant from pH 5.3 to 7.3, as shown in Table 1. This is because both negative and positive charges in the CHAPS or CHAPSO micelle-coated stationary phase are so strong that they are almost independent of the pH of the mobile phase.

Conventional LC system. Figure 4 shows a chromatogram of a mixture of inorganic analytes obtained using the conventional LC system with phosphate buffer as the mobile phase. Figure 5 shows the chromatogram of β-3,4-dihydroxyphenylalanine, phenylalanine and tryptophan obtained using phosphate buffer as the mobile phase. Compared with the separation obtained using pure water as the mobile phase [10], the separation coefficient of EIC for the separation of organic zwitterions was also improved by the addition of ions to the mobile phase.

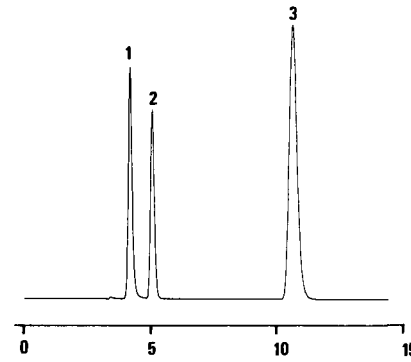

Fig. 5. Chromatogram of a mixture of amino acids. Separation conditions as in Fig. 4. Analyte: 1 mM each of (1) β-3,4-dihydroxyphenylalanine, (2) phenylalanine, and (3) tryptophan.

Separation of α-amylase

Over a wide pH range, proteins are also organic zwitterions. For the separation of proteins, α-amylase was chosen. It is found in human saliva and acts as a digestive enzyme. Figure 6 shows the chromatogram of α-amylase. The compound

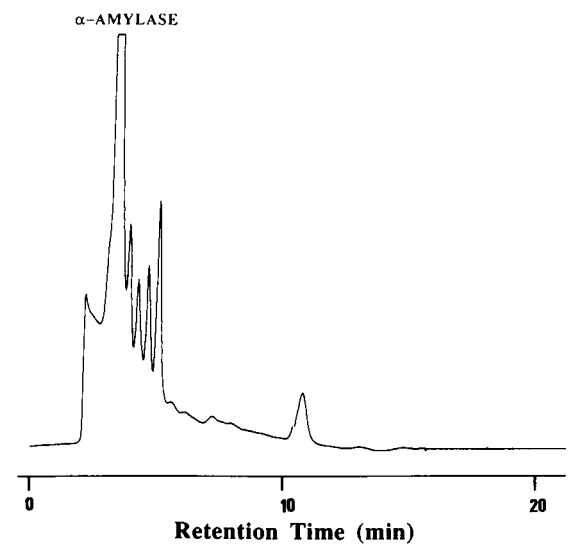

Fig. 6. Chromatogram of α-amylase. Separation conditions as in Fig. 4. Analyte: saturated aqueous solution of α-amylase.

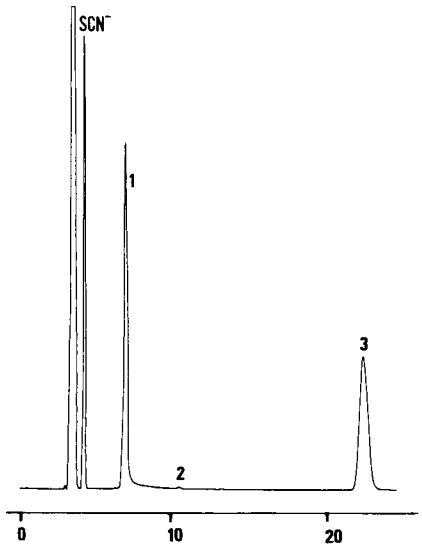

Fig. 7. Chromatogram of a mixture of inorganic anions and amino acids. Separation conditions as in Fig. 4 except for the column. Column coated with CHAPS monomers. Analyte: 0.5 mM each of nitrite, nitrate, iodide, thiocyanate, (1) β-3,4-dihydroxyphenylalanine, (2) phenylalanine and (3) tryptophan.

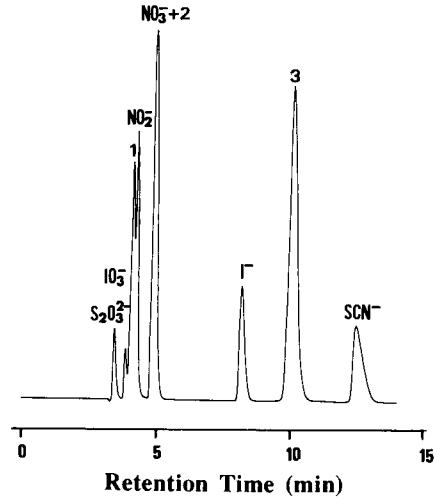

Fig. 8. Chromatogram of a mixture of inorganic anions and amino acids. Separation conditions as in Fig. 4. Analyte: 0.5 mM each of thiosulphate, iodate, nitrite, nitrate, iodide, thiocyanate, (1) β-3,4-dihydroxyphenylalanine, (2) phenylalanine and (3) tryptophan.

which eluted at 3.49 min is α-amylase. Other UV-absorbing organic compounds in the standard α-amylase solution were eluted after α-amylase. These compounds are present because the quality of the standard α-amylase obtained form *Bacillus subtilis* is poor.

Structural effect of micelle-coated stationary phase

It was demonstrated in previous work [12,13] that bile micelles adsorbed on ODS surfaces keep their helical structures as they do in the micellar mobile phase. For a further investigation of the effect of the helical structures of the bile micelle-coated stationary phase, a similar ODS column (L-Column, 250 × 4.6 mm i.d.) coated with CHAPS monomers (1 mM CHAPS aqueous

TABLE 2

Concentrations of inorganic and organic components in human saliva [a]

Sample No.	Found (mM)					
	α-Amylase [b]	Trp [c]	NO_2^-	NO_3^-	I^-	SCN^-
1	+	0.001	0.45	0.34	0.01	0.43
2	+	ND [d]	0.81	1.23	ND	0.25
3	+	0.003	0.76	0.89	ND	0.35
4	+	ND	1.02	0.96	ND	2.13
5	+	ND	0.67	2.01	0.13	3.12
6	+	0.001	0.24	0.86	ND	2.10
7	+	ND	1.21	0.25	ND	0.31

[a] Determination conditions as in Fig. 4. The concentrations of NO_2^-, NO_3^-, I^- and SCN^- were determined twice by using UV absorption and conductivity detectors. [b] Concentration of α-amylase is not shown in this table because a high-quality standard was not available. + = α-Amylase was detected. [c] Tryptophan. [d] ND = not detected.

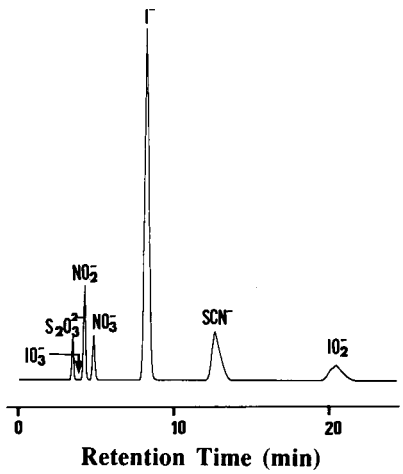

Fig. 9. Stability testing. Separation conditions as in Fig. 4. The peak of iodite ions is produced from iodate ions over a period of 3 months.

solution was passed through the column for 5 h and then washed with pure water for at least 50 min) was prepared. Figure 7 shows a chromatogram of a mixture of inorganic anions and UV-absorbing amino acids obtained using a CHAPS monomer-coated stationary phase. Compared with the results shown in Fig. 8 obtained using a CHAPS micelle-coated stationary phase, the retention times of inorganic anions were decreased and the separation coefficient became poor, whereas for the organic zwitterions the retention times became longer. The separation coefficient for the anions became poorer because the volume of CHAPS coated on the ODS stationary phase decreased in the CHAPS monomer-coated stationary phase. The retention time of organic zwitterions became longer because the CHAPS monomer-coated ODS stationary phase still showed some reversed-phase activity after coating with CHAPS monomers. These experimental results indicate that the micelle-coated stationary phase is more useful than the monomer-coated stationary phase for the simultaneous separation of inorganic anions and organic zwitterions.

Stability of the stationary phase

Figure 9 shows a chromatogram obtained using a CHAPS micelle-coated column after 3

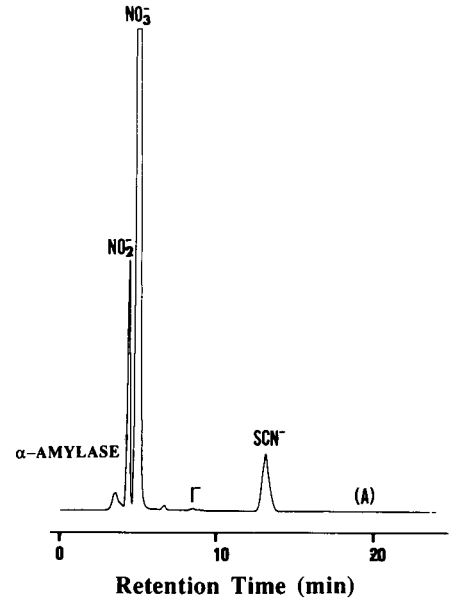

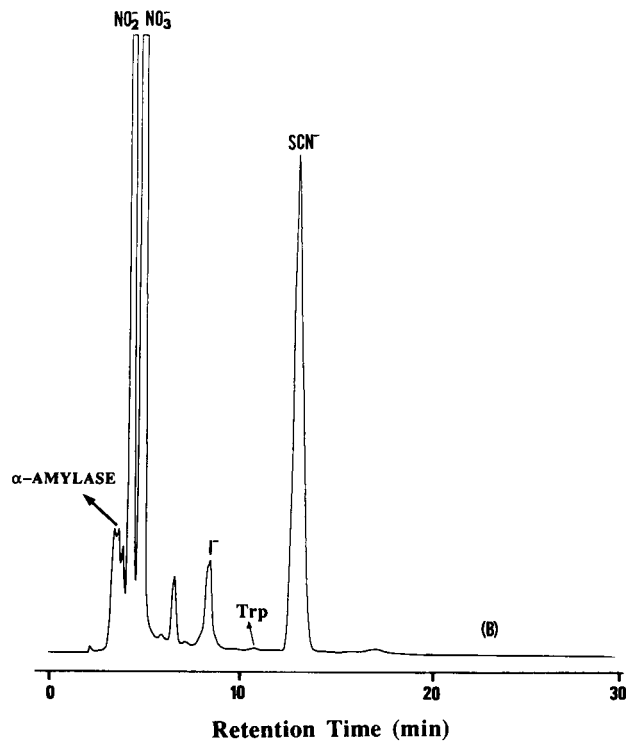

Fig. 10. Chromatograms of human saliva. (A) Separation conditions in Fig. 4. (B) Obtained with the sample as in (A) but with increased detector sensitivity.

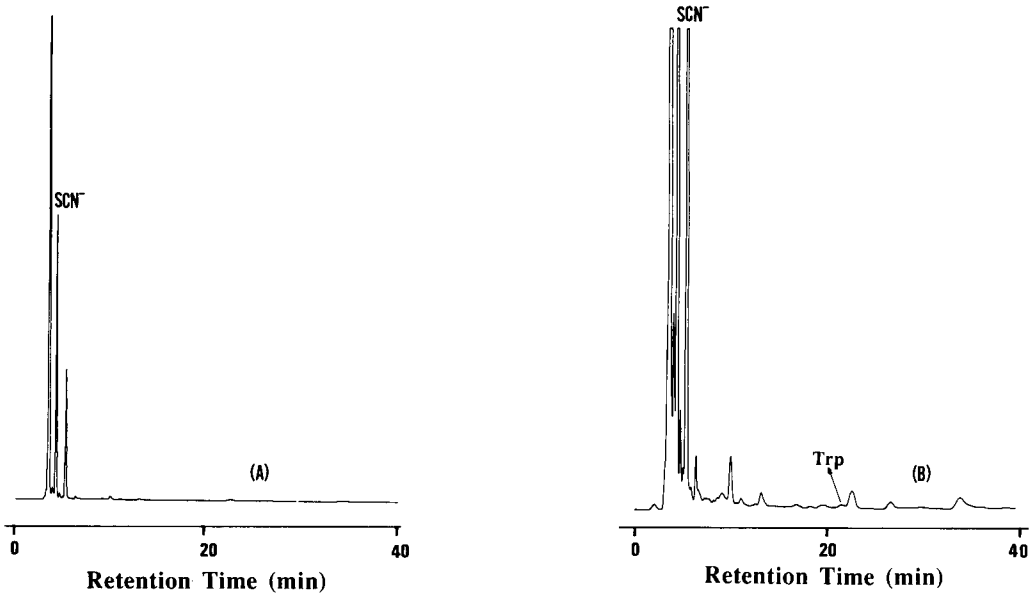

Fig. 11. Chromatogram of humans saliva. (A) Separation conditions as in Fig. 7. (B) Obtained with the same sample as in (A) but with increased detector sensitivity.

months of use. During this time, more than 200 saliva and standard samples were analysed with the column. No differences in the retention time and separation coefficient were observed.

Practical application

The conventional EIC system using a CHAPS micelle-coated stationary phase with phosphate buffer as the mobile phase was used for the simultaneous determination of organic zwitterions and inorganic anions in human saliva samples. The saliva sample was collected by means of a syringe. To remove all solid particles, the tip of the syringe was covered with cotton-wool, which was removed before the sample was injected into the separation system. Figure 10 shows chromatograms of human saliva. As can be seen, α-amylase, nitrite, nitrate, iodide, tryptophan, and thiocyanate contained in human saliva were simultaneously determined using the present system. The concentrations of inorganic and organic species in human saliva are summarized in Table 2.

The saliva samples were also analysed using the CHAPS monomer-coated stationary phase (Fig. 11). As can be seen, using the CHAPS monomer-coated stationary phase it takes 35 min for elution of the compounds in saliva, whereas using CHAPS micelle-coated stationary phase it takes only 15 min for elution.

REFERENCES

1 T.F. Maliszewski and D.E. Bass, J. Appl. Physiol., 8 (1955) 289.
2 P.M. Densen, B. Davidow, H.E. Bass and E.W. Jones, Arch. Environ. Health, 14 (1967) 865.
3 T. Chikamoto and T. Maitani, Anal. Sci., 2 (1986) 161.
4 X. Cai and Z. Zhao, Anal. Chim. Acta, 212 (1988) 43.
5 A.B. Bendtsen and E.H. Hansen, Analyst, 166 (1991) 647.
6 Y. Michigami, K. Fujii, K. Ueda and Y. Yamamoto, Analyst, 177 (1992) 1855.
7 M.N. Kurnosov, Lab. Delo, 3 (1991) 34.
8 A. Onoshi and K. Okaniwa, Jpn. Kokai Tokkyo Koho, JP 0326, 967 [9126, 967], 23 (1989) 8.
9 J.A. Beeley, D. Sweeney, J.C.B. Lindsay, M.L. Buchanan, L. Sarna and K.S. Khao, Electrophoresis, 12 (1991) 1032.
10 W. Hu, T. Takeuchi and H. Haraguchi, Anal. Chem., 65 (1993) 2209.
11 J.H. Knox and G.R. Laird, J. Chromatogr., 122 (1976) 17.
12 W. Hu, T. Takeuchi and H. Haragichi, Chromatographia, 33 (1992) 63.
13 W. Hu and H. Haraguchi, Bull. Chem. Soc. Jpn., 66 (1993) 1967.

Analytica Chimica Acta, 285 (1994) 343–351
Elsevier Science B.V., Amsterdam

Determination of alcohols and amines, labelled with 4-(*N*,*N*-dimethylaminosulfonyl)-7-(2-chloroformylpyrrolidin-1-yl)-2,1,3-benzoxadiazole, by liquid chromatography with conventional and laser-induced fluorescence detection

Toshimasa Toyo'oka, Yi-Ming Liu, Nobumitsu Hanioka, Hideto Jinno and Masanori Ando

Division of Environmental Chemistry, National Institute of Health Sciences, 1-18-1 Kamiyoga, Setagaya-ku, Tokyo 158 (Japan)

(Received 7th June 1993; revised manuscript received 13th September 1993)

Abstract

The utility of the fluorescence derivatization reagents, 4-(*N*,*N*-dimethylaminosulfonyl)-7-(2-chloroformylpyrrolidin-1-yl)-2,1,3-benzoxadiazole [*R*(+)-DBD-Pro-COCl and *S*(−)-DBD-Pro-COCl] with compounds having various functional groups has been evaluated. Enantiomers of DBD-Pro-COCl were equally reactive with alcohols, amines, phenol and aniline, whereas carboxylic acids and thiols did not yield fluorescent derivatives. The reaction conditions were optimized with a model alcohol (1-heptanol) and a model amine (*n*-heptylamine). Derivatization of alcohols and amines in benzene with 1% pyridine provides optimum yields of the corresponding fluorescence ester and amide derivatives. The excitation (ca. 450 nm) and emission (ca. 560 nm) maxima were essentially the same for all alcohols and amines tested. The corresponding derivatives of nine alcohols and three amines were completely separated by reversed-phase chromatography. The detection limits (signal-to-noise ratio of 2) with conventional fluorescence detection using a xenon arc lamp were from 10 fmol to 500 fmol, while those with laser-induced fluorescence (LIF) detection using argon-ion at 488 nm were in the range of 2 fmol to 10 fmol.

Keywords: Liquid chromatography; Fluorimetry; Alcohols; Amines; Laser-induced fluorescence detection; Pre-column derivatization

Various fluorescent derivatization reagents have been developed for the detection of amines by liquid chromatography (LC) [1,2]. Many of them have been successfully used for the determination of amino acids and amino containing drugs in biological samples. In contrast, the derivatization of alcoholic compounds is more difficult because of the limited reactivity of the hydroxyl functional group with electrophiles and the instability of the reagent itself. Some derivatization reagents for hydroxyls have been reported [3–18]. The reactive functional groups of the reagents divided into four classes; (1) isocyanates [3–6], e.g., naphthylisocyanate [3,4] and 7-dimethylaminocoumarin-3-isocyanate [6], (2) carbonyl azides [7,8], e.g., 7-methoxycoumarin-3-carbonyl azide [7] and 3,4-dihydro-6,7-dimethoxy-4-methyl-3-oxoquinoxaline-2-carbonyl azide [8], (3) carbonyl nitriles [9–11], e.g., 4-dimethylamino-1-naphthoyl nitrile [9] and 1- or 9-anthroyl nitrile [10], and (4) carbonyl chlorides [12–17], e.g., 2-dansylethyl chloroformate [14], 7-[(chlorocarbonyl)methoxy]-4-methylcoumarin [12], 3,4-dihydro-6,7-dimeth-

Correspondence to: T. Toyo'oka, Division of Environmental Chemistry, National Institute of Health Sciences, 1-18-1 Kamiyoga, Setagaya-ku, Tokyo 158 (Japan).

SSDI 0003-2670(93)E0523-A

oxy-4-methyl-3-oxoquinoxaline-2-carbonyl chloride (DMEQ-COCl) [13], 2-(5-chlorocarbonyl-2-oxazolyl)-5,6-methylenedioxybenzofuran (OMB-COCl) [16] and 6-methoxy-2-methylsulfonylquinoline-4-carbonyl chloride [17]. Although these reagents were used for the determination of alcohols by LC, those methods utilizing these reagents are not always satisfactory with respect to reactivity and sensitivity. Furthermore, the fluorescence wavelengths of the resulting derivatives, which are in the relatively short wavelength region, are not ideal for the detection in real samples, because interference by intrinsic compounds is always a possibility.

In a previous paper [19], we reported the syntheses of chiral derivatization reagents, 4-(*N*,*N*-dimethylaminosulfonyl)-7-(2-chloroformylpyrrolidine-1-yl)-2,1,3-benzoxadiazole (DBD-Pro-COCl) [*S*(−)- and *R*(+)-enantiomers], for the resolution of alcohol enantiomers by LC. The reagents are not only easily obtained with adequate purity with one step reactions, but are also stable as solids. Each pair of diastereomers derived from the reaction of selected aliphatic alcohol enantiomers with these reagents are well separated by normal-phase LC. The detection limits of alcohol enantiomers are at the sub-pmol level. The fluorescent properties with excitation near 450 nm and emission near 560 nm are advantageous for complex matrices. The excitation and emission maxima are at longer wavelengths than those of other reported reagents such as DMEQ-COCl [13] and OMB-COCl [16]. DBD-Pro-COCls are applicable for the determination of alcohols and amines, etc., even when enantiomeric separation is not required.

This paper describes the utility of these reagents with compounds having various hydroxyl, and primary and secondary amino functional groups. The fluorescence characteristics of the derivatives are also studied. Optimal conditions for the derivatization reactions with model alcohols and amines are established by investigation of important reaction parameters. The resulting derivatives are analyzed by reversed-phase LC with conventional fluorescence (FL) and laser-induced fluorescence (LIF) detection under the optimum elution conditions.

EXPERIMENTAL

Materials and reagents

4-(*N*,*N*-Dimethylaminosulfonyl)-7-(2-chloroformylpyrrolidine-1-yl)-2,1,3-benzoxadiazoles [*R*(+)- and *S*(−)-DBD-Pro-COCl] were synthesized as previously described [19]. 1-Heptanol, 1-octylalcohol, 1-nonanol, 1-decanol, 1-undecanol, 1-dodecanol, 1-tridecylalcohol, 1-tetradecanol, *n*-heptylamine, *n*-octylamine, *R*(−)-1-cyclohexylethylamine, phenol, aniline, methylamine (abs. 30% sol.), diethylamine, triethylamine and pyridine were purchased from Wako (Tokyo). 1-Azabicyclo[2,2,2]octane (quinuclidine), 1,8-diazabicyclo[5,4,0]-7-undecene (DBU) (Nacalai Tesque, Kyoto), and 1-pentadecanol (Aldrich, Milwaukee, WI) were used as received. Benzene, tetrahydrofuran, acetonitrile and water were of LC grade (Wako). All other chemicals were of analytical-reagent grade and were used without further purification.

LC

The liquid chromatograph consisted of two LC-9A pumps (Shimadzu) and an SCL-6B system controller (Shimadzu). Sample solutions, cooled with sample cooler (Shimadzu), at 5°C were injected with a SIL-10A auto injector (Shimadzu). The analytical column was a 5-μm Inertsil ODS-2 (150 × 4.6 mm i.d.) (GL Sciences, Tokyo). The column was maintained at 40°C with a 655A-52 column oven (Hitachi, Tokyo). A Shimadzu RF-550 fluorescence monitor equipped with a 12-μl flow cell was employed for the detection. The excitation and emission wavelengths were fixed at 450 nm and 560 nm, respectively. A LF-8010 monitor, equipped with a 5-μl flow cell and an interference filter at 540 ± 20 nm, was employed for the laser-induced fluorescence (LIF) detection (Tosoh, Tokyo). The peak areas obtained from the fluorescence and LIF monitors were calculated with a C-R4A chromatopac (Shimadzu). All mobile phases were de-gassed with an on-line degasser (DGU-3A, Shimadzu). The flow-rate of the eluent was 1.0 ml/min.

Reactivity of DBD-Pro-COCl

A solution prepared by mixing 30-μl aliquots of 10 mM DBD-Pro-COCl in anhydrous solvent

(benzene, THF or acetonitrile), and 1 mM 1-heptanol or *n*-heptylamine in anhydrous benzene, THF or acetonitrile with 2% pyridine, triethylamine, quinuclidine or DBU was sealed in a capped 1.5-ml mini-vial (GL Science). The reaction was allowed to proceed for over 4 h at room temperature or heated at 50, 80 or 100°C. At the fixed time intervals, one vial was removed from the dry heat block, and cooled in ice-water. Then a 690-μl portion of a 1% methylamine in acetonitrile solution was added to stop the derivatization reaction. An aliquot (10 μl) of the diluted solution was automatically injected into an Inertsil ODS-2 column, and the fluorescence peak area of the resulting diastereomer was calculated with an integrator. The reagent blanks without 1-heptanol or *n*-heptylamine were treated in the same manner.

For the fluorescent spectra measurements, 50 μl of the diluted solution was injected onto the column and the peak corresponding to the derivative was collected from outlet of the detector (ca. 2 ml portion). The fluorescence spectra of the derivatives corresponding to the other alcohols and amines were also measured as described for 1-heptanol or *n*-heptylamine.

Derivatization procedure for alcohols or amines

To 0.5 ml (low nmol–pmol) of a test solution containing 2% pyridine in benzene in a 1.5-ml mini-vial was added 0.5 ml of 10 mM DBD-Pro-COCl [*R*(+)- or *S*(−)-enantiomer] in anhydrous benzene. The vials were tightly capped and heated at 80°C (for alcohols) or 50°C (for amines) for 150 min (alcohols) or 30 min (amines) in the dark. Then a suitable volume of 1% methylamine in acetonitrile was added to the reaction mixture, cooled in ice–water (0–5°C), to stop the derivatization reaction. An aliquot (10 μl) of the diluted solution was chromatographed with an Inertsil ODS-2 column with water–acetonitrile. The fluorescence peak area of the derivative was calculated with an integrator. The reagent blanks without alcohol or amine were treated in the same manner.

RESULTS AND DISCUSSION

Derivatization conditions

Among the various types of derivatization reagents, carbonyl chlorides are suitable for alcohols. Therefore, many reagents for alcohols have a carbonyl chloride functional group as the reactive site. Although the carbonyl chlorides have been widely employed as the derivatization reagents for alcohols and amines, the susceptibility of hydrolysis to the parent acids makes them difficult to maintain in a pure form. Furthermore, accurate and precise results are difficult to achieve because of the limited stability of the reagents. As described in a previous paper [19], the proposed derivatization reagent, DBD-Pro-COCl [*S*(−)- or *R*(+)-enantiomer], a carbonyl chloride type reagent, was prepared in pure form from the optically active DBD-Pro. Both enantiomers were fairly stable and applied to the resolution of some alcohol enantiomers by nor-

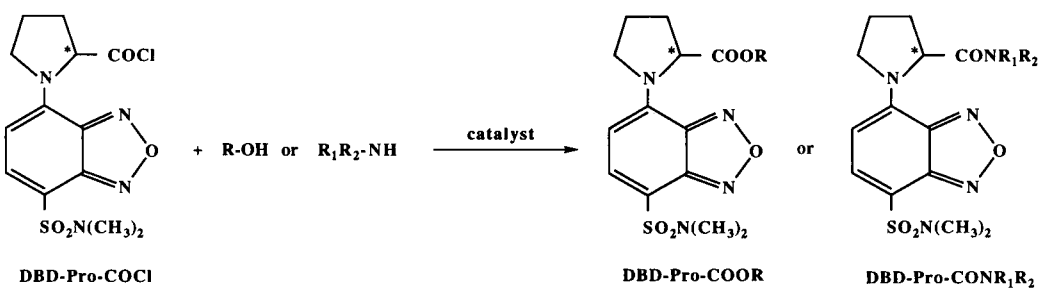

Fig. 1. Derivatization reaction of alcohols and amines.

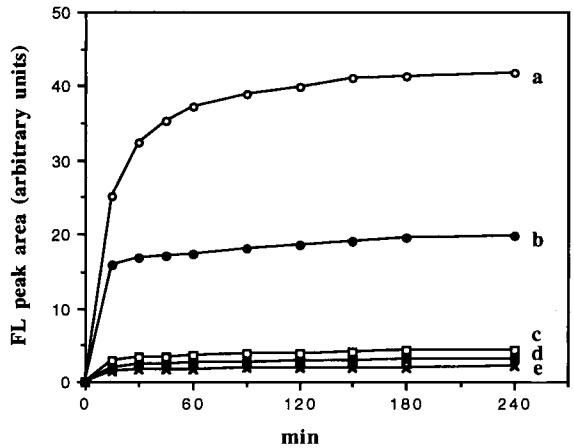

Fig. 2. Effect of solvent on the derivatization reaction of 1-heptanol with *S*(−)-DBD-Pro-COCl. (a) Benzene at 50°C; (b) benzene at room temp. (RT); (c) THF at 50°C; (d) THF at RT; (e) acetonitrile at RT. Eluent, H_2O–CH_3CN (3:7); fluorescence detection, 560 nm (excitation at 450 nm). Other LC conditions are given in the Experimental section.

mal-phase chromatography. Figure 1 shows the derivatization reaction of DBD-Pro-COCl with alcohols and amines in the presence of catalyst.

The solvent effect on the derivatization of alcohols was investigated in anhydrous benzene, tetrahydrofuran and acetonitrile. The time course of the derivatization reaction of 1-heptanol with *S*(−)-DBD-Pro-COCl in three solvents containing 1% pyridine was shown in Fig. 2. The reaction in benzene provided the highest reaction yield at both temperatures [50°C and RT (ca. 25°C)]. The results suggest that the derivatization in a hydrophobic solvent gives higher yield than in hydrophilic solvent (benzene > tetrahydrofuran > acetonitrile). Since even trace amounts of water in the reaction medium will hydrolyze the derivatization reagent, the product yield seems to depend upon the water content of the reaction mixture. The acids liberated by water partially consume the basic catalyst that is required in the acylation reaction. If the water content in the medium can be kept low, the derivatization reaction will quantitatively and quickly proceed with mild heating. Therefore, the solvents used in the reaction should be thoroughly dried with suitable reagents such as molecular sieves or sodium wire. Based on the above considerations, benzene which was stored over molecular sieves in order to decrease the water content was chosen as the reaction solvent in the following experiments.

TABLE 1

Effect of catalyst on the derivatization reaction of 1-heptanol in benzene at 80°C

Catalyst [a]	Concentration (mM)	Relative peak area (%)
Pyridine	63	100 [b]
Quinucridine	63	27.9
Triethylamine	63	23.7
DBU	63	1.2
No catalyst	0	2.5

[a] Quinucridine: 1-azabicyclo[2,2,2]octane; DBU: 1,8-diazabicyclo[5,4,0]-7-undecene. [b] The peak area obtained from 1-heptanol derivative in the presence of pyridine was tentatively taken as 100%.

Since the derivatization reaction requires a basic reagent as the catalyst, which forms salt with hydrogen chloride, compounds such as triethylamine and pyridine were tested. As shown in Table 1, pyridine was much more powerful catalyst among four reagents tested. Although quinuclidine and triethylamine also accelerated the derivatization reaction, their efficiencies were approximately one-fourth that of pyridine. The relative peak area obtained without the catalyst was only 2.5%. When DBU was used as the catalyst, the yield of the derivative was lower than that without the catalyst (only 1.2%). Instead, a large peak appeared at a retention time much longer than that of the derivative obtained from 1-heptanol. Judging from the results, the low yield seems to be due to the side reaction of DBU with DBD-Pro-COCl. The fluorescence peak areas for 1-heptanol were increased with increasing pyridine concentration and maximal yield was achieved at 63 mM pyridine (Table 2). Comparable yields were obtained at 126 mM concentration. Thus, 1% pyridine (126 mM) was selected as the catalyst.

Reaction temperature is a critical parameter for the derivatization reaction. The effect was tested in benzene containing 1% pyridine. The rate of the reaction of alcohol with DBD-Pro-COCl increases with temperature. However, the absolute yields were not determined due to the limited amount of the derivatization reagent

TABLE 2

Effect of pyridine concentration on the derivatization reaction of 1-heptanol in benzene at 80°C

Pyridine concentration mM (%)	Relative peak area (%)
3.16 (0.025)	15.2
6.32 (0.05)	30.1
12.6 (0.10)	43.9
31.6 (0.25)	79.9
63.2 (0.50)	100 [a]
126.0 (1.0)	97.2

[a] The peak area of 1-heptanol derivative obtained from 63.2 mM pyridine was tentatively taken as 100%.

available. The results for 1-heptanol are shown in Fig. 3. The peak areas reached a maximum after 150 min at 80°C and remained constant for 240 min. Since no peak reduction was observed at 80°C, the derivative seems to be stable for at least 240 min. However, at 100°C the peak areas steadily decrease with time. Thus, 150 min at 80°C in benzene containing 1% pyridine was selected for the determination of alcohols.

Amines are much more reactive with the derivatization reagent because the nucleophilicity of the amino functional group is higher than that of hydroxyl functional group. Therefore, the rate of the formation of the derivative of *n*-heptylamine with the reagent was studied with and

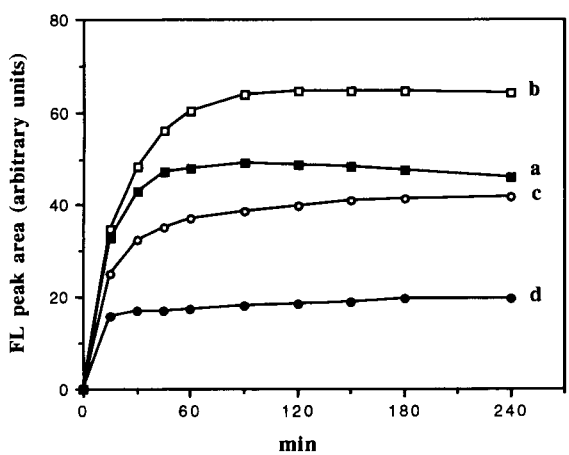

Fig. 3. Effect of temperature on the derivatization reaction of 1-heptanol with *S*(−)-DBD-Pro-COCl. (a) 100°C; (b) 80°C; (c) 50°C; (d) RT. LC conditions are the same as those in Fig. 2.

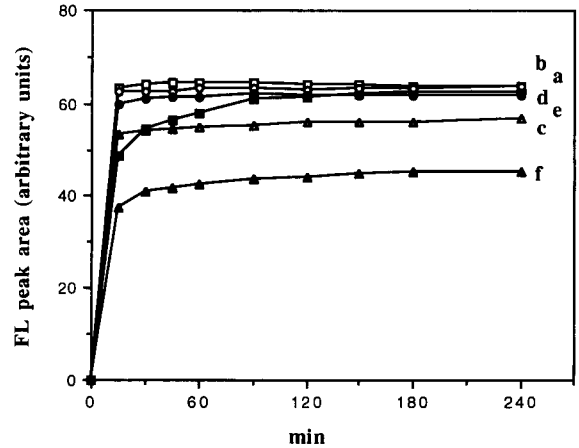

Fig. 4. Time course of the derivatization of *n*-heptylamine with *S*(−)-DBD-Pro-COCl in benzene (a) with pyridine at 80°C; (b) with pyridine at 50°C; (c) with pyridine at RT; (d) without pyridine at 80°C; (e) without pyridine at 50°C; (f) without pyridine at RT. Eluent, H_2O–CH_3CN (1:1); fluorescence detection, 560 nm (excitation at 450 nm). Other LC conditions are given in the Experimental section.

without pyridine in benzene as a function of time. The reaction rates appear to be faster than those of 1-heptanol at all temperatures tested. This is illustrated in Fig. 4. As observed with alcohols, the derivatization reaction was accelerated by pyridine. Even in the absence of the catalyst in the reaction medium at 80°C, good results were obtained (Fig. 4). Since the best results were obtained at 50°C in benzene containing 1% pyridine, 30 min reaction at 50°C was selected as the derivatization conditions for the determination of amines.

Fluorescence characteristics of the derivatives

The proposed derivatization reagent (DBD-Pro-COCl) yielded useful derivatives with alcohols, primary and secondary amines, phenols and anilines. The fluorescence properties of the derivatives were examined in acetonitrile–water which have widely been used as the components of mobile phases in reversed-phase chromatography. The fluorescence excitation and emission maxima of some derivatives are listed in Table 3. The resulting ester and amido derivatives showed almost the same excitation and emission maxima. The results suggest that the fluorescence is inde-

TABLE 3

Fluorescence properties of the derivative obtained from DBD-Pro-COCl

Compound	λmax (nm)		Medium [a]
	Excitation	Emission	
Ethanol	451	559	A
n-Butanol	451	560	A
Isoamyl alcohol	451	559	A
1-Hexanol	452	562	B
1-Heptanol	452	561	B
1-Phenylethanol	452	561	B
	451	559	A
Phenol	450	566	B
	447	562	C
1-Cyclohexylethylamine	451	565	B
Aniline	454	566	C

[a] Medium: A, H_2O–CH_3CN (4:6); B, H_2O–CH_3CN (1:1); C, H_2O–CH_3CN (55:45).

pendent of the compounds tested, but are dependent upon the fluorescence properties of the derivatization reagent itself. The fluorescence in long wavelength region must be an advantage for the determination of alcohols and amines in real samples, because the likelihood of interference by endogeneous substances in the short wavelength region is negligible. Furthermore, the excitation wavelength at around 450 nm is useful for the determination with LIF detection as previously demonstrated with 4-(*N*,*N*-dimethylaminosulfonyl)-7-(3-aminopyrrolidine-1-yl)-2,1,3-benzoxa-4-diazole (DBD-APy) derivatives of carboxylic acids [20,21].

LC separation of the derivatives

The separation of the derivatives obtained from alcohols and amines was studied with a reversed-phase column (Inertsil ODS-2) with aqueous acetonitrile. As shown in Tables 4 and 5, the elution order was dependedent upon the molecular weights of the alcohols and amines tested. Studies with *n*-heptylamine and 1-heptanol suggest that amido derivatives elute faster than ester derivatives. The same order of elution was observed with aniline and phenol derivatives. Nine aliphatic alcohols and three aliphatic amines were adequately resoluted with 80% acetonitrile and 50% acetonitrile, respectively. Typical chromatograms are shown in Figs. 5A and 6A. The detection limits (signal-to-noise ratio of 2) for the alcohols and amines, calculated from chromatograms, were in 10–500 fmol range for an injection volume of 10 μl. Greater sensitivity is achieved using other derivatization reagents such as DMEQ-COCl [13] and OMB-COCl [16]. An improvement in the sensitivity would be expected

TABLE 4

Retention behavior and detection limits of hydroxyl derivatives by reversed-phase chromatography [a]

Hydroxyl	Retention time (min)	*k'*	Detection limit with LIF, fmol ($S/N = 2$)	Eluent
1-Heptanol	5.02	4.02	2.3	A
	6.39	5.39	5.3	B
	9.00	8.00	ND	D
1-Octanol	6.31	5.31	3.8	A
	8.35	7.35	6.2	B
1-Nonanol	8.15	7.15	4.4	A
	11.17	10.17	7.7	B
1-Decanol	10.76	9.76	5.6	A
	15.23	14.23	11	B
1-Undecanol	5.78	4.78	2.7	C
	14.45	13.45	7.7	A
	21.09	20.09	15	B
1-Dodecanol	7.08	6.08	5.7	C
	19.70	18.70	16	A
1-Tridecylalcohol	8.79	7.79	33	C
	27.08	26.08	12	A
1-Tetradecanol	11.04	10.04	4.6	C
	37.52	36.52	19	A
1-Pentadecanol	13.98	12.98	10	C
	52.25	51.25	50	A
Phenol	3.79	2.79	ND	D
	6.24	5.24	ND	E
	12.89	11.89	140	F

[a] ND = not determined. $t_0 = 1.0$ min. Determination of detection limits: hydroxyl compounds (25 nM) reacted with DBD-Pro-COCl (5 mM) in benzene containing 1% pyridine. After heating at 80°C for 150 min, 450 μl of 1% methylamine in acetonitrile was added to 50 μl of the reaction solution cooled (final concentration, 2.5 pmol/ml). Then 5–60 μl (12.5–150 fmol) of the solution was subjected to LC and the detection limits were calculated from the comparison of peak height and variation of baseline noise. LC conditions, column: Inertsil ODS-2 (150×4.6 mm i.d., 5 μm) at 40°C, eluent: A, H_2O–CH_3CN (20:80); B, H_2O–CH_3CN (25:75); C, H_2O–CH_3CN (10:90); D, H_2O–CH_3CN (30:70); E, H_2O–CH_3CN (40:60); F, H_2O–CH_3CN (50:50); flow-rate: 1.0 ml/min, LIF detection, 15 mW argon ion.

with a LIF detector, relative to conventional fluorescence detector using xenon lamp, because the excitation wavelengths of the DBD-Pro-COOR and DBD-Pro-CONHR are close to light emission of argon-ion (488nm). As shown in Tables 4 and 5, the detection limits of alcohols and amines were improved by about two-orders of magnitude with LIF detection (2–10 fmol). In the case of phenol, the sensitive detection was not obtained with fluorescence or LIF detection (Table 4). It might be due to aromatic-OH group in phenol structure. Figures 5B and 6B show typical chromatograms with LIF detection at 15 mW. Under the proposed procedure with LIF detection, good linearities were obtained in the range from 2.5 nM (25 fmol/10 μl injection) to 0.5 μM (5 pmol/10 μl injection) of 1-heptanol (slope, 971; $r > 0.999$) and from 5.0 nM (50 fmol/10 μl injection) to 0.5 μM (5 pmol/10 μl injection) of *n*-heptylamine (slope, 480; $r > 0.999$). The coefficient of variation (C.V.) at 50 nM (0.5 pmol/10 μl injection) concentration of 1-heptanol and *n*-heptylamine were 6.0% ($n = 5$) and 9.1% ($n = 5$), respectively. With respect to stability of the derivatives, the loss of peak areas derived from alcohols and amines were less than 5% after 2 days at 5°C. Since the labelled analyte in the sample solution is fairly stable, sequence analysis of multiple samples seems to be possible with autoinjector equipped with cooling unit.

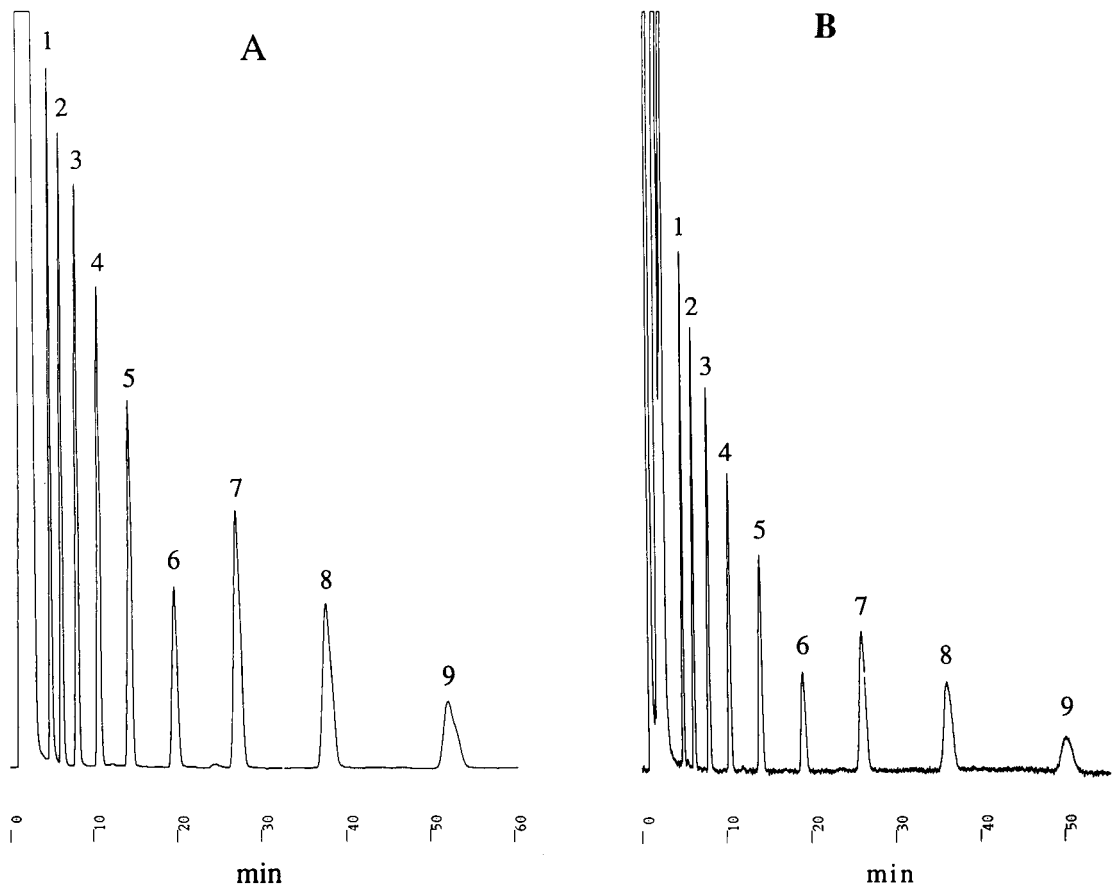

Fig. 5. Reversed-phase chromatography of alcohol derivatives obtained with *S*(−)-DBD-Pro-COCl. (A) FL detection at 560 nm (excitation, 450 nm), each peak corresponding to 5 pmol; (B) LIF detection at 15 mW, each peak corresponding to 0.2 pmol. Peaks: (1) 1-heptanol, (2) 1-octanol, (3) 1-nonanol, (4) 1-decanol, (5) 1-undecanol, (6) 1-dodecanol, (7) 1-tridecylalcohol, (8) 1-tetradecanol, (9) 1-pentadecanol. Eluent, H_2O–CH_3CN (2:8). Other LC conditions are given in the Experimental section.

The proposed derivatization reagents (DBD-Pro-COCls) exhibit excellent reactivity with alcohols and amines. The resulting derivatives are relatively stable and completely resolved by reversed-phase LC. While the detection limits obtained with conventional fluorescence detection are not as good as those compared with obtained with previously reported reagents, the detectiability at low fmol with LIF detection is one of most sensitive methods available. The long wavelength excitation and emission maxima of the derivatives might be another advantage for the detection in real samples because the likelihood of interference by intrinsic compounds, which emit at shorter wavelengths, is substantially reduced. Furthermore, the reagents may be also preferable for ultra trace analysis by peroxyoxalate chemiluminescence, since the fluorescence wavelengths

TABLE 5

Retention behavior and detection limits of amine derivatives by reversed-phase chromatography [a]

Amine	Retention time (min)	k'	Detection limit with LIF, fmol ($S/N = 2$)	Eluent
Methylamine	2.77	1.77	ND	A
Diethylamine	5.52	4.52	ND	A
n-Heptylamine	12.54	11.54	7.9	A
	6.11	5.11	ND	B
n-Octylamine	19.48	18.48	11	A
	8.29	7.29	ND	B
R(−)-1-Cyclohexyl-ethylamine	11.19	10.19	8.9	A
	19.70	18.70	ND	C
Aniline	6.26	5.26	4.6	A

[a] ND = not determined. $t_0 = 1.0$ min. Determination of detection limits: amines (50 nM) reacted with DBD-Pro-COCl (5 mM) in benzene containing 1% pyridine. After heating at 50°C for 30 min, 450 μl of 1% methylamine in acetonitrile was added to 50 μl of the reaction solution cooled (final concentration, 5 pmol/ml). Then 5–20 μl (25–100 fmol) of the solution was subjected to LC and the detection limits were calculated from the comparison of peak height and variation of baseline noise. LC conditions, column: Inertsil ODS-2 (150×4.6 mm i.d., 5 μm) at 40°C, eluent: A, H_2O–CH_3CN (50:50); B, H_2O–CH_3CN (40:60); C, H_2O–CH_3CN (55:45); flow-rate: 1.0 ml/min, LIF detection, 15 mW argon ion.

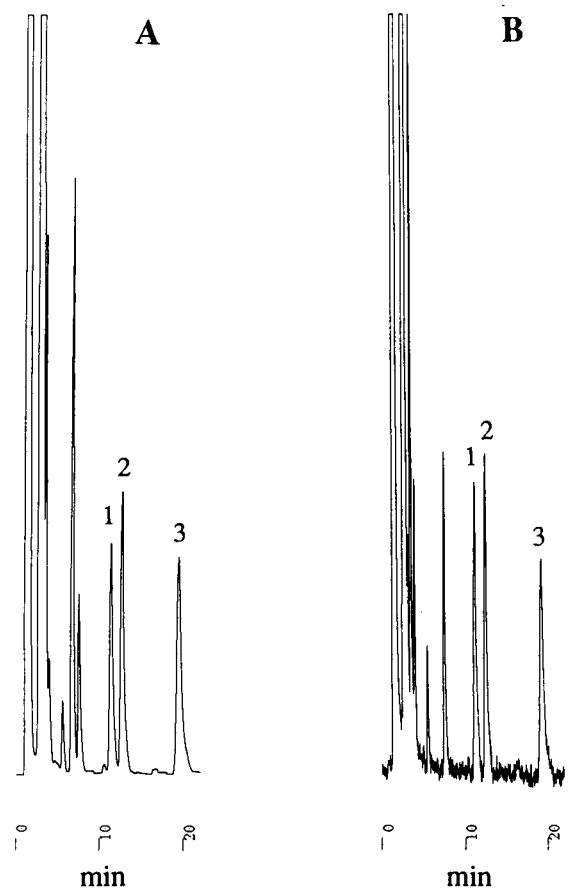

Fig. 6. Reversed-phase chromatography of amine derivatives obtained with *S*(−)-DBD-Pro-COCl. (A) FL detection at 560 nm (excitation, 450 nm), each peak corresponding to 2.5 pmol; (B) LIF detection at 15 mW, each peak corresponding to 0.1 pmol. Peaks: (1) *R*(−)-1-cyclohexylethylamine, (2) *n*-heptylamine, (3) *n*-octylamine. Eluent, H_2O–CH_3CN (1:1). Other LC conditions are given in the Experimental section.

are similar to those of DBD-APy derivatives which are detected at sub-attomole as reported in previous work [22]. Hence, the proposed method using DBD-Pro-COCl might serve for the determination of alcohols and amines in water and air. Further studies are currently in progress and the results will be reported.

The authors thank Dr. C.R. Warner, Food and Drug Administration in Washington DC, for reviewing the manuscript.

REFERENCES

1 K. Imai and T. Toyo'oka, in R.W. Frei and K. Zech (Eds.), Selective Sample Handling and Detection in High-performance Liquid Chromatography, Part A, J. Chromatogr. Library, Elsevier, Amsterdam, 1988, p. 209.
2 H. Lingeman, W.J.M. Underberg, A. Takadate and A. Hulshoff, J. Liq. Chromatogr., 8 (1985) 789.
3 R. Wintersteiger and G. Wenninger-Weinzierl, Fresenius' Z. Anal Chem., 309 (1981) 201.
4 R. Wintersteiger, G. Wenninger-Weinzierl and W. Pacha, J. Chromatogr., 237 (1982) 399.
5 R. Wintersteiger, J. Liq. Chromatogr., 5 (1982) 897.
6 H. Fujino, M. Eguchi and S. Goya, Yakugaku Zasshi, 110 (1990) 155.
7 A. Takadate, M. Irikura, T. Suehiro, H. Fujino and S. Goya, Chem. Pharm. Bull., 33 (1985) 1164.
8 M. Yamaguchi, T. Iwata, M. Nakamura and Y. Ohkura, Anal. Chim. Acta, 193 (1987) 209.
9 J. Goto, S. Komatsu, N. Goto and T. Nambara, Chem. Pharm. Bull., 29 (1981) 899.
10 J. Goto, N. Goto and T. Nambara, Chem. Pharm. Bull., 30 (1982) 4597.
11 J. Goto, N. Goto, F. Shamsa, M. Saito, S. Komatsu, K. Suzaki and T. Nambara, Anal. Chim. Acta, 147 (1983) 397.
12 K.E. Karlsson, D. Wiesler, M. Alsandro and M. Novotny, Anal. Chem., 57 (1985) 229.
13 T. Iwata, M. Yamaguchi, S. Hara, M. Nakamura and Y. Ohkura, J. Chromatogr., 362 (1986) 209.
14 A. Takadate, M. Iwai, H. Fujino, K. Tahara and S. Goya, Yakugaku Zasshi, 103 (1983) 962.
15 C. Matsuoka, H. Nohta, N. Kuroda and Y. Ohkura, J. Chromatogr., 341 (1985) 432.
16 H. Nagaoka, H. Nohta, Y. Kaetsu, M. Saito and Y. Ohkura, Anal. Sci., 5 (1989) 525.
17 T. Yoshida, Y. Moriyama and H. Taniguchi, Anal. Sci., 5 (1992) 355.
18 A. Takadate, T. Tahara, H. Fujino and S. Goya, Chem. Pharm. Bull., 30 (1982) 4120.
19 T. Toyo'oka, M. Ishibashi, T. Terao and K. Imai, Analyst (London), 118 (1993) 759.
20 T. Toyo'oka, M. Ishibashi and T. Terao, J. Chromatogr., 625 (1992) 357.
21 T. Toyo'oka, M. Ishibashi and T. Terao, Anal. Chim. Acta, 278 (1993) 71.
22 T. Toyo'oka, M. Ishibashi and T. Terao, J. Chromatogr., 627 (1992) 75.

Analytica Chimica Acta, 285 (1994) 353–358
Elsevier Science B.V., Amsterdam

Methods for assay of trimethoprim and sulphadiazine in broiler tissues using liquid chromatography

M. Dagorn and J.M. Delmas

CNEVA, Laboratoire des Médicaments Vétérinaires, La Haute Marche, 35133 Javene (France)

(Received 1st February 1993)

Abstract

A process for the extraction of sulphadiazine (SDZ) and trimethoprim (TMP) from broiler fortified tissues (plasma, lung, liver, kidney, fat, muscle, skin) was developed and a liquid chromatographic (LC) method for their determination is described. After extraction in acidic medium (pH 6.8) with ethyl acetate or dichloromethane, the extracts were purified with hexane–chloroform in an acidic buffer. Reversed-phase LC separation with gradient elution (phosphate buffer–acetonitrile) was applied. The values obtained for the quantification limit for both drugs are 0.100 $\mu g\ ml^{-1}$ for plasma, 0.100 $\mu g\ g^{-1}$ for lung and 0.050 $\mu g\ g^{-1}$ for the other tissues. The detection limits range from 0.010 to 0.015 $\mu g\ g^{-1}$ or ml^{-1} and from 0.020 to 0.025 $\mu g\ g^{-1}$ or ml^{-1} for SDZ and TMP, respectively. Recoveries, established by comparison of peak areas obtained with standards and those with fortified tissue, ranged between 85.7 and 67.2%, depending on the tissue.

Keywords: Liquid chromatography; Biological samples; Broiler tissues; Extraction; Pharmaceuticals; Sulphadiazine; Trimethoprim

In veterinary medicine, a combination of trimethoprim (TMP) and sulphadiazine (SDZ) is used to treat poultry via the drinking water for several consecutive days [1]. Notwithstanding their extensive use, only a few published data are available on the pharmacokinetics of these drugs in poultry. To judge the efficacy of TMP–SDZ, it is necessary to obtain data on concentrations at the sites where they must be active, especially the plasma and the lungs. These concentrations must be compared with the minimum inhibitory concentrations of the drugs in order to verify if the combination SDZ–TMP will be active or not. From a public health viewpoint, complete information about the pharmacokinetics of the combination of SDZ and TMP in broilers is desirable, because the maximum residue limits recommended for these drugs by EEC Council Regulation No. 675/92 are 50 and 100 $\mu g\ kg^{-1}$ for TMP and SDZ, respectively.

A liquid chromatographic (LC) method has already been described for broiler plasma [2], but there is no information about the assay of SDZ and TMP in broiler tissues. Therefore, it was necessary, before undertaking residue studies in broilers, to devise a sensitive method in order to determine TMP and SDZ. The aim of this study was to develop a suitable method for the simultaneous measurement of these two drugs.

Correspondence to: M. Dagorn, CNEVA, Laboratoire des Médicaments Vétérinaires, La Haute Marche, 35133 Javene (France).

EXPERIMENTAL

Apparatus and reagents

A Jouan K81 centrifuge, a Heidolph rotary magnetic stirrer, a Vortex magnetic stirrer, a

SSDI 0003-2670(93)E0543-G

Black and Decker electric chopper or Moulinex Mouli-grater manual rasp and a Buchi rotary evaporator were used.

Liquid chromatograph. A Varian Model 5500 gradient system equipped with a 200-μl sample loop, a Varian UV 200 variable-wavelength detector set at 270 nm, a 4 mm × 4 mm i.d. precolumn packed with RP-18 (LiChrospher 100, end-capped, 5 μm; Merck), a 12.5 cm × 4 mm i.d. column packed with RP-18 (LiChrospher, end-capped, 5 μm; Merck) and a Varian Vista 402 or Merck D 2000 computer for quantification were employed.

Mobile phase. An elution gradient of aqueous phase (0.01 M KH_2PO_4)–acetonitrile was applied as follows: time 0, 92% aqueous phase–8% acetonitrile; 10 min, 70% aqueous phase–30% acetonitrile; 10.1 min, 92% of aqueous phase–8% acetonitrile; 16 min, end of gradient. All solvents and chemicals were of analytical-reagent grade (Merck).

Standard solutions. Stock standard solutions (500 μg ml^{-1}) are prepared as follows. In 100-ml volumetric flasks, dissolve 49.75 mg of base SDZ (Welcome, batch DY 55.0, analytical grade, 100.5%), TMP (Welcome, batch 7987-84, analytical grade, 100.1%) in methanol and dilute to volume with methanol.

For working standard solutions, dilute aliquots of the stock standard solution in 0.01 M KH_2PO_4 buffer to 0.05, 1 and 10 μg ml^{-1}.

For fortification solutions, dilute aliquots of the stock solution to obtain 250, 50, 25, 5, 1, 0.5 and 0.1 μg ml^{-1} solutions in ultra-purified water for lung and plasma fortifications or in 0.1% acid for the other tissues.

Tissue grinding. Take about 20 g of thawed control tissue (muscle, liver, kidney, fat), cut it into small pieces and grind for 30 s. For skin, rasp about 20 g of frozen tissue (−80°C) with a manual rasp.

Distribute 1-g amounts, exactly weighed, into centrifugation tubes fitted with glass caps. Deep-freeze at −20°C, pending fortification. For lung tissue, the grinding is performed after fortification.

Fortifications. All the plasma fortifications are performed on the same day. Dilute as needed to obtain plasma fortifications at 0.1, 0.5, 1, 5 and 10 μg ml^{-1} in a ratio of 200 μl of standard to 10 g of plasma. Mix with a Heidolph rotary stirrer at 100 rpm for 15 min. Keep the fortified plasmas at −20°C until assayed.

For lung, to 10 g of tissue add 10 ml of standard solutions in order to obtain the chosen concentrations of 0.1, 0.5, 1, 5 and 10 μg g^{-1}. Mix with a Heidolph rotary stirrer for 15 min, then allow to settle for 30 min. Keep at −20°C until assayed.

Fortifications of muscle, liver, kidney, skin and fat were done every day on aliquots of 1 g of ground tissue by adding a volume of 1 ml to obtain tissue concentrations of 0.05, 0.1, 0.2, 0.5 and 1 μg g^{-1}.

For the control or treated broiler samples, 1 ml of 0.1% HCl is added to the ground tissues, except for lung, where water is added instead of HCl, so that its weight is the same as the lung sample.

Extraction and purification

For all the tissues, the extraction process was nearly the same (Table 1). To the sample in the centrifuge tube, add 200 μl (for plasma) or 500 μl (for lung, kidney, liver, fat, skin) of phosphate buffer (1 or 2 M KH_2PO_4, pH 6.8) except for muscle (100 μl of 1 M NaOH) and extract with ethyl acetate (plasma, lung, muscle) or dichloromethane (other tissues). Centrifuge for 10 min at 4000 *g*, then transfer 4.8 ml of the supernatant into a 20-ml round-bottomed flask. Evaporate to dryness under reduced pressure in a 30°C water-bath. Dissolve the residue in 1.6 ml of the hexane–chloroform, then add either 0.8 ml of 0.1% HCl for muscle, kidney, liver, fat and skin or 0.8 ml of 0.01 M KH_2PO_4 for lung or plasma. Mix gently with a Heidolph rotary stirrer at 35 rpm for 15 min. Transfer into a centrifuge tube, centrifuge for 30 min at 4000 *g* and inject the supernatant into the sample loop of the chromatograph.

Validation

The concentration range studied was between 10 and 0.05 μg g^{-1} for muscle, liver, kidney, fat and skin. For plasma and lung, the concentra-

TABLE 1

Extraction steps

Extraction step	Plasma	Lung	Muscle	Kidney, liver	Fat, skin
Add KH_2PO_4 buffer	1 M, 200 µl	1 M, 500 µl	0 µl	2 M, 500 µl	2 M, 500 µl
Add 1 M NaOH	No	No	100 µl	No	No
Shake : Manual	10 s	No	No	No	No
Vortex	No	15 s	15 s	15 s	10 s
Eliminate fat	No	No	No	No	Add 2 ml hexane Mix with Heidolph rotary stirrer at 100 rpm for 5 min Centrifuge for 5 min at 3000 *g* Discard upper hexane phase
Add 6 ml	Ethyl acetate			Dichloromethane	
Mix with Heidolph rotary stirrer	100 rpm for 30 min			100 rpm for 15 min	
Settle for 15 min	Yes	No	No	No	No
Add 2 ml of water	Yes	No	No	No	No
Mix for 10 s with Vortex	Yes	No	No	No	No
Centrifuge for 10 min at 4000 *g*	Yes	Yes	Yes	Yes	Yes
Discard aqueous phase and tissue pieces present in this phase	No	No	No	Yes	Yes
Place 4.8 ml of supernatant in round-bottomed flask	Yes	Yes	Yes	Yes	Yes

tions were between 10 and 0.100 µg ml^{-1} or g^{-1}. The validation was performed by confirming the response linearity coupled with a study of the reproducibility and repeatability after analysis of extracts obtained from fortified tissues. As the response of the detector to these compounds is known, the amounts in fortified samples were calculated by comparing the chromatographic peak areas with those for standards. These tests were carried out by the same technician using the same equipment on different days.

Statistical analysis of the areas measured was performed to verify the linearity and the sensitivity [3]. Repeatability and reproducibility were tested according to the recommendations of the standard NF X 06-041 [4].

The recoveries were evaluated by comparison between peak areas for fortified tissues and standards.

RESULTS

Some examples of chromatograms for control and fortified tissues are shown in Figs. 1 and 2. The chromatograms of control tissues do not show any interferents with similar retention times to those found for SDZ and TMP. The retention times, $t_R = 6.80$ min for SDZ and 10.20 min for TMP, are only approximate. As the LC system was not thermostated, they vary according to the ambient temperature. The detector response to these two compounds, based on peak area, is linear over the concentration range 0.05–10 µg ml^{-1}.

The results of the fidelity study are given in Table 2 for repeatability and in Table 3 for reproducibility. Generally, the confidence limits were < 20%, whatever the concentration of SDZ and TMP tested. However, for the assays of TMP in

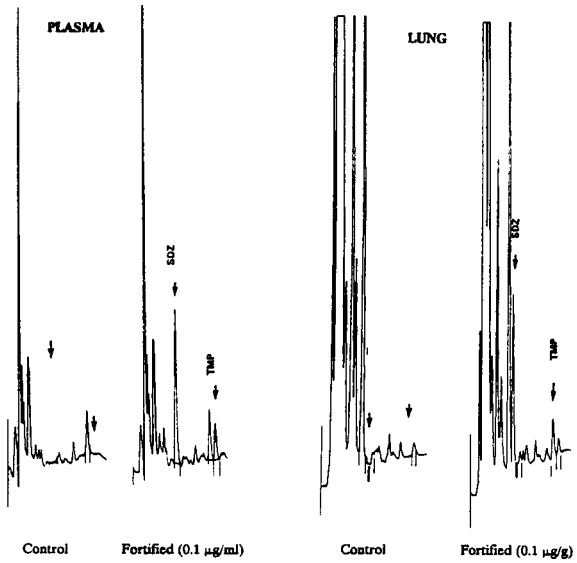

Fig. 1. Chromatograms of control and fortified plasma and lung with SDZ and TMP at 0.1 μg ml^{-1} or g^{-1} (limit of quantification).

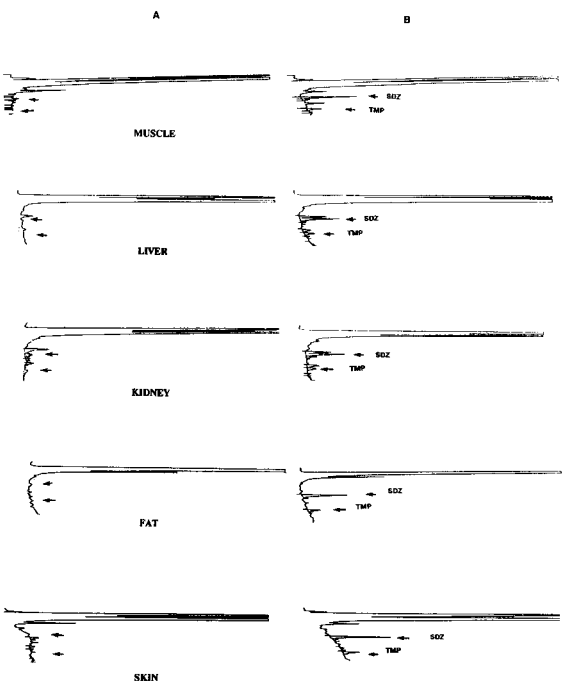

Fig. 2. Chromatograms of (A) tissue control and (B) fortified tissues with SDZ and TMP at 0.05 μg g^{-1} (limit of quantification).

TABLE 2

Repeatability: relative standard deviation (%) ($n = 5$ per concentration per tissue. In total 50 measurements per tissue)

Drug	Tissue	Concentration (μg g^{-1} or ml^{-1})				
		0.1	0.5	1.0	5.0	10.0
SDZ	Plasma	12.2	6.0	4.8	5.0	5.8
	Lung	9.1	4.8	5.7	3.6	3.8
TMP	Plasma	17.9	3.2	6.7	2.4	6.9
	Lung	25.8	8.6	7.1	4.2	2.5
		Concentration (μg g^{-1})				
		0.05	0.1	0.2	0.5	1.0
SDZ	Muscle	2.6	1.9	5.1	2.6	1.5
	Liver	13.5	10.8	2.0	2.2	2.2
	Kidney	10.3	4.5	1.3	3.0	2.7
	Fat	12.1	9.6	3.4	2.0	1.7
	Skin	9.1	10.7	2.1	1.3	2.7
TMP	Muscle	12.1	7.6	3.7	5.2	3.1
	Liver: area	31.3	35.2	8.9	10.4	6.4
	height	20.1	9.0	5.5	3.9	3.6
	Kidney	13.9	17.8	9.1	4.6	7.3
	Fat	16.6	13.6	6.0	2.5	4.1
	Skin	12.3	15.4	5.6	5.7	3.5

liver, the confidence intervals were close to 35% for concentrations under 0.1 μg g^{-1}. As the baseline noise for the control liver was high, the TMP

TABLE 3

Reproducibility: relative standard deviation (%) ($n = 5$ per concentration per tissue. In total 50 measurements per tissue)

Drug	Tissue	Concentration (μg g^{-1} or ml^{-1})				
		0.1	0.5	1.0	5.0	10.0
SDZ	Plasma	14.0	17.0	12.1	8.0	7.4
	Lung	12.9	7.8	10.6	9.3	10.3
TMP	Plasma	17.9	17.2	6.9	11.4	9.0
	Lung	25.8	15.7	7.1	10.0	8.4
		Concentration (μg g^{-1})				
		0.05	0.1	0.2	0.5	1.0
SDZ	Muscle	11.1	18.6	12.5	9.6	0.1
	Liver	21.8	20.9	13.2	12.0	12.4
	Kidney	13.7	16.6	8.7	5.2	7.6
	Fat	12.1	18.7	7.6	7.2	10.5
	Skin	10.6	11.8	18.0	4.4	13.2
TMP	Muscle	16.4	14.9	5.9	8.4	8.9
	Liver: area	33.9	37.8	13.4	16.0	18.2
	height	37.6	9.0	15.2	20.8	20.5
	Kidney	17.5	24.3	10.7	13.8	10.4
	Fat	20.2	21.3	16.3	7.9	13.5
	Skin	16.8	15.4	17.3	7.0	9.6

TABLE 4

SDZ recovery

Tissue	Concentration ($\mu g\ g^{-1}$ or ml^{-1})	Recovery [a] (%)	Mean recovery ± s.d. (%) and extract tissue equation [b]
Plasma	0.10	81.7 ± 3.4	
	0.50	82.0 ± 4.6	
	1.00	81.4 ± 2.2	83.53 ± 4.18
	5.00	88.4 ± 2.4	$y = -525.36 + 120584x$
	10.00	84.0 ± 2.2	($r = 0.999$)
Lung	0.10	75.6 ± 3.3	
	0.50	75.0 ± 2.0	
	1.00	69.3 ± 2.5	74.71 ± 4.03
	5.00	74.6 ± 2.5	$y = -15319.99 + 135204.3x$
	10.00	79.0 ± 2.3	($r = 0.999$)
Muscle	0.05	83.8 ± 3.7	
	0.10	83.0 ± 6.2	
	0.20	83.8 ± 4.2	83.81 ± 4.26
	0.50	85.2 ± 3.2	$y = 59.43 + 146526.3x$
	1.00	83.3 ± 3.9	($r = 0.996$)
Liver	0.05	71.0 ± 4.6	
	0.10	69.6 ± 3.4	
	0.20	69.0 ± 2.6	69.06 ± 3.83
	0.50	68.0 ± 3.0	$y = 452.32 + 115061.3x$
	1.00	68.0 ± 5.7	($r = 0.996$)
Kidney	0.05	70.1 ± 3.3	
	0.10	69.5 ± 3.9	
	0.20	71.8 ± 2.1	69.99 ± 2.75
	0.50	70.0 ± 1.2	$y = 614.97 + 116258.2x$
	1.00	68.6 ± 1.8	($r = 0.999$)
Fat	0.05	79.4 ± 3.3	
	0.10	77.5 ± 4.9	
	0.20	78.1 ± 2.0	78.15 ± 3.15
	0.50	79.1 ± 1.9	$y = -580.7 + 137109.5x$
	1.00	79.4 ± 2.8	($r = 0.998$)
Skin	0.05	67.7 ± 2.5	
	0.10	68.9 ± 2.8	
	0.20	66.9 ± 4.0	67.24 ± 3.18
	0.50	65.3 ± 2.9	$y = -155.1 + 130250.2x$
	1.00	67.5 ± 3.0	($r = 0.998$)

[a] Mean ± s.d. ($n = 10$). y = Area ($\mu V\ s^{-1}$); x = concentration in extract tissue ($\mu g\ g^{-1}$ or ml^{-1}).

concentrations were evaluated by measurement of either peak area or peak height.

Limits of quantification and detection and recovery

The quantification limits were evaluated as the smallest amount of SDZ or TMP assayed during the validation and were 0.1 $\mu g\ ml^{-1}$ or g^{-1} for plasma and lung and 0.05 $\mu g\ g^{-1}$ for all the tissues. The detection limits (2σ) were defined graphically: for TMP, 0.020 $\mu g\ ml^{-1}$ or g^{-1} for plasma and muscle and 0.025 $\mu g\ g^{-1}$ for lung, liver, skin, fat and kidney; for SDZ, 0.010 $\mu g\ ml^{-1}$ or g^{-1} all the tissues except for lung (0.015 $\mu g\ g^{-1}$).

At each concentration, ten assays of fortified tissue and five assays of standards were carried out. The results are given in Tables 4 and 5. The average extraction recoveries ranged between 83.8 and 67.2% for SDZ (lowest value for skin), and from 85.7 to 65.5% for TMP (lowest value for liver).

TABLE 5

TMP recovery

Tissue	Concentration ($\mu g\ g^{-1}$ or ml^{-1})	Recovery [a] (%)	Mean recovery ± s.d. (%) and extract tissue equation [b]
Plasma	0.10	86.0 ± 4.8	
	0.50	82.9 ± 4.9	
	1.00	85.8 ± 2.7	85.74 ± 3.94
	5.00	86.8 ± 3.4	$y = -1003.7 + 38409.17x$
	10.00	87.3 ± 2.7	($r = 0.999$)
Lung	0.10	73.7 ± 7.3	
	0.50	68.7 ± 3.7	
	1.00	67.3 ± 1.6	69.37 ± 4.44
	5.00	69.5 ± 2.0	$y = -137.39 + 32870.75x$
	10.00	67.6 ± 1.9	($r = 0.999$)
Muscle	0.05	87.2 ± 5.7	
	0.10	81.6 ± 5.0	
	0.20	76.2 ± 2.0	79.22 ± 6.07
	0.50	76.9 ± 2.9	$y = 238.48 + 34254.15x$
	1.00	74.1 ± 3.0	($r = 0.997$)
Liver	0.05	71.0 ± 8.4	
	0.10	67.9 ± 9.0	
	0.20	65.7 ± 3.0	66.03 ± 6.77
	0.50	64.7 ± 3.5	$y = 532.62 + 27201.8x$
	1.00	60.9 ± 3.7	($r = 0.997$)
Kidney	0.05	75.5 ± 4.6	
	0.10	73.4 ± 6.1	
	0.20	67.6 ± 2.5	69.17 ± 5.86
	0.50	65.2 ± 3.0	$y = 449.24 + 28868.6x$
	1.00	64.3 ± 2.2	($r = 0.999$)
Fat	0.05	73.4 ± 5.8	
	0.10	85.3 ± 6.2	
	0.20	87.6 ± 4.8	84.61 ± 4.93
	0.50	82.7 ± 2.2	$y = -111.2 + 38915.4x$
	1.00	84.1 ± 3.8	($r = 0.998$)
Skin	0.05	76.6 ± 4.4	
	0.10	77.5 ± 9.0	
	0.20	76.6 ± 4.4	76.26 ± 4.98
	0.50	74.3 ± 1.8	$y = -77.98 + 39516.05x$
	1.00	76.4 ± 2.5	($r = 0.998$)

[a] Mean ± s.d. ($n = 10$). [b] x and y as in Table 4.

Conclusion

The analytical methods proposed should allow the detection and quantification of these analytes, in tissues of broilers treated with a combination of TMP and SDZ, at the maximum residue level (50 $\mu g\ kg^{-1}$ and 100 $\mu g\ kg^{-1}$ for TMP and SDZ, respectively). It is also suitable to evaluate their kinetics in broiler plasma and lung.

REFERENCES

1 S.R.M. Bushby, J. Am. Vet. Med. Assoc., 176 (1980) 1049.
2 W. Löscher, C.P. Fabbender, M. Weissing and M. Kietzmann, J. Vet. Pharmacol. Ther., 13 (1990) 309.
3 Traitement des Résultats de Mesure. Utilisation de Grandeurs de Référence dans les Méthodes de Mesure, AFNOR NF X 06-045, AFNOR, Paris, 1985.
4 Fidélité des Méthodes d'Essais. Détermination de la Répétabilité et de la Reproductibilité d'une Méthode d'Essai Normalisée par des Essais Interlaboratoires, AFNOR NF X 06-041 (ISO 5725), AFNOR, Paris, 1987.

Analytica Chimica Acta, 285 (1994) 359–364
Elsevier Science B.V., Amsterdam

Evaluation of some wet decomposition methods for mercury determination in biological and environmental materials by cold vapour atomic absorption spectroscopy

S.B. Adeloju, H.S. Dhindsa [a] and R.K. Tandon

Centre for Electrochemical Research and Analytical Technology, Department of Chemistry, University of Western Sydney, Nepean, P.O. Box 10, Kingswood, NSW 2747 (Australia)

(Received 6th June 1993; revised manuscript received 4th October 1993)

Abstract

Four of the most commonly used wet digestion methods were evaluated for the accurate determination of mercury in biological and environmental materials by cold vapour atomic absorption spectroscopy. The method based on the use of HNO_3–H_2SO_4 mixture was found to be most suitable for the reliable determination of the element. The recovery efficiencies of the method for mercury in fish homogenate and horse kidney samples were 95.9 and 105.7%, respectively for the inorganic form, and 89.0 and 99.8% for the organic form. The method based on the use of HNO_3–H_2O_2 mixture also gave similar recoveries for the organic and inorganic mercury in these samples. In comparison, the recoveries of the organic mercury in the fish and kidney samples by the use of HNO_3 only and HNO_3–$HClO_4$ mixture were $< 50\%$, but their recovery efficiencies for the inorganic mercury were close to 100%. The application of the method utilizing the HNO_3–H_2SO_4 mixture to a range of biological and environmental standard reference materials gave the most accurate and reproducible analytical data. The suitability of the digestion method for the reliable determination of mercury in soil samples was also demonstrated.

Keywords: Atomic absorption spectrometry; Mercury; Wet decomposition methods; Environmental materials; Soil; Fish; Horse kidney; Bovine liver

Cold vapour atomic absorption spectroscopy (CV-AAS) is one of the most sensitive and simple techniques for the determination of trace and ultra-trace concentrations of mercury in biological and environmental materials [1]. However, the direct determination of the element in these materials is not feasible because of the enormous matrix effects usually encountered, particularly in solid samples. The accurate determination of mercury in these materials, therefore, often requires the decomposition of the organic matrices and the conversion of the mercury to the inorganic divalent form.

The two types of decomposition methods commonly employed for the determination of trace elements in biological and environmental materials are wet digestion and dry ashing [1,2]. Dry ashing is not suitable for mercury determination because of the low boiling points of mercury and its associated compounds. Consequently, wet digestion at relatively low temperatures (< 100°C) is often employed for this purpose.

The suitability of wet digestion methods for the CV-AAS determination of mercury was eval-

Correspondence to: S.B. Adeloju, Centre for Electrochemical Research and Analytical Technology, Department of Chemistry, University of Western Sydney, Nepean, P.O. Box 10, Kingswood, NSW 2747 (Australia).

[a] Current address: Department of Biological Sciences, Faculty of Health Sciences, University of Sydney, Lidcombe, NSW 2141 (Australia).

SSDI 0003-2670(93)E0560-T

uated about 20 years ago when the technique was still in its infancy [3,4]. Over this period, several major improvements have been made to the technique and its application to a diverse range of sample matrices has been reported. However, the need for the re-evaluation of the existing wet digestion methods for the CV-AAS determination of mercury in biological and environmental materials was recently highlighted by the inconsistencies observed in the use of different digestion methods with the technique [5]. Furthermore, there is still a general tendency to adopt any wet decomposition method for the determination of mercury by this technique despite the previous evaluation of various wet digestion methods. The danger of adopting such an approach has also been demonstrated in a recent study which indicated that the mercury response can be significantly influenced by the presence of some acids [6].

Based on the survey of the literature for the past 20 years, the four most commonly employed wet digestion methods have been evaluated in this study for the determination of trace and ultra-trace concentrations of mercury in biological and environmental materials. The chosen decomposition methods include wet digestion with (a) HNO_3 only, (b) HNO_3–H_2SO_4, (c) HNO_3–$HClO_4$, and (d) HNO_3–H_2O_2. The effectiveness of these methods for the CV-AAS determination of mercury has been compared by the use of three standard reference materials representing a diverse range of biological and environmental materials. Also, the applicability of the best wet digestion method for the determination of mercury in polluted and unpolluted soil samples has been investigated.

EXPERIMENTAL

Reagents and standards

All reagents used in this study were of analytical grade. Mercury stock solution (2 g/l) was prepared by dissolving appropriate amount of mercuric chloride in 20% (v/v) hydrochloric acid. A mercury standard (0.1 mg/l) was prepared daily by diluting the stock in 2% (v/v) hydrochloric acid. Stock solution of organic mercury (1 g/l) was prepared by dissolving appropriate amount of methylmercury chloride in ethanol (12 ml of 96%, v/v) and diluting to volume (100 ml) with water. Stannous chloride solution (30%, w/v) was prepared daily by dissolving appropriate amount in 20% (v/v) hydrochloric acid and stabilised by the addition of a piece of tin. All solutions were prepared with Milli-Q water.

The standard reference materials fish homogenate (Ma-A-2) and horse kidney (H-8) were obtained from IAEA, Vienna, while the bovine liver (1577b) was from NIST, USA.

All glassware and plastic containers were soaked in nitric acid (2 M) for at least 24 h and rinsed 4–5 times with Milli-Q water prior to use.

Instrumentation and glassware

All CV-AAS measurements were performed on a GBC Model 902 atomic absorption spectrophotometer operated in a single beam mode. The conditions employed for the measurements were: wavelength, 253.7 nm; slit width, 0.5 nm; lamp current, 0.3 mA; and cell temperature, 40°C.

Procedure

CV-AAS measurement. A 100-ml Erlenmeyer flask containing 20 ml sample or standard solution was connected to the mercury vapour generation system, 1 ml of stannous chloride solution was added and the contents of the flask were stirred with a magnetic stirrer at maximum speed for 3 min. The resulting mercury vapour was displaced from the flask to the mercury cell by the water displacement method [7] at a rate of 10 ml/s. After recording the mercury response, the cell was flushed out with pure argon.

Wet digestion methods. For simplicity, the wet digestion methods utilizing HNO_3, HNO_3–H_2SO_4, HNO_3–$HClO_4$ and HNO_3–H_2O_2 mixtures are referred to as methods M1, M2, M3 and M4, respectively. The digestion of the fish homogenate with concentrated HNO_3 (M1) and the (2.25:1 by volume) mixture of concentrated HNO_3 and concentrated H_2SO_4 (M2) involved the accurate weighing of 0.2 g of the sample (or 0.1 g horse kidney or 3.0 g bovine liver) into a precleaned 100-ml Erlenmeyer flask, followed by the

addition of 2.5 ml (or 6.0 ml for bovine liver) of the acid or the mixture and heating of the loosely stoppered flask at 90°C for 90 and 60 min, respectively. The flask was then cooled to room temperature and the stopper as well as the sides of the wall were rinsed with Milli-Q water. The final volume was made up to 20 ml and this was used for the mercury measurement, as previously described.

The digestion of the fish homogenate with the HNO_3–$HClO_4$ (M3) and HNO_3–H_2O_2 (M4) was performed initially as described for method M1, but heating only for 30 min. After this period, the flask was cooled to room temperature, 1.0 ml (or 2.0 ml for bovine liver) of concentrated $HClO_4$ or H_2O_2 was added and the flask was further heated for 30 min. The flask was then cooled, and the solution was made up and measured as described above for M1 and M2.

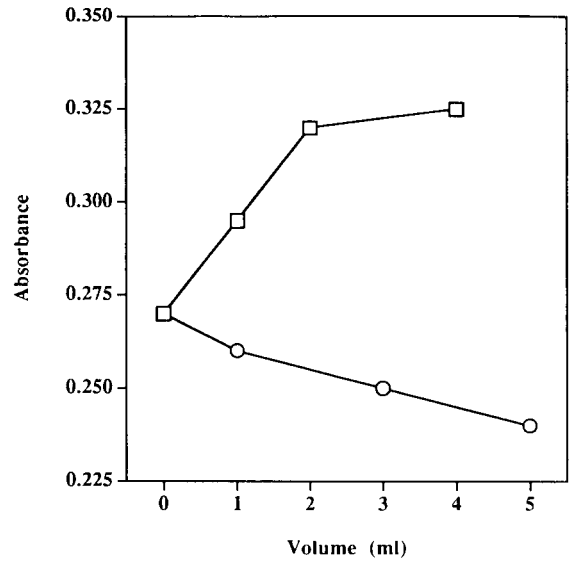

Fig. 1. Influence of increasing volume of components of the HNO_3–H_2SO_4 mixture on the mercury response. Initial acid volumes at zero addition are 1.7 ml HNO_3 and 0.8 ml H_2SO_4; 0.2 μg Hg. Key: □ = H_2SO_4; ○ = HNO_3.

RESULTS AND DISCUSSION

Influence of digestion mixtures on mercury response

Table 1 shows the influence of the digestion mixtures on the detection limit and sensitivity of CV-AAS technique for mercury determination. In general, there appears to be no significant advantage in using any of the digestion mixtures over the others. However, this trend may be significantly altered when employed for the decomposition of biological and environmental materials, depending on the effectiveness of the mixture in breaking down the organic matrix and releasing the mercury in its inorganic form. Also, in this regard the residual amount of the digestion mixture component may have some influence on the sensitivity of the CV-AAS method.

TABLE 1

Influence of digestion mixtures on the detection limit and sensitivity of CV-AAS

Digestion mixture	Detection limit (ng) [a]	Sensitivity (ng/0.0044 Abs.)
HNO_3	3.3	2.9
HNO_3–H_2SO_4	4.1	2.7
HNO_3–$HClO_4$	2.3	2.7
HNO_3–H_2O_2	3.2	2.9

[a] Based on three times standard deviation; $n = 6$.

Figure 1 shows that the increasing addition of individual component of the HNO_3–H_2SO_4 mixture affected the sensitivity of the mercury response significantly. While the addition of increasing volume of sulphuric acid enhanced the mercury response, the presence of more nitric acid results in slight suppression of the response. It appears, as previously reported [6], that the increasing addition of sulphuric acid increased the sensitivity of the mercury response by enhancing the partition coefficient of the element between vapour and solution. In contrast, the increasing addition of nitric acid slightly suppressed the partition coefficient.

The increasing addition of the individual component of the HNO_3–$HClO_4$ and HNO_3–H_2O_2 mixture only had slight effect on the mercury response. This observation indicates that the variation in the residual amount of the HNO_3–$HClO_4$ and HNO_3–H_2O_2 mixtures will have the least effect on the sensitivity of the mercury response. In contrast, the variation in the residual amount

TABLE 2

Recovery efficiencies of digestion methods in fish homogenate and horse kidney samples[a]

Digestion methods	Inorganic ($HgCl_2$)		Organic (CH_3HgCl)	
	FH (%)	HK (%)	FH (%)	HK (%)
M1	87.9	103.7	–	43.0
M2	95.9	105.7	89.0	99.8
M3	103.2	101.0	46.6	43.9
M4	108.0	99.4	84.3	109.5

[a] $n = 3$.

of the HNO_3–H_2SO_4 mixture components will tend to have more influence on the mercury response. Nevertheless, the effectiveness of the digestion mixtures in breaking down the organic matrices in solid biological and environmental materials may be a more significant factor in obtaining reliable and accurate mercury concentrations by CV-AAS.

Recovery of inorganic and organic mercury

The effectiveness of the digestion methods in recovering inorganic and organic mercury spikes in the reference materials is given in Table 2. With the exception of the low recovery of mercury in the fish homogenate obtained with HNO_3 digestion, the recovery efficiencies for the inorganic mercury were close to 100% in all cases. These results show that most wet decomposition methods are adequate for the recovery of the inorganic form of mercury in most biological and environmental materials. The comparatively low recovery (87.9%) of the inorganic mercury in the fish homogenate by method M1 indicates that the sample matrix is more difficult to decompose with nitric acid than the horse kidney.

The digestion methods were however not as effective in recovering organic mercury in the fish homogenate and horse kidney samples. Digestion methods M1 and M3 were inadequate for the complete recovery of organic mercury from both samples (Table 2). Riisgard and Hansen [8] have recently reported that the recovery of organic mercury by digestion with HNO_3–KOH mixture decreased from 108 to 77% when the amount of organic mercury was increased from 2.5 to 20 ng. The use of digestion methods M1 and M3 may, therefore, be inadequate for the complete recovery of the 50 ng of organic mercury employed in the present study. In contrast, the recovery efficiencies obtained for the organic mercury in both samples with the digestion methods M2 and M4 were much higher. Even the mixtures used in these digestion methods only gave 89% (M2) and 84.3% (M4) recovery for the organic mercury in the fish homogenate. Nevertheless, full recovery of the organic mercury in the horse kidney sample was obtained by both digestion methods. It can, therefore, be concluded that the recovery of the organic mercury is influenced by the nature of the sample matrix and the oxidising strength of the digestion mixtures.

Other considerations

Among the important considerations in the selection of a suitable digestion method for the determination of mercury in biological and environmental materials by CV-AAS are blank levels, required digestion time and safety. The blank levels obtained for the digestion mixtures were generally comparable. Further improvement of the blank levels beyond those obtained in this study may be obtained by the use of ultra-pure reagents.

The required digestion time of 90 min for the complete release of mercury with M1 was 30 min longer than required by the other digestion methods. This is due to the lower oxidising power of nitric acid on its own, but the time factor can be quite significant when dealing with large number of samples. In this regard, the digestion methods utilizing M2, M3 and M4 mixtures are more time-efficient.

The use of digestion method M2 is relatively simple and less explosive compared to methods M3 and M4, but exothermic and violent reactions may be caused by this mixture when large amounts of sample material is digested. Under these conditions the pre-wetting of the sample with water, prior to the wet decomposition is recommended. The necessary safety considerations must be made when employing perchloric acid and hydrogen peroxide as digestion mixture. In contrast, the use of nitric acid does not create any problem with

respect to safety, but its effectiveness in the decomposition of biological and environmental materials for reliable and accurate mercury determination by CV-AAS is a major concern. The use of HNO_3–H_2SO_4 provides the best compromise between safety and effectiveness for the reliable and accurate determination of the element.

Application to reference materials and soil samples

Table 3 shows that the concentrations of mercury obtained in the fish homogenate digested with methods M1, M2 and M3 were comparable and all agreed with the certified value. However, the mercury concentration obtained with the HNO_3–H_2O_2 mixture was much higher and outside the certified range. On the basis of the accurate result obtained for the sample digested with HNO_3, the higher concentration obtained with M4 may be due to the interference of H_2O_2 or its digestion product with the CV-AAS measurement.

Similarly the concentrations of mercury obtained for the horse kidney and bovine liver samples by all digestion methods agreed favourably with the certified value. The higher mercury concentration obtained for the bovine liver with the HNO_3 digestion may be due to interference from the presence of incompletely digested sample or the presence of nitrogen oxides. The effect of the latter can be removed by the addition of urea or sulphamic acid [6].

On the basis of the results obtained for the reference materials and the previous recovery efficiencies for inorganic and organic mercury, the most effective digestion mixture for the wet decomposition of biological and environmental materials for the reliable and accurate determination of mercury by CV-AAS is the HNO_3–H_2SO_4 mixture. The effectiveness of this digestion method is further demonstrated by its application to the determination of mercury in uncontaminated and contaminated soil samples. Table 4 shows that the recovery of mercury in the spiked soil samples was close to 100%.

TABLE 3

Mercury concentrations obtained in standard reference materials with the digestion methods

Digestion methods	Fish homog. ($\mu g/g$) [a]	Horse kidney ($\mu g/g$) [a]	Bovine liver ($\mu g/g$) [a]
M1	0.467 ± 0.030	0.877 ± 0.021	0.0042 ± 0.0009
M2	0.472 ± 0.004	0.884 ± 0.040	0.0023 ± 0.0006
M3	0.475 ± 0.030	0.876 ± 0.016	0.0027 ± 0.0007
M4	0.545 ± 0.008	0.901 ± 0.004	0.0022 ± 0.0009
Certified Value [b]	0.47 ± 0.03	0.91 ± 0.07	0.003 [c]

[a] Based on mean deviation. [b] Based on standard deviation. [c] Non-certified value; $n = 3$.

TABLE 4

Mercury concentrations obtained in soil samples with the HNO_3–H_2SO_4 digestion method

Sample	Nature of sample	Amount added ($\mu g/g$)	Amount found ($\mu g/g$)
S1	Uncontaminated	–	0.018 ± 0.003
S2	Uncontaminated	–	0.126 ± 0.005
S3	Uncontaminated	–	0.074 ± 0.006
S4	Spiked	1.0	0.995 ± 0.005 [a]
S5	Spiked	1.0	$0,977 \pm 0.006$ [a]
S6	Spiked	1.0	0.964 ± 0.004 [a]
S7	Contaminated	–	0.465 ± 0.007

[a] After correcting for the concentration of mercury in sample; $n = 3$.

Conclusions

The use of wet decomposition methods for the accurate determination of mercury in biological and environmental materials by cold vapour atomic absorption spectroscopy requires careful consideration of the choice of digestion mixture. The wet decomposition of these materials with the HNO_3–H_2SO_4 mixture was found to be most effective for the complete recovery of inorganic and organic mercury. The decomposition method also proved to be most satisfactory for the reliable determination of mercury in fish homogenate, horse kidney, bovine liver and soil samples.

The technical assistance provided by Mr. Bert Aarts is gratefully acknowledged. Prof. S.B. Adeloju acknowledges a research seed grant received from the University of Western Sydney, Nepean for this study.

REFERENCES

1 J.E. Marcovecchio, V.J. Moreno and A. Perez, Sci. Total Environ., 75 (1988) 181.
2 S.B. Adeloju, Analyst, 114 (1989) 455.
3 I. Skare, Analyst, 97 (1972) 148.
4 C. Feldman, Anal. Chem., 46 (1974) 1606.
5 D.C. Baxter and W. Frech, Anal. Chim. Acta, 236 (1990) 377.
6 S.B. Adeloju and T.F. Mann, Anal. Lett., 20 (1987) 985.
7 J.F. Chapman and L.S. Dale, Anal. Chim. Acta, 101 (1978) 203.
8 H.U. Riisgard and S. Hansen, Mar. Ecol. Prog. Ser., 62 (1990) 259.

Analytica Chimica Acta, 285 (1994) 365–368
Elsevier Science B.V., Amsterdam

Selective extractive spectrophotometric determination of germanium with *N*-hydroxy-*N*,*N*′-diphenylbenzamidine and iodide

Neena Nashine and R.K. Mishra

School of Studies in Chemistry, Pt. Ravishankar Shukla University, Raipur-492010, M.P. (India)

(Received 16th April 1993; revised manuscript received 12th August 1993)

Abstract

A simple and rapid spectrophotometric method for the determination of germanium is described. It is based on the reaction of Ge(IV) with I^- in 4.2–8.4 M H_2SO_4, and extraction of the tetraiodogermanate(IV) complex so formed into chloroform with *N*-hydroxy-*N*,*N*′-diphenylbenzamidine. The apparent molar absorptivity of the yellow coloured complex formed is 1.5×10^4 l mol^{-1} cm^{-1} at $\lambda_{max} = 395$ nm. The detection limit is 0.1 μg Ge ml^{-1}. The method is highly selective as few of the tested common metal ions and anions interfere.

Keywords: Spectrophotometry; Germanium; *N*-Hydroxy-*N*,*N*′-diphenylbenzamidine; Iodide; Extraction

Many spectrophotometric methods for the determination of trace amounts of germanium in complex materials are reported. The classical iodide method is not sensitive and it suffers from interference of other elements which give coloured complexes with iodide [1]. Various reagents and dyes such as *N*-(4-chlorophenyl)-2-fluorohydroxamic acid [2], phenylfluorone [3,4] rhodamine B and C [5,6], bromopyrogallol red [7], malachite green [8] and molybdoheteropoly acid [9], are reported. Most of these methods need rigid control of pH, temperature, reagents, etc. and are also time consuming [9]. These methods have generally low reproducibility and are also not selective as many of the common species which are generally found associated with germanium such as Ga(III), Ti(IV), Sn(IV), As(III), Bi(III), Fe(III), Nb(V), Ta(V), Zr(IV), V(V) and Ce(IV) interfere [2].

Correspondence to: R.K. Mishra, School of Studies in Chemistry, Pt. Ravishankar Shukla University, Raipur-492010, M.P. (India).

In the present investigation an effort was made to develop a highly selective, reproducible and rapid method for the spectrophotometric determination of trace germanium. The method is based on the selective extraction of germanium as its tetraiodocomplex into chloroform with *N*-hydroxy-*N*,*N*′-diphenylbenzamidine (HDPBA). Most of the common ions associated with germanium in real samples do not interfere. Moreover, this method doubles the sensitivity compared to the classical iodide method.

EXPERIMENTAL

Apparatus

A Carl-Zeiss Jena Spekol spectrophotometer with EK-5 attachment and matched 1-cm quartz cells was used for absorbance measurements.

Reagents

All chemicals used were of analytical reagent grade (BDH and Merck). A standard solution of

SSDI 0003-2670(93)E0536-G

Ge(IV) was prepared by dissolving a weighed amount of GeO_2 in alkaline solution (0.1 M NaOH) and diluting to 1 l with distilled water. Freshly prepared potassium iodide 33% (w/v) (2 M) and ascorbic acid 10% (w/v) (0.56 M) solutions were used. A 14 M H_2SO_4 solution was employed for extraction work. *N*-Hydroxy-*N*,*N*'-diphenylbenzamidine (HDPBA) was synthesized as reported in the literature [10], and a 0.1% (w/v) (0.0035 M) solution in chloroform was used.

Procedure

An aliquot of the solution containing up to 45 μg Ge(IV) is taken in a 125-ml separatory funnel. To this 4 ml H_2SO_4 is added and the funnel is dipped in a thermostat bath having a temperature of 15 ± 2°C. The analyte is treated with 1 ml of KI solution and 1 ml of ascorbic acid solution and the final volume is made to 10 ml with distilled water. This is equilibrated by shaking with 10 ml chloroform solution of HDPBA for 2 min. The yellow chloroform extract is separated and dried over anhydrous sodium sulphate (ca. 2 g) in a 25-ml beaker. The aqueous phase is washed twice with 2 ml fresh chloroform.

The combined extracts, after drying, are transferred to a 10-ml volumetric flask, and the latter is filled to the mark with chloroform. The absorbance of the extract is measured at λ_{max} of the complex against the reagent blank.

A known amount of the samples were treated with concentrated nitric acid and evaporated to dryness. The dried samples were heated with (1 : 1) H_2SO_4 until fumes of sulphuric acid ceased. The residues were leached with about 50 ml of hot water, cooled and made up to 100 ml with double distilled water in a volumetric flask. Aliquots of this solution were taken and the Ge(IV) content was determined according to the recommended procedure.

RESULTS AND DISCUSSION

Absorption spectra

The absorption spectra obtained for tetraiodogermanate(IV)–HDPBA in chloroform show an absorption maximum at 395 nm against reagent blank (Fig. 1). In this region, the reagent blank exhibits appreciable absorbance, hence it was used as a reference for all measurements.

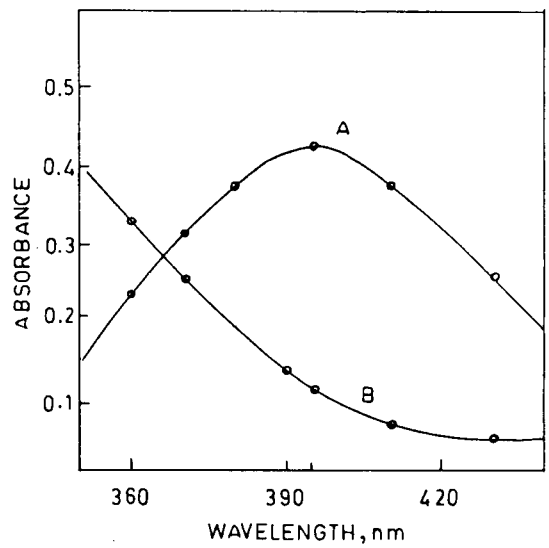

Fig. 1. Absorption spectra of the tetraiodogermanate(IV) complex. (A) Absorption spectra of the complex in chloroform. $C_{Ge} = 2.7 \times 10^{-5}$ M (2.0 μg Ge(IV) ml^{-1}); $C_{KI} = 0.2$ M; $C_{H_2SO_4} = 5.6$ M. (B) Reagent blank.

Effect of solvents

The effect of various solvents (1-pentanol, methyl isobutyl ketone, ethyl acetate, diethyl ether, chloroform, carbon tetrachloride, benzene, toluene and cyclohexane) on the extraction of the tetraiodogermanate(IV) complex with HDPBA were studied. Of these, diethyl ether, carbon tetrachloride and cyclohexane were unable to extract the complex. The other solvents extracted the complex quantitatively but their nature greatly affects the λ_{max} (nm) and molar absorptivity (ϵ, l mol^{-1} cm^{-1}) values for the complex: 1-pentanol (ϵ, 12 000; λ_{max}, 410), ethyl acetate (ϵ, 8000; λ_{max}, 420), methyl isobutyl ketone (ϵ, 7500; λ_{max}, 420), benzene (ϵ, 13 500; λ_{max}, 400), toluene (ϵ, 13 000; λ_{max}, 400), chloroform (ϵ, 15 000; λ_{max}, 395). In the case of polar solvents the extraction is not selective and the colour of the extract is unstable. Chloroform was chosen as extraction solvent because of large absorbance and stability of the complex and the relatively high distribution of the reagent in the solvent.

TABLE 1

Determination of Ge(IV) in standard, sphalerite and lead–zinc ore concentrate samples

Sample	Germanium found		% Relative standard deviation of the present method ($n = 5$)
	Present method	AAS	
A	0.006%	0.0058%	1.4
B	0.0075%	0.0072%	1.3
C	16.0 $\mu g\ g^{-1}$	14.8 $\mu g\ g^{-1}$	1.3
USGS [a]			
SDO-I	1.29 $\mu g\ g^{-1}$	1.29 $\mu g\ g^{-1}$	1.2
G-2	1.13 $\mu g\ g^{-1}$	1.14 $\mu g\ g^{-1}$	1.3

[a] Sphalerite ore obtained from (A) Dhariba, Udaipur, Rajasthan, India; (B) Agucha, Udaipur, Rajasthan, India. Lead–zinc ore concentrate obtained from (C) Zawar, Udaipur, Rajasthan, India. USGS = United States Geological Survey Standards, Arlington, VA, USA. Certified Ge(IV) content in $\mu g\ g^{-1}$: SDO-I = 1.3, G-2 = 1.15.

Effect of acidity

Extraction of the metal with iodide and HDPBA was carried out in a sulphuric acid medium. The complete extraction of the complex into chloroform and maximum absorbance was found in an acid concentration range of 4.2–8.4 M H_2SO_4 (Fig. 2). Hydrochloric acid could not be used since it decreases the absorbance.

Effect of ascorbic acid and optimal reagent concentration

In the present investigation ascorbic acid is used to remove iodine liberated by any oxidizing species present in the solution; 0.045 M to 0.17 M ascorbic acid is sufficient for complete and maximum development of the complex. At least 2.8×10^{-3} M HDPBA in chloroform is required for development of the complex and no adverse effect was observed up to 1.0×10^{-2} M HDPBA. The maximum and constant extraction of the metal is achieved over the range 0.16 M to 0.48 M KI in the aqueous solution. Beyond these limits, incomplete extraction of the metal and high blank absorbance was observed. Hence in the present investigation the extraction of the metal was carried out with 0.2 KI and 3.5×10^{-3} HDPBA.

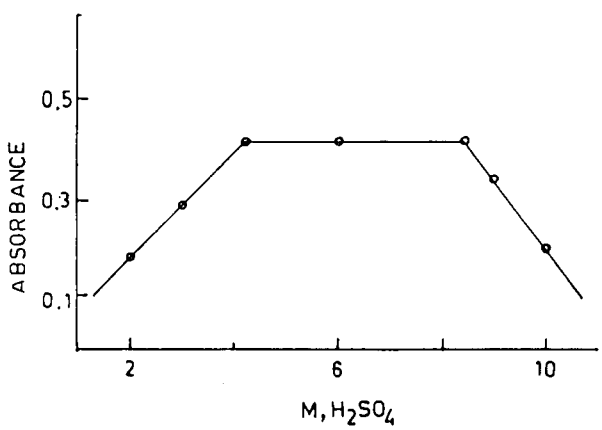

Fig. 2. Acidity range. $C_{Ge} = 2.7 \times 10^{-5}$ M; $C_{KI} = 0.2$ M; $C_{AA} = 0.056$ M; AA = ascorbic acid.

Calibration, molar absorptivity and precision

The system gives a linear calibration graph up to 4.5 μg Ge(IV) ml^{-1} with I^- and HDPBA. The apparent molar absorptivity of the tetraiodogermanate(IV) complex is 1.5×10^4 l mol^{-1} cm^{-1} at $\lambda_{max} = 395$ nm. The precision of the method was checked by taking 10 replicate measurements on solutions each containing 20 μg of Ge(IV) per 10 ml of organic phase after extraction. The relative standard deviation of the method is 1.3%. The detection limit (2σ) is 0.1 μg Ge ml^{-1} in the original aqueous solution.

Stoichiometry of the complex

The stoichiometry of the complex was determined by plotting log distribution ratio [$D = A_{eq}/(A_{max} - A_{eq})$] of the metal versus log molar concentration of iodide or log molar concentration of (A = absorbance, eq and max refer to the equilibrium and maximum values, respectively). The data obtained show the involvement of $4I^-$ and 2HDPBA for each Ge(IV) to give neutral chloroform-extractable species.

Effect of diverse ions

The effect of diverse ions in the determination of 20 μg of Ge(IV) was studied as in the above procedure. Most ions did not interfere. The tolerance limits for these ions (in mg), i.e., those causing an error $< \pm 2\%$ are shown in parenthesis: Sb(V), Sn(IV) (0.15); As(V), Cu^{2+}, Pd^{2+}, Se(IV), Mo(VI) (0.3); Re(VII), Hg^{2+} (0.5); Ag^+, Bi(III), Zr(IV) (0.75); Cd^{2+}, Pb^{2+}, Al^{3+} (1.0); W(VI), V(V) (1.5); Be^{2+}, Ca^{2+}, La^{3+}, NO_3^- (2.0);

Mn^{2+}, Ni^{2+}, Fe^{3+} (5.0); EDTA, F^-, citrate (10.0). Arsenic(V) may be masked with 1 ml of 1% (w/v) sodium thiosulphate solution.

Application

The method has been applied for the determination of Ge(IV) in standard, sphalerite and lead–zinc ore concentrate samples.

The data obtained were compared by analysing the sample by atomic absorption spectrometry (AAS). The results obtained were found to be highly satisfactory.

REFERENCES

1 K. Tanaka and N. Takagi, Anal. Chim. Acta, 48 (1969) 357.
2 Y.K. Agrawal and V.J. Bhatt, Analyst, 111 (1986) 761.
3 Z. Marczenko, M. Krasieiko and A. Klebek, Microchem. J., 34 (1986) 121.
4 H. Kurihara, H. Kuwabara and T. Kurihara, Bunseki Kagaku, 29 (1980) 560.
5 F.V. Mirzoyan, N.P. Sarkisyan and A.A. Petrosyan, Ukr. Khim. Zh., 53 (1987) 391.
6 S. Xu and H. Liu, Fenxi Huaxue, 14 (1986) 909.
7 D.T. Burns and D. Dadgar, Analyst, 105 (1980) 1082.
8 S. Sato and H. Tanaka, Talanta, 36 (1989) 391.
9 V. Hernandis, L. Macia and J.V. Sala, Analyst, 112 (1987) 1007.
10 K. Satyanarayana and R.K. Mishra, Anal. Chem., 46 (1974) 1609.

Analytica Chimica Acta, 285 (1994) 369–375
Elsevier Science B.V., Amsterdam

Study of the kinetic characteristics of D-amino acid oxidase using 2,2′-azinodi(3-ethylbenzothiazoline-6-sulphonic acid) as oxygen acceptor

S. Ignjatovic and N. Majkic-Singh

Department of Medical Biochemistry, Pharmaceutical Faculty, 11000 Belgrade (Yugoslavia)

(Received 24th June 1992; revised manuscript received 14th September 1992)

Abstract

A simple kinetic method for assay of D-amino acid oxidase (D-AAO) catalytic activity using 2,2′-azinodi(3-ethylbenzothiazoline-6-sulphonic acid) (ABTS) as chromogen is described. Hydrogen peroxide produced in the reaction catalysed by D-AAO stoichiometrically oxidizes ABTS in a peroxidase-catalysed reaction. The absorbance of the chromogen measured at 410 nm is directly proportional to D-AAO activity. The estimated values of the Michaelis–Menten constants (K_m) for D-alanine, D-proline, D-valine, D-2-aminobutyrate and D-leucine, determined in 100 mM pyrophosphate buffer (pH 8.8) at 30°C, were 2.60, 3.40, 4.60, 1.98 and 0.14 mM, respectively. The pH optima for the D-AAO activity was found to be between 8.6 and 8.8. The optimum temperature was about 30°C and the activation energy 8.89 kJ mol^{-1}. The K_m values for peroxidase, as an auxiliary enzyme in the indicator reaction, were 19.0, 20.8, 17.3 and 27.2 U l^{-1} for D-alanine, D-proline, D-2-aminobutyrate and D-leucine, respectively, as substrates. The K_m value for ABTS was 1.16 mM. The inhibition by sodium benzoate was found to be competitive with an inhibition constant, K_i, of 2.7×10^{-5} M. In all experiments, 50.5 μM of free flavine adenine dinucleotide was added to the reaction mixture to avoid dissociation of the holoenzyme.

Keywords: Enzymatic methods; Kinetic methods; Amino acid oxidase; Catalytic activity

D-Amino acid oxidase [D-amino acid: oxygen oxidoreductase (deaminating), EC 1.4.3.3, D-AAO] is a flavoenzyme that catalyses the oxidative deamination of various D-amino acids. It is strictly stereospecific, reacting only with D-amino acids. The enzyme has a high degree of specificity for oxygen as hydrogen acceptor [1]. D-AAO is found in the kidney, liver and brain of all mammals and some other vertebrates [2,3], although D-AAO substrates, D-amino acids, are rare in the metabolism of vertebrates [4]. However, recently detectable levels of four free D-amino acids (phenylalanine, tyrosine, tryptophan and leucine) were found in human urine using a liquid chromatographic coupled column (i.e., achiral–chiral) method [5].

Methods for the assay of D-AAO catalytic activity are based on the measurement of the 2-keto acid formed by the enzyme action [6,7] or on the oxygen consumption [8,9]. D-AAO activity can also be measured via hydrogen peroxide [10,11] or ammonia liberated from D-amino acids as sub-

Correspondence to: S. Ignjatovic, Department of Medical Biochemistry, Pharmaceutical Faculty, 11000 Belgrade (Yugoslavia).

SSDI 0003-2670(92)00274-6

strates [12–14]. A "sandwich" type of enzyme immunoassay for the determination of D-AAO concentration has also been described [15].

The aim of this study was to investigate the kinetic characteristics of D-amino acid oxidase using 2,2′-azinodi(3-ethylbenzothiazoline-6-sulphonic acid) (ABTS) as an oxygen acceptor on the basis of the following reactions:

$$\text{D-amino acid} + H_2O + O_2 \xrightarrow{\text{D-AAO}} \text{2-keto acid} + NH_3 + H_2O_2 \quad (1)$$

$$H_2O_2 + ABTS_{red} \xrightarrow{POD} ABTS_{ox} + H_2O \quad (2)$$

The specific property of ABTS is to give a stable radical cation by oxidation with hydrogen peroxide in the presence of peroxidase (POD). By optimizing the conditions characterizing the above-postulated coupled D-AAO–POD reactions, a simple kinetic method for measuring D-AAO activity was developed. The absorbance of oxidized ABTS measured at 410 nm is directly proportional to D-AAO activity.

EXPERIMENTAL

Apparatus

All kinetic measurement were carried out with a Unicam SP 8-100 UV–visible spectrophotometer equipped with a cuvette thermostated by an external circulating water-bath and a Hewlett-Packard HP 97 S recorder.

Chemicals

A crystalline suspension of D-amino acid oxidase from porcine kidney in 3.2 M ammonium sulphate (specific activity 14–17.6 U mg^{-1}, 5 mg protein ml^{-1}) and D-amino acids were obtained from Sigma (St. Louis, MO), the diammonium salt of ABTS (crystallized) and horseradish peroxidase (type I, specific activity 250 U mg^{-1}) from Boehringer (Mannheim, Germany) and the disodium salt of flavin adenine dinucleotide tetrahydrate from Calbiochem-Behring (La Jolla, CA). All other chemicals were of analytical-reagent grade and redistilled water was used throughout.

Solutions

On the basis of the investigations of kinetic characteristics the following solutions were adopted for the kinetic assay of D-AAO activity.

Reagent solution. This contained 10 mM D-leucine, 2.5 mM ABTS, 500 U l^{-1} POD and 100 mM pyrophosphate (PPi) buffer (pH 8.8) or 200 mM Tris–HCl buffer (pH 8.6). Instead of 10 mM D-leucine, alternatively 40 mM D-2-aminobutyrate, 60 mM D-alanine or D-proline and 80 mM D-valine can be used. When stored at 4°C the reagent solution is stable for about 3 weeks.

Flavin adenine dinucleotide solution. This contained 5.05 mM FAD and was prepared just before use.

D-Amino-acid oxidase solution (ca. 500 U l^{-1}). For investigation of the kinetic characteristics of D-AAO, commercially available D-amino acid oxidase was used. D-Amino acid oxidase solution was prepared by dilution of a crystalline suspension of D-AAO in 3.2 M ammonium sulphate with FAD solution in an approximate ratio of 1:500. The D-AAO solution was prepared just before use.

Optimized procedure for D-amino acid oxidase assay

The assay was initiated by addition of 0.01 ml of D-AAO solution (containing a final concentration of 50.5 μM FAD) to 1.0 ml of reagent solution (preincubated at 30°C) in semimicro cuvette. The absorbance was recorded at 410 nm for 3 min against air as blank. All experiments were done in triplicate and results are given as mean values.

Calculation and statistics

The D-AAO activity was calculated as $\Delta A_{410\,nm}/\text{min} \times 3961$ on the basis of the molar absorptivity $ABTS_{ox}$, which is 2550 m^2 mol^{-1} [16,17].

The mean value ($\bar{x}$), standard deviation (S.D.), relative standard deviation (R.S.D.) and standard error (S.E.) were calculated using standard statistical methods.

Values for all the substrates were plotted according to the Lineweaver–Burk method and values of the Michaelis–Menten constants (K_m) were calculated from the regression equations.

The parameters *a* (intercept with abscissa) and *b* (slope of regression line) were calculated by the least-squares method [18].

RESULTS

Effect of dilution on D-AAO holoenzyme and cofactor requirement

Preliminary experiments confirmed the instability of enzyme solutions after dilution of commercial D-AAO preparation. This is due to the spontaneous dissociation of D-AAO holoenzyme into apoenzyme and FAD, and is fully reversible on addition of FAD [8]. The stability of the catalytic activity of D-AAO after dilution with distilled water, 100 mM PPi, 200 mM Tris buffer and 3.2 M ammonium sulphate in the presence and absence of FAD was studied by monitoring the absorption changes of oxidized ABTS at 410 nm formed in ABTS–peroxidase reactions.

The results showed that the catalytic activity of D-AAO did not change significantly during 90 min after dilution with 3.2 M ammonium sulphate or buffer containing 5.05 mM FAD. The stability of D-AAO is shown in Fig. 1.

The enzymatic activity of D-AAO as a function of FAD concentration was also investigated. The range of the optimum FAD concentrations was broad, and therefore 50.5 μM FAD should be added to the assay mixture to prevent any loss of enzyme activity caused by its dissociation.

D-AAO substrate specificity for various D-amino acids

Michaelis–Menten constants for D-AAO were determined using D-alanine, D-valine, D-proline, D-2-aminobutyrate and D-leucine as substrates. Solutions of the D-amino acids were prepared in PPi or Tris–HCl buffer to give final concentrations of 0.05–100 mM. For each substrate concentration tested the reaction rate was measured and V_{max} and K_m values were calculated from double-reciprocal plots. In all experiments, the correlation coefficients of the regression lines used in the calculations were greater than 0.99.

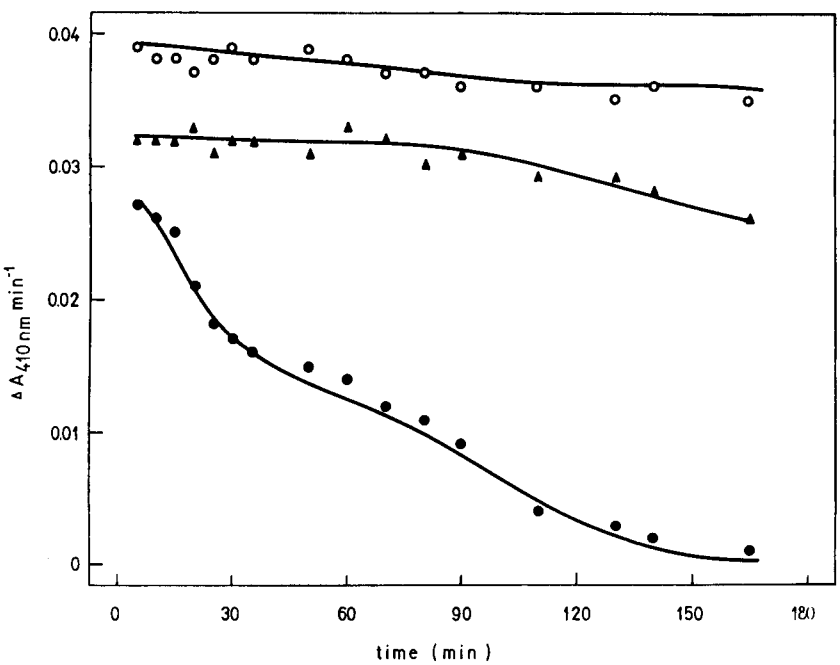

Fig. 1. Stability of D-AAO after dilution with 100 mM PP1 buffer (pH 8.8), followed (○) in the presence of 3.2 M ammonium sulphate, (▲) in the presence of 5.05 mM FAD and (●) in the absence of FAD.

TABLE 1

D-AAO substrate specificity for various D-amino acids tested by ABTS as oxygen acceptor

Substrate	V (relative) [a]	K_m (mM)	Conditions
D-Alanine	1.00	2.60	100 mM PPi buffer, pH 8.8, 30°C
D-Valine	0.43	4.60	
D-Proline	0.90	3.40	
D-2-Amino-butyrate	0.47	1.98	
D-Leucine	1.49	0.14	
D-Alanine	–	5.40	200 mM Tris–HCl buffer, pH 8.6, 30°C

[a] V represents the maximum velocity relative to that for D-alanine.

The kinetic data obtained for D-AAO specificity to five different substrates are summarized in Table 1. The lowest K_m value was obtained with D-leucine as substrate. As maximum activities were achieved with 60 mM D-alanine or D-proline, 80 mM D-valine, 40 mM D-2-aminobutyrate and 10 mM D-leucine in the final assay mixture, these concentrations were used in further investigations.

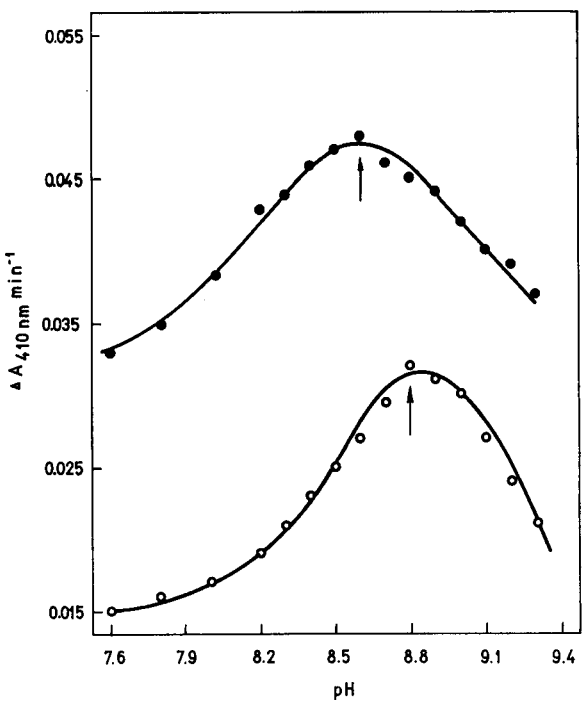

Fig. 2. Effect of pH on the catalytic activity of D-AAO determined with D-alanine as substrate in (●) 200 mM Tris–HCl buffer and (○) 100 mM PPi buffer.

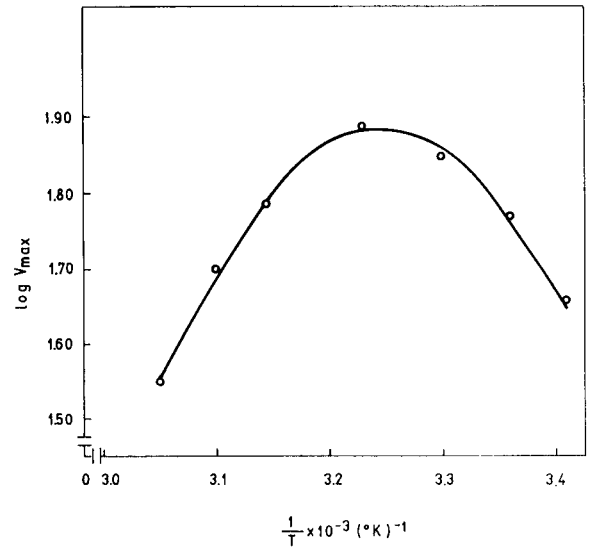

Fig. 3. Temperature dependence of D-AAO activity plotted according to the Arrhenius equation.

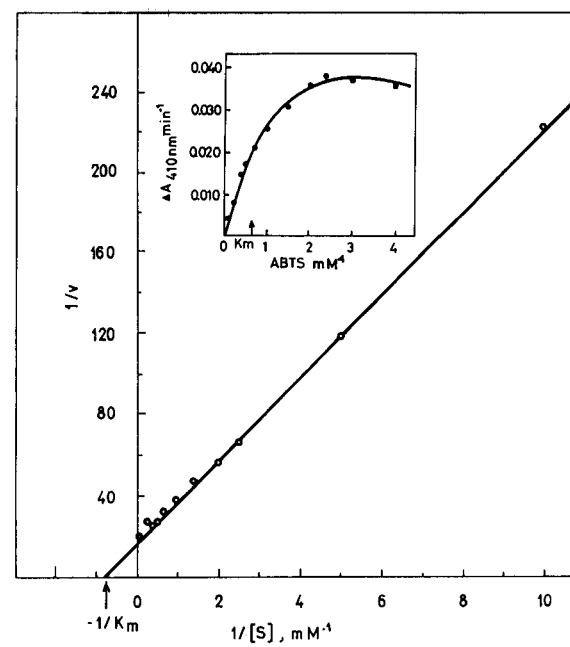

Fig. 4. Lineweaver–Burk plot for ABTS concentrations used in D-AAO assay with D-alanine ($y = 17.642 + 20.387x$; $r = 0.999$; $K_m = 1.156$ mM). Inset: Michaelis–Menten plot.

Effect of pH on the reaction velocity

To determine the optimum pH for D-AAO assay, the enzyme activity was determined with 200 mM Tris–HCl and 100 mM PPi buffer of different pH values. D-Alanine was used as substrate. The maximum reaction velocity was at pH 8.6 using Tris–HCl buffer and at pH 8.8 with PPi buffer (see Fig. 2).

Temperature dependence

Under the established optimum conditions, the temperature dependence of D-AAO catalytic activity was investigated in the range 20–55°C. The results are plotted in Fig. 3 according to the Arrhenius equation [19]. From the slope values and integrated forms of the Arrhenium equation an activation energy of 8.89 kJ mol^{-1} was calculated. Although the maximum activity was obtained between 30 and 37°C, all further D-AAO activity assays were made at 30°C, as recommended by IFCC [20].

Optimum concentrations of ABTS and peroxidase

The stoichiometric amount of hydrogen peroxide produced in the reaction catalysed by D-AAO oxidizes the chromogen ABTS by means of the added peroxidase. As the D-AAO reaction has to be rate limiting, excess of ABTS and peroxidase is needed. In order to determine the relationship between the enzyme reaction velocity and ABTS concentration, the amounts of $ABTS_{red}$ were varied in the range 0.04–4 mM. A Lineweaver–Burk plot from the data obtained is presented in Fig. 4.

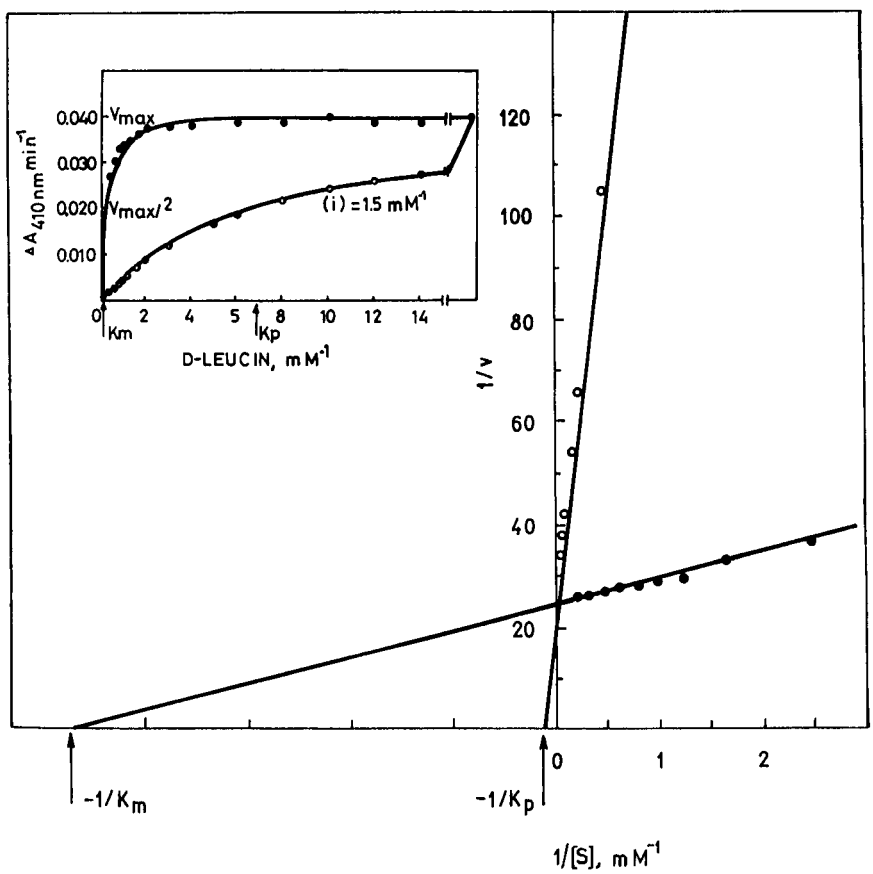

Fig. 5. Double reciprocal plot of D-leucine oxidation by D-AAO in (●) the absence of inhibitor ($y = 24.384 + 5.126x$, $r = 0.999$, $K_m = 0.211$ mM) and (○) the presence of 1.375 mM sodium benzoate ($y = 23.099 + 185.279x$, $r = 0.999$, $K_{app} = 8.021$ mM).

The Michaelis–Menten constant for ABTS in 100 mM PPi buffer (pH 8.8) with D-alanine as substrate was 1.16 mM. As the maximum velocity was obtained with 2.5 mM ABTS, this concentration was adopted in subsequent studies.

To obtain the optimum concentration of POD, as auxiliary enzyme in the indicator reaction, its concentration in the reaction mixture was varied from 4 to 160 U l^{-1}, under the established optimum conditions. Michaelis–Menten constants for POD, calculated from the regression lines, were 19.0, 20.8, 17.3 and 27.2 U l^{-1} for D-alanine, D-proline, D-2-aminobutyrate and D-leucine as substrates, respectively. The maximum velocity for all substrates was reached with 60–100 U l^{-1} POD and the reaction rate was unaffected by further increases in POD concentration up to 5000 U l^{-1}. To ensure an excess of POD, a concentration of 500 U l^{-1} was used in all further experiments.

Effect of catalase

Catalase (hydrogen peroxide : hydrogen peroxide oxidoreductase, EC 1.11.1.6) decomposes the hydrogen peroxide formed in reaction of D-AAO with D-amino acids, causing a decrease in the actual $ABTS_{ox}$ absorbance which corresponds to D-AAO catalytic activity. To check whether catalase is present in an enzyme sample, 5 mM sodium azide, as inhibitor of catalase, was added to the reaction mixture. The addition of sodium azide had no effect on the D-AAO activity, so it was concluded that commercially available D-AAO was free from catalase. If D-AAO activity is assayed in tissue preparations, sodium azide has to be added to the mixture.

Inhibition of D-AAO catalytic activity by sodium benzoate

It is known that certain aromatic acids inhibit D-AAO activity [21]. The inhibitory effect of sodium benzoate with D-leucine as substrate was examined. First, it was found that 1.375 mM sodium benzoate when added to D-leucine inhibits the oxidation by 50%. The effect of sodium benzoate on the enzyme reaction was investigated kinetically by the optimized procedure with concentrations of D-leucine in the range 0.1–18 mM. Under these conditions, benzoate is a competitive inhibitor. The inhibition constant (K_i) value was determined by a double reciprocal plot, and was calculated to be 2.7×10^{-5} M. A double reciprocal plot of 1/rate versus 1/[D-leucine] in the presence or absence of sodium benzoate is shown in Fig. 5.

DISCUSSION

Some kinetic characteristics and the optimum conditions for the measurement of D-amino acid oxidase catalytic activity using ABTS as chromogen were determined. The activity of D-AAO was assayed in a coupled reaction. On the basis of reactions (1) and (2), each step of the reaction scheme was evaluated and optimized.

The well recognized activation of D-AAO by FAD was demonstrated. In the presence of 50.5 μM FAD in the assay mixture the inactivation of D-AAO, after dilution, was also investigated. The results showed that D-AAO activity did not change significantly during 90 min after dilution with buffers containing 5.05 mM FAD and 3.2 M ammonium sulphate.

The activity of D-AAO was studied as a function of substrate concentration using various D-amino acids. All K_m values, calculated from the Lineweaver–Burk equation, were of the order 10^{-3}–10^{-4} M (see Table 1). The substrate with the lowest value of K_m was D-leucine, followed by D-alanine and D-proline. These results are in agreement with previously published data [22].

By investigating the effect of pH with 100 mM PPi and 200 mM Tris–HCl buffers, broad pH optima were found at 8.8 and 8.6, respectively (Fig. 2). Therefore, these values were chosen for the assay of D-AAO catalytic activity.

The activation energy calculated from the temperature dependence was 8.89 kJ mol^{-1} (see Fig. 3).

The absorption changes of the oxidized chromogen ($ABTS_{ox}$) at 410 nm are proportional to D-AAO activity. For the assay of D-AAO catalytic activity the most important conditions are the optimum concentrations of both ABTS and POD. As the maximum activity of D-AAO was achieved

with 2.5 mM ABTS in the reaction mixture (see Fig. 4), this concentration was used in the optimized method.

The maximum reaction velocity was reached with 60–100 U l^{-1} peroxidase. However, the concentration of POD, as an auxiliary enzyme in the indicator reaction, is the rate-limiting factor for the main reaction, and a concentration of 500 U l^{-1} was used as optimum to ensure an excess.

It should be noted that inhibition of the D-AAO system as measured spectrophotometrically by the ABTS method was observed. Sodium benzoate was found to inhibit the oxidation in competition with D-leucine, and inhibition constant (K_i) was calculated to be 2.7×10^{-5} M (Fig. 5).

In summary, the method proposed here is based on the determination of the initial enzyme velocity of ABTS oxidation by use of peroxidase. Optimizing the reaction conditions, the reagent solution with all the necessary components for D-AAO determination was obtained: 10 mM D-leucine, 2.5 mM ABTS, 500 U l^{-1} POD in 100 mM PPi buffer (pH 8.8). The chromogen used, ABTS, was characterized by high solubility and acceptable molar absorptivity of the oxidized product. This has been confirmed in previously described methods [16,17].

In subsequent work the analytical characteristics of the ABTS method (linearity, sensitivity, precision and correlation with LDH–NADH method) will be investigated.

REFERENCES

1 M. Dixon and K. Kleppe, Biochim. Biophys. Acta, 96 (1965) 368.
2 W.R. Weimar and A.H. Neims, J. Neurochem., 28 (1977) 559.
3 K. Horiike, R. Arai, H. Tojo, T. Yamano, M. Nozaki and T. Maeda, Acta Histochem. Cytochem., 18 (1985) 539.
4 M.S. Huynh, K. Horiike, H. Tojo, M. Katagiri and T. Yamano, Comp. Biochem. Physiol., 80B (1985) 425.
5 D.W. Armstrong, J.D. Duncan and S.H. Lee, Amino Acids, 1 (1991) 97.
6 Biochemica Information, Boehringer, Mannheim, 1973, p. 39.
7 J.J. Corrigan, D. Wellner and A. Meister, Biochim. Biophys. Acta, 73 (1963) 50.
8 M. Dixon and K. Kleppe, Biochim. Biophys. Acta, 96 (1965) 357.
9 M. Grassl, in H.U. Bergmeyer (Ed.), Methods of Enzymatic Analysis, Vol. 4, Verlag Chemie, Weinheim, 1974, p. 1686.
10 G.G. Guilbault and J.E. Hieserman, Anal. Biochem., 26 (1968) 1.
11 M. Le Hir, Anal. Biochem., 102 (1980) 233.
12 D.J. Holme and D.M. Goldberg, Biochim. Biophys. Acta, 377 (1975) 61.
13 G.G. Guilbault and E. Hrabankova, Anal. Chim. Acta, 56 (1971) 285.
14 T.J. Dunn and T.G. Perkoff, Biochim. Biophys. Acta, 73 (1963) 327.
15 M. Katagiri, H. Tojo, K. Horiike, N. Kasuga, K. Imagawa and T. Yamano, Biomed. Res., 5 (1984) 125.
16 N. Majkic, S. Djordjevic-Spasic and I. Berkes, Clin. Chim. Acta, 65 (1975) 227.
17 N. Majkic and I. Berkes, Clin. Chim. Acta, 80 (1977) 121.
18 L.E. Baner, in Statistical Methods for Chemists, Academic, New York, 1971, p. 71.
19 I. Segel, in Biochemical Calculations, Wiley, New York, 2nd edn., 1974, p. 96.
20 Approved Recommendations of IFCC Methods for the Measurement of Catalytic Concentrations of Enzymes, Part 1, General Considerations, Clin. Chim. Acta, 98 (1979) 163F.
21 J.R. Klein and H. Kamin, J. Biol. Chem., 138 (1941) 507.
22 H.U. Bergmeyer, K. Gawehn and M. Grassl, in H.U. Bergmeyer (Ed.), Methods of Enzymatic Analysis, Vol. 1, Verlag Chemie, Weinheim, 1974, p. 431.

Analytica Chimica Acta, 285 (1994) 377–389
Elsevier Science B.V., Amsterdam

Expert system for the voltammetric determination of trace metals

Part V. Methods for determining total iron, manganese(II), aluminium and titanium

M. Esteban and C. Ariño

Departament de Química Analítica, Universitat de Barcelona, Av. Diagonal 647, 08028 Barcelona (Spain)

I. Ruisánchez, M.S. Larrechi and F.X. Rius

Departament de Química, Universitat Rovira i Virgili (Tarragona), Pl. Imperial Tàrraco 1, 43005 Tarragona (Spain)

(Received 14th May 1993; revised manuscript received 14th July 1993)

Abstract

A previously described expert system for the voltammetric determination of Cu, Zn, Cd, Pb, In, Ni, Co, Tl, Hg, V, Se, Te, Cr(III), Cr(V), As(III) and As(V) is enlarged and improved by including methods for the determination of total Fe, Mn(II), Al and Ti. Pulse polarographic and stripping voltammetric techniques are considered. Although in some cases solid electrodes are mentioned, mercury drop electrodes are mostly recommended. The expert system is developed using the commercially available building tool KES.

Keywords: Voltammetry; Aluminium; Expert system; Iron; Manganese; Titanium; Chemometrics; Trace metals

In previous papers [1,2], a knowledge-based expert system was described for the voltammetric determination of Cu, Zn, Cd, Pb, In, Ni, Co, Tl, Hg, V, Se, Te, As(III), As(V), Cr(III) and Cr(VI). The main techniques implemented were differential pulse polarography (DPP), differential pulse anodic stripping voltammetry (DPASV), differential pulse cathodic stripping voltammetry (DPCSV) and differential pulse adsorptive stripping voltammetry (DPAdSV), using mainly mercury drop electrodes (SMDE and HMDE).

The expert system is designed for those users who have some knowledge in electrochemical analysis but cannot be considered as specialists. Furthermore, it can be a valuable tool for teaching electroanalysis and for showing the applicability of expert systems.

In this paper, an enlargement of the previously described expert system is reported, which is devoted to the determination of total iron, manganese (II), aluminium and titanium.

As the second most abundant metal in the earth's crust, iron is present in almost all waters. However, its electrochemistry is generally very complicated and very dependent on pH and the presence of complexing agents [3]. The redox reactions of Fe(II) and Fe(III) species permit their convenient polarographic measurement by

Correspondence to: M. Esteban, Departament de Química Analítica, Facultat de Química, Universitat de Barcelona, Av. Diagonal 647, 08028 Barcelona (Spain).

SSDI 0003-2670(93)E0460-O

DPP and alternating current polarography (ACP). ASV at mercury electrodes is not easily applicable to iron because of its low solubility in mercury, interferences from the hydrogen evolution reaction, and formation of various intermetallic compounds [4]. More recently, AdSV procedures, based on the adsorption of iron complexes onto the HMDE and subsequent reduction of the complex, have been used to measure trace levels of iron [5].

Although manganese has three common oxidation states only Mn(II) is soluble in aqueous solution, Mn(III) and Mn(IV) being completely hydrolysed and present as non-stoichiometric oxides. Concentrations of Mn(II) of up to 1 μM and 0.1 mM commonly occur in oxygenated and anoxic waters, respectively. The electrochemical reduction of Mn(II) to the metal is easily measured by DPP. Manganese has also been measured in natural waters using ASV. It is readily stripped from mercury at slow scan rates. Furthermore, adsorption of organic compounds on the electrode may distort ASV peaks in natural waters, so that DPP should be used preferably when the concentration of Mn(II) is greater than 10^{-7} M [3].

A considerable interest has been developed on the role of aluminium in environmental and biological systems. The concentration of dissolved aluminium in non-contaminated sea water generally lies between 5 nM and 40 nM. Its direct electrochemical determination is difficult since the reduction potential of Al(III) is very negative (−1.75 V vs. SCE), its irreversible wave being distorted by the hydrogen evolution [6]. A more convenient way to determine Al(III) is the use of voltammetric techniques after its complexation with different dyes [7]. Then, the reduction potentials are more positive than those of hydrogen or aluminium itself.

Determination of titanium in some natural samples such as sea water is not a simple matter since Ti occurs at very low concentrations between 2 and 300 pM [8]. Inductively coupled plasma atomic emission spectrometry, UV–visible spectrophotometry and ion-exchange spectrophotometry have been used to determine titanium in sea water but they are not sufficiently sensitive to detect picomolar levels [9]. The direct polarographic reduction from Ti(IV) and Ti(III) is not useful for trace levels, and AdSV has been used to determine titanium in sea water.

THE EXPERT SYSTEM

The present paper describes an enlargement of a previously reported expert system. Therefore the type of final end user, the domain expert, the rule-building tool used, the development steps and the validation of the system are the same as previously reported [1,2].

KNOWLEDGE BASE

Sample treatment

This part contains information about the steps to be followed for removing the organic matter of the sample. It was explained in detail in Part I [1].

Determination of total iron

Because of the complex electrochemistry of iron and the diversity of samples available, the use of voltammetric techniques in the present expert system has been restricted to well-known methods for the determination of total iron.

Three main options are considered. Option 1 is devoted to relatively high concentrations and it recommends the use of DPP [10]. Figure 1 shows the information received by the user when this option is selected. For lower concentrations, Option 2 (Fig. 2) recommends the use of DPAdSV onto an HMDE [11]. For still lower concentrations, Option 3 (Fig. 3) is also based on AdSV [12], but using catechol instead of 1-nitroso-2-naphthol (Option 2).

Determination of manganese(II)

The knowledge base for the determination of Mn(II) is divided into two options. Option 1 (Fig. 4) recommends a method for concentrations above 10^{-7} M based on the use of DPP [3]. Inside this option, a note indicates that for concentrations above 2×10^{-6} M literature recommends sampled direct current polarography instead of DPP [3].

Figure 1. Determination of total Fe by using Differential Pulse Polarography (DPP) onto the Dropping Mercury Electrode (DME) or the Static Mercury Drop Electrode (SMDE).

Which of the following cations are to be determined?

1. Cu,Zn,Cd,Pb
2. Ni, Co
3. Tl
4. Se
5. Hg
6. V
7. Cr
8. As
9. Fe
10. Mn
11. Al
12. Ti
13. others

=? **9**

The methods recommended here are developed to analyze natural waters whether polluted or otherwise. These methods have been selected because of the relevance of their performance characteristics published in the literature.

Do you know the approximate concentration of total iron $[Fe]_T$?

1. yes
2. no

=? **1**

What is the concentration of total iron in the sample?

1. 5 μg/l (9 10^{-8} M) < $[Fe]_T$
2. 58 ng/l (1 10^{-9} M) < $[Fe]_T$ < 2.3 μg/l (4 10^{-8} M)
3. 34 ng/l (6 10^{-10} M) < $[Fe]_T$ < 2.8 μg/l (5 10^{-8} M)

Note: The methods indicated in options 2 and 3 are very similar. The main difference between them is the reagent used. In both cases (options 2 and 3) concentration ranges given are orientative, because they depend on the preconcentration time.

= ? **1**

You should use Differential Pulse Polarography (DPP) onto a Dropping Mercury Electrode (DME) or a Static Mercury Drop Electrode (SMDE).

The medium conditions are:

The determination of total Fe in natural waters requires the removal of natural organic matter in the sample by either UV-irradiation or H_2O_2-oxidation. The conditions of the cell-medium are: 0.02 M catechol and 0.02 M

PIPES (piperazine-N,N'-bis-2-ethane sulphonic acid) buffer (pH=8). After 15 minutes of purging with a N_2 stream, measurement can be performed.

The instrumental parameters are:

E_r = Ag/AgCl or Standard Calomel Electrode, E_w = DME or SMDE.
E_{aux} = Pt or glassy carbon.
scan mode DP.
pulse= 25 mV (in general, between 10 and 100 mV) , v = 20 mV/s.
$t_{(pulse)}$ = 100 ms (in general, between 30 and 100 ms).
E_i = -0.250 V, E_f = -0.550 V, (both vs. Ag/AgCl).

Set up the polarograph according to the conditions mentioned; connection is established with external program which plots the voltammogram. The voltammogram is:

... (The voltammogram corresponding to the experimental conditions is shown here).....

Did you observe different peaks in the voltammograms?

1. yes
2. no

= ? 1

If the potential value is : Ep = -0.41 vs Ag/AgCl, the peak will be due to the presence of Fe in the original solution.

Could you measure the peak height precisely ?

1. yes
2. no

=? 1

The quantitative procedure is based on the multiple standard addition method and the standard Iron solution used is prepared by dissolving metallic iron in 6 M hydrochloric acid (1 mg Fe/ ml).

Parameters of the calibration curve:

slope = ... (value according to input experimental data)
intercept (at y=0) = ... (value according to input experimental data)

The concentration of the cation Fe given in mol/l, is the absolute value of ..... (value according to input experimental data).

Figure 2. Determination of total Fe by using Adsorptive Stripping Voltammetry (AdSV) onto the Hanging Mercury Drop Electrode (HMDE).

What is the concentration of total iron in the sample?

1. 5 μg/l (5 10^{-8} M) < $[Fe]_T$
2. 58 ng/l (1 10^{-9} M) < $[Fe]_T$ < 2.3 μg/l (4 10^{-8} M)
3. 34 ng/l (6 10^{-10} M) < $[Fe]_T$ < 2.8 μg/l (5 10^{-8} M)

Note: The methods indicated in options 2 and 3 are very similar. The main difference between them is the reagent used. In both cases (options 2 and 3) concentration ranges given are orientative, because they depend on the preconcentration time.

= ? 2

You should use Adsorptive Stripping Voltammetry (AdSV) onto the Hanging Mercury Drop Electrode (HMDE).

The medium conditions are:

The application of the method recommended requires a sample free of organic matter at the moment of the accumulation step. The conditions of the cell-medium are: 0.01 M of PIPES buffer (pH=6.9) and 10^{-4} M of 1-Nitroso-2-naphthol.

The instrumental parameters are:

E_r = Ag/AgCl or Standard Calomel Electrode, E_w = HMDE.
E_{aux} = Pt or glassy carbon,
E_{ads} = -0.15 V vs Ag/AgCl.
t_{ads} = 60 - 600 s, t_r = 30 s.
E_i = -0.15 V, E_f = -0.7 V (both vs Ag/AgCl).
scan mode DC, v= 20 mV/s.

Did you observe different peaks in the voltammograms?

1. yes
2. no

=? 1

If the potential value is E_p = -0.5 V (vs Ag/AgCl) the peak will be due to the presence of Fe in the original solution.

Figure 3. Determination of total Fe by using Adsorptive Stripping Voltammetry (AdSV) onto the Hanging Mercury Drop Electrode (HMDE).

What is the concentration of total iron in the sample?

1. 5 μg/l (5 10^{-8} M) < $[Fe]_T$
2. 58 ng/l (1 10^{-9} M) < $[Fe]_T$ < 2.3 μg/l (4 10^{-8} M)
3. 34 ng/l (6 10^{-10} M) < $[Fe]_T$ < 2.8 μg/l (5 10^{-8} M)

Note: The methods indicated in options 2 and 3 are very similar. The main difference between them is the reagent used. In both cases (options 2 and 3) concentration ranges given are orientative, because they depend on the preconcentration time.

= ? 3

You should use Adsorptive Stripping Voltammetry (AdSV) onto the Hanging Mercury Drop Electrode (HMDE).

The medium conditions are:

The application of the method to water samples requires the removal of natural organic matter in the sample. The conditions of the cell-medium are: 0.008 M of PIPES buffer (pH=6.9) and 4 10^{-4} M of catechol and 2 10^{-4} M EDTA (for masking Cu and Pb if their concentrations are above 10^{-7} M).

The instrumental parameters are:

E_r = Ag/AgCl or Standard Calomel Electrode E_w = HMDE.
E_{aux} = Pt or glassy carbon.
E_{ads} = -0.1 V, t_{ads} = 1 - 5 min, t_r = 30 s.
E_i = -0.1 V, E_f = -0.5 V, (both vs. Ag/AgCl).
scan mode DC, v = 20 mV/s

Did you observe different peaks in the voltammograms?

1. yes
2. no

= ? 1

If Ep = -0.35 V (vs Ag/AgCl) the peak will be due to the presence of Fe in the original solution.

Figure 4. Determination of Mn(II) by using Differential Pulse Polarography (DPP) onto the Dropping Mercury Electrode (DME) or the Static Mercury Drop Electrode (SMDE).

Do you know the approximate metal-ion concentration ?

1. yes
2. no

=? 1

What is the concentration of Mn (II) in the sample?

1. if [Mn(II)] > 5.5 μg/l (1 10^{-7} M)
2. if 1.1 μg/l (2 10^{-8} M) < [Mn(II)] < 5.5 μg/l (1 10^{-7} M)

Note: Manganese has been measured in natural waters at levels of 10^{-9} - 10^{-10} M, but using a mercury film electrode, which is out of the scope of this expert system. For additional details see, R. O'Halloran, Anal.Chim.Acta, 140 (1982) 51.

=? 1

You should use Differential Pulse Polarography (DPP) onto the Dropping Mercury Electrode (DME) or the Static Mercury Drop Electrode (SMDE).

Note: According to the literature (W.Davison, J.Buffle and R. de Vitre, Pure Appl. Chem, 60 (1988) 1535) DPP should be used in the concentration range from 1 10^{-7} M to 2 10^{-6} M, although calibration curves tend to be slightly convex at the high concentration end. Thus, for concentrations above 2 10^{-6} M Sampled Direct Current Polarography should be the preferred technique. In such a case, medium conditions, electrodes and initial and final potentials are as in DPP.

The medium conditions are:

0.1 M NaCl. Several supporting electrolytes have been used such as 0.02 M $NaHCO_3$ or 0.1 M KCl + 5 10^{-3} M $NaHCO_3$ or 0.1 M $Na_2B_4O_7.10\ H_2O$. In all cases the pH range 5 - 8 is recommended.

The instrumental parameters are:

E_r = Ag/AgCl or Standard Calomel Electrode, E_w = SMDE or DME.
E_{aux} = Pt or glassy carbon.
DP mode, pulse = 25 mV, v = 10 mV/s.
E_i = -0.9 V, E_f = -1.6 V, (both vs. Ag/AgCl)

Did you observe different peaks in the voltammograms?

1. yes
2. no

= ? 1

If Ep = -1.3 V vs (Ag/AgCl) the peak will be due to the presence of Mn(II).

Figure 5. Determination of Mn(II) by using Differential Pulse Anodic Stripping Voltammetry (DPASV) onto the Hanging Mercury Drop Electrode (HMDE).

What is the concentration range of Mn (II) in the sample?

1. if [Mn(II)] > 5.5 μg/l (1 10^{-7} M)
2. if 1.1 μg/l (2 10^{-8} M) < [Mn(II)] < 5.5 μg/l (1 10^{-7} M)

Note: Manganese has also been measured in natural waters at levels of 10^{-9} - 10^{-10} M, but using a mercury film electrode, which is out of the scope of this expert system. For additional details see, R. O'Halloran, Anal.Chim.Acta, 140 (1982) 51.

=? 2

You should use Differential Pulse Anodic Stripping Voltammetry (DPASV) onto the Hanging Mercury Drop Electrode (HMDE).

The medium conditions are:

0.1 M NaCl. Several supporting electrolytes have been used such as 0.02 M $NaHCO_3$,0.1 M KCl + 5 10^{-3} M $NaHCO_3$ or 0.1 M $Na_2B_4O_7$ 10 H_2O. In all cases the pH range 5 - 8 is recommended.

The instrumental parameters are:

E_r = Ag/AgCl or Standard Calomel Electrode, E_w = HMDE.
E_{aux} = Pt or glassy carbon.
E_{pe} = -1.7 V vs. Ag/AgCl during t_{pe} = 1 - 5 min, t_r = 30 s.
DP mode, pulse = 50 mV, v = 2 mV/s.
E_f= -1.0 V.

Note: Because of the quasi-reversible charge-transfer mechanism of Mn(II)/Mn(Hg), slow scan rates are recommended for the satisfactory determination of Mn(II). For additional information, see R.J. O'Halloran and H. Blutstein, J. Electroanal. Chem, 125 (1981) 261.

Did you observe different peaks in the voltammograms?

1. yes
2. no

=? 1

If you observe a peak at Ep = -1.5 V (vs Ag/AgCl), the peak will be due to the presence of Mn(II).

Figure 6. Determination of Al by using Adsorptive Stripping Voltammetry (AdSV), onto the Hanging Mercury Drop Electrode (HMDE).

Do you know the approximate metal-ion concentration?

1. yes
2. no

=? 1

Which is the concentration of Al in the sample?

1. if 5 μg/l (1.85 10^{-7} M) < [Al] < 100 μg/l (3.7 10^{-6} M)
2. if [Al] < 16 μg/l (5.92 10^{-7} M)

Note: The methods recommended in all cases use dyes to complex Al and to enhance the Al voltammetric signal. The second method corresponds to the official method of HMSO.

(Enter a number)
=? 1

You should use Adsorptive Stripping Voltammetry (AdSV) onto the Hanging Mercury Drop Electrode (HMDE).

The medium conditions are:

The conditions of the cell medium are: 1 10^{-6} M of Eriochrome Violet B (SVRS) and a 0.2 M acetate buffer at pH = 4.5.

The instrumental parameters are:

E_r = Ag/AgCl, E_{aux} = Pt or glassy carbon, E_w = HMDE.
E_{ac} = -0.45 V (vs. Ag/AgCl), t_{ac} = 2 min, t_r = 15 s.
scan mode DC or DP, $v_{(scan\ rate)}$ = 50 mV / s.
E_i = -0.45 V, E_f = -1 V. (both vs. Ag/AgCl)

Note: Before the voltammetric measurement, the solution containing the sample and standards, 0.2 M acetate buffer and 1 10^{-6} M of SVRS is heated during 10 min. at 90°C. After heating, the solution is allowed to cool at room temperature for 15 min. Then it is transferred to the electrochemical cell and degassed with nitrogen.

Did you observe different peaks in the voltammograms?

1. yes
2. no

=? **1**

If you observe a peak at Ep = -0.61 V, the peak will be due to the presence of Al(III).

Figure 7. Determination of Al by using Differential Pulse Adsorptive Stripping Voltammetry (DPAdSV), onto the Hanging Mercury Drop Electrode (HMDE).

Which is the concentration range of Al in the sample?

1. if 5 μg/l (1.85 10^{-7} M) < [Al] < 100 μg/l (3.7 10^{-6} M)
2. if [Al] < 16 μg/l (5.92 10^{-7} M)

=? **2**

You should use Differential Pulse Adsorptive Stripping Voltammetry (DPAdSV), onto the Hanging Mercury Drop Electrode (HMDE).

The medium conditions are:

The application of the method requires a neutral pH which is allowed with 10^{-2} M BES (M-M'- bis- (2-hydroxyethyl)- 2 -amino-ethane sulphonic acid) in NaOH, and the 10^{-5} M Alizarine Red S or DASA (1,2-dihydroxyanthraquinone - 3 - sulphonic acid).

The instrumental parameters are:

E_r = Ag/AgCl, E_{aux} = Pt or glassy carbon, E_w = HMDE.
E_{ac} = -0.9 V, t_{ac} = 1 min, t_r = 10 s.
scan mode DP, pulse = 25 mV, t_p = 100 ms, $v_{(scan\ rate)}$ = 20 mV/s.
E_i = -0.9 V, E_f = -1.3 V.

Note: Only Zn interferes on the determination of Al by this method, as it may be present at enhanced levels because of sample contamination. Interfering levels (> 5 10^{-2} M) of Zn(II) can be masked by adsorbing at -1 V and starting the scan from -0.9 V, or by addition of 10^{-4} M of EDTA .

Did you observe different peaks in the voltammograms?

1. yes
2. no

=? 1

If you observe a peak at Ep = -1.1 V, the peak will be due to the presence of Al(III).

Figure 8. Determination of Ti by using Adsorptive Stripping Voltammetry (AdSV), onto the Hanging Mercury Drop Electrode (HMDE).

Do you know the approximate metal-ion concentration?

1. yes
2. no

=? 1

Which is the concentration of Ti in the sample?

1. if 1 μg/l (2 10^{-8} M) < [Ti] < 20 μg/l (4 10^{-7} M).
2. if [Ti] < 1 μg/l (2 10^{-8} M).

Note: Methods recommended use AdSV: in the first choice with Eriochrome Violet B and in the second one with mandelic acid.

=? 1

You should use Adsorptive Stripping Voltammetry (AdSV), onto the Hanging Mercury Drop Electrode (HMDE).

The medium conditions are:

The application of the method requires as optimal conditions a pH 5.1 buffer solution of acetic/acetate and 1.5 10^{-6} M of Eriochrome Violet B, as complexing agent. The chelate formation is allowed during deareation of the solution.

The instrumental parameters are:

E_r = Ag/AgCl or Standard Calomel Electrode (SCE). E_w = HMDE.
E_{aux} = Pt or glassy carbon.
E_{ac} = -0.42 V, t_{ac} = 5 min, t_r = 15 s.
scan mode DC or DP, v = 50 mV / s.
E_i = -0.42 V, E_f = -1.0 V.

Did you observe different peaks in the voltammograms?

1. yes
2. no

=? 1

If you observe a peak at Ep = -0.54 V, the peak will be due to the presence of Ti in the original solution.

Figure 9. Determination of Ti by using Differential Pulse Adsorptive Stripping Voltammetry (DPAdSV), onto the Hanging Mercury Drop Electrode (HMDE).

Which is the concentration of Ti in the sample?

1. if 1 μg/l (2 10^{-8} M) < [Ti] < 20 μg/l (4 10^{-7} M).
2. if [Ti] < 1 μg/l (2 10^{-8} M).

=? 2

You should use Differential Pulse Adsorptive Stripping Voltammetry (DPAdSV), onto the Hanging Mercury Drop Electrode (HMDE).

The medium conditions are:

The application of the method requires the presence on the cell of 4.5 10^{-2} M potassium chlorate and 4 10^{-3} M mandelic acid. The pH of the solution should be adjusted between 3 and 3.3 with ammonia.

The instrumental parameters are:

E_r = Ag/AgCl, E_{aux} = Pt or glassy carbon, E_w = HMDE.
E_{ac} = -0.1 V, t_{ac} = 3 min, t_r = 20 s.
scan mode DP, pulse = 25 mV, scan rate = 20 mV / s.
E_i = -0.75 V, E_f = -1.2 V.

Note1: Mo(VI) is present at a background concentration of ca. 10^{-7} M in sea waters, and the catalytic effect of chlorate on the reduction of molybdenum is greater than that on titanium. To avoid the interference of Mo , after the preconcentration on the electrode surface, the potential is switched to -0.75 V, that is more negative than the reduction peak of molybdenum.

Note2: The catalytic effect of chlorate on the reduction of Ti(IV) is used in this method to enhance the sensitivity of the AdSV signal of titanium. If the concentration levels of titanium on the sample are not as low as choice 2 recommends, you can use this method without the addition of chlorate.

Did you observe different peaks in the voltammograms?

1. yes
2. no

=? 1

If you observe a peak at Ep = -0.9 V, the peak will be due to the presence of Ti(IV) in the original solution.

At concentrations in the range of 2×10^{-8} to 1×10^{-7} M, a method based on DPASV onto an HMDE [13] is preferred (Fig. 5). For natural waters as well as other type of samples containing Mn(II) at 10^{-9}–10^{-10} M, a note included in the information shown on the screen indicates the convenience of using a mercury film electrode (TMFE) [14].

Determination of aluminium

The knowledge base for the determination of Al at the very low concentrations present in natural water, environmental and biological samples [6,15] is divided in two options. Methods of both options are based on AdSV by using a dye as complexing agent: Eriochrome violet B in Option 1 (Fig. 6), and Alizarin Red S in Option 2 (Fig. 7).

Determination of titanium

The formation of a surface active chelate of titanium with Eriochrome Violet B [16], and its adsorptive accumulation onto an HMDE, is recommended in Option 1 for measuring very low concentrations of Ti (Fig. 8). For still lower concentrations, literature recommends the use of AdSV [9], through the catalytic effect of chlorate on the reduction peak obtained in presence of mandelic acid (Fig. 9). For higher concentrations of Ti, this method can be used without the addition of chlorate [17].

Conclusions

The enhancement here described of the expert system for the voltammetric determination of trace metals may be very useful for solving problems concerned with the determination of total iron, divalent manganese, aluminium and titanium. For this goal, well-tested methods and very common voltammetric techniques are recommended. At the moment, speciation of iron is still out of the scope of this expert system.

Economic support from the Spanish Ministry of Education and Science is acknowledged (DGICYT, projects No. BP90-0453 and BP90-0821).

REFERENCES

1 M. Esteban, I. Ruisánchez, M.S. Larrechi and F.X. Rius, Anal. Chim. Acta, 268 (1992) 95, 107; Trends Anal. Chem., 11 (1992) 135.
2 M. Esteban, C. Ariño, I. Ruisánchez, M.S. Larrechi and F.X. Rius, Anal. Chim. Acta, 284 (1993) 435; 285 (1994) 193.
3 W. Davison, J. Buffle and R. Devitre, Pure Appl. Chem., 60 (1988) 1535.
4 F. Vydra, K. Stulik and E. Julakova, Electrochemical Stripping Analysis, Ellis Horwood, Chichester, 1976.
5 J. Wang and J. Mahmoud, Fresenius' Z. Anal. Chem., 327 (1987) 789.
6 J. Wang, P.A.M. Farias and J.S. Mahmoud, Anal. Chim. Acta, 173 (1985) 57.
7 H.H. Willard and J.A. Dean, Anal. Chem., 22 (1950) 1264.
8 K.J. Oriaus, E.A. Boyle and K.W. Bruland, EOS, 71 (1990) 90.
9 K. Yokoi and C.M.G. van den Berg, Anal. Chim. Acta, 245 (1991) 167.
10 Metrohm, Application Bulletin No. 123.
11 The determination of Trace Metals in Marine and Other Waters by Voltammetry or AAS, HMSO, London, 1988.
12 C.M.G. van den Berg and Z. Qiang Huang, J. Electroanal. Chem., 177 (1984) 269.
13 R.J. O'Halloran and H. Blutstein, J. Electroanal. Chem., 125 (1981) 261.
14 R.J. O'Halloran, Anal. Chim. Acta, 140 (1982) 51.
15 C.M.G. van den Berg, K. Murphy and J.P. Riley, Anal. Chim. Acta, 188 (1986) 177.
16 J. Wang and J.S. Mahmoud, J. Electroanal. Chem., 208 (1986) 383.
17 H. Li and C.M.G. van den Berg, Anal. Chim. Acta, 221 (1989) 269.

Analytica Chimica Acta, 285 (1994) 391–399
Elsevier Science B.V., Amsterdam

Ionic equilibria in non-aqueous solvents

Part 3. Effect of homoconjugation

Martí Rosés

Departament de Química Analítica, Universitat de Barcelona, Diagonal 647, 08028 Barcelona, Catalonia (Spain)

(Received 11th June 1993)

Abstract

Equations for the calculation of pH in non-aqueous solvents are derived. The equations consider dissociation of the acid or base, formation of salt ion pairs and formation of acid–anion or base–cation homoconjugates. The effect of homoconjugation on titration curves and buffer capacities in solvents of low and high dielectric constant is investigated. Computer programs to plot titration and buffer capacity curves and to compute simultaneously dissociation and homoconjugation constants of the acid or base and the salt from potentiometric data are presented. The equations and programs are tested on data from the literature in different non-aqueous solvents.

Keywords: Potentiometry; Titrimetry; Dissociation constants; Homoconjugation; Ionic equilibria; Non-aqueous solvents

In Parts 1 and 2 of this series [1,2], equations and computer programs for the calculation of pH, dissociation constants and reference potentials from potentiometric data in non-aqueous solvents were developed. The equations take into account the formation of ion pairs in solvents of low dielectric constants, but they do not consider homoconjugation equilibria. Homoconjugation reactions are produced in aprotic solvents because of the inability of the medium to solvate the dissociated ions, which instead are stabilized by forming a hydrogen-bonded complex with the undissociated acid or base.

The formation of hydrogen-bonded acid–anion complexes was first invoked by Maryott [3] to explain the conductance maxima obtained at about the mid-point of conductometric titration curves in benzene and 1,4-dioxane. The formation of these hydrogen-bonded complexes was confirmed by cryoscopic [4], infrared [5–7] and other conductimetric studies [8,9]. Van der Heijde [10] was the first to explain the abnormal shape of some potentiometric titration curves (additional potential rise at half-neutralization) by homoconjugation reactions. His results provided evidence that homoconjugation occurs not only in non-polar solvents, but also in some polar solvents, such as acetone, pyridine or acetonitrile. Harlow and co-workers [11,12] observed inflections near the half-neutralization points of potentiometric titration curves in benzene, toluene, gasoline and sulpholanes, which they explained by the formation of acid–anion and base–cation hydrogen-bonded complexes.

More quantitative studies were performed by Kolthoff and co-workers [13–29], Coetzee and co-workers [30–35], Pawlak and co-workers [36–41] and others [42–47]. They determined homoconjugation constants of acids and bases in acetonitrile (by far the most studied solvent) [13–

Correspondence to: M. Rosés, Departament de Química Analítica, Universitat de Barcelona, Diagonal 647, 08028 Barcelona, Catalonia (Spain).

SSDI 0003-2670(93)E0519-D

20,22,23,29,32–35], dimethyl sulphoxide [21,29], *N*,*N*-dimethylformamide [24,29,42], methyl isobutyl ketone [26], propylene carbonate [28,41,45], nitromethane [36], nitrobenzene [36,44], acetone [37–40], oxydipropionitrile [43] and pyridine [46].

Usually, a combination of different techniques (solubility, potentiometry, conductimetry and spectrophotometry) is used to determine the dissociation constant of the acid or base and the formation constant of the acid–anion or base–cation homoconjugate. Potentiometry alone can be used to determine both constants. In this instance, after standardization of the potentiometric system, the dissociation constant of the acid or base is computed from the half-neutralization potential of a titration curve and the homoconjugation constant from the other points on the curve. However, this method can be applied only in solvents of high dielectric constant, where the salt formed during titration is completely dissociated. Formation of salt ion pairs shifts the titration curve [1,2,48,49], and does not allow a direct relationship between the dissociation pK and the pH of half-neutralization. Even in solvents of high dielectric constant the method has the disadvantage that the acid or base constant is computed from only one potential value, which may be poorly buffered because of the potential jump in the half-neutralization region.

Without demeriting the traditional computation methods, appropriate for the limited possibilities at that time, modern computer facilities offer more effective methods for simultaneous computation of the equilibrium constants which affect potentiometric titration curves. In previous work, general equations for the calculation of pH during a titration were derived [1] and computer programs for calculating dissociation constants of acids, bases and salts from potentiometric data were developed [2]. In this paper the equations are extended to include homoconjugation, and the new equations are incorporated in two of the computer programs (CORVAL and PKSIMULT). CORVAL computes pH values from given equilibrium constants and simulates and displays titration curves and buffer capacities. It allows the observation of the effect of homoconjugation on titration curves. Of special interest are titration curves in solvents of low dielectric constant, as the effects of simultaneous acid or base dissociation, salt association and homoconjugation have hardly been studied. PKSIMULT allows the simultaneous computation of acid or base, salt and homoconjugation constants from potentiometric data and also the *s*-parameter, which accounts for medium variations caused by the addition or formation of a solvent different from the main titration solvent [1,2]. Copies of the programs are available on request.

IONIC EQUILIBRIA IN NON-AQUEOUS SOLVENTS

Non-aqueous solvents usually contain small amounts of substances (e.g., water) capable of competing with the main solvent, solvating H^+ ions or giving other basic ions different from S^- (the lyate ion). In order to account for these ions, a solvent constant ($K_{solvent}$) different from the autoprotolysis constant has been defined and used in non-aqueous solvents [1,2,48–50]:

$$K_{solvent} = \Sigma[H^+]\Sigma[S^-]y^2 \quad (1)$$

where $\Sigma[H^+]$ indicates the overall proton concentration (solvated by any solvent), $\Sigma[S^-]$ the overall lyate concentration coming from all the "solvents" present in the medium and y the mean ionic molar activity coefficient. For simplicity, the activity coefficients of all ions involved in the studied equilibria will be considered to be equal, despite the differences in size of the ions.

In non-aqueous solvents, the dissociation of an acid is usually described in two steps (ionization, K_i, and dissociation, K_d), but an overall acidity constant (K_a) is used:

$$HA \overset{K_i}{\rightleftharpoons} H^+A^- \overset{K_d}{\rightleftharpoons} H^+ + A^-$$

$$K_a = \Sigma[H^+][A^-]y^2/\Sigma[HA] \quad (2)$$

where $\Sigma[HA] = [HA] + [H^+A^-] = (1 + K_i)[HA]$. In the same way, dissociation of a base is described by an overall basicity constant (K_b):

$$B + HS \overset{K_i}{\rightleftharpoons} BH^+S^- \overset{K_d}{\rightleftharpoons} BH^+ + S^-$$

$$K_b = [BH^+]\Sigma[S^-]y^2/\Sigma[B] \quad (3)$$

where $\Sigma[B] = [B] + [BH^+S^-] = (1 + K_i)[B]$.

In some non-aqueous solvents, the low dielectric constant favours the formation of ion pairs and a dissociation constant for the salt (K_{salt}) must be considered:

$$BH^+A^- \rightleftharpoons BH^+ + A^-$$

$$K_{salt} = [BH^+][A^-]y^2/[BH^+A^-] \quad (4)$$

Equilibria 1–4 were used in previous studies [1,50] for the derivation of the proposed equations, but additional homoconjugation equilibria will be considered in this paper.

In weak hydrogen-bonding solvents, the ions are poorly solvated by the solvent. However, they can be solvated by solutes with appropriate hydrogen bond capabilities. Therefore, A^- ions (hydrogen bond acceptors) can be solvated by acids (hydrogen bond donors) according to the equilibrium

$$A^- + HA \rightleftharpoons HA_2^-$$

$$K^f_{HA_2^-} = [HA_2^-]/[A^-][HA] \quad (5)$$

where $K^f_{HA_2^-}$ is the acid homoconjugation constant defined as usual. However, another slightly different homoconjugation constant $[K^f_{homo(HA)}]$ will be defined here:

$$K^f_{homo(HA)} = [HA_2^-]/[A^-]\Sigma[HA] = K^f_{HA_2^-}/(1 + K_i) \quad (6)$$

where K_i is the ionization constant of the acid according to the equilibria 2. This homoconjugation constant simplifies the computation of pH in solvents of low dielectric constant, as [HA] and $[H^+A^-]$ cannot be computed separately unless K_i is known. In a solvent of high dielectric constant, where there is no formation of ion pairs, $K_i \rightarrow 0$ and $K^f_{homo(HA)} \rightarrow K^f_{HA_2^-}$.

Some bases (e.g., amines) have electron pairs capable of hydrogen bonding with hydrogen bond donors (e.g., ammonium ions). In poor solvating solvents, these bases can form homoconjugated complexes:

$$BH^+ + B \rightleftharpoons B_2H^+$$

$$K^f_{B_2H^+} = [B_2H^+]/[BH^+][B] \quad (7)$$

$$K^f_{homo(B)} = [B_2H^+]/[BH^+]\Sigma[B] = K^f_{B_2H^+}/(1 + K_i) \quad (8)$$

where $K^f_{B_2H^+}$ and $K^f_{homo(B)}$ are homoconjugation constants of the base.

COMPUTATION OF pH

In a mixture of an acid and its salt, the mass and charge balances are

$$c_a = \Sigma[HA] + [HA_2^-] + \Sigma[H^+] - \Sigma[S^-] \quad (9)$$

$$c_{salt} = [BH^+] + [BH^+A^-] \quad (10)$$

$$\Sigma[H^+] + [BH^+] = \Sigma[S^-] + [A^-] + [HA_2^-] \quad (11)$$

where c_a and c_{salt} are the analytical concentrations of the acid and salt, respectively. Because many non-aqueous solvents have a low $K_{solvent}$ value, $\Sigma[H^+] \gg \Sigma[S^-]$ even for low c_a values, and $\Sigma[S^-]$ can be neglected in Eqns. 9 and 11.

From Eqns. 2 and 6:

$$\Sigma[HA] = K_a^{-1}\Sigma[H^+][A^-]y^2 \quad (12)$$

$$[HA_2^-] = K^f_{homo(HA)}K_a^{-1}\Sigma[H^+][A^-]^2y^2 \quad (13)$$

Substituting Eqns. 12 and 13 in Eqn. 9, neglecting $\Sigma[S^-]$ and rearranging terms:

$$\Sigma[H^+] = \frac{c_a}{1 + K_a^{-1}[A^-]y^2 + K^f_{homo(HA)}K_a^{-1}[A^-]^2y^2} \quad (14)$$

From Eqns. 4 and 10:

$$\Sigma[BH^+] = \frac{c_{salt}}{1 + K_{salt}^{-1}[A^-]y^2} \quad (15)$$

Substituting Eqns. 13–15 in Eqn. 11, neglecting $\Sigma[S^-]$ and rearranging terms, the following equation is obtained:

$$\left[K^f_{homo(HA)}K_{salt}^{-1}K_a^{-1}y^4\right][A^-]^4 + \left[K_{salt}^{-1}K_a^{-1}y^4 + K^f_{homo(HA)}K_a^{-1}y^2 + K^f_{homo(HA)}K_{salt}^{-1}K_a^{-1}c_a y^4\right] \times [A^-]^3 + \left[K_{salt}^{-1}y^2 + K_a^{-1}y^2 + K^f_{homo(HA)} \times K_a^{-1}(c_a - c_{salt})y^2\right][A^-]^2 + \left(1 - K_a^{-1}c_{salt}y^2 - K_{salt}^{-1}c_a y^2\right)[A^-] - (c_{salt} + c_a) = 0 \quad (16)$$

Equation 16 is similar to the equation derived previously [1], but it includes homoconjugation.

When homoconjugation is negligible, $K^{f}_{homo(HA)} = 0$, and Eqn. 16 becomes

$$(K^{-1}_{salt}K^{-1}_{a}y^4)[A^-]^3 + (K^{-1}_{salt}y^2 + K^{-1}_{a}y^2)[A^-]^2 + (1 - K^{-1}_{a}c_{salt}y^2 - K^{-1}_{salt}c_a y^2)[A^-] - (c_{salt} + c_a) = 0 \quad (17)$$

which is the equation derived in Part 1 [1].

Equation 16 can be solved by a similar iterative procedure to that described for Eqn. 17 [1]. When $[A^-]$ has been computed, $\Sigma[H^+]$ is calculated by means of Eqn. 14, and the pH from

$$pH = -\log(\Sigma[H^+]y) \quad (18)$$

The pH of a solution of an acid alone can also be computed from Eqn. 16, taking $c_{salt} = 0$.

A parallel derivation for base–salt mixtures (of analytical concentrations c_b and c_{salt}, respectively) leads to the equation

$$[K^{f}_{homo(B)}K^{-1}_{salt}K^{-1}_{b}y^4][BH^+]^4 + [K^{-1}_{salt}K^{-1}_{b}y^4 + K^{f}_{homo(B)}K^{-1}_{b}y^2 + K^{f}_{homo(B)}K^{-1}_{salt}K^{-1}_{b}c_b y^4] \times [BH^+]^3 + [K^{-1}_{salt}y^2 + K^{-1}_{b}y^2 + K^{f}_{homo(B)} \times K^{-1}_{b}(c_b - c_{salt})y^2][BH^+]^2 + (1 - K^{-1}_{b}c_{salt}y^2 - K^{-1}_{salt}c_b y^2)[BH^+] - (c_{salt} + c_b) = 0 \quad (19)$$

which can be solved for $[BH^+]$ in the same manner as Eqn. 16 for $[A^-]$, and pS and pH computed from the following equations:

$$\Sigma[S^-] = \frac{c_b}{1 + K^{-1}_{b}[BH^+]y^2 + K^{f}_{homo(B)}K^{-1}_{b}[BH^+]^2y^2} \quad (20)$$

$$pS = -\log(\Sigma[S^-]) \quad (21)$$

$$pH = pK_{solvent} - pS \quad (22)$$

RESULTS AND DISCUSSION

The effect of homoconjugation on titration curves and buffer capacities in solvents of high dielectric constant have been investigated by Kolthoff and co-workers [17,25,27,29] and Coetzee [35]. In this work, the CORVAL program, which computes pH during titration by means of Eqns. 14, 16 and 18–22, and plots it against the titrated fraction, is used to study and compare the effect of homoconjugation in solvents of high dielectric constant and the effect of simultaneous homoconjugation and ion-pair association in solvents of low dielectric constant.

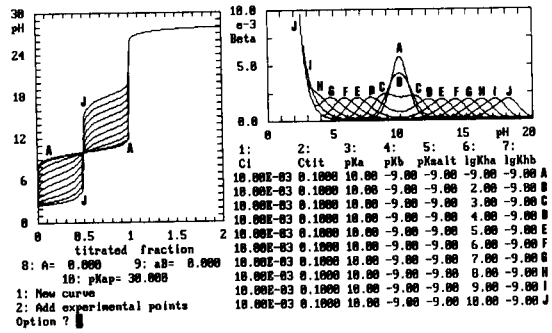

Fig. 1. Effects of homoconjugation on titration curve and buffer capacity in a solvent of high dielectric constant computed by the CORVAL program. A 0.01 M (Ci) solution of a weak acid of $pK_a = 10$ (pKa) is titrated with a 0.1 M (Ctit) solution of a base completely dissociated (pKb = −9). The salt formed is completely dissociated (pKsalt = −9) and the base does not form homoconjugated complexes (lg Khb = −9). The log $K^{f}_{homo(HA)}$ (lg Kha) changes from −9 (curves A, no homoconjugation) to 10 (curves J).

Figure 1 shows the output of CORVAL for titration of a 0.01 M solution of a typical weak acid of $pK_a = 10$ with a 0.1 M strong base, forming a salt completely dissociated (letters A–J have been added to identify the curves). The $pK_{solvent}$ value is assumed to be 30, and activity coefficients to be unity (the Debye–Hückel A and aB parameters are set to zero). It can be observed that the shapes of the titration and buffer capacity curves depend strongly on the homoconjugation constant. Homoconjugation decreases $[A^-]$ and [HA] by formation of HA_2^-, and according to equilibrium 2, this favours acid dissociation when $[A^-] < \Sigma[HA]$, but is unfavourable when $[A^-] > \Sigma[HA]$. Therefore, in comparison to an acid without homoconjugation (curve A), the titration curve is shifted to lower pH values before the half-neutralization point, but to higher pH values after it. When homoconjugation becomes important, a pH jump appears in the half-neutralization region. Anyway, all the curves cross at the half-neutrali-

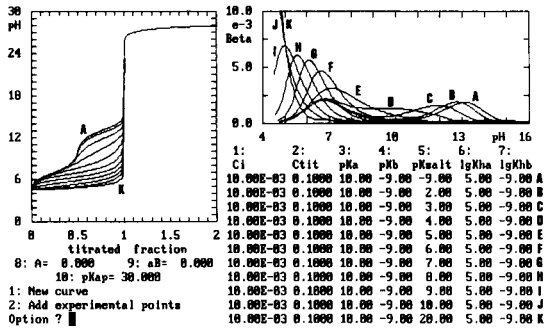

Fig. 2. Effects of salt ion-pair formation on titration curve and buffer capacity of a weak acid suffering homoconjugation. Concentrations and constants as in Fig. 1, except $\log K^{f}_{homo(HA)} = 5$ and pK_{salt} changes from -9 (curves A, no ion-pair formation) to 20 (curves K).

zation point, which has a pH equal to pK_a, showing that the pH of this point is not affected because $[A^-] = \Sigma[HA]$.

As homoconjugation increases, the buffer capacity curve, initially bell-shaped and with a maximum at $pH = pK_a$, widens and decreases the maximum until two bell-shaped symmetrical arms, each with its corresponding maximum, appear. The two arms are also symmetrical with respect to the $pH = pK_a$ point, and the higher the homoconjugation the greater is the distance of the maxima to this point. When $\log K^{f}_{homo(HA)}$ approaches the pK_a, the more acidic arm of the buffer capacity curve becomes exponential shaped, as the A^- anions are almost completely homoconjugated with the acid, and a further neutralization of the latter hardly affects $[A^-]$ and, therefore, acid dissociation and pH.

Figure 2 shows the output of CORVAL for the titration of the same acid under the same conditions as in Figure 1 for different pK_{salt} values, taking $\log K^{f}_{homo(HA)} = 5$. When there is no salt ion-pair formation the titration and buffer capacity curves (A) are the same as the curves E in Fig. 1. The titration curve shows a pH break at the half-neutralization point, but when salt association increases (higher pK_{salt} values), $[A^-]$ decreases according to Eqn. 4, and this favours acid dissociation according to Eqn. 2, as has been explained earlier [1,2,48–50]. The increase in acid dissociation increases $[H^+]$ and moves the titration curve to lower pH values. Since this effect depends on the salt concentration, the higher the titrated fraction, the greater is the shift of the titration curve, and as pK_{salt} increases the pH jump at the half-neutralization region diminishes and disappears.

The buffer capacity curve consequently moves with the pH variation. As the pK_{salt} increases, the basic arm of the double bell-shaped curve moves toward lower pH values. When pK_{salt} approaches $\log K^{f}_{homo(HA)}$, the basic arm of the curve joins the acidic arm and an unsymmetrical bell-shaped curve is obtained. As pK_{salt} increases, this curve narrows and the maximum β value increases and shifts to lower pH values. For pK_{salt} values similar to or higher than the pK_a value, an exponential-shaped curve is obtained because the salt association is very strong, and $[A^-]$ and $[H^+]$ are hardly affected by the acid neutralization.

Comparison of Figs. 1 and 2 shows that the half-neutralization point has a pH value equal to pK_a only when salt association is negligible. The invariance of the pH value of the half-neutralization point, or of mixtures of acid and salt at the same concentration, have been used to compute the pK_a value of acids subject to homoconjugation [17–19,24,28,29,43] but, as Figure 1 reveals, these mixtures are well buffered only if the homoconjugation is weak. Therefore, pK_a should be better determined from mixtures of acids and salts at different concentrations but, as the pH of these mixtures is affected by homoconjugation, $\log K^{f}_{homo(HA)}$ must be known or simultaneously calculated. The PKSIMULT program, described previously [2], has been modified in this way, changing the previously used Eqn. 17 by Eqn. 16. It allows the simultaneous computation of both constants.

The simultaneous computation of pK_a and $\log K^{f}_{homo(HA)}$ has been tested with the potentiometric literature data of Kolthoff and co-workers [17–19] for some acids in acetonitrile (dielectric constant $\epsilon = 36$). The data were obtained from prepared acid–tetraalkylammonium salt mixtures instead of titration of an acid with a base, and the input of the program was consequently modified to accept c_a, c_{salt} and pH values instead of volume and pH data. The program computes by

non-linear regression the equilibrium constant values, which minimizes the squared residuals, weighted according to the buffer capacity of the solution [2]. The Debye–Hückel limiting law was used for computation of activity coefficients, taking $A = 1.64$. The results obtained are presented in Table 1, together with the results obtained by Kolthoff and co-workers using the classical methods. The simultaneous computation of pK_a and log $K^f_{homo(HA)}$ gives values comparable to those of Kolthoff and co-workers but with lower standard deviations as all the data are used in the computation.

The salts of the acids presented in Table 1 have been considered to be completely dissociated except for 3,5-dinitrophenol. Kolthoff et al. [19] gave a pK_{salt} value of 2.00 for this phenolic compound and they used it in computation of the homoconjugation constant. When this pK_{salt} value is used in the program, the same results as given by Kolthoff et al. are obtained. However, if the pK_{salt} value is also simultaneous computed, the best fit gives slightly lower pK_a and log $K^f_{homo(HA)}$ values and a negative pK_{salt} value. This means that the salt ion-pair formation is negligible in these solutions and therefore pK_{salt} cannot be estimated accurately.

If the dielectric constant of the solvent decreases, the salt ion-pair formation increases, pK_{salt} has a greater effect on pH and, therefore, it should be possible to estimate its value more accurately. This can be illustrated by calculation of the equilibrium constants of 3,5-dinitrobenzoic acid in methyl isobutyl ketone ($\epsilon = 12.9$, Debye–Hückel $A = 7.36$). Juillard and Kolthoff [26] determined conductimetrically a pK_{salt} value of 4.15 for its tetraethylammonium salt, and from potentiometric data pK_a and log $K^f_{homo(HA)}$ values of 18.75 ± 0.2 and 4.3 ± 0.2, respectively, by an iterative graphical method, as the usual method cannot be applied because of the appreciable salt association. If pK_{salt} is set to 4.15, and pK_a and log $K^f_{homo(HA)}$ are simultaneously calculated by the PKSIMULT program, using Juillard and Kolthoff's data, values of 18.89 ± 0.01 and 4.41 ± 0.01, respectively, are obtained from seven points and with an overall standard error of $\sigma = 1.0 \times 10^{-2}$. If the three constants are simultaneously calculated, the best fit is obtained for $pK_a = 18.49 \pm 0.09$, $pK_{salt} = 3.46 \pm 0.23$ and log $K^f_{homo(HA)} = 4.02 \pm 0.09$, with $\sigma = 5.7 \times 10^{-3}$. If the salt is assumed to be completely dissociated the results are $pK_a = 18.24 \pm 0.01$, log $K^f_{homo(HA)} = 3.77 \pm 0.01$ and $\sigma = 5.6 \times 10^{-3}$.

TABLE 1

Acidity and homoconjugation constants of acids in acetonitrile computed by the PKSIMULT program from Kolthoff and co-workers' potentiometric data [17–19]

Acid	PKSIMULT				Kolthoff and co-workers		
	pK_a	Log $K^f_{homo(HA)}$	σ [a]	N [b]	pK_a	Log $K^f_{homo(HA)}$	N [c]
2,5-Dichlorobenzenesulphonic	6.41 ± 0.01	2.66 ± 0.01	1.1×10^{-2}	12	6.23	2.59 ± 0.04	8
Methanesulphonic	9.84 ± 0.03	3.82 ± 0.03	4.1×10^{-2}	16	10.0	3.75 ± 0.13	16
Picric	10.98 ± 0.01	0.47 ± 0.12	1.9×10^{-2}	13	11.0	≈ 0.30	
Salicylic	16.79 ± 0.01	3.37 ± 0.02	5.0×10^{-2}	23	16.7	3.28 ± 0.08	20
3,5-Dinitrobenzoic	17.00 ± 0.02	4.07 ± 0.02	6.4×10^{-2}	23	16.9	3.99 ± 0.14	23
4-Nitrobenzoic	18.80 ± 0.01	3.84 ± 0.01	3.6×10^{-2}	12	18.7	3.82 ± 0.10	11
3-Bromobenzoic	19.65 ± 0.01	3.83 ± 0.02	5.8×10^{-2}	18	19.5	3.74 ± 0.10	15
Benzoic	20.75 ± 0.01	3.71 ± 0.02	3.7×10^{-2}	19	20.7	3.59 ± 0.12	16
4-Hydroxybenzoic	20.83 ± 0.02	3.09 ± 0.07	6.7×10^{-2}	9	20.8	3.04 ± 0.13	5
3,5-Dinitrophenol [d]	20.50 ± 0.01	4.65 ± 0.01	4.7×10^{-2}	18	20.5	4.65 ± 0.10	15
3,5-Dinitrophenol [e]	20.42 ± 0.01	4.57 ± 0.01	4.4×10^{-2}	18			

[a] σ = Standard error. [b] Number of points used in the computation of the acidity and homoconjugation constants. [c] Number of points used in the computation of the homoconjugation constant. [d] Taking $pK_{salt} = 2.00$ [19]. [e] Assuming salt completely dissociated.

From these results, it can be deduced that in the presence of homoconjugation, pK_{salt} is difficult to estimate even when its effect on pH is appreciable. The simultaneous calculation of the three parameters tends to give pK_a, log $K^f_{homo(HA)}$ and pK_{salt} values lower than the real values. As has been explained for Fig. 2, an increase in pK_{salt} value shifts the titration curve to lower pH values and decreases the pH jump at half-neutralization. However, the same effects are produced by a decrease in pK_a and log $K^f_{homo(HA)}$ values, and a similar curve would be obtained for lower pK_a, log $K^f_{homo(HA)}$ and pK_{salt} values. Therefore, there are multiple combinations of pK_a, log $K^f_{homo(HA)}$ and pK_{salt} values which can give similar fits for the experimental data and it is difficult to choose the correct one based only on the goodness of the fit.

The accurate determination of pK_a and log $K^f_{homo(HA)}$ values is difficult not only if pK_{salt} must be simultaneously determined, but also if the medium changes during titration. In Parts 1 and 2 [1,2] it was demonstrated that in many non-aqueous titrations the titration medium changes because the titrant is dissolved in another solvent or water is formed in the neutralization reaction. This medium change implies a change in pH, which has been assumed to be proportional to the volume fraction of titrant added, and the proportionality coefficient, s, has been proposed as a parameter measuring the effect of the medium change [1]. This parameter is simultaneously estimated from the potentiometric data together with the equilibrium constants [2]. However, as, in an acid titration, homoconjugation shifts the pH toward lower values before the half-neutralization point and toward higher values after it, this effect is similar to that produced by the medium change and, therefore, the simultaneous estimation of s and log $K^f_{homo(HA)}$ would be uncertain.

Persin and Gal [43] determined the acidity and homoconjugation constants of some acids in oxydipropionitrile, which can illustrate this point. The results obtained by the PKSIMULT program from Persin and Gal's data are presented in Table 2, together with the results calculated by them using the classical method [pK_a from the half-neutralization point and log $K^f_{homo(HA)}$ from the other titration points]. The variation in activity coefficients has not been considered because of the constancy of the ionic strength (0.1 M in tetrabutylammonium perchlorate) in the solutions studied. The salt formed in the titration of the acids with butylamine has been considered to be completely dissociated because of the high dielectric constant of the solvent ($\epsilon = 66.6$). When pK_a and log $K^f_{homo(HA)}$ are simultaneously computed,

TABLE 2

Acidity and homoconjugation constants of acids in oxydipropionitrile computed by the PKSIMULT program from Persin and Gal's potentiometric data [43]

Acid	PKSIMULT					Persin and Gal		
	pK_a	Log $K^f_{homo(HA)}$	s	σ [a]	N [b]	pK_a	Log $K^f_{homo(HA)}$	N [c]
Sulphuric (I) [d]	5.04 ± 0.01	2.49 ± 0.02		1.4×10^{-2}	9	5.1	2.7 ± 0.2	8
Sulphuric (I) [e]	4.68 ± 0.02		−73 ± 3	1.5×10^{-2}	9			
Hydrochloric [d]	7.48 ± 0.02	3.18 ± 0.03		5.1×10^{-2}	9	7.6	3.2 ± 0.2	8
Hydrochloric [e]	6.48 ± 0.03		−201 ± 5	3.1×10^{-2}	9			
Nitric [d]	7.49 ± 0.01	2.30 ± 0.03		1.8×10^{-2}	9	7.5	2.2 ± 0.2	8
Nitric [e]	7.23 ± 0.02		−52 ± 3	1.8×10^{-2}	9			
Salicylic [d]	13.69 ± 0.01	2.54 ± 0.03		2.2×10^{-2}	9	13.7	2.5 ± 0.2	8
Salicylic [e]	13.30 ± 0.02		−79 ± 3	1.9×10^{-2}	9			
Benzoic [d]	16.30 ± 0.02	2.19 ± 0.12		4.8×10^{-2}	8	16.4	1.7	4
Benzoic [e]	16.08 ± 0.06		−43 ± 10	4.9×10^{-2}	8			

[a] σ = Standard error. [b] Number of points used in the computation of the acidity and homoconjugation constants. [c] Number of points used in the computation of the homoconjugation constant. [d] Assuming there is homoconjugation, but not a medium change. [e] Assuming there is a medium change, but not homoconjugation.

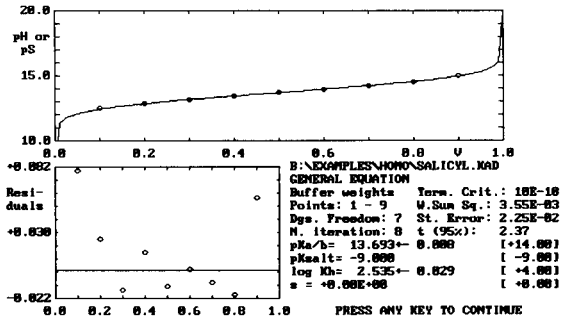

Fig. 3. Simultaneous computation of dissociation (pKa/b) and homoconjugation constants (log Kh) of salicylic acid in oxydipropionitrile by means of the PKSIMULT program.

assuming there is no medium change, results similar to those of Persin and Gal are obtained, but with better standard deviations. The PKSIMULT program even allows the inclusion of pH points neglected by Persin and Gal because of the weakness of the acid, such as the points after the half-neutralization of benzoic acid. However, if it is assumed that there is a medium change, but not homoconjugation, and pK_a and s are the parameters simultaneously computed, similar fits are obtained, but with different pK_a results.

The difference in the results obtained can be observed in Figs. 3 and 4, where the outputs of PKSIMULT for salicylic acid are presented. The plots of pH or residuals vs. volume in both figures are almost identical, despite the fact that the numerical results are different, Figure 3 shows the results for the simultaneous computation of pK_a and log $K^f_{homo(HA)}$ and Figure 4 those for

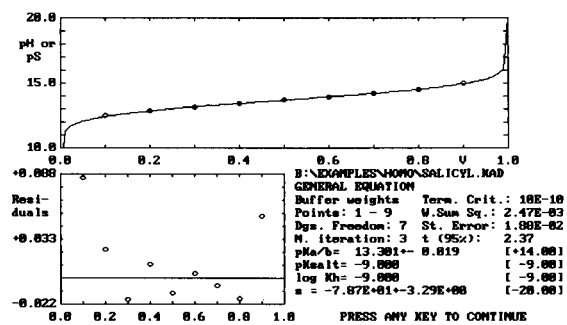

Fig. 4. Simultaneous computation of dissociation constant (pKa/b) of salicylic acid in oxydipropionitrile and medium change parameter (s) by means of the PKSIMULT program.

pK_a and s. The difference in the pK_a results can be explained because the pK_a value computed simultaneously with log $K^f_{homo(HA)}$ agrees with the pH of half-neutralization, but the pK_a value computed simultaneously with s is the extrapolation to the pure initial solvent, that is, to $V = 0$.

It can be concluded that simultaneous computation of acidity (or basicity) and homoconjugation constants overcomes some of the problems of the traditional potentiometric methods, such as computation of pK_a from only the half-neutralization point. However, it does not allow an accurate simultaneous computation of salt ion-pair formation constant or medium change parameter, because of the similarity of the effect of these parameters and the effect of homoconjugation. Therefore, as in the traditional methods, these parameters must be known if accurate results are to be obtained.

The financial support from the DGICYT (project PB91-0262) is gratefully acknowledged.

REFERENCES

1 M. Rosés, Anal. Chim. Acta, 276 (1993) 211.
2 M. Rosés, Anal. Chim. Acta, 276 (1993) 223.
3 A.A. Maryott, J. Res. Natl. Bur. Stand., 38 (1947) 527.
4 S. Kaufman and C.R. Singleterry, J. Phys. Chem., 56 (1952) 604.
5 G.M. Barrow and A. Yerger, J. Am. Chem. Soc., 76 (1954) 5211.
6 A. Yerger and G.M. Barrow, J. Am. Chem. Soc., 77 (1955) 4474.
7 G.M. Barrow, J. Am. Chem. Soc., 78 (1956) 5802.
8 P.J.R. Bryant and A.W.H. Wardrop, J. Chem. Soc., (1957) 895.
9 D.B. Bruss and G.A. Harlow, Anal. Chem., 30 (1958) 1836.
10 H.B. van der Heijde, Anal. Chim. Acta, 16 (1957) 392.
11 G.A. Harlow and D.B. Bruss, Anal. Chem., 30 (1958) 1833.
12 D.H. Morman and G.A. Harlow, Anal. Chem., 39 (1967) 1869.
13 I.M. Kolthoff, S. Bruckenstein and M.K. Chantooni, Jr., J. Am. Chem. Soc., 83 (1961) 3927.
14 I.M. Kolthoff and M.K. Chantooni, Jr., J. Phys. Chem., 66 (1962) 1675.
15 I.M. Kolthoff and M.K. Chantooni, Jr., J. Am. Chem., Soc., 85 (1963) 426.
16 I.M. Kolthoff and M.K. Chantooni, Jr., J. Am. Chem. Soc., 87 (1965) 1004.
17 I.M. Kolthoff and M.K. Chantooni, Jr., J. Am. Chem. Soc., 87 (1965) 4428.

18 I.M. Kolthoff and M.K. Chantooni, Jr., J. Phys. Chem., 70 (1966) 856.
19 I.M. Kolthoff, M.K. Chantooni, Jr., and S. Bhowmik, J. Am. Chem. Soc., 88 (1966) 5430.
20 I.M. Kolthoff and M.K. Chantooni, Jr., Anal. Chem., 39 (1967) 1080.
21 I.M. Kolthoff, M.K. Chantooni, Jr., and S. Bhowmik, J. Am. Chem. Soc., 90 (1968) 23.
22 I.M. Kolthoff and M.K. Chantooni, Jr., J. Am. Chem. Soc., 91 (1969) 4621.
23 I.M. Kolthoff and M.K. Chantooni, Jr., J. Phys. Chem. 73 (1969) 4029.
24 I.M. Kolthoff, M.K. Chantooni, Jr., and H. Smagowski, Anal. Chem., 42 (1970) 1622.
25 I.M. Kolthoff, Pure Appl. Chem., 25 (1971) 305.
26 J. Juillard and I.M. Kolthoff, J. Phys. Chem., 75 (1971) 2496.
27 I.M. Kolthoff, Anal. Chem., 46 (1974) 1992.
28 K. Izutsu, I.M. Kolthoff, T. Fujinaga, M. Hattori and M.K. Chantooni, Jr., Anal. Chem., 49 (1977) 503.
29 I.M. Kolthoff and P.J. Elving (Eds.), Treatise on Analytical Chemistry, Part I, Vol. 2, Wiley, New York, 2nd edn., 1979.
30 J.F. Coetzee and G.R. Padmanabhan, J. Phys. Chem., 66 (1962) 1708.
31 J.F. Coetzee and D.K. McGuire, J. Phys. Chem., 67 (1963) 1810.
32 J.F. Coetzee, G.R. Padmanabhan and G.P. Cunningham, Talanta, 11 (1964) 93.
33 J.F. Coetzee and G.R. Padmanabhan, J. Am. Chem. Soc., 87 (1965) 5005.
34 J.F. Coetzee and G.R. Padmanabhan, J. Phys. Chem., 69 (1965) 3193.
35 J.F. Coetzee, Prog. Phys. Org. Chem., 4 (1967) 45.
36 Z. Pawlak and T. Jasinski, Zesz. Nauk. Wydz. Mat. Fiz. Chem., Uniw. Gdanski, Chem., 1 (1971) 51; C.A., 78 (1973) 123818r.
37 Z. Pawlak, Rocz. Chem., 47 (1973) 641; C.A. 79 (1973) 52631g.
38 Z. Pawlak, T. Jasinski and C. Dobrogowska, Rocz. Chem., 48 (1974) 1609; C.A., 82 (1975) 77697h.
39 Z. Pawlak, B. Nowak and M.F. Fox, J. Chem. Soc., Faraday Trans. 1, 78 (1982) 2157.
40 S. Kuna, Z. Pawlak and M. Tusk, J. Chem. Soc., Faraday Trans. 1, 78 (1982) 2685.
41 Z. Pawlak and J. Magoński, J. Chem. Soc., Faraday Trans. 1, 78 (1982) 2807.
42 E. Roletto and J. Juillard, J. Solut. Chem., 3 (1974) 127.
43 M. Persin and J.Y. Gal, Can. J. Chem., 59 (1981) 2491.
44 Z. Pawelka and M.C. Haulait-Pirson, J. Phys. Chem., 85 (1981) 1052.
45 A.K. Srivastava and L.M. Mukherjee, J. Electroanal. Chem., 157 (1983) 53.
46 I. Yamakawa and T. Nakajima, Nippon Kapako Kaishi, 3 (1988) 260; C.A., 110 (1989) 23219g.
47 E.P. Serjeant, Potentiometry and Potentiometric Titrations, Wiley, New York, 1984.
48 E. Bosch and M. Rosés, Talanta, 36 (1989) 623.
49 E. Bosch and M. Rosés, Talanta, 36 (1989) 627.
50 E. Bosch and M. Rosés, Talanta, 36 (1989) 615.

Analytica Chimica Acta, 285 (1994) 401–406
Elsevier Science B.V., Amsterdam

BOOK REVIEWS

David L. Andrews (Ed.), *Applied Laser Spectroscopy: Techniques, Instrumentation and Applications*, VCH Publishers, Weinheim, 1992 (ISBN 3-527-28072-3). ix + 471 pp. Price £81.00/DM 198.00.

This book is a comprehensive description of laser spectroscopy and its increasing importance not only for academic but also for commercial applications, written by distinguished scientists. The book motivates its readers into delving further into this interesting field of science and its manifold applications in physics, chemistry and biology.

The first two chapters give an introduction to basic principles and aspects of instrumentation for laser spectroscopy. The reasons why lasers have become established in modern analytical techniques are shown very well. The current state of the art in laser technology is reviewed. Although knowledge of lasers themselves is not necessary to understand this book; a short chapter concerning laser theory would have been helpful. The remaining eight chapters cover the most important fields of applications of laser spectroscopy, such as absorption spectroscopy, fluorescence spectroscopy, high-resolution infrared spectroscopy, Raman spectroscopy, laser mass spectrometry and ultrafast spectroscopic methods. All chapters are divided clearly and contain principles, special instrumentation and applications of each described method. In some chapters commercial applications especially could have been treated in more detail, according to the title of the book. Each chapter features a comprehensive reference list providing the reader with a good basis for further reading.

The editor has been successful in producing a homogeneous, well-balanced book. The reader can recognize clearly that laser spectroscopy has become an important routine analytical tool.

Christoph Schnürer-Patschan

R.P.W. Scott, *Silica Gel and Bonded Phases*, Wiley, Chichester, 1993 (ISBN 0-471-93985-4). xi + 261 pp. Price £35.00.

Contrary to the wide-spread use of bonded silicas in liquid chromatography (LC) only a few monographs have been published on this important subject. Raymond Scott, who is one of the pioneers of modern column LC, provides an authoritative and historical perspective of this field.

The main focus of the book is on the treatment of the decisive properties of silica and its bonded phases and on the basic principles which govern retention and selectivity in LC, emphasizing the most important contributions of the author.

The book is divided into eleven chapters. The first two provide a short review on the formation and the manufacturing processes of porous silica (silica gel). Chapter 3 deals with the characterization of microparticulate silicas and column packing procedures. Chapter 4 surveys the important features with respect to the chemical nature of silica. The exclusion properties and the solvent–solute interactions of silica are discussed in the following two chapters. The core of the book is chapters 7 to 10 where the most important aspects of the synthesis, characterization and chromatographic application of reversed-phase silicas are critically reviewed. The book concludes with a summary of retention mechanisms in LC (chapter 11).

The book is well-structured. The subjects are thoroughly treated, clearly described and illustrated by numerous examples. It will be especially valuable to experienced chromatographers and analytical chemists who wish further to understand basic principles in LC.

K.K. Unger

T.R. Crompton, *The Analysis of Natural Waters*, Vols. 1 and 2, Oxford Science Publications, Ox-

ford, 1993 [ISBN 0-19-855395-1 (Vol. 1), 0-19-855394-3 (Vol. 2), 0-19-855752-3 (set)]. xi + 249 pp. (Vol. 1), xi + 216 pp. (Vol. 2). Price £75.00 (set).

The general title of this two volume set is somewhat misleading because the content relates exclusively to preconcentration techniques. Nonetheless it is undoubtedly a crucial aspect of the overall analytical process for the determination of species in both saline and, to a lesser degree, non-saline waters. The two volumes are classified in terms of complex-formation preconcentration (volume 1) and direct preconcentration (volume 2) techniques, although the distinction is not particularly clearcut. Volume 1 provides a general introduction and describes chelation-solvent extraction, macroreticular non-polar resins, cation exchange resins and anion exchange resins. Volume 2 covers solid organic adsorbents and chelators (e.g. Chelex-100), metal oxides and metal adsorbents, active carbon, co-precipitation techniques, solvent extraction, purge and trap and head space techniques.

This twin volume set follows a similar style to the recently published *Comprehensive Water Analysis* by the same author [see *Anal. Chim. Acta*, 281 (1993) 223]. It is primarily a factual compilation of literature material referring mainly to citations from the 1970s and 1980s, with some additional general background and basic theoretical principles at the start of each chapter. Most of the chapters are divided into sections covering metal cations, anions, organics and organometallic compounds with some additional sub-division of sections into non-saline waters and sea water (presumably including brackish waters). It would have been easier to follow the book and use the material as a practical guide if the theoretical sections had been followed by species specific applications rather than method specific applications.

Therefore, although these two books summarise a significant body of information from the primary literature (with good use of tables), the content is not critical or comprehensive. For example there is no mention of flow-injection techniques for preconcentration although it is well established as a rapid, clean and simple approach particularly for metals using iminodiacetate based resins. This is partially because the intended audience is broad based, encompassing not only water chemists, but also analytical chemists with an interest in preconcentration (as a means of improving detection limits), environmental scientists, water management personnel and the general public. Nonetheless it is a useful overview of an increasingly important area of environmental analytical chemistry.

Paul J. Worsfold

I.M. Kolthoff and J.D. Winefordner (Eds.), *Treatise on Analytical Chemistry*, Part I, Vol. 13, *Thermal Analysis*, Wiley, New York, 1993 (ISBN 0-471-80647-1). xviii + 406 pp. Price £29.00.

The Treatise on Analytical Chemistry was first produced in the 1950s and is a worldwide comprehensive treatment on analytical chemistry. This book is an up-date of the first edition of volume 13. Thermal Analysis methods have grown very much in the last decade. This edition does not describe techniques which are now currently used as analytical tools, such as differential scanning calorimetry and microcalorimetry or techniques useful for the analysis of polymers.

The book is divided in six chapters: Application to Kinetic Evaluation of Thermal Degradation, Thermometric Titrations and Enthalpimetric Analysis, Thermogravimetry, Application of Thermodilatometry to the Study of Ceramics, Pyrolysis Techniques and Application of Thermal Analysis to Problems in Cement Chemistry.

The style is very clear and easy to read. Each part has been written by experts. Despite some lack of description of modern instrumentation, this book offers a very valuable reference for theoretical background and interpretation in the area treated.

D. Giron

J.C. Miller and J.N. Miller, *Statistics for Analytical Chemistry*, 3rd edn., Ellis Horwood, Chichester, 1993 (ISBN 0-13-030990-7). 233 pp. Price US $23.00.

It is a pleasure to review the 3rd edition of a text that one was able warmly to commend in both its earlier versions. The format and bulk of the text remain the same but, based on the authors' experience, that of other teachers using this popular text, and recent publications, changes and updates have been made to most chapters. Significant changes have been made to sections dealing with curvilinear regression methods, robust statistical methods, outliers in univariate statistics, calibration methods, initial data examination, experimental design and on optimisation. Very commendably these revisions are properly incorporated within the text which thus remains coherent and almost the same size as before.

This is an excellent text for students and for practitioners of analytical chemistry and remains in the "essential to purchase" classification.

D. Thorburn Burns

Richard C. Graham, *Data analysis for the chemical sciences. A guide to statistical techniques*, VCH, Weinheim, 1993 (ISBN 1-56081-048-3). xx + 536 pp. Price DM 78.00/£32.00.

This text unlike that of Miller and Miller (reviewed above) is addressed to chemists in general and aims to provide the tools necessary to determine the suitability of synthetic methods, quality of analytical results, relationships between data, structure in a data set, spatial similarities in data sets, temporal trends of data sets and patterns in data sets. Much of the material is standard, e.g., test for comparison of means, but well explained and put in context with a wealth of worked examples. Less common but useful material provided includes that on transformation of instrument data, quality assurance and software sources. Future editions could usefully include discussion of optimisation techniques, of interest to synthetic and analytical chemists alike.

Overall this is an interesting book for teacher and student; sections like that including a diagram illustrating the relation between samples and population should engender a moment of complete clarity of concept in all. It is a good reference text for third level college library purchase.

D. Thorburn Burns

Kim Kinoshita, *Electrochemical Oxygen Technology*, Wiley, New York, 1992 (ISBN 0-471-57043-5). xiv + 431 pp. Price £98.00.

Oxygen is life, yet, paradoxically, it has also within it the seeds of corruption. Without oxygen there would be no life, at least in the form that we know it. But at the same time, whilst mechanisms of change and decay may not be fully understood, it is clear that highly active oxygen plays no small part in degrading the world around us and in propelling us inexorably to the grave.

Happily, the same properties of oxygen which make it so corrupting, especially the high, positive standard potential, means it plays an important role in a wide range of technologies in general, and, in particular, in a number of electrochemical technologies, especially for fuel cells and metal/air batteries. Unfortunately, although perhaps fortunately for us, the kinetics of oxygen reduction are rather slow and its uses as an energy source have been rather limited. A significant part of this book surveys the research that has gone into the preparation and properties of electrodes suitable for oxygen reduction (chapter 3) and into their application to fuel cells (chapter 4) and metal/air batteries (chapter 5), the efficient performance of both of which continues to be a Holy Grail which energy oriented electrochemists have spent, and are likely to continue to spend, many hours pursuing. Anyone wishing to join the quest would be well served by this part of the book and would have a comprehensive reference list from which to start. They might find some guidance on the route to take from the chapter devoted to the electrochemistry of oxygen (chapter 2), but, like knights of old, they need to

beware of false trails, half truths, and contradictory advice for, as the author points out, the mechanisms of oxygen electrode processes are still controversial and far from settled. Perhaps the only crumb of comfort for any valiant electrochemist in search of glory is that when it comes to the physicochemical properties of oxygen there are some reasonably reliable data, and these are usefully collected and summarised in chapter 1. At the end of the day it may be that discretion should become the better part of valour and a latter day electrochemical knight should set out on a slightly easier, although not much less daunting, quest, and seek to slay a few dragons in areas of oxygen recombination in batteries (chapter 6), or of industrial processes which use or generate oxygen, or of electrochemical sensors for oxygen (chapter 7). And, of course, if none of these appeal then there are many valiant deeds to be done and maidens to be rescued from the clutches of the marauding oxygen as it goes about corroding anything that is weaker or less electrochemically positive than itself — which is the topic which is dealt with, albeit rather cursorily, by the author at the end of this volume and with which we started this short review.

This is undoubtedly a book that any electrochemist involved with oxygen (and which one is not to some extent or other) would find useful to have available for reference, although at £98.00 it is rather expensive. There is very little analytical chemistry, in the usual meaning of that term, within it. The only sections with any analytical content are those dealing with the physicochemical properties of oxygen (chapter 1) and with sensors (chapter 7). There are, though, a number of other texts which deal more adequately with these matters and so it is unlikely that this is a book an analytical chemist would be likely to find of much value. Unless, of course, they wish to try and win their spurs by bringing to bear analytical expertise to some of the problems which undoubtedly exist, and which this book highlights, in electrochemical oxygen technology.

Michael L. Hitchman

P.K. Hopke (Editor), *Receptor Modelling for Air Quality Management*, Data Handling in Science and Technology, Vol. 7, Elsevier, Amsterdam 1991 (ISBN 0-444-88218-9). xiv + 329 pp. Price £100.00.

Receptor Modelling For Air Quality Management is a fitting tribute to Dr. Thomas G. Dzubay, to whom this book is dedicated. As volume 7 in the series *Data Handling in Science and Technology* it demands that the reader is proficient in a wide range of statistical and chemometric techniques, if the reader is to gain the full benefit of this work. Nevertheless, the non-specialist will be fully informed as to what may be accomplished through the manipulation of analytical data obtained from the analysis of air samples.

Starting with an introduction to the important concepts of mass balance calculations, a multidisciplinary approach is adopted with sections covering air sampling systems, from PM-10 reference methods through to filter-based units and denuder tube assemblies. This approach is then developed with a discussion on post-sample analysis techniques, although this takes place only at a superficial level. Having discussed how air quality data are obtained the use of chemical mass balance mathematics is presented and apportionment techniques are described, along with proforma methodologies and protocols for undertaking such studies. This theme of data analysis continues to be developed with multivariant approaches proposed as complementary procedures to the chemical mass balance methodologies previously presented. Finally, in this middle section of the book, pattern recognition techniques for use in conjunction with scanning electron microscopy are shown to enable sampled particulate material to be assigned to their appropriate sources.

Case studies form the final part of this work with volatile organic compounds, particulate matter and applications to localised air quality problems all presented in detail.

Aimed at the specialist with substantial experience in at least one of the areas covered this is a challenging text. The editor and contributing authors have presented a complicated and difficult

subject well in producing what appears to be a comprehensive source book on this subject.

C.P. Thomas

S.M. Khopkar, *Basic Concept of Analytical Chemistry*, Wiley Eastern Ltd., New Delhi, 1984, Third Reprint 1992 (ISBN 0-85226-461-5). xvi + 368 pp. Price 70 Rupees.

Above the publishers name on the title page is the statement "Publishing for one world". It is clearly not one world when students in one geographical region are sold a straight reprint of a text in a rapidly changing subject that is 10 years old. It is unacceptable that methods now so routine as flow-injection analysis and chiral chromatography are omitted from a student level text. In 1984 this was a well balanced book and a credit to its author. With careful and sensitive revision it could again be of great value. It is to be hoped that the publishers will follow this course of action and demonstrate that they know the differences between useful classical methods and out of date instrumentation and technologies.

Cees van Dijk (Ed.), *Analytical Biotechnology*, Elsevier, Amsterdam, 1993 (ISBN 0-444-81640-2) iv + 202 pp. Price Dfl. 265.00, US $151.50.

This is a collection of papers, previously published in *Anal. Chim. Acta*, Vol. 279, presented at Anabiotec '92, the *Fourth International Symposium on Analytical Methods, Systems and Strategies in Biotechnology*, held at Noordwijkerhout, The Netherlands, September 21–23, 1992. The papers are arranged in sections dealing with process control (7 papers), chromatography, etc. (6), antibodies (1), biosensors (3), instrumental techniques (4), enzymatic analysis (1) and colloidal carbon particles (1). As such they present a good cross-section of the applications of analytical chemistry to analyses in the biotechnology area, and of biotechnology to facilitate analytical measurements, and provide a record of a popular symposium.

A.A. Szalay, L.J. Kricka and P. Stanley (Eds.), *Bioluminescence and Chemiluminescence, Status Report*, Wiley, Chichester, 1993 (ISBN 0-471-94164-6). xvi + 548 pp. Price £90.00.

These are the proceedings of the *VIIth International Symposium on Bioluminescence and Chemiluminescence*, held in Banff, Canada, 14–18th March 1993, and produced, unreviewed, with commendable speed in camera-ready format. Each author is restricted to 5 pages. The material is divided amongst 5 sections, viz. instrumentation for light detection (10 papers), molecular biology and biochemistry (37), chemiluminescent and bioluminescent assays (42), cellular luminescence (12) and chemiluminescence and bioluminescence (8). There is a mixed subject/author index. The presentation is generally very clear, and there is a tremendous coverage of current developments in a very topical area.

Michael Buback and Hans Peter Vogele, FT-NIR Atlas, VCH, Weinheim, 1993 (ISBN 3-527-28563-9). xiv + 1067 pp. Price DM 880.00.

The core of this publication is the hard copy of the library of 1957 digital FT-near IR spectra, mostly of individual compounds, held by Chemical Concepts, part of the VCH Publishing Group, and founded under an initiative by the German Ministry of Research and Technology. The spectra appear in alphabetical order (starting with BBr_3 and finishing with H_2O), with the vast majority relating to carbon compounds, which appear in traditional *Chemical Abstracts* order. Much other information (molar mass, density, m.p., b.p., CAS Reg. No.) is also included, as are the frequencies of the most intense peaks. Information retrieval is via a formula index, compound name index, CAS Reg. No. index. The information is also available in electronic form. The format is designed to be as similar as possible to the Merck FT-IR Atlas (VCH, 1988), and the Atlases may be purchased as a pair at a reduced price.

I. Matsumoto (Ed.), *Advances in Chemical Diagnosis and Treatment of Metabolic Disorders*, Vol. 1, Wiley, Chichester, 1992 (ISBN 0-471-93615-4). xviii + 165 pp. Price £30.00.

This volume is the updated proceedings of the *First* and *Second Symposia on Clinical Diagnosis of Medical Disorders*, Kanazawa, Japan, May 1989 and May 1990. As the foreword states, it "combines analytical aspects of the diagnosis of metabolic disorders with the results of the analyses applied to the treatment of these disorders". The seventeen chapters cover lactic acidemic, organic acidemia, urea-cycle disorders and drug-induced metabolic defects and there are two papers dealing directly with analytical techniques (LC and LC–MS for acylcarnitine and peptide hormones, respectively). The collection of individual papers shows how essential are modern analytical techniques to medical progress and the diagnosis of disease, and gives an appreciation of how they are used in these areas. There is a good subject index included.

ANALYTICA CHIMICA ACTA, VOL. 285 (1994)

AUTHOR INDEX

Announcement from the Publisher

Elsevier encourages submission of articles on floppy disk.

All manuscripts may now be submitted on computer disk, with the eventual aim of reducing production times still further.

The preferred storage medium is a 5¼ or 3½ inch disk in MS-DOS format, although other systems are welcome, e.g. Macintosh.

After **final acceptance**, your disk plus one final, printed and exactly matching version (as a printout) should be submitted together to the editor. **It is important that the file on disk and the printout are identical.** Both will then be forwarded by the editor to Elsevier.

Illustrations should be provided in the usual manner.

Please follow the general instructions on style/arrangement and, in particular, the reference style of this journal as given in 'Instructions to Authors'.

Please label the disk with your name, the software & hardware used and the name of the file to be processed.

For further information on the preparation of compuscripts please contact:

Elsevier Science B.V.
Analytica Chimica Acta
P.O. Box 330
1000 AH Amsterdam, The Netherlands
Phone: (+31-20) 5862 758 Fax: (+31-20) 5862 459

ELSEVIER SCIENCE B.V.

ANALYTICAL BIOTECHNOLOGY

Proceedings of the 4th International Symposium on Analytical Methods, Systems and Strategies in Biotechnology (ANABIOTEC '92), Noordwijkerhout, The Netherlands, 21-23 September 1992

Edited by **C. van Dijk**

Previously published as part of the 1993 subscription to the journals *Analytica Chimica Acta* and *Journal of Biotechnology*

ANABIOTEC '92 focused on the further integration of biotechnology and analytical chemistry. The results of this symposium clearly demonstrated that a substantial progress could be reported in the application of both conventional and new analytical techniques, the latter essentially based on natural analytical tools such as biomolecules. The main themes covered during this meeting are fermentation monitoring, chromatography, instrumental analysis, biosensors and bioanalysis.

A selection of the contents.
Preface.
Process Control. Monitoring and control of recombinant protein production (K. Schügerl *et al.*). Rapid and quantitative analysis of bioprocesses using pyrolysis mass spectrometry and neural networks: application to indole production (R. Goodacre, D.B. Kell). Characterization of a sampling unit based on tangential flow filtration for on-line bioprocess monitoring (T. Buttler, L. Gorton, G. Marko-Varga). Automated monitoring of biotechnological processes using on-line ultrafiltration and column liquid chromatography (N.C. Van de Merbel *et al.*). On-line monitoring of penicillin V during penicillin fermentations: a comparison of two different methods based on flow-injection analysis (M. Carlsen *et al.*). Development of an on-line method for the monitoring of vicinal diketones and their precursors in beer fermentation (C. Mathis *et al.*). Monitoring of fermentation by infrared spectrometry. Alcoholic and lactic fermentations (D. Picque *et al.*).
Chromatography and other Separation Techniques. Chromatographic analysis of biopolymers distribution in "poly-hemoglobin", an intermolecularly crosslinked hemoglobin solution (J. Simoni, G. Simoni, M. Feola). Application of multivariate mathematical-statistical methods for the comparison of the retention behaviour of porous graphitized carbon and octadecylsilica columns (E. Forgács, T. Cserháti, B. Bordás).
Antibodies. Catalytic antibodies: new developments (R. Hilhorst).
Biosensors. Measurements of nitric oxide in biological materials using a porphyrinic microsensor (T. Malinski *et al.*). Reusable fiber-optic-based immunosensor for rapid detection of imazethapyr herbicide (R.B. Wong, N. Anis, M.E. Eldefrawi). Biosensor monitoring of blood lactate during open-heart surgery (M. Kyröläinen *et al.*).
Instrumental Techniques. Introduction to the dielectric estimation of cellular biomass in real time, with special emphasis on measurements at high volume fractions (C.L. Davey *et al.*). Spectral analysis of interactions between proteins and dye ligands (J. Hubble, A.G. Mayes, R. Eisenthal).
Enzymatic Analysis. Preservation of shelf life of enzyme based analytical systems using a combination of sugars, sugar alcohols and cationic polymers or zinc ions (T.D. Gibson, J.N. Hulbert, J.R. Woodward).
Colloidal Carbon Particles. Colloidal carbon particles as a new label for rapid immunochemical test methods: Quantitative computer image analysis of results (A. van Amerongen *et al.*). Author Index.

© 1993 208 pages Hardbound
Price: Dfl. 265.00 (US $ 151.50)
ISBN 0-444-81640-2

ORDER INFORMATION

For USA and Canada
ELSEVIER SCIENCE INC.
P.O. Box 945
Madison Square Station
New York, NY 10160-0757
Fax: (212) 633 3880

In all other countries
ELSEVIER SCIENCE B.V.
P.O. Box 330
1000 AH Amsterdam
The Netherlands
Fax: (+31-20) 5862 845

US$ prices are valid only for the USA & Canada and are subject to exchange rate fluctuations; in all other countries the Dutch guilder price (Dfl.) is definitive. Customers in the European Community should add the appropriate VAT rate applicable in their country to the price(s). Books are sent postfree if prepaid.

ELSEVIER SCIENCE B.V.

PUBLICATION SCHEDULE FOR 1994

	S'93	O'93	N'93	D'93	J	F	M	A	M			
Analytica Chimica Acta	281/1 281/2 281/3	282/1 282/2 282/3	283/1 283/2	283/3 284/1 284/2	284/3 285/1–2 285/3	286/1 286/2 286/3	287/1–2 287/3 288/1	288/2 288/3 289/1	289/2–3 290/1 290/2			
Vibrational Spectroscopy		6/1			6/2		6/3		7/1			

INFORMATION FOR AUTHORS

Detailed "Instructions to Authors" for *Analytica Chimica Acta* was published in Volume 256, No. 2, pp. 373–376. Free reprints of the "Instructions to Authors" of *Analytica Chimica Acta* and *Vibrational Spectroscopy* are available from the Editors or from: Elsevier Science B.V., P.O. Box 330, 1000 AH Amsterdam, The Netherlands. Telefax: (+31-20) 5862459.

Manuscripts. The language of the journal is English. English linguistic improvement is provided as part of the normal editorial processing. Authors should submit three copies of the manuscript in clear double-spaced typing on one side of the paper only. *Vibrational Spectroscopy* also accepts papers in English only.

Rapid publication letters. *Letters* are short papers that describe innovative research. Criteria for letters are novelty, quality, significance, urgency and brevity. Submission data: max. of 2 printed pages (incl. Figs., Tables, Abstr., Refs.); short abstract (e.g., 3 lines); *no* proofs will be sent to the authors; submission on floppy disc; *no* revision will be possible.

Abstract. All papers and reviews begin with an Abstract (50–250 words) which should comprise a factual account of the contents of the paper, with emphasis on new information.

Figures. Figures should be prepared in black waterproof drawing ink on drawing or tracing paper of the same size as that on which the manuscript is typed. One original (or sharp glossy print) and two photostat (or other) copies are required. Attention should be given to line thickness, lettering (which should be kept to a minimum) and spacing on axes of graphs, to ensure suitability for reduction in size on printing. Axes of a graph should be clearly labelled, along the axes, outside the graph itself. All figures should be numbered with Arabic numerals, and require descriptive legends which should be typed on a separate sheet of paper. Simple straight-line graphs are not acceptable, because they can readily be described in the text by means of an equation or a sentence. Claims of linearity should be supported by regression data that include slope, intercept, standard deviations of the slope and intercept, standard error and the number of data points; correlation coefficients are optional.

Photographs should be glossy prints and be as rich in contrast as possible; colour photographs cannot be accepted. Line diagrams are generally preferred to photographs of equipment. Computer outputs for reproduction as figures must be good quality on blank paper, and should preferably be submitted as glossy prints.

Nomenclature, abbreviations and symbols. In general, the recommendations of IUPAC should be followed, and attention should be given to the recommendations of the Analytical Chemistry Division in the journal *Pure and Applied Chemistry* (see also *IUPAC Compendium of Analytical Nomenclature, Definitive Rules*, 1987).

References. The references should be collected at the end of the paper, numbered in the order of their appearance in the text (*not* alphabetically) and typed on a separate sheet.

Reprints. Fifty reprints will be supplied free of charge. Additional reprints (minimum 100) can be ordered. An order form containing price quotations will be sent to the authors together with the proofs of their article.

Papers dealing with vibrational spectroscopy should be sent to: Dr J.G. Grasselli, 150 Greentree Road, Chagrin Falls, OH 44022, U.S.A. Telefax: (+1-216) 2473360 (Americas, Canada, Australia and New Zealand) or Dr J.H. van der Maas, Department of Analytical Molecular Spectrometry, Faculty of Chemistry, University of Utrecht, P.O. Box 80083, 3508 TB Utrecht, The Netherlands. Telefax: (+31-30) 518219 (all other countries).

0003-2670/94/$07.00

This issue is printed on acid-free paper.

PRINTED IN THE NETHERLANDS

ANABIOTEC 94

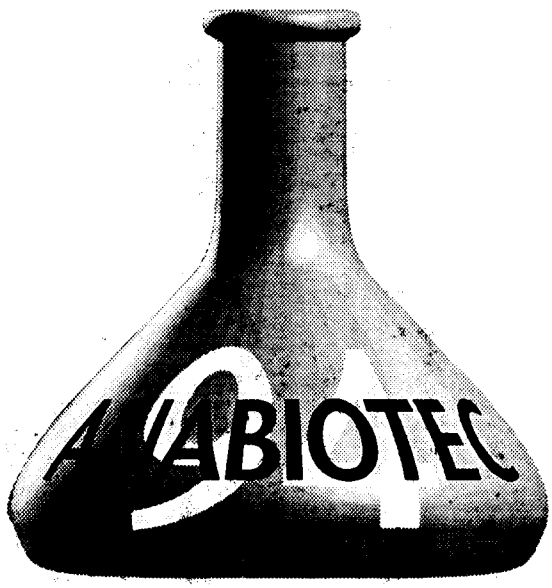

5th International Symposium on Analytical Techniques, Systems & Strategies in Biotechnology

31 October – 2 November 1994

Minneapolis Hilton & Towers, USA

Learn of the new instruments and techniques for analytical chemistry
Improve monitoring of industrial scale processes
Update your strategies for clinical diagnosis
Meet international colleagues and contacts

The analytical chemistry of complex matrices involving species of a biological origin is a rapidly developing research frontier.

ANABIOTEC 94 – consisting of plenary sessions, selected original papers, posters and an exhibition – will address the wide array of research issues involved in this field. This symposium is the ideal forum for information exchange between the fields of analytical chemistry, biochemistry, clinical chemistry and biotechnology: you need to be there!

For further information send a copy of this advert, complete with your address details to:

Anabiotec 94 Conference Secretariat, Elsevier Science Ltd,
PO Box 150, Kidlington, Oxford OX5 1AS, UK.
Tel: +44 (0) 865 512242
Fax: +44 (0) 865 310981

anabiotec.bk+12) 12.93

0003-2670(19940128)285:3;1-4